Acta morphologica et anthropologica 25 (3–4)

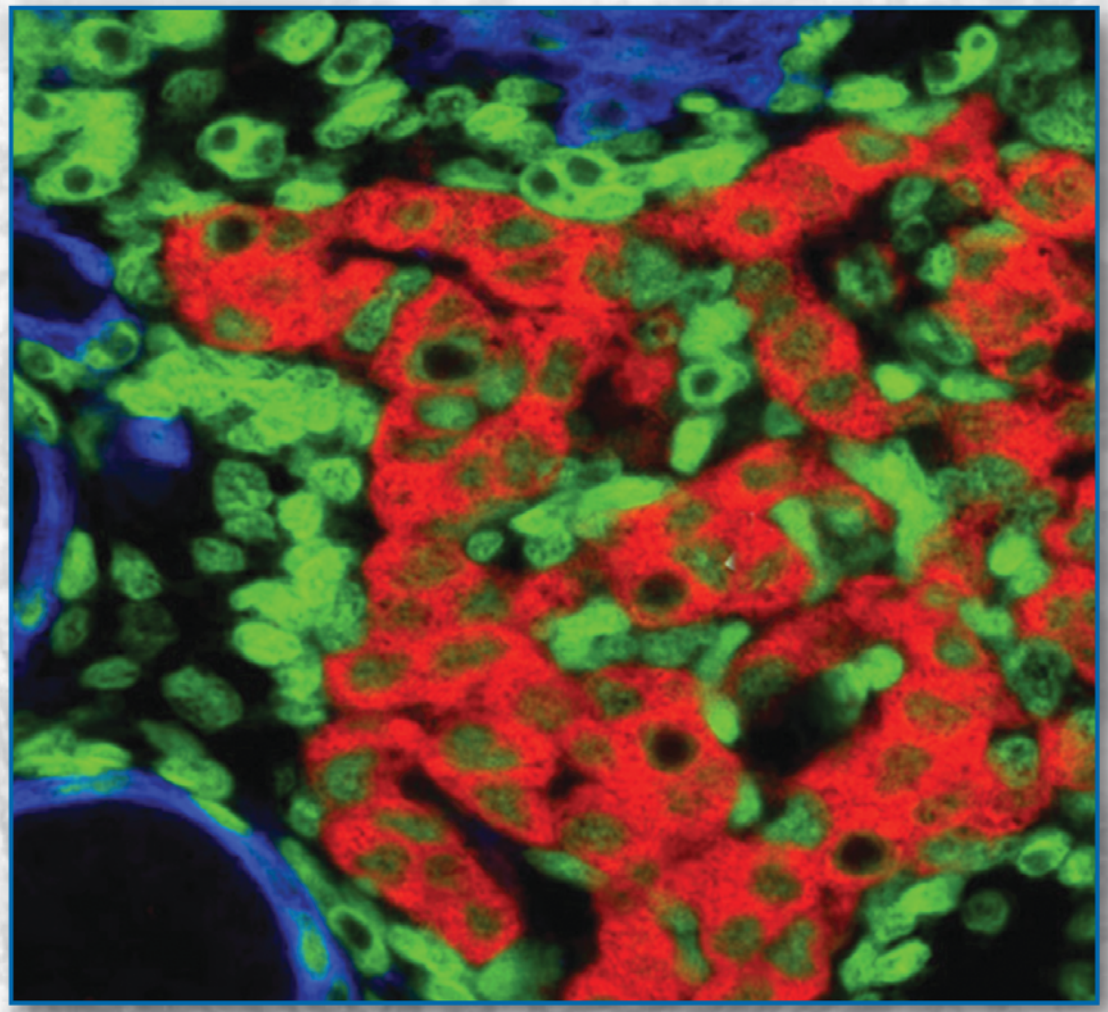

Prof. Marin Drinov Publishing House
of Bulgarian Academy of Sciences

Acta morphologica et anthropologica

is the continuation of Acta cytobiologica et morphologica

Editor-in-Chief: Prof. Nina Atanassova
e-mail: ninaatanassova@yahoo.com; ninaatanassova@bas.bg
+359 2 979 2342
Deputy Editor-in-Chief: Prof. Dimitar Kadiysky
e-mail: dkadiysky@yahoo.com; dimkad@bas.bg
+359 2 979 2311
Executive Secretary: Assoc. Prof. Y. Gluhcheva
e-mail: ygluhcheva@hotmail.com
+359 2 979 2344

Editorial Correspondence
Institute of Experimental Morphology, Pathology and Anthropology with Museum
Bulgarian Academy of Sciences
Acta morphologica et anthropologica
Acad. Georgi Bonchev Str., Bl. 25
1113 Sofia, Bulgaria
E-mail: ygluhcheva@hotmail.com; iempam@bas.bg
Tel.: +359 2 979 2311

Издаването на настоящия том 25, книжки 3 и 4 е осъществено с финансовата подкрепа на Фонд „Научни изследвания“

Prof. Marin Drinov Publishing House of Bulgarian Academy of Sciences
Bulgaria, 1113 Sofia, Acad. Georgi Bonchev Str., Bl. 6

Graphic designer Veronika Tomcheva
Format 70×100/16 Printed sheets 11.50

Printing Office of Prof. Marin Drinov Publishing House of Bulgarian Academy of Sciences
Bulgaria, 1113 Sofia, Acad. Georgi Bonchev Str., Bl. 5

ISSN 1311-8773 (print)
ISSN 2535-0811 (online)

Acta morphologica et anthropologica

25 (3-4)

25 (3-4) ● Sofia ● 2018
Institute of Experimental Morphology, Pathology and Anthropology with Museum
Bulgarian Anatomical Society

Contents

Anthropology and Anatomy

Review Articles

Institute of Experimental Morphology, Pathology and Anthropology with Museum
Bulgarian Anatomical Society

Acta morphologica et anthropologica, 25 (3-4)
Sofia ● 2018

Editorial

VII National Conference with International Participation "Morphological Days", Sofia, 8-10 of June, 2018

Nina Atanassova[*]

Institute of Experimental Morphology, Pathology and Anthropology with Museum, Bulgarian Academy of Sciences, Sofia, Bulgaria

* Corresponding author e-mail: ninaatanassova@yahoo.com

The traditional 7th National Conference with International Participation "Morphological Days" was held on 8th – 10th of June, 2018 in Sofia. The organizer of this event was the Institute of Experimental Morphology, Pathology and Anthropology with Museum at the Bulgarian Academy of Sciences and the venue of the Conference was the National Anthropological Museum of the Institute.

The opening of the conference started by welcome addresses from Professor Svetlozara Petkova - Director of the Institute and Professor Nina Atanassova - President of the Organizing Committee. They were followed by official ceremony of giving awards to Professor Vasil Vasilev on his 90th anniversary and Professor Christo Chouchkov on his 80 anniversary for their great recognition for development of morphological science, education in anatomy and Bulgarian Anatomical Society.

The main topics of the conference included all the fields of anatomy, histology, cytology, embryology, pathology and anthropology. The conference was attended by more than 120 participants from Germany, Netherlands, Belarus, Georgia, Serbia, Macedonia, Egypt and Bulgaria. In national aspect, the meeting integrated scientists from biomedical institutes of the Bulgarian Academy of Sciences, Sofia University "St Kliment Ohridski", Plovdiv University "Paisii Hilendarski", all Medical Universities – in Sofia, Plovdiv, Varna, Pleven, Trakia University in Stara Zagora, University of Forestry – Faculty of Veterinary Medicine, as well as clinical specialists from University Hospitals.

The conference was organized in ten scientific sessions with 94 presentations. Plenary lectures were given by Professor Katja Teerds from Wageningen University in Netherlands, Professor Michail Davidoff from University of Hamburg, Germany and Acad. Vladimir Ovtscharoff, President of the Bulgarian Anatomical Society.

The conference was funded by the project “Creation and development of young high-qualified scientists and lecturers for innovative interdisciplinary research of great importance for biomedicine”, Grant No BG05M20P001-2.009-0019-C01/02.06.2017, financed by the Operational Programme “Science and Education for Smart Growth” 2014-2020, co-financed by the European Union via the European Structural and Investigation Funds. The conference was included in the action plan of the project and all the presentations were attended by the project target group of PhD students, PostDocs, young researchers and lecturers.

The venue of the conference – The National Anthropological Museum provided nice atmosphere around the museum expositions and anthropological reconstructions of the head of great Bulgarians as King Kaloyan, King Samuil, Thracian Princess, Georgi Rakovski, Luben Karavelov, Zahari Stoyanov, Bacho Kiro and all the participants enjoyed the meeting.

Institute of Experimental Morphology, Pathology and Anthropology with Museum
Bulgarian Anatomical Society

Acta morphologica et anthropologica, 25 (3-4)
Sofia ● 2018

Morphology

Immunohistochemical Expression of KISS-1 Protein and KISS-1R in Breast Cancer

Desislava Ankova[*]*, Despina Pupaki, Pavel Rashev*

Institute of Biology and Immunology of Reproduction „Acad. Kiril Bratanov“,
Bulgarian Academy of Sciences, Sofia, Bulgaria

*Corresponding author e-mail: dessislava_ankova@abv.bg

Numerous studies have shown that the *kiss-1* gene countervails the metastatic aptitude of several cancer cell lines and solid-tumor neoplasms. However, there still remains ambiguity regarding its role in breast cancer and literature has arisen asserting that Kiss-1 protein may be linked to an aggressive phenotype and malignant progression. We investigated the localization of KISS-1 and its receptor KISS-1R in breast cancer tissue compared to non-cancerous mammary tissue. Immunohistochemical localization was investigated using rabbit polyclonal antibodies against KISS-1 and KISS-1R. A total of 30 tumor formations and 20 samples from non-tumorous mammary tissue were examined. Our study showed that KISS-1 and KISS-1R proteins were significantly higher in breast cancer compared to normal tissue. These results further support the role of the KISS-1/ KISS-1R system in breast cancer biology and might be useful in developing effective therapeutic strategies aimed at modulating the KISS-1/KISS-1R pathway.

Key words: KISS-1, KISS-1R, breast cancer

Introduction

Breast cancer is a progressive and potentially fatal disease that affects women of all ages. It is the most common type of cancer and the leading cause of cancer-related deaths in women in most developed countries [14]. Its high mortality rate is in fact not due to the primary breast tumor burden but rather its metastatic deposits. The metastatic spread of cancer cells is a complex and sequential process that requires detachment from the primary site, survival in the circulation, attachment to and invasion of distant tissues [7]. Tumor cell invasion and metastasis involves genetic and epigenetic modifications of numerous molecular mediators, leading to alterations in various signaling pathways. Numerous studies have shown that the KISS-1 gene countervails the metastatic aptitude of several cancer cell lines and solid-

tumor neoplasias. However, there still remains ambiguity regarding its role in breast cancer and literature has arisen asserting that KISS-1 expression may be linked to an aggressive phenotype and malignant progression.

The *kiss-1* gene encodes a group of biologically active peptides collectively known as kisspeptins (KPs) which play a major regulatory role in puberty onset and reproductive function [1, 3, 8, 28]. Kisspeptins are the endogenous ligands for the G protein-coupled receptor KISS-1R [12]. Activation of this pathway results in stimulation of the phosphatidylinositol-3-kinase/Akt and mitogen activated protein kinase (MAPK) pathways [19].

In non-malignant tissues, KISS-1 expression has been shown to be particularly abundant in the placenta [22], contributing to trophoblast invasion during pregnancy [2, 10, 13, 26], followed by a widespread expression in several central nervous system regions and moderate-to-weak expression in the testis, pancreas, liver, intestine, kidney, lungs and prostate [16, 22, 25]. This tissue distribution pattern is compatible with mRNA localization of GPR54, which is highly expressed in the placenta and central nervous system, and less prominent in intestine, kidney, lungs, and prostate [16, 22, 25]. KISS-1 and KISS-1R expression has been investigated in a variety of cancers including gestational trophoblastic disease [5], melanoma [16, 31], breast cancer [30, 17], hepatocellular carcinoma [11], pancreatic cancer [23], gastric carcinoma [6], esophageal carcinoma [12], papillary thyroid cancer [27], bladder cancer [29], ovarian cancer [15, 9], prostate cancer [32] and pheochromocytoma [24]. The KISS-1/GPR54 system has also been implicated in the pathophysiology of endometriosis [18]. In most malignancies, the *kiss-1* gene seems to act as an anti-metastatic agent and loss of KISS-1 expression is associated with tumor progression and advanced disease. In breast cancer, however, the role of kisspeptin remains elusive due to limited and conflicting data, and it is possible that increased KISS-1 expression correlates with disease progression and poor patient prognosis in this particular type of cancer.

The present study aimed at determining KISS-1 and KISS-1R protein expression in breast cancer tissues compared to non-malignant mammary tissues.

Materials and Methods

Thirty samples of invasive ductal carcinoma (18 cases of moderately differentiated ductal carcinoma and 12 cases of low-differentiated ductal carcinoma) and 20 samples from non-tumorous mammary tissue, were included in the study.

Immunohistochemical (IHC) method. Tissue samples were fixed in 10% buffered formalin, dehydrated and embedded in paraffin. Paraffin sections, 5 μm thick, were stained with haematoxylin and eosin for histopathological evaluation. Antigen retrieval was performed in Citrate Buffer, pH 6.0 (ScyTek Laboratories Inc., USA) at 95°C for 20 min. Endogenous peroxidase activity was blocked with 3% H_2O_2 for 10 min at room temperature. Subsequently, the sections were washed in TTBS (tris-buffered saline + 0,05% Tween 20) and incubated with primary antibodies against KISS-1 (1:150, rabbit polyclonal, Elabscience Biotechnology Inc., USA) and KISS-1R (1:150, rabbit polyclonal, Elabscience Biotechnology Inc., USA). Biotin-Streptavidin HRP detection system (ScyTek Laboratories Inc., USA) with DAB as chromogen was used.

Results

The intensity of the reaction was significantly higher in tumours compared to normal tissue. KISS-1 and KISS-1R showed stronger staining in the cytoplasm of tumour cells

with additional membrane reaction for KISS-1R. In low-differentiated invasive ductal carcinomas the reaction was stronger compared to that in moderately differentiated ductal carcinomas (**Fig. 1**).

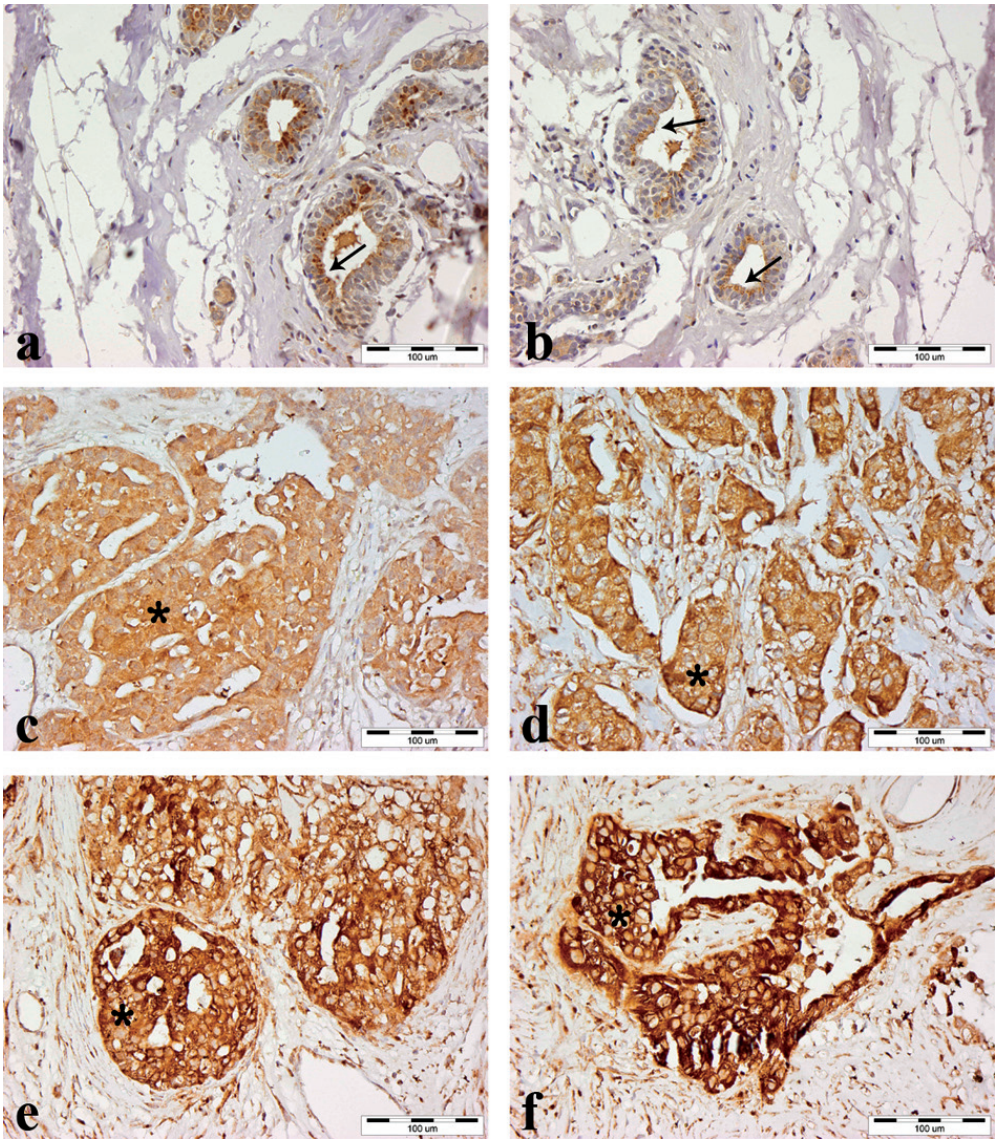

Fig. 1. Immunohistochemical expression of KISS-1 (a, c, e) and KISS-1R (b, d, f) in normal breast epithelium (a, b), invasive moderately differentiated ductal carcinoma (c, d) and invasive low-differentiated ductal carcinoma (e, f). Weak cytoplasmic and more intensive apical reaction for both KISS-1 and KISS-1R in normal breast epithelium was observed (arrows). Stronger staining of the cytoplasm of tumor cells in invasive moderately differentiated ductal carcinomas and low-differentiated ductal carcinoma (asterisk).

Discussion

The class of proteins known as metastasis suppressors can prevent metastasis without affecting the growth of primary tumour and has recently attracted much attention as it may provide useful mechanistic insight for the development of targeted-therapeutic strategies including drug induced restoration of metastasis suppressor genes and emerged pathways. The kiss-1 gene was initially identified as a candidate metastasis suppressor in 1996, when it was found that its expression was differentially up-regulated in C8161 melanoma cells that were rendered non-metastatic by microcell-mediated transfer of an intact copy of the human chromosome. However, even though the *kiss-1* gene has been identified as a strong suppressor of metastasis in a variety of cancers, limited and conflicting data have been subjected to the intertwined relationship between KISS-1 system and breast cancer, and its biological role in that particular cancer remains to be elucidated [11, 21, 20]. Reports on the expression of KISS-1 and KISS-1R in different types of tumours are quite controversial. In some studies, KISS-1 expression has been shown to decrease in high-grade tumours, which is associated with increased metastatic potential and unfavourable prognosis. Such relation has been found in gastric adenocarcinoma [11], oesophageal carcinoma [33], ovarian carcinoma [9], etc. Studies on breast cancer, however, have demonstrated the opposite phenomenon. Higher-grade tumours show increased expression of KISS-1 and KISS-1R, which correlates with increased metastatic potential and poor prognosis [35]. Our results show that the expression of KISS-1 and KISS-1R is higher in cancer tissue compared to non-malignant breast tissue. The expression of KISS-1 was also significantly and positively related to the expression of KISS-1R. Our findings are consistent with previous studies conducted by Martin et al. [21] and Marot et al. [20], that have also demonstrated higher expression of KISS-1 is breast cancer compared to normal breast parenchyma. It has been previously shown that ERα plays a key role in controlling KISS-1/KISS-1R signalling. Under physiological conditions, in the presence of ERα, the activation of KISS-1R is associated with growth and remodelling of the gland. Loss of ERα in breast cancer, however, results in increased transcription of KISS-1 and/or KISS-1R. Increased transcription in these cases is not associated with the physiological role of KISS-1 as a metastatic suppressor, but rather, it stimulates invasiveness by EGFR transactivation by KISS-1R. This ligand-independent activation of EGFR further stimulates cellular invasiveness in breast cancer. Furthermore, the transactivation of EGFR by KISS-1R is necessary for the secretion and activation of MMP-9 [35], and the effects of active MMP-9 are associated with stimulation of tumour cell invasion and angiogenesis [34]. Increased KISS-1R signalling in breast cancer has also been associated with induction of EMT, which enables them to assume a mesenchymal phenotype, which includes enhanced migratory capacity, invasiveness, elevated resistance to apoptosis, and greatly increased production of ECM components [4].

Conclusions

In conclusion, present study demonstrated that protein expression of both KISS-1 and KISS-1R was significantly higher in invasive breast cancer compared to normal breast tissue. The lower tumor differentiation was, the higher KISS-1 and KISS-1R expression was observed. These results further support the role of the KISS-1/KISS-1R system in breast cancer biology and might be useful in developing effective therapeutic strategies aimed at modulating the KISS-1/KISS-1R pathway.

References

1. **Aparicio, S. A.** Kisspeptins and GPR54–the new biology of the mammalian GnRH axis. – *Cell. Metab.*, **1**, 2005, 293-296.
2. **Bilban, M., N. Ghaffari-Tabrizi, E. Hintermann, S. Bauer, S. Molzer, C. Zoratti, R. Malli, A. Sharabi, U. Hiden, W. Graier, M. Knofler, F. Andreae, O. Wagner, V. Quaranta, G. Desoye.** Kisspeptin-10, a KiSS-1/metastin-derived decapeptide, is a physiological invasion inhibitor of primary human trophoblasts. – *J. Cell. Sci.*, **117**, 2004, 1319-1328.
3. **Castellano, J. M., V. M. Navarro, R. Fernández-Fernández, R. Nogueiras, S. Tovar, J. Roa, M. J. Vazquez, E. Vigo, F. F. Casanueva, E. Aguilar, L. Pinilla, C. Dieguez, M. Tena-Sempere.** Changes in hypothalamic KiSS-1 system and restoration of pubertal activation of the reproductive axis by kisspeptin in undernutrition. – *Endocrinology*, **146**, 2005, 3917-3925.
4. **Cvetković, D., A. V. Babwah, M. Bhattacharya.** Kisspeptin/KISS1R system in breast cancer. – *Journal of Cancer*, **4(8)**, 2013, 653-661.
5. **Dhillo, W. S., P. Savage, K. G. Murphy, O. B. Chaudhri, M. Patterson, G. M. Nijher, V. M. Foggo, G. S. Dancey, H. Mitchell, M. J. Seckl, M. A. Ghatei, S. R. Bloom.** Plasma kisspeptin is raised in patients with gestational trophoblastic neoplasia and falls during treatment. – *Am. J. Physiol. Endocrinol. Metab.*, **291**, 2006, E878-884.
6. **Dhar, D. K., H. Naora, H. Kubota, R. Maruyama, H. Yoshimura, Y. Tonomoto, M. Tachibana, T. Ono, H. Otani, N. Nagasue.** Downregulation of KiSS-1 expression is responsible for tumor invasion and worse prognosis in gastric carcinoma. – *Int. J. Cancer.*, **111**, 2004, 868-872.
7. **Fidler, I. J.** The pathogenesis of cancer metastasis: the 'seed and soil' hypothesis revisited. – *Nat. Rev. Cancer.*, **3**, 2003; 453-458.
8. **Funes, S., J. A. Hedrick, G. Vassileva, L. Markowitz, S. Abbondanzo, A. Golovko, S. Yang, F.J. Monsma, E.L. Gustafson.** The KiSS-1 receptor GPR54 is essential for the development of the murine reproductive system. – *Biochem. Biophys. Res. Commun.*, **312**, 2003, 1357-1363.
9. **Hata, K., D. K. Dhar, Y. Watanabe, H. Nakai, H. Hoshiai.** Expression of metastin and a G-protein-coupled receptor (AXOR12) in epithelial ovarian cancer. – *Eur. J. Cancer.*, **43**, 2007, 1452-1459.
10. **Horikoshi, Y., H. Matsumoto, Y. Takatsu, T. Ohtaki, C. Kitada, S. Usuki, M. Fujino.** Dramatic elevation of plasma metastin concentrations in human pregnancy: metastin as a novel placenta-derived hormone in humans. – *J. Clin. Endocrinol. Metab.*, **88**, 2003, 914-919.
11. **Ikeguchi, M., Y. Hirooka, N. Kaibara.** Quantitative reverse transcriptase polymerase chain reaction analysis for KiSS-1 and orphan G-protein-coupled receptor (hOT7T175) gene expression in hepatocellular carcinoma. – *J. Cancer. Res. Clin. Oncol.*, **129**, 2003, 531-535.
12. **Ikeguchi, M., K. Yamaguchi, N. Kaibara.** Clinical significance of the loss of KiSS-1 and orphan G-protein-coupled receptor (hOT7T175) gene expression in esophageal squamous cell carcinoma. – *Clin. Cancer. Res.*, **10**, 2004, 1379-1383.
13. **Janneau, J.L., J. Maldonado-Estrada, G. Tachdjian, I. Miran, N. Motte, P. Saulnier, J. C. Sabourin, J. F. Cote, B. Simon, R. Frydman, G. Chaouat, D. Bellet.** Transcriptional expression of genes involved in cell invasion and migration by normal and tumoral trophoblast cells. – *J. Clin. Endocrinol. Metab.*, **87**, 2002, 5336-5339.
14. **Jemal, A., R. Siegel, J. Xu, E. Ward**. Cancer statistics. – *CA Cancer J. Clin.*, **60**, 2010, 277-300.
15. **Jiang, Y., M. Berk, L. S. Singh, H. Tan, L. Yin, C. T. Powell, Y. Xu.** KiSS1 suppresses metastasis in human ovarian cancer via inhibition of protein kinase C alpha. – *Clin. Exp. Metastasis*, **22**, 2005, 369-376.
16. **Lee, J. H., M. E. Miele, D. J. Hicks, K. K. Phillips, J. M. Trent, B. E. Weissman, D. R. Welch**. KiSS-1, a novel human malignant melanoma metastasis-suppressor gene. – *J. Natl. Cancer Inst.*, **88**, 1996, 1731-1737.
17. **Lee, J. H., D. R. Welch.** Suppression of metastasis in human breast carcinoma MDA-MB-435 cells after transfection with the metastasis suppressor gene, KiSS-1. – *Cancer Res.*, **57**, 1997, 2384-2387.
18. **Makri, A., P. Msaouel, C. Petraki, D. Milingos, A. Protopapas, A. Liapi, A. Antsaklis, C. Magkou, M. Koutsilieris.** KISS1/KISS1R expression in eutopic and ectopic endometrium of women suffering from endometriosis. – *In Vivo*, **26**, 2012, 119-127.
19. **Makri, A., N. Pissimissis, P. Lembessis, C. Polychronakos, M. Koutsilieris.** The kisspeptin (KiSS1)/GPR54 system in cancer biology. – *Cancer Treat. Rev.*, **34**, 2008, 682-692.

20. **Marot, D., I. Bieche, C. Aumas, S. Esselin, C. Bouquet, S. Vacher, G. Lazennec, M. Perricaudet, F. Kuttenn, R. Lidereau, N. de Roux.** High tumoral levels of Kiss1 and G-protein-coupled receptor 54 expression are correlated with poor prognosis of estrogen receptor-positive breast tumors. – *Endocr. Relat. Cancer.*, **14**, 2007, 691-702.
21. **Martin, T. A., G. Watkins, W. G. Jiang.** KiSS-1 expression in human breast cancer. – *Clin. Exp. Metastasis*, **22**, 2005; 503-511.
22. **Muir, A. I., L. Chamberlain, N. A. Elshourbagy, D. Michalovich, D. J. Moore, A. Calamari, P. G. Szekeres, H. M. Sarau, J. K. Chambers, P. Murdock, K. Steplewski, U. Shabon, J. E. Miller, S. E. Middleton, J. G. Darker, C. G. Larminie, S. Wilson, D. J. Bergsma, P. Emson, R. Faull, K. L. Philpott, D. C. Harrison.** AXOR12, a novel human G protein-coupled receptor, activated by the peptide KiSS-1. – *J. Biol. Chem.*, **276**, 2001, 28969-28975.
23. **Nagai, K., R. Doi, F. Katagiri, T. Ito, A. Kida, M. Koizumi, T. Masui, Y. Kawaguchi, K. Tomita, S. Oishi, N. Fujii, S. Uemoto**. Prognostic value of metastin expression in human pancreatic cancer. – *J. Exp. Clin. Cancer Res.*, **28**, 2009, 9.
24. **Ohta, S., E. W. Lai, A. L. Pang, F. M. Brouwers, W. Y. Chan, G. Eisenhofer, R. de Krijger, L. Ksinantova, J. Breza, P. Blazicek, R. Kvetnansky, R. A. Wesley, K. Pacak.** Downregulation of metastasis suppressor genes in malignant pheochromocytoma. – *Int. J. Cancer.*, **114**, 2005, 139-143.
25. **Ohtaki, T, Y. Shintani, S. Honda, H. Matsumoto, A. Hori, K. Kanehashi, Y. Terao, S. Kumano, Y. Takatsu, Y. Masuda, Y. Ishibashi, T. Watanabe, M. Asada, T. Yamada, M. Suenaga, C. Kitada, S. Usuki, T. Kurokawa, H. Onda, O. Nishimura, M. Fujino.** Metastasis suppressor gene KiSS-1 encodes peptide ligand of a G-protein-coupled receptor. – *Nature*, **411**, 2001, 613-617.
26. **Qiao, C., D. L. Cheng, S. L. Zhang, C. H. Wang, Q. D. Lin.** The role of KiSS-1 and matrix metalloproteinase-9 in regulation of invasion of trophoblasts. – *Zhonghua Yi Xue Za Zhi*., **85**, 2005, 839-842.
27. **Ringel, M. D., E. Hardy, V. J. Bernet, H. B. Burch, F. Schuppert, K. D. Burman, M. Saji.** Metastin receptor is overexpressed in papillary thyroid cancer and activates MAP kinase in thyroid cancer cells. – *J. Clin. Endocrinol. Metab*., **87(5)**, 2002, 2399-2402.
28. **Sam, A. H.,. W.S. Dhillo.** Kisspeptin: a critical regulator of puberty and reproductive function. – *Curr. Drug Targets*, **11**, 2010, 971-977.
29. **Sanchez-Carbayo, M., P. Capodieci, C. Cordon-Cardo.** Tumor suppressor role of KiSS-1 in bladder cancer loss of KiSS-1 expression is associated with bladder cancer progression and clinical outcome. – *Am. J. Pathol.*, **162**. 2003, 609-617.
30. **Stark, A. M., K. Tongers, N. Maass, H. M. Mehdorn, J. Held-Feindt**. Reduced metastasis-suppressor gene mRNA-expression in breast cancer brain metastases. – *J. Cancer Res. Clin. Oncol.*, **131**, 2005, 191-198.
31. **Shirasaki, F., M. Takata, N. Hatta, K. Takehara.** Loss of expression of the metastasis suppressor gene KiSS1 during melanoma progression and its association with LOH of chromosome 6q16.3-q23. – *Cancer Res.*, **61**, 2001, 7422-7425.
32. **Wang, H., J. Jones, T. Turner, Q. P. He, S. Hardy, W. E. Grizzle, D. R. Welch, C. Yates**. Clinical and biological significance of KISS1 expression in prostate cancer. – *Am. J. Pathol.*, **180**, 1170-1178.
33. **Yao, H. L, Z. L. Yang, Y. G. Li, G. W. Liu.** In situ hybridization study on the expression of Kiss-1 and KAI-1 metastasis suppressor genes in gastric cancer. – *Zhonghua Wei Chang Wai Ke Za Zhi*, **10**, 2007, 274–7.
34. **Yu, Q, I. Stamenkovic.** Cell surface-localized matrix metalloproteinase-9 proteolytically activates TGF-β and promotes tumor invasion and angiogenesis. – *Genes Dev.*, **14**, 2000, 163–176.
35. **Zajac, M., J. Law, D. D. Cvetkovic, M. Pampillo, L. McColl, C. Pape, G. M. Di Guglielmo, L. M. Postovit, A. V. Babwah, M. Bhattacharya.** GPR54 (KISS1R) transactivates EGFR to promote breast cancer cell invasiveness. – *PLoS One*, **6**, 2011, e21599.

Institute of Experimental Morphology, Pathology and Anthropology with Museum
Bulgarian Anatomical Society

Acta morphologica et anthropologica, 25 (3-4)
Sofia ● 2018

Cell Cultures as Reliable Models in Experimental-Oncopharmacology

Radostina Alexandrova[1], Tanya Zhivkova[1], Lora Dyakova[2], Milena Glavcheva[1]*

[1] Institute of Experimental Morphology, Pathology and Anthropology with Museum, Bulgarian Academy of Sciences, Sofia, Bulgaria
[2] Institute of Neurobiology, Bulgarian Academy of Sciences, Sofia, Bulgaria

* Corresponding author e-mail: rialexandrova@hotmail.com

The aim of our study was to summarize the role of various cancer cell cultures (human, rat, chicken; established from different types of cancer; monolayer cell cultures and 3D cancer cell colonies; primary cell cultures and permanent cell lines, tumor and non-tumor cells) used in our investigations for the evaluation of cytotoxic / antitumor activity of compounds (a total of 24 compounds) with different chemical structures and chemical / physicochemical characteristics – ammonium vanadate (NH_4VO_3) and as well as ionophore antibiotics (monensin), non-steroidal anti-inflammatory drugs (NSAIDs, meloxicam), cholic acids (ursodeoxycholic acid, UDCA), Mannich bases (BAMP = N,N'-bis(4-antipyrylmethyl)-piperazine; TAMEN = N,N'-tetra-(antipyryl-1-methyl)-1,2-diaminoethane) and their metal complexes. The advantages and disadvantages of cell cultures used as model systems in the experiments as well as strategies to meet the challenges of such *in vitro* models are presented.

Key words: cell cultures, model systems, cancer, cytotoxicity, experimental oncopharmacology

Introduction

Cell cultures have successfully served as experimental models for investigations in the fields of experimental oncology and oncopharmacology for many years and have contributed to our understanding of tumor biology and mechanisms of cancerogenesis as well as to the introduction of diagnostic, prophylactic and treatment strategies in clinical practice [6, 11, 13]. There are different types of cell cultures, including primary cell cultures (PCC) and permanent cell lines (PCL); tumor and non-tumor cell cultures; suspension, monolayer (2D) and 3D cell cultures; cell cultures established from different organisms and from different histological types of tumors, etc. Each cell culture has its unique biological properties. Knowing the advantages and disadvantages of individual cell lines will facilitate the choice of the most appropriate model systems for certain scientific purposes and will help us to improve their predictive capacity for cancer drug development / discovery. The aim of the present study was to summarize the potential role of various cell cultures used by our group for the evaluation of cytotoxic / antitumor activity of compounds with different chemical structures and chemical / physico-chemical characteristics.

Materials and Methods

The cytotoxic activity of 24 compounds was evaluated using a wide range of cancer cell lines: i) chicken - LSCC-SF-Mc29 (hepatoma), ii) rat - LSR-SF-SR (sarcoma) and iii) human – A549 (non-small cell lung cancer), MCF-7 (luminal A type breast cancer), SK-BR-2 (Her-2 positive breast cancer), Caco-2 (colorectal cancer), HeLa (carcinoma of the uterine cervix); HepG2 (liver cancer), 8MGBA (glioblastoma multiforme), A431 (squamous cell carcinoma) and its multidrug resistant clones A431-MDR1, A431-MRP1 and A431-ABCG2. Non-tumor human (embryonal Lep-3 and MRC-5) as well as bovine (MDBK - Madin Darby bovine kidney cells) cell lines were also included in the experiments. The compounds tested for cytotoxic activity as well as cell cultures used as model systems are presented in Table 1.

The cells were grown as monolayer (2D) cultures in Dulbecco's modified Eagle's medium (D-MEM) supplemented with 5-10% fetal bovine serum and antibiotics (100 U/ml penicillin and 100 µg/ml streptomycin) or as 3D cancer cell colonies in a mixture of 2X DMEM medium and 0.9% agar (1 : 1, vol. : vol.). The investigations were performed by short-term (24-72h) experiments with monolayer cell cultures and methods with different molecular targets and mechanisms of action (MTT test, neutral red uptake assay, crystal violet staining, trypan blue dye exclusion technique, double staining with acridine orange and propidium iodide) and long-term experiments (14-30 days) with 3D colony-forming method as it was earlier described [1, 4].

Results and Discussion

The cytotoxic activity of 24 compounds with different chemical structures and chemical / physicochemical properties was evaluated in our investigations using a wide range of cancer permanent cell lines (**Table 1**): human, rat, chicken; cultures established from different types of cancer; grown as 2D- or 3D- cell cultures; sensitive and multidrug resistant cancer cells. The examined compounds were found to reduce to varying degrees the viability and proliferation of the treated cells, each cell culture expressed different rate of sensitivity to the cytotoxic effect of each individual compound. Examples of hierarchical orders based on the chemosensitivity of the model cell lines are presented in **Table 2**. The results / experience obtained by us can be summarized as follows:

i) Chicken hepatoma and rat sarcoma cells

LSCC-SF-Mc29 chicken hepatoma and LSR-SF-SR rat sarcoma cells were found to be highly sensitive to the cytotoxic activity of the compounds examined. Both cell lines (LSCC-SF-Mc29 and LSR-SF-SR) are valuable model systems for the search of new anticancer agents because of at least five reasons: i) they are easily grown as 2D cell cultures and 3D cancer cell colonies; ii) implanted subcutaneously in immunocompetent chickens or rats, respectively, the cells induce tumor development and are useful for *in vivo* investigations in the fields of experimental oncopharmacology and tumor immunology; iii) these cells contain / express *v-myc* (LSCC-SF-Mc29) or *v-src* (LSR-SF-SR) oncogene. The cellular analogues of these genes are known to be involved (when their expression and/or activity is / are not properly regulated) in the pathogenesis of a wide range of cancers in humans and animals. Myc and Src genes and their products are attractive targets for the development of innovative new anticancer strategies [7, 12]; iv) the high sensitivity of chicken hepatoma and rat sarcoma cells makes them suitable models for primary screening for new anticancer agents; v) while a large number of mammalian (for example human, mouse) cell lines are known, the amount of the available avian permanent cell lines is quite limited. The relatively low

Table 1. Compounds tested and cell cultures used as model systems for the evaluation of their cytotoxic activity

	Compound(s)	Number of the compounds tested	Cell cultures used as experimental models
1.	Meloxicam (Mel) and its Zn(II), Cu(II), Co(II) and Ni(II) complexes	5	LSCC-SF-Mc29; LSR-SF-SR, HeLa, 8MGBA
2.	Monensin and its Mg(II), Ca(II), Mn(II), Co(II), Ni(II) and Zn(II) complexes	7	LSCC-SF-Mc29; LSR-SF-SR, MCF-7, HeLa, A549, HepG2, 8MGBA, A431 and its multidrug resistant clones A431-MDR1, A431-MRP1 and A431-ABCG2, Lep-3
3.	Ursodeoxycholic acid (UDCA) and its Zn(II), Cu(II) and Ni(II) complexes	4	LSCC-SF-Mc29; LSR-SF-SR, MCF-7, HeLa, A549, HepG2, Lep-3
4.	Complexes of Ni(II) with Mannich type ligands BAMP or TAMEN	6	LSCC-SF-Mc29; LSR-SF-SR, MCF-7, SK-BR-3, Caco-2, HepG2, 8MGBA
5.	Mixed ligand Cu(II) complex Cu_2BAMPdipyCl_4	1	LSCC-SF-Mc29; LSR-SF-SR, A431, A431-MDR, A431-MRP, A431-ABCG2
6.	Ammonium vanadate (NH_4VO_3)	1	LSCC-SF-Mc29; LSR-SF-SR, MCF-7, HeLa, HepG2, Lep-3, MRC-5, MDBK
Total		24 compounds	13 cell cultures – 10 tumor and 3 non-tumor

BAMP = N,N'-bis(4-antipyrylmethyl)-piperazine; TAMEN = N,N'-tetra-(antipyryl-1-methyl)-1,2-diaminoethane; dipy = 2,2 bipyridyl

amount of commercially available monoclonal antibodies against avian and rat antigens limits to some extent the possible applications of these cell lines in laboratory practice.

ii) Human cervical carcinoma cells

HeLa was the first human cell line established in culture [5]. HeLa cells are well studied and used for many decades all over the world as a model system to carry out a wide range of investigations [13]. It is worth to be mentioned here that two Nobel prizes for physiology or medicine have been awarded for discoveries achieved by the "help" of HeLa cells: the link between human papilloma virus (HPV) and cervical cancer (2008, Harald zur Hausen) and the role of telomeres and the enzyme telomerase in preventing the ends of chromosomes from degradation (2009, Elizabeth Blackburn, Carol Greider, and Jack Szostak). HeLa cells are particularly suitable in the search for new diagnostic, prognostic and therapeutical approaches for human cervical cancer. The results obtained by us reveal that these cells exhibit moderate sensitivity to the cytotoxic effect of the compounds investigated as compared to the other human cancer cells and are more resistant than rat sarcoma and especially chicken hepatoma cells (**Table 2**). The HeLa cells contain human papilloma virus type 18 (HPV – 18) [3, 10]. It will be interesting to evaluate comparatively the influence of one and the same agent on the viability and proliferation of human cervical carcinoma cells containing different high-risk oncogenic (e.g. HPV-16, HPV-18) and low-risk oncogenic (e.g. HPV-6, HPV-11) types HPV.

iii) Human breast cancer cell lines

MCF-7 and SK-BR-3 cell lines were established from different subtypes of human breast cancer: luminal type A (MCF-7) and HER-2 positive (SK-BR-3) breast cancer.

Table. 2. Hierarchic orders of cell lines according to their sensitivity to the cytotoxic effect of compounds examined

Compound	Method	Treatment period, h	Hierarchic order
$Ni_2B(CH_3COO)_4$	MTT	72	MCF-7 (57.2)* > HepG2 (81.8) > 8MGBA (100.8) > Caco2)172.3) > SKBR-3 (2016.1)
Ni_2BCl_4	MTT	72	MCF-7 (94) > HepG2 (149.5) > 8MGBA (221.6) > Caco-2 (238.8) > SKBR-3 (268.3)
Cu-Mel	MTT	72	LSCC-SF-Mc29 (32) > LSR-SF-SR (53) > 8MGBA (304) > HeLa (306)
Co-Mel	MTT	72	LSCC-SF-Mc29 (42) > LSR-SF-SR (45) > 8MGBA (313) > HeLa (429)
Zn-UDCA	MTT	72	LSCC-SF-Mc29 (68) > LSR-SF-SR (102) > HepG2 (143) > HeLa (149) > A549 (161) > Lep3 (>200)
Cu-UDCA	MTT	72	LSR-SF-SR (<50) > LSCC-SF-Mc29 (37) > HepG2 (159) > A549 (169) > 8MGBA (>200) = HeLa (>200) = Lep3 (>200)
NH_4VO_3	MTT	72	LSR-SF-SR (1.0) > MRC-5 (1.0) > LSCC-SF-Mc29 (1.5) > HepG2 (2.1) > HeLa (7.0) > MCF-7 (7.7) > Lep3 (8.0)
	NR	72	LSCC-SF-Mc29 (1.4) > LSR-SF-SR (2.0) > HepG2 (3.8) > HeLa (4.4) > MRC-5 (7.8) > MCF-7 (8.4)

* – Cytotoxic concentration 50 (CC_{50}, μM) that reduce the percent of viable cells by 50% as compared to the non-treated control; All hierarchic orders start with the most sensitive cell line (with the lowest CC_{50} value of the compound); MTT – thiazolyl blue tetrazolium bromide test; NR – neutral red uptake cytotoxicity assay; B = BAMP = N,N'-bis(4-antipyrylmethyl)-piperazine.

The experimental data obtained showed that SK-BR-3 cells were less sensitive to the cytotoxic activity of Ni(II) complexes with BAMP ($Ni_2(BAMP)(CH_3COO)_4$ and $Ni_2(BAMP)(Cl)_4$) as compared to MCF-7 cells (Table 2). In addition, MDA-MB-231 (triple negative breast cancer, TNBC) cell line was more resistant to the cytotoxic activity of Zn(II)/Au(I) and Zn(II)/Ag(I) complexes with Schiff bases (Salen, Salampy and Saldmen) than MCF-7 cells [14]. The observed difference in sensitivity of these cells can be explained at least partially by tumor heterogeneity phenomenon [2] that makes each tumor / tumor cell line a unique biological system. At the same time, luminal A type breast cancer has a more favorable prognosis as compared to Her-2 positive and triple negative breast cancer. Investigations performed with cell lines established from different breast cancer cell types will allow better understanding of breast cancer biology and behavior and will facilitate the identification of new treatment strategies, especially for TNBC for which currently there is no targeted / specific treatment available.

iv) Multidrug resistant cancer cells

The cell line A431 (human squamous cell carcinoma) and its clones expressing mdr1 (A431-MDR1), mrp1 (A431-MRP1) or abcg2 (A431-ABCG2) gene were also included in our studies. It was found that mixed ligand complex $Cu_2BAMPdipyCl_4$ as well as monensin and its metal complexes decrease significantly viability and proliferation of both – sensitive parental A431 cell line and resistant cell clones. Drug resistant cancer cell lines can be established by genetic manipulation; continuous culturing in the presence of gradually increasing concentrations of particular anticancer agent(s) (starting by non-toxic concentration); cultivating the primary cell culture derived from tumor tissue in medium containing high concentration of antitumor agent/s. The last

two technical approaches represent the well known situations in clinical practice where oncology patients can develop drug resistance during the prolonged course of cancer treatment (acquired drug resistance) or demonstrated drug resistance from the very beginning of chemotherapy (pre-existing, intrinsic drug resistance) [9]. Drug resistance is among the main obstacles preventing successful managing of cancer diseases. (Multi) drug resistant cancer cell lines are absolutely necessary for better understanding of this phenomenon as well as for the discovery of sensitizing agents and effective treatment strategies.

v) 2D- and 3D- cell cultures

Monolayer (2D) cell cultures were used in our investigations to evaluate the "quick" cytotoxic effect of the compounds tested (in short-term experiments lasting usually 24-72h) by MTT, NR, CV, TB and AO/PI assays. In order to examine the 'duration" of the cytotoxic effect we carried out CFM based on the natural ability of cancer cells for anchorage-independent 3D growth in semi-solid medium. These long-term experiments last 2-4 weeks and provide more adequate information about cytotoxic activity of the compounds tested. Conventional monolayer cell cultures are easier to maintain, suitable for routine culturing, well studied and allow application of wide range cytotoxicity assays. 3D-cell cultures are more "realistic" model systems and represent better tumor / tumor cell biology and behavior.

vi) Primary cultures

Permanent cell lines were proved to be suitable tools for the needs of biomedicine and biotechnology. They have many advantages as model systems in experimental oncopharmacology such as adaptation for propagation in laboratory conditions, accessibility and availability, their biological features are well characterized, etc. On the other hand, a large number of *in vitro* passages of PCL can result in significant genetic and epigenetic changes that do not exist in the tissue of origin. Even one and the same PCL cultured in different laboratories / conditions may show some different characteristics. That is why primary cell cultures are more "close" to the initial tissue. PCC can be useful in the search for new anticancer agents and for the needs of personalized medicine. From practical point of view the establishment of PCC meets some challenges such as the presence of unwanted stromal fibroblasts, possible microbial contamination (for example in the case of gastric or colorectal cancer), short life, etc.

vii) Non-tumor cell cultures

Non-tumor permanent cell lines were included for comparative purposes in our investigations. The results obtained reveal that these non-tumor cells are usually also highly sensitive to the cytotoxic activity of the compounds examined. This is not surprising because the non-tumor PCL are usually established from embryonal tissues – it is well known that tumor and embryonal cells share some common characteristics including high proliferative activity, expression of some antigens. In addition, embryonal cells are highly sensitive to the influence of the chemical agents in their microenvironment whereas cancer cells have been selected during tumor progression to become more and more aggressive and well adapted [2]. In our opinion, PCC obtained from transplantable tumors in laboratory animals and healthy cells from the same tumor-bearing animals (lymphocytes, macrophages, bone marrow cells, etc) are suitable model systems in the field of experimental oncology representing the situation of patients under cancer chemotherapy. Special attention deserve bone marrow, liver, kidney and heart cells (tissues that are frequently attacked during cancer chemotherapy), but the establishment of such PCC is challenging and can be with low success.

Conclusion

Cell cultures are suitable model systems in the search for new agents with promising antitumor properties and identification of their molecular target(s) and mechanism(s) of action. Each cell line has its own individual features and advantages providing specific benefits for the implementation of various biomedical studies. The improvement of cell culture systems (especially 3D cell cultures, co-cultures) will increase significantly their predictive value and facilitate the translation of "*in vitro*" experimental data into results of importance to clinical practice.

Acknowledgements: The work was supported by the National Science Fund, Bulgarian Ministry of Education and Science, Grant № Б 02 30/12.12.2014 and Operational Programme "Science and Education for Smart Growth" 2014-2020, co-financed by the European Union through the European Structural and Investment Funds, Grant BG05M2OP001-2.009-0019-C01 from 02.06.2017.

References

1. **Alexandrova, R., A. Vachevs, M. Kirilova, G. Miloshev, E.-M. Mosoarca, R. Tudose, O. Costisor.** Investigations on cytotoxic and antiproliferative effects in vitro of a newly synthesized mixed ligand copper (II) complex. – *Acta Morphol. Anthropol.*, **12**, 2007, 72-78.
2. **Alexandrova, R.** Tumour heterogeneity. – *Exp. Pathol. Parasitol.*, **4**(6), 2001, 57-67.
3. **Boshart, M., L. Gissmann, H. Ikenberg, A. Kleinheinz, W. Scheurlen, H. zur Hausen**. A new type of papillomavirus DNA, its presence in genital cancer biopsies and in cell lines derived from cervical cancer. – *EMBO J.*, **3**(5), 1984, 1151-1157.
4. **Dyakova, L., D.-C. Culita, G. Marinescu, M. Alexandrov, R. Kalfin, L. Patron, R. Alexandrova.** Metal (ZnII, CuII, NiII) complexes of ursodeoxycholic acid as putative anticancer agent. – *B. & BE.*, **28**(3), 2014, 543-551.
5. **Gey, G. O., W. D. Coffman, M. T. Kubicek**. Tissue culture studies of the proliferative capacity of cervical carcinoma and normal epithelium. – *Cancer Res.*, **12**, 1952, 264–265.
6. **Goodspeed, A., L. M. Heiser, J. W. Gray, J. C. Costello.** Tumor-derived cell lines as molecular models of cancer pharmacogenomics. – *Mol. Cancer Res.*, **14**(1), 2016, 3-13.
7. **Kumar, A., A. S. Jaggi, N. Singh.** Pharmacology of Src family kinases and therapeutic implications of their modulators. – *Fundam. Clin. Pharmacol.*, **29**(2), 2015, 115-130.
8. **Landry, J. J., P. T. Pyl, T. Rausch, T. Zichner, M. M. Tekkedil, A. M. Stütz, A. Jauch, R. S. Aiyar, G. Pau, N. Delhomme, J. Gagneur, J. O. Korbel, W. Huber, L. M. Steinmetz**. The genomic and transcriptomic landscape of a HeLa cell line. – *G3 (Bethesda)*, **3**(8), 2013, 1213-1224.
9. **Lippert, T. H., H. J. Ruoff, M. Volm**. Intrinsic and acquired drug resistance in malignant tumors. The main reason for therapeutic failure. – *Arzneimittelforschung*, **58**(6), 2008, 261-264.
10. **Porass, C., C. Bennett, M. Safaeian, S. Coseo, A. C. Rodriguez, P. Gonzaález, M. Hutchinson, S. Jimenez, M. E. Sherman, S. Wacholder, D. Solomon, V. Doorn Leen-Jan, C. Bougelet, W. Quint, M. Schiffman, R. Herrero, A. Hildeshein**. Determinants of seropositivity among HPV16/18DNA positive young women. – *BMC Infect. Dis.*, **10**, 2010, 238.
11. **Sharma, S.V., D. A. Haber, J. Settleman**. Cell line-based platforms to evaluate the therapeutic efficacy of candidate anticancer agents. – *Nat. Rev. Cancer*, **10**(4), 2010, 241-253.
12. **Stine, Z. E., Z. E. Walton, B. J. Altman, A. L. Hsieh, C.V. Dang.** MYC,Metabolism, and Cancer. – *Cancer Discov.*, **5**(10), 2015, 1024-1039.
13. **Wilding, J. L., W. F. Bodmer**. Cancer cell lines for drug discovery and development. – *Cancer Res.*, **74**(9), 2014, 2377-2384.
14. **Zhivkova, T.** Influence of metal complexes with different ligands on viability and proliferation of tumor cells. *PhD thesis*, 2018, Sofia, Bulgaria [in Bulgarian]

Institute of Experimental Morphology, Pathology and Anthropology with Museum
Bulgarian Anatomical Society

Acta morphologica et anthropologica, 25 (3-4)
Sofia ● 2018

Experimental Approach as Research Strategy for Cytocompatibility Assessment of New Materials for Bone Implants

Boyka Andonova-Lilova[1], Tanya Zhivkova[1], Lora Dyakova[2], Abedulkadir Abudalleh[1], Diana Rabadzieva[3], Stefka Tepavitcharova[3], Nabanita Saha[4], Virginija Jankauskaitė[5], Radostina Alexandrova[1]*

[1] Institute of Experimental Morphology, Pathology and Anthropology with Museum, Bulgarian Academy of Sciences, Sofia, Bulgaria
[2] Institute of Neurobiology, Bulgarian Academy of Sciences, Sofia, Bulgaria,
[3] Institute of General and Inorganic Chemistry, Bulgarian Academy of Sciences, Sofia, Bulgaria
[4] Centre of Polymer Systems, University Institute, Tomas Bata University in Zlin, Czech Republic
[5] Kaunas University of Technology, Kaunas, Lithuania

***** Corresponding author e-mail: rialexandrova@hotmail.com

The study presents experimental design (direct and indirect experiments, assays, cell cultures) used by our group for the initial cytocompatibility assessment of new materials for bone implants. Some advantages and drawbacks of cell cultures (primary cultures and permanent cell lines; non-tumor and tumor cells) applied as model systems in the investigations are also discussed.

Key words: bone disease, bone implants, cytocompatibility, cell cultures

Introduction

The global incidence of bone diseases and conditions is rising steadily and is expected to double by 2020. The most affected are people over the age of 50 with reduced physical activity and obesity. The treatment of bone and joint degenerative and inflammatory processes, fractures, spinal pain, osteoporosis, scoliosis and other musculoskeletal problems requires the use of permanent, temporary or biodegradable materials/devices [4]. Suitable model systems and experimental strategies are needed for biocompatibility assessment of new materials for bone implants and estimation of their osteoinductive and osteoconductive properties [2, 9].

The aim of this study was to present the advantages and challenges of experimental strategies used by our group for cytocompatibility assessment of new materials for bone implants.

Materials and Methods

The cytocompatibility of 25 materials for bone implants from three different groups was investigated in our study: i) di- and tricalcium phosphate fine powders; ii) composite materials (Zn(13)-b-$Ca_3(PO)_4$ and hydrogels prepared from gelatin, xanthan gum and carrageenan; iii) cements. The cell cultures used as model systems are presented in **Table 1**.

Table 1. Cell cultures used as model systems in our investigations

Origin	Type (PCL / PCC; T /NT)	Established from (Name)
Rat	PCC, NT	Bone morrow
Mouse	PCC, NT	Bone marrow
	PCC, NT	Bone explants
	PCL, NT	Embryonal fibroblasts (BALB/c 3T3)
Bovine	PCL, NT	Kidney (MDBK)
Human	PCL, NT	LEP-3, MRC-5 – embryonic fibroblasts
	PCL, T	Osteosarcoma (Saos-2)
	PCL, T	Carcinoma of the uterine cervix (HeLa)
	PCL, T	Breast cancer (MCF-7)

PCL = permanent cell line; PCC = primary cell culture; T = tumor; NT = non-tumor

Primary cell cultures (PCC) were established as described earlier [5, 6]. Permanent cell lines (PCL) were obtained from the Cell Culture Collection of the Institute of Experimental Morphology, Pathology and Anthropology with Museum – Bulgarian Academy of Sciences. The cells were grown in Dulbecco's modified Eagle's medium (D-MEM) medium supplemented with 5-10% fetal bovine serum (FBS), 100 U/mL penicillin and 100 μg/mL streptomycin and kept in a humidified incubator (Thermo Scientific, HEPA Class 100) at 37°C under 5% CO_2 in air. For routine passages the monolayer cell cultures were detached using a mixture of 0.05% trypsin and 0.02 % EDTA.

The effect of the compounds on cell viability and proliferation was studied in direct (the cells were seeded on the material) and indirect (the cells were grown in culture medium in which the material was pre-incubated) experiments using one or more of the following cytotoxicity assays - thiazolyl blue tetrazolium bromide (MTT) test, neutral red uptake assay, crystal violet staining (CVS), trypan blue dye exclusion technique (TBT). Double staining with acridine orange & propidium iodide (AO/PI) and/or hematoxylin & eosin (HE), single cell gel electrophoresis (Comet assay), light/fluorescent microscopy and scanned electron microscopy (SEM) were also performed [5, 6, 7].

Results and Discussion

The investigations were performed by:

Indirect experiments (IDE) – the "material extracts" were prepared by incubating the materials in culture medium (D-MEM) for various periods of time (for example 1h, 4h, 8h, 24h, 3 days, 6 days, 10 days). The parent "extracts" (100%) were then diluted in D-MEM to obtain a series of dilutions with concentrations of 75%, 50%, 25%, 10% and 1% which were

used further for cell viability/proliferation tests. IDE can be carried out by a wide range of cytotoxicity assay, cytological, (immuno) cytochemical and other methods.

Direct experiments (DE) – the cells were cultivated directly on the material's surface. DE provide valuable information about the interactions between the material and the cells, including the ability of the material to allow and support cell viability, adhesion, proliferation and differentiation. However, the application of some cytotoxicity assays in this approach may require additional modification depending on the physicochemical properties of the material examined.

Various cell cultures were used as model systems for cytocompatibility assessment of the materials. Our decision to include bone marrow cells (BMCs) in the experiments was not occasional because of at least three reasons: 1) the possible contact of BMCs with the material in the body; ii) BMCs are characterized by low or absent expression of P-glycoprotein which makes them extremely sensitive to the toxic effects of xenobiotics; iii) BMCs are mixture of various stem / progenitor cells including mesenchymal stem cells (MSCs) that are suitable for application in bone tissue engineering [1, 3, 13].

Primary cultures from bone explants of laboratory animals are attractive model systems because represent at least partially the regenerative process of damaged bone in laboratory conditions.

MCF-7 and HeLa cells were used in our investigations because they are established from two of the most common cancers in women – breast cancer and carcinoma of the uterine cervix. Both cancers are known to induce bone metastasis that may cause major morbidity including fractures [8, 11]. In addition, endocrine treatment of hormone-dependent breast cancer increases the risk for osteoporosis and fractures [10]. That is why data on the potential effect of bone substitutes on the proliferation of cancer cells are needed.

Some advantages and drawbacks of cell cultures used as model systems in our experiments are presented in **Table 2.**

One of the most important questions is what kind of cell cultures to be used as model systems in biocompatibility asssessment of new materials for bone implants. On one hand, osteoblasts, that are known to produce calcified bone matrix and contribute to bone formation and remodeling [14] as well as their progenitors seem to be the most appropriate model systems for this purpose. On the hand, human body is a highly coordinated complex system, where different organs/tissues have overlapped and interconnected functions. One can suggest that the local bone implant will more or less interact with the whole organism (through body fluids that "wash" the material, by switching on or off various signaling pathways).

In this relation various cell cultures must be taken into account when examining the potential cytotoxicity of bone implants including liver and kidney cells. The challenge is that we need information coming from normal cells. Most of the available human kidney and liver cell lines were obtained from cancer tissues and as a result exhibit different biology/behavior as compared to normal cells. Even permanent cell lines established from healthy liver or kidney can possess genetic/epigenetic alterations obtained during prolonged cultivation in laboratory conditions. Most of the available non-tumor kidney and liver PCL are of non-human origin.

Theoretically, a better option to solve this problem is to use primary cultures from healthy tissues. In reality, there is some difficulty in doing this at least because healthy human tissue is not easily accessible and the establishment of primary cell cultures has a low successful rate.

Primary cell cultures obtained from the same type "starting material" and following the same protocol can differ in some of their characteristics.

The mesencymal stem cells (MSCs) are among the most appropriate model systems for biocompatibility assessment of new materials for bone implants and bone tissue

Table 2. Advantages and drawbacks of cell cultures used as model systems for cytocompatibility assessment of new materials for bone implants

Cell culture	Advantages	Drawbacks
Fibroblasts	Important for bone tissue growth and regeneration Well known and readily accessible permanent cell lines are available	Terminally differentiated cells (their conversion into functional osteoblasts for the needs of bone tissue engineering may require special strategies)
Bone marrow cells	(Possible) contact with material in the body The stem/progenitor nature of these cells	Heterogeneous population The cells grow (with some exceptions such as MSCs) in suspension that requires adequate cytotoxicity assays (For example MTS test instead of MTT test)
Primary cultures from animal (rat, mouse) bone explants	*In vitr*o model of an *in vivo* bone regeneration	Heterogeneous population? Each cell culture has its individual own characteristics (low repeatability) The type/nature of the cells has to be determined
Osteosarcoma cells	Their (osteoblast/osteocyte) origin	The biology and behavior of cancer cells differ from those of normal osteoblasts/osteocytes.

engineering. The main advantages of MSCs include their high ability to proliferate, self-renew and differentiate into osteoblasts and chondroblasts; the possibility to be isolated from various embryonic and adult tissues; immunomodulating properties and the lack of teratogenic potential.

Co-cultures, including fibroblasts, endothelial cells and osteoblasts can be helpful for the evaluation of bone implant materials [13].

In conclusion, the successful development of improved new biomaterials for bone implants requires adequate experimental strategies and cell culture models to test their biocompatibility, osteoinductive and osteoconductive properties and to provide valuable predictive information.

Acknowledgement: This study was supported by Operational Programme "Science and Education for Smart Growth" 2014-2020, co-financed by the European Union through the European Structural and Investment Funds, Grant BG05M2OP001-2.009-0019-C01 from 02.06.2017; National Science Fund, Ministry of Education and Science, Bulgaria (Grants № DFNI T 02-5 and № DFNI Б 02 30 from 12.12.2014) and a bilateral project between Bulgarian Academy of Sciences (IEMPAM) and Kaunas University of Technology, Lithuania.

References

1. **Alexandrova, R.** Multidrug resistance and P-glycoprotein. Minireview. – *Exp. Pathol. Parasitol.*, **1**, 1998, 62-66.
2. **Alexandrova, R., A. Abudalleh, T. Zhivkova, L. Dyakova, B. Andonova-Lilova, O. Alexandrov, N. Saha**. Briefly about bone defects and new strategies to treat them. – *Acta Morphol. Anthropol.,* **22**, 2015, 142-149.
3. **Alexandrova, R., T. Zhivkova, L. Dyakova, B. Andonova-Lilova, D. Dinev, A. Abudalleh, N. Saha, V. Jankauskaitė, O. Alexandrov**. Briefly about mesenchymal stem cells - one of the main players in bone tissue engineering. – *Adv. Cytol. Pathol*., **3**(1), 2018, 15–18.
4. **Amini, A. R., Laurencin, C. T., Nukavarapu, S. P.** Bone Tissue engineering: recent advances and challenges. – *Crit. Rev. Biomed. Eng*., **40**(5), 2012, 363–408.
5. **Andonova-Lilova, B., R. Alexandrova, D. Rabadjieva, S. Tepavitcharova**. Application of cultured murine cells for initial evaluation of the biocompatability of Mg and Zn-modified tri-calcium phosphates. – *Compt. Rend. Acad. Bulg. Sci.*, **65** (8), 2012, 1099-1104. .
6. **Andonova-Lilova, B., T. Zhivkova, L. Dyakova, D. Rabadjieva, S. Tepavitcharova, R. Alexandrova**. Viability and proliferation of rat bone marrow cells cultured in the presence of newly synthesized composite materials for bone implants. In: *The Proceedings of the Sixth Edition of the Symposium with International Participation "New Trends and Strategies in the Chemistry of Advanced Materials"*, 8-9 November 2012, Timisoara, Romania, pp.7-10.
7. **Andonova-Lilova, B., T. Zhivkova, L. Dyakova, M. Alexandrov, D. Rabadjieva, S. Tepavitcharova, R. Alexandrova**. Application of various cytotoxicity assays for the initial evaluation of biocompatibility of a Sr-modified dicalcium phosphate dihydrate. – *Acta Morphol. Anthropol.,* **19**, 2012, 10-14.
8. **Coleman, R., J. J. Body, M. Aapro, P. Hadji, J. Herrstedt**. ESMO guidelines working group. Bone health in cancer patients: ESMO clinical practice guidelines. – *Ann. Oncol.,* **25** Suppl 3, 2014, 124-137.
9. **Kumar, P,, B. Vinitha, G. Fathima.** Bone grafts in dentistry. – *J. Pharm. Bioallied. Sci.,* **5**(Suppl 1), 2013, S125-S127.
10. **Kalder, M., P. Hadji**. Breast cancer and osteoporosis – Management of cancer treatment-induced bone loss in postmenopausal women with breast cancer. – *Breast Care (Basel).*, **9**(5), 2014, 312–317.
11. **Nartthanarung, A., K. Thanapprapasr, U. Udomsubpayakul, D. Thanapprapasr**. Age and survival of cervical cancer patients with bone metastasis. – *Asian Pac. J. Cancer Prev.*, **15**(19), 2014, 8401-8404.
12. **Oryan, A., A. Kamali, A. Moshiri, M. Eslaminejad**. Role of mesenchymal stem cells in bone regenerative medicine: What is the evidence? – *Cells Tissues Organs,* **204**(2), 2017, 59-83.
13. **Wein, F., A. Bruinink**. Human triple cell co-culture for evaluation of bone implant materials. – *Integr. Biol. (Camb)*, **5**(4), 2013, 703-711.
14. **Yamamoto, K., T. Kishida, Y. Sato, K. Nishioka, A. Ejima, H. Fujiwara, T. Kubo, T. Yamamoto, N. Kanamura, O. Mazda**. Direct conversion of human fibroblasts into functional osteoblasts by defined factors. – *Proc. Natl. Acad. Sci. USA*, **112**(19), 2015, 6152-6157.

Institute of Experimental Morphology, Pathology and Anthropology with Museum
Bulgarian Anatomical Society

Acta morphologica et anthropologica, 25 (3-4)
Sofia ● 2018

Trichinella britovi, Etiologic Agent of Trichinellosis in Wild Carnivores in Bulgaria

Valeria Dilcheva[*]*, Svetlozara Petkova*

Institute of Experimental Morphology,Pathology and Anthropology with Museum – Bulgarian Academy of Sciences, Sofia, Bulgaria

* Corresponding author e-mail: val_dilcheva@yahoo.com

Trichinellosis is one of the most common helminthozoonoses in Bulgaria. While in previous years the main source of infection were wild boars, today there is a shift in the tendency towards the domestic breed of swine as well as to the consumption of meat from bears, badgers, etc. which constitute a major link in the epidemiological chain of Trichinellosis. The objective of the present study was to better characterize the Trichinella genotypes found in wild boars and wildlife carnivores from different regions in Bulgaria. A molecular characterization by PCR of 24 Trichinella isolates from a variety of game has been performed. The prevalence of *T. britovi* among the wild animals in the country was confirmed.

Key words: Trichinella britovi, species determination, polymerase chain reaction (PCR)

Introduction

Trichinellosis is a food-borne parasitic disease caused by nematodes of the genus *Trichinella* which are zoonotic parasites with cosmopolitan distribution and major socio-economic importance. Human infection is acquired through consumption of undercooked meat from domestic or wild animal. Penetration of trichinella larvae into striated skeletal muscle cells results in ultrastructural and metabolic changes [2]. Migration of larvae causes the typical symptoms and signs of the disease. The severity of the symptoms depends on the number of ingested trichinella larvae and the immune response of the host [1, 2]. Based on epidemiological observation, [3] it is assumed that approximately 100 and 300 larvae of *Trichinella spiralis* cause disease and an intake of 1,000 to 3,000 or more larvae can cause severe disease. The incubation period for development of the disease after consumption of contaminated meat or meat products ranges from 1 to 51 days [5]. The main reason for global distribution of this parasite is the fact that trichinella has a wide range of hosts and can infect more than 150 species of animals, including humans. It is evaluated that around 11 million people may be infected by trichinella [4]. Until recently it has been accepted that the cause of trichinellosis in all animal species was the same – *Trichinella spiralis*. However, the implementation of molecular biology methods proved the existence of a significant diversity of species and differences in the taxonomy, the geographical dissemination and the epidemiology of trichinellosis [10]. Today, nine species and three genotypes are recognized in this genus [6, 9].

In Bulgaria, Kurdova et al. [7] investigated parasite isolates obtained upon 15 epidemic outbreaks. Received results showed the predominance of *T. britovi* (etiological agent in 10 outbreaks) while *T. spiralis* was found in 5 outbreaks. For the period from 2008 to 2014, 29 outbreaks were recorded in Bulgaria. Of 1 670 people who consumed meat or meat products contaminated with trichinella larvae, 710 were infected. The annual incidence of human trichinellosis for the period varied from 0.22 to 5.82 per 100,000 population [12]. An in-depth analysis based on molecular research, performed with 120 trichinella isolates was made by Lalkovski [8]. He found the appearance of two species: *Trichinella britovi* and *Trichinella spiralis*. *T. britovi* predominated over *T. spiralis* – 113 isolates (94.17%) and 7 (5.83%) respectively. Both species were identified in domestic pigs and wild boars, with *T. britovi*:*T. spiralis* ratios in 45:1 in wild boars and 1:1 in domestic pigs. *T. britovi* was the geographically more widespread species. (**Fig. 1**).

Fig.1. *Trichinella britovi* larvae within the diaphragm muscle of mouse.

Materials and Methods

The studies were carried out following the reference method of digestion using a magnetic stirrer according to Regulation (EU) 2015/1375. Muscle larvae were preserved in ethanol. *Trichinella spp.* larvae were identified at the species level by multiplex PCR, which has been developed for the simple and unequivocal differentiation of trichinella species and genotypes. Partial DNA sequence data were generated from the internal transcribed spacers ITS1 and ITS2 and from the expansion segment V region of the rRNA repeat from different trichinella species and genotypes.

Twenty four *Trichinella spp*. isolates were tested, typified and sorted according to the laboratory protocol of The European Union Reference Laboratory for Parasites (Rome, Italy).

Results

A total number of 24 isolates typified and sorted as followed:

Table 1. The Data obtained from the multiplex PCR.

N	Source of infection	Type of muscle in the original host	Species identification PCR	Number of larvae/g diaphragm	Number of passages *in vivo*	Place of origin locality	Latitude longitude
1	w. boar	masseter diaphragm	Tb	4	2	Elhovo	42° 31′N 26° 71˘ E
2	w. boar	masseter diaphragm	Tb	8	2	Grudovo	42° 41′N 27° 17˘ E
3	w. boar	masseter diaphragm	Tb	9	2	Chiprovci	43° 45′N 22° 79˘ E
4	w. boar	masseter diaphragm	Tb	5	2	Bankia	42° 78′N 22° 63˘ E
5	w. boar	masseter diaphragm	Tb	6	2	Melnik	41° 32′N 23° 45˘ E
6	fox	masseter diaphragm	Tb	2	2	Rudarci	42° 33′N 23° 19˘ E
7	jackal	masseter diaphragm	Tb	3	2	Peshtera	42° 05′N 23° 90˘ E
8	jackal	masseter diaphragm	Tb	2	2	Elena	43° 00′N 25° 86˘ E
9	Jackal	masseter diaphragm	Tb	7	2	Kula	43° 89′N 22° 51˘ E
10	jackal	masseter diaphragm	Tb	4	2	Razlog	41° 82′N 23° 46˘ E
11	jackal	masseter diaphragm	Tb	3	2	Govedarci	42° 36′N 23° 53˘ E
12	wild cat	masseter diaphragm	Tb	4	2	Anton	42° 69′N 24° 38˘ E
13	m. foina	masseter diaphragm	Tb	6	2	Belchin	42° 44′N 23° 41˘ E
14	m. foina	masseter diaphragm	Tb	4	2	Kostenec	42° 56′N 23° 98˘ E
15	badger	masseter diaphragm	Tb	14	1	Svoge	42° 91′N 23° 32˘ E
16	badger	masseter diaphragm	Tb	7	2	Iskretc	42° 94′N 23° 26˘ E
17	rat	masseter diaphragm	Tb	23	1	Sofia	42° 44′N 23° 21˘ E

N	Source of infection	Type of muscle in the original host	Species identification PCR	Number of larvae/g diaphragm	Number of passages *in vivo*	Place of origin locality	Latitude longitude
18	rat	masseter diaphragm	Tb	14	2	Elin Pelin	42° 43′N 23° 29˘ E
19	rat	masseter diaphragm	Tb	25	1	Slivnitca	42° 51′N 23° 15˘ E
20	wolf	masseter diaphragm	Tb	11	2	Grudovo	42° 21′N 27° 26˘ E
21	wolf	masseter diaphragm	Tb	9	2	Mramor	42° 75′N 22° 60˘ E
22	bear	masseter diaphragm	Tb	17	1	Madan	41° 42′N 24° 91˘ E
23	bear	masseter diaphragm	Tb	6	2	Batak	41° 88′N 24° 20˘ E
24	otter	masseter diaphragm	Tb	12	2	Samokov	42° 19′N 23° 34˘ E

Discussion

The results obtained in the study of the trichinella species from wild animals:wild boars - 5 specimens, fox-1, waiting-5, wild cat - 1, m. foina-2, badjer-2, rat-3, wolf-2, bear-2 and 1 otter showed that parasites cause of infection belong to *T. britovi*.

The detection of only *T. britovi* in wild animals shows that this species is prevalent in wildlife. Our results confirm the opinion of Pozio et al. [11] that in most countries of the European Union, including Bulgaria, *T. britovi* was the more prevalent species. These results confirm the assumption that wild animals (wild boar, fox, jackal, etc.) represent wildlife reservoir for *T. britovi* in Bulgaria. Previous investigation of trichinella isolates obtained upon 15 epidemic outbreaks revealed the predominance of *T. britovi*, as a cause of infection. Therefore, when people fail to properly breed domestic pigs this parasite reaches the domestic environment as it is registered in three outbreaks caused by the consumption of pork from backyard pigs [7]. As data indicate a steady increase in the number of outbreaks and of sporadically occurred individual cases, as well as due to public health importance of the disease, many questions remain open. We think that the main efforts should have been focused on the control or elimination of trichinella from the food chain and hope that our discoveries may have an impact on the transmission and control of trichinellosis in Bulgaria.

Acknowledgements: The work was supported by the Operational Programme "Science and Education for Smart Growth" 2014-2020, co-financed by the European Union through the European Structural and Investment Funds, Grant BG05M2OP001-2.009-0019-C01 from 02.06.2017 and Programme for support of young scientists and scholars (Contract No. 17-9/24.07.2017).

References

1. **Capo, V, D. Despommier**. Clinical aspects if infection with, *Trichinella spp*. – *Clin. Microbiol. Rev.*, **9** (1), 1996, 47–54.
2. **Despommier, D.D**. How does *Trichinella spiralis* make itself at home? – *Parasitol.* Today, **14**,1998, 318–323.
3. **Dupouy-Camet, J., F. Bruschi.** Management and diagnosis of human trichinellosis. In: *FAO/WHO/ OIE guidelines for the surveillance, management, prevention and control of trichinellosis. Food & Agriculture Org.*, (Eds. J. Dupouy-Camet, K.D. Murrell), 2007.
4. **Dupouy-Camet, J**. Trichinellosis: a worldwide zoonosis. – *Vet. Parasitol.*, **93**, 2000, 191–200. doi: 10.1016/S0304-4017(00)00341-1
5. **Gottstein, B., E. Pozio, K. Nockler**. Epidemiology, treatment andcontrol of Trichinellosis. – *Clin. Microbiol. Rev*., **22**(1), 2009, 127–145. doi:10.1128/CMR.00026-08
6. **Korhonen, P. K.,E. Pozio, G. La Rosa, B. C. Chang, A. V. Koehler, E. P. Hoberg**, **P. R. Boag, P. Tan, A. R. Jex, A. Hofmann, P. W. Sternberg, N. D. Young, R. B. Gasser**. Phylogenomic and biogeographic reconstruction of the *Trichinella* complex. – *Nat. Commun.* **7**, 2016, 10513. doi: 10.1038/ncomms1051
7. **Kurdova, R., N. Muller, N. Tsvetkova, L. Michov,D. Georgieva, M. Ivanova, B. Gottstein**. Characterisation of *Trichinella* isolates from Bulgaria by moleculartyping and cross-breeding. – *Vet. Parasitol*, **123**, 2004, 179–188.
8. **Lalkovski, N**. Species composition of *Trichinella* in domestic and wild animals in Bulgaria. – *Bulg. J. Vet. Med.,* 2017(online first).
9. **Pozio, E., D. S. Zarlenga**. New pieces of the *Trichinella puzzle*. – *Int. J. Parasitol*., **43**, 2013, 983–997. doi: 10.1016/j.ijpara.2013.05.010
10. **Pozio, E., D. S. Zarlenga**. Recent advanceson the taxonomy, systematics andepidemiology of *Trichinella*. – *Int. J. Parasitol.*, **35**, 2005, 1191–1204.
11. **Pozio E, Rinaldi L, Marucci G, Musella V, Galati F, Cringoli G, Boireau P, La Rosa G.** Hosts and habitats of *Trichinella spiralis* and *Trichinella britovi* in Europe. – Int. J. Parasitol. **39**(1), 2009, 71-79**.**
12. **Rainova, I., I. Kaftandjiev, R. Harizanov, N. Tsvetkova, D. Jordanova, I. Marinova, R. Kurdova, T. Kantardjiev, N. Lalkovski.** Outbreaks of human trichinellosis, still a challenge for the public health authorities in Bulgaria. – *J.Pub. Health*, *24*(4), 2016, 291-297.

Institute of Experimental Morphology, Pathology and Anthropology with Museum
Bulgarian Anatomical Society

Acta morphologica et anthropologica, 25 (3-4)
Sofia ● 2018

Experimental Acupuncture of the Human ST_{36} Acupoint

Nikolay Dimitrov[1], Dimitrinka Atanasova[1,2], Nikola Tomov[1], Sevinch Hamza[1], Dimitar Sivrev[1]*

[1] *Department of Anatomy, Faculty of Medicine, Trakia University, Stara Zagora, Bulgaria*

[2] *Institute of Neurobiology, Bulgarian Academy of Sciences, Sofia, Bulgaria*

* Corresponding author e-mail: nikolaydd@abv.bg

The aim of the present study is to examine the structures that interact with the acupuncture needle. For this purpose, we examined the vicinity of the needle tract formed after experimental acupuncture in ST_{36} acupoint in humans. We used the method for needle tract visualization, developed by us, to demonstrate the tissues in a condition, maximally close to the condition during the needling. As a result of acupuncture the integrity of the epithelium, dermis, subcutis and striated muscles is disrupted and folds are formed in the direction of the needle tract. Elastic and collagen fibers in dermis and subcutis are partially destroyed. We observed hair follicles, nerve fibers, blood vessels, and muscle spindles in the vicinity of the needle tract. Some of them are partially destroyed by the acupuncture needle. Larger blood vessels and nerves are not affected by it. Needling of the acupoint generally causes displacement and destruction of the soft tissue.

Key words: acupoint, Zusanli (ST_{36}), muscle spindles, needle tract

Introduction

Traditional Chinese Medicine (TCM) and acupuncture in particular continue to gain more and more popularity in Bulgaria, Europe, and all over the world in the last years, which is one of the reasons for our struggle to clarify the morphological basis of this ancient healing method. Acupuncture points (acupoint) are important for treatment in TCM and they can be found by applying the method of standard proportions of anatomical structures under the control of an apparatus measuring skin resistance [12]. Acupuncture point ST_{36} is one of the most important acupoints used for treatment in TCM. In human, ST_{36} acupoint is located on the stomach meridian – from ST_{35} ('lateral eye of the knee', at the level of the knee joint space) 3 cun (1 handbreadth) down and 1 fingerbreadth lateral to the anterior crest of the tibia, on the tibialis anterior muscle [8]. In TCM for therapeutic intention, acupuncture needles are inserted into the acupoint. The depth of the needling ST_{36} acupoint in the human is 1–1.5 cun [8]. Researchers investigate the mechanism of acupuncture and the nature of acupuncture points [1, 13], but there is a lot of uncertainty and controversy. Some physicians use the electrical conductance of the skin at the acupuncture points, for diagnostic purposes [2].

The aim of the present study is to examine the structures that interact with the acupuncture needle. For this purpose, we examined the vicinity of the needle tract formed after experimental acupuncture in ST_{36} acupoint in humans.

Materials and Methods

We used the method for needle tract visualization, developed by us in rats and explained in detail in previous publications [3, 5, 6] to demonstrate the tissues in a condition, maximally close to the condition during needling. This method enables the investigator to demonstrate the tissues in a condition, maximally close to the condition during the needling process, after retracting the needle. This method was applied on human cadavers to obtain samples from ST_{36} acupoint. The experiments were carried out on six human cadavers of different ages available at the Department of Anatomy in the Faculty of Medicine of the Trakia University. ST_{36} acupoint was located, defined and marked using the method of standard proportion of anatomical structures – 3 cun down from ST_{35} and 1 fingerbreadth lateral to the anterior crest of the tibia, on the tibialis anterior muscle [8]. We used standard steel acupuncture needles with size 0.30 × 40 mm. Acupuncture needles were inserted 25 mm deep into ST_{36} acupoint. Samples from ST_{36} acupoint with different size 10 × 10-15× 25 mm was excised together with the needle and fixed in formalin for 48h – 96h. Tissue was paraffin-embedded and sectioned on a conventional microtome in 5 μm sections. The acupuncture needle remained in the paraffin block and was taken out immediately before its plane was reached by the microtome blade. We used classical histological techniques of staining: H&E, Orcein and Van Gieson for visualization of morphological structures in the vicinity of the needle tract.

Results

The method used successfully visualizes needle tract formed after experimental acupuncture in ST_{36} acupoint in humans (**Fig. 1, 2**). We demonstrate the needle tract and tissues in the vicinity in a condition, maximally close to the condition during the needling. The needle tract defect seen is with a minimum size and is observed across all tissues through which the needle has passed. The needle tract is visible from the surface of the ST_{36} acupoint point to its depth. The acupuncture needle destroys and shifts the tissues through which it passes.

As a result of acupuncture the integrity of the epithelium, dermis, subcutis and striated muscles is disrupted and folds are formed in the direction of the needle tract. We observed indentation of the epidermis and compression and displacement of the connective tissue from acupuncture needle (**Fig. 1A**). The needle tract formed as a result of acupuncture is clearly visible in the depth of investigated tissues (**Fig. 1, 2**) Changes in the structure are most clearly differentiated in the vicinity of the needle tract formed by the acupuncture needle. Particles of loose connective tissue and collagen and elastic fibers fall inside the needle tract into the plane of disrupted striated muscle. We observed destroyed elastic and collagen fibers in dermis, subcutis and striated muscles in the needle tract (**Fig. 2A-D**). We also observed hair follicles, nerve fibers, blood vessels, sebaceous glands, sweat glands, lymph vessels, striated muscle fibers (**Fig. 1**) and muscle spindles in the vicinity of needle tract (**Fig. 2C**). Some of them are also destroyed from the acupuncture needle (**Fig. 1B-D; 2B**). Very interesting observation was the presence of blood vessels (**Fig 1B; 2B**), hair follicles (**Fig. 1B**) particles of striated muscles (**Fig. 2C**) and muscle spindles (**Fig. 1D**) inside in the needle tract.

The destroyed blood vessels in the needle tract were cut into two parts by the needle. The muscle spindle observed in the needle tract was removed from its normal position between striated muscles by the needle and moved along the needle tract (**Fig. 1D**). Blood vessels with reduced cross section and in various degrees of compression were found in the vicinity of the needle tract (**Fig. 1B**). The larger blood vessels and larger nerves deeper in tissue were not affected by the needle.

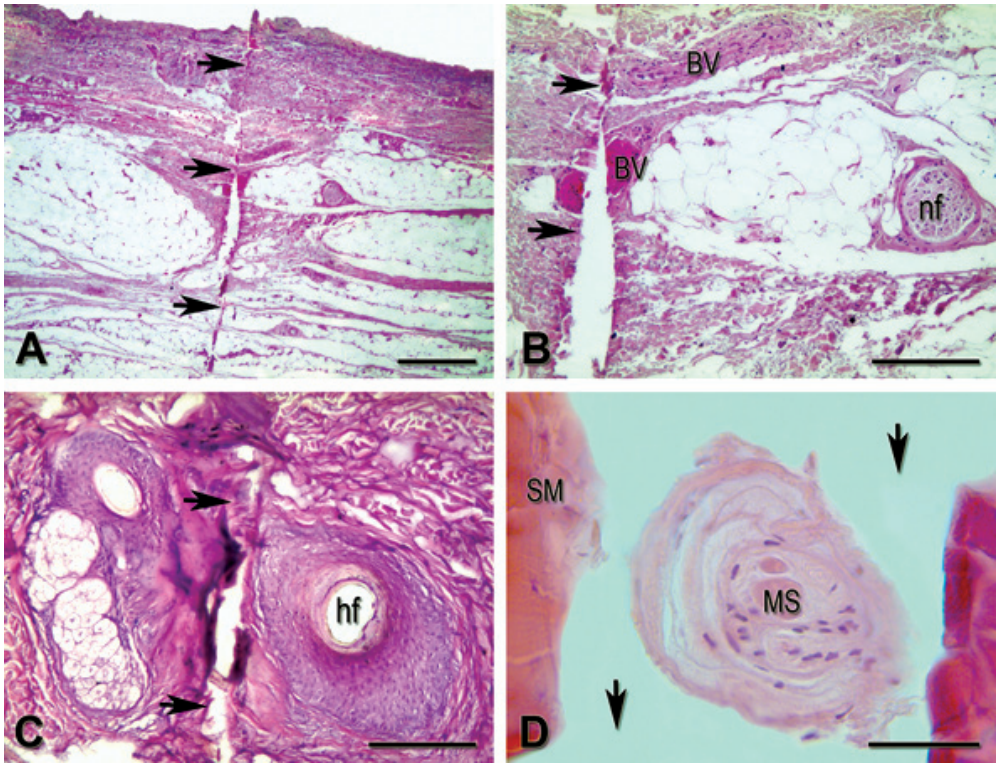

Fig. 1. The representative Hematoxylin & Eosin (H&E)-stained structures in the vicinity of the needle tract formed after acupuncture in ST_{36} acupoint in humans. (**A)** The needle tract (arrow) formed after acupuncture and structures in the vicinity of the needle tract. **(B)** Needle tract formed after acupuncture (arrow) and nerve fibers (nf), and blood vessels (BV) in the vicinity of the needle tract (arrow). **(C)** Hair follicles (hf) in the vicinity of the needle tract (arrow) destroyed by the acupuncture needle. (**D)** The muscle spindle (ms) in the needle tract (arrow) destroyed by the acupuncture needle between striated muscles (SM). Scale bars: 500 µm (A), 200 *µm* (B), 100 *µm* (C), 50 *µm* (D).

Discussion

In our previous investigation of morphology of ST_{36} acupoint in the human we demonstrated normal anatomical structures in this acupoint: skin, subcutaneous adipose tissue, blood vessels, nerves, sebaceous and sweat glands, and mast cells. In some areas of the skin indentations and differences in the thickness of the epidermis and the loose connective tissue layers were found, but these differences were not pronounced [7]. In this study we observed normal anatomical structures in this acupoint in the human but

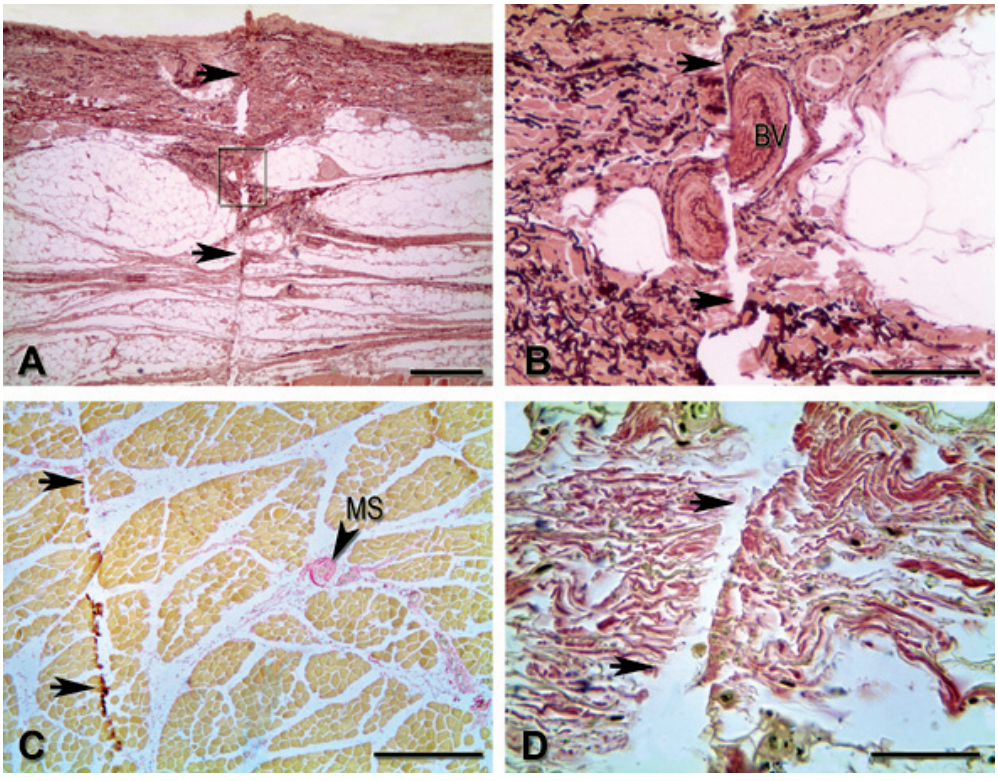

Fig. 2. The structures in the vicinity of the needle tract formed after acupuncture in ST_{36} acupoint in humans. **(A)** Needle tract (arrow) formed after acupuncture and elastic fibers in dermis and subcutis in the vicinity of the needle tract, partially destroyed by the acupuncture needle (Orcein). **(B)** Elastic fibers and blood vessels (BV) in the vicinity of the needle tract (arrow) destroyed by the acupuncture needle (Orcein). **(C)** The needle tract (arrow) destroyed striated muscles. Muscle spindles (MS) in the vicinity of needle tract (arrow) (Van Gieson). **(D)** Collagen fibers in the vicinity of the needle tract, partially destroyed by the acupuncture needle (arrow) (van Gieson). Scale bars: 500 μm (A, C), 100 μm (B), 50 μm (D).

also alterations of the structure of elastic and collagen fibers in the vicinity of needle tract. Our previous results in rats ST_{36} acupoint show normal anatomical structures and the presence of a thicker layer of loose connective tissue in some areas of the skin, indentations and differences in the thickness of the epidermis and folding of the deep fascia [4]. Following acupuncture in ST_{36} in rats, a needle tract is formed in the tissues, affected by the needle. The influence of the acupuncture needle in ST_{36} in rats induces morphological changes in the examined tissues – compression and displacement of the connective tissue in the vicinity of the needle tract. The integrity of derma, subcutis, deep fascia, epimysium and striated muscle was disrupted by the acupuncture needle [3]. Changes in the structure of elastic and collagen fibers in ST_{36} in rats are most clearly defined in the vicinity of the needle tract formed by the acupuncture needle. The defect is seen with a minimum size, mainly because tissue integrity recovers fast after the removal of the needle [5]. In this study we successfully visualized needle tract formed after experimental acupuncture in ST_{36} acupoint in humans and tissues in the vicinity of this tract. We observed analogous to those in experimental animals changes in the structure of elastic and collagen fibers in the vicinity of the needle tract. In this

study we observed destroyed muscle spindles in the needle tract. This indicates that the acupuncture needle is able to destroy at least some of muscle spindles. We also observed large nerve fibers and large blood vessels in ST_{36} acupoint in the humans. However, they were not affected. This confirms our previous investigation in rats, which shows that larger neurovascular structures remain relatively intact following needling of the acupoint [3]. All this leads to the conclusion that morphological alterations following experimental acupuncture in ST_{36} acupoint in humans and rats are similar. Other researchers have observed the needle tract in the tissue of acupoints. In its vicinity, they observed nerve fibers, small vessels and muscle spindles in canine acupoints [9]. This confirms our investigation in humans. Observed changes after acupuncture that occur in the connective tissue are important because they are probably related to the effect of acupuncture. Some investigators have suggested that the mechanism of the acupuncture effects is the reaction of the connective tissue near the needle tract [10, 11, 14]. The investigators suggest that collagen fibers play an important role in the degranulation of mast cells and acupuncture analgesia [14]. This shows the important role of the changes of connective tissue observed after insertion of acupuncture needle, which we confirm on a morphological level.

Conclusion

The method for needle tract visualization, developed by us successfully visualizes needle tract formed after experimental acupuncture in ST_{36} acupoint in humans. Needling of the acupoint generally causes displacement and destruction soft tissue. The alterations are mainly in the connective tissue of the acupoint. However, smaller blood vessels and nerve structures, such as muscle spindles, are also affected. The observed morphological effects of acupuncture are probably related to at least some of the mechanisms of post-acupuncture reactions.

References

1. **Bowsher, D. Mechanisms of acupuncture**. – In: *Medical Acupuncture: A Western Scientific Approach*, Edinburg, Churchill Livingstone, 1998, 69-82.
2. **Comunetti, A., S. Laage, N. Schiessl, A. Kistler.** Characterization of human skin conductance at acupuncture points. – *Experientia,* **51**, 1995, 328-331.
3. **Dimitrov, N**. Morphological changes in biologically active point /BAP/ ST36 after acupuncture in rat. – *Acta morphol. anthropol.,* **19**(1), 2012, 30-33.
4. **Dimitrov, N.** Normal morphology of biologically active point BAP/ST36 rat. – *Acta morphol. anthropol.*, **19**(1)*,* 2012, 34-37.
5. **Dimitrov, N., D. Atanasova, J. Staykova, N. Pirovski, D. Sivrev**. Changes in collagen and elastic fibers in biological active point ST_{36} of rats after experimental acupuncture. – *Acta morphol. anthropol.,* **21**, 2015, 115-118.
6. **Dimitrov, N., D. Atanasova, N. Tomov, D. Sivrev, N**. **Lazarov.** Acupuncture causes serotonin release by mast cells. – *Rom. J. Morphol. Embryol.*, **58**(3), 2017, 961-968.
7. **Dimitrov, N., D. Sivrev, D. Atanasova.** Histological structure of the human biologically active point (BAP) ST36. – *TJS,* **13** (2), 2015, 67-69.
8. **Focks, C.** Atlas of acupuncture. China, Churchill Livingstone Elsevier, 2008, 168.
9. **Kim, M., T. Nam, M. Kim, J. Kim, D. Kim, K. Lee, C. Song.** Histological observation of canine acupoints. – *J. Vet. Clin*., **23** (2), 2006, 102-104.
10. **Langevin, H., N. Bouffard, G. Badger, D. Churchill, A. Howe.** Subcutaneous tissue fibroblast cytoskeletal remodeling induced by acupuncture: evidence for a mechanotransduction-based mechanism. – *J. Cell Physiol.*, **207**(3), 2006, 767-774.

11. **Langevin, H., N. Bouffard, D. Churchill, G. Badger**. Connective tissue fibroblast response to acupuncture: dose-dependent effect of bidirectional needle rotation. – *J. Altern. Complement. Med., **13***(3), 2007*,* 355–360.
12. **White, A., M. Cummings, J. Fishie. How to locate acupuncture points.** – In: *An introduction to western medical acupuncture*. Churchill Livingstone Elsevier, 2008, 185-189.
13. **Wick, F., M. Wick, MC. Wick.** Morphological analysis of human acupuncture points through immunohistochemistry. – *Am. J. Phys. Med. Rehabil*., **86**(1), 2007, 7-11.
14. **Yu, X., G. Ding, W. Yao, R. Zhan, M. Huang.** The role of collagen fiber in "Zusanli" (ST 36) in acupuncture analgesia in the rat. – *Chinese Acupuncture & Moxibustion*, **28**, 2008, 207-213.

Institute of Experimental Morphology, Pathology and Anthropology with Museum
Bulgarian Anatomical Society

Acta morphologica et anthropologica, 25 (3-4)
Sofia ● 2018

Effect of Disulfiram on Viability and Proliferation of Virus Transformed Rat Sarcoma Cells

Desislav Dinev[1], Lora Dyakova[2], Rossen Spasov[3], Radostina Alexandrova[1]*

[1] Institute of Experimental Morphology, Pathology and Anthropology with Museum Bulgarian Academy of Sciences, Sofia, Bulgaria
[2] Institute of Neurobiology, Bulgarian Academy of Sciences, Sofia, Bulgaria
[3] Department of Pathology, Faculty of Medicine, Sofia University "St.Kliment Ohridski", University Hospital Lozenetz, Sofia, Bulgaria

* Corresponding author e-mail: rialexandrova@hotmail.com

The aim of our study was to evaluate the influence of disulfiram (Antabuse) on viability and proliferation of cultured retrovirus-transformed rat sarcoma cells (permanent cell line LSR-SF-SR). The investigations were performed by thiazolyl blue tetrazolium bromide (MTT) test, crystal violet staining, double staining with acridine orange and propidium iodide in short-term (24-72h) experiments with monolayer cultures as well as in long-term experiments (30 days) by 3D-colony forming method. The results obtained reveal that applied at a concentration range of 0.3 –100 μg/ml disulfiram expresses significant cytotoxic effect that is time- and concentration- dependent.

Key words: disulfiram, Rous sarcoma virus, rat sarcoma, cell culture, cytotoxicity

Introduction

Disulfiram (DS), an FDA (Food and Drug administration, USA) approved drug for the treatment of alocoholism has been also reported to express promising antitumor activity in cellular and animal models as well as in humans [7, 10]. According to the literature available, in this study we report for the first time data about inhibitory effect of disulfiram on 2D- and 3D-growth of cultured LSR-SF-SR rat sarcoma cells transformed by Rous sarcoma virus strain Schmidt-Ruppin (SR-RSV). The cells contain *v-src* gene - the cellular analogues of this gene are known to be involved (when their expression and functioning are disturbed) in pathogenesis of various malignancies in humans and animals [9, 11].

Materials and Methods

Tetraethylthiuram disulfide (Disulfiram) was provided by Sigma-Aldrich Co (Germany, Lot #BCBN4962V). Disulfiram was dissolved in dimethylsulfoxide (DMSO – the

concentration of DS in the stock solution was 1 mg/ml containing 2 % DMSO) and then diluted in culture medium.

Permanent cell line LSR-SF-SR established from a transplantable sarcoma in rat, induced by Rous sarcoma virus strain Schmidt-Ruppin (SR-RSV) [1] was used as an experimental model in our study. RSV, as well as cells transformed by the virus, contain *v-src* gene [11]. The influence of disulfiram on cell viability and proliferation was studied as it was previously described [2, 4], in short-term (24-72h, with monolayer cultures) experiments by MTT test (MTT), crystal violet staining (CV) and double staining with acridine orange and propidium iodide (AO/PI) as well as in long-term experiments (30 days) with 3D-colony-forming method (CFM). Statistical analysis was done using one-way analysis of variance (ANOVA) followed by Dunnett post-hoc test and Origin 6.1™ .

Results

The results obtained reveal that applied at a concentration range of 1-100 μg/ml for 24 – 72h disulfiram significantly decreases viability and proliferation of LSR-SF-SR rat sarcoma cells in a time- and concentration-dependent manner (**Fig. 1A, Table 1**). The cytotoxic activity of DS has been confirmed by MTT test (that measures the ability of the mitochondrial enzyme succinate dehydrogenase to convert yellow thiazolyl blue tetrazolium bromide into purple formazane) – accepted as a gold standard for cytotoxicity assays [14] and staining with crystal violet dye that binds to proteins and DNA [5] (**Fig. 1B, Table 1**). Cytopathological alternations such as cellular polymorphism are observed in LSR-SF-SR cells cultured for 72 h in the presence of DS applied at concentrations of 0.39 to 25 μg/ml. Individual cell size varies up to 4-5 times. Giant cells (of about 30 μm in diameter) and large optically dense cytoplasmic vacuoles have been observed. The nuclei are intact and multiple nucleoli (2 or more) are visible. Cytoplasmic morphology is erased. Apoptotic changes of the cell membrane are found only in single cells with dimensions less than 10 μm. Mitotic activity is missing (**Fig. 2**).

The rapid cytotoxic effect of disulfiram observed after short treatment intervals (24-72h) has been found to persist over time – the long-term experiments (30 days) carried out by CFM show that administered at concentrations ≥ 3.12 μg/ml DS completely inhibits 3D growth of rat sarcoma cells in a semisolid medium.

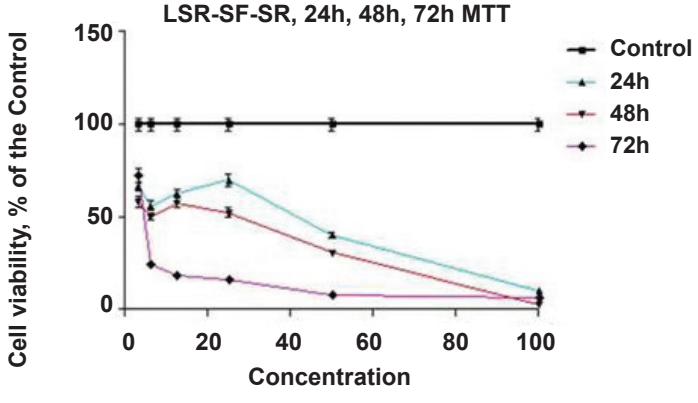

A

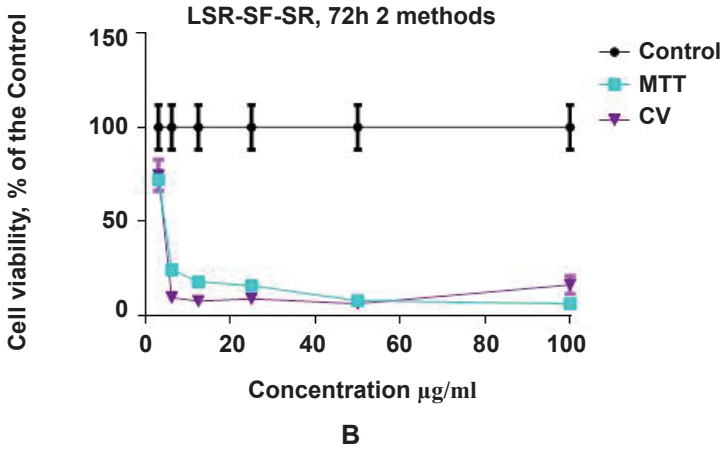

Fig.1 Effect of disulfiram on viability and proliferation of LSR-SF-SR rat sarcoma cells. The investigations are performed by MTT test (MTT) after 24, 48 and 72 h of treatment (Fig. 1A) as well as by MTT test and crystal violet staining (CV) after 72 h incubation period (Fig. 1B).

Table 1. Cytotoxic concentrations 50 (CC_{50}, μg/ml) and 90 (CC_{90}, μg/ml) of disulfiram for LSR-SF-SR rat sarcoma cells determined by MTT test (MTT) and crystal violet staining (CV)

Cytotoxicity assay	**MTT**			**CV**
Treatment period	24h	48h	72h	72h
CC_{50}	42.1	27.2	4.4	4.3
CC_{90}	n.d.	85.4	45.0	6.24

n.d. – not determined

Discussion

Disulfiram has been used for the treatment of chronic alcohol dependence since 1951. The promising anticancer properties of DS have also been reported – DS induces apoptosis in cancer cells, inhibits their proliferation and dissemination (metastases). Various mechanisms clarifying at least partially the antineoplastic potential of DS have been suggested including inhibition of proteasome functions and topoisomerase and matrix metalloproteinase activity, ability to suppress cancer STAT3 signaling, inhibition of TGF-beta-induced epithelial mesenchymal transition via ERK/NF-kB/Snail pathway, etc. Important feature of DS's anticancer activity is its ability to suppress cancer stem cells. DS has the potential to enhance the activity of anticancer agents and to overcome drug resistance (for example to alkylating agents) [6, 7, 8, 10, 12]. The protective effect of DS against the doxorubicin-induced cardiotoxicity has been documented [13]. The cytotoxicity of disulfiram is copper-dependent. The thiol groups

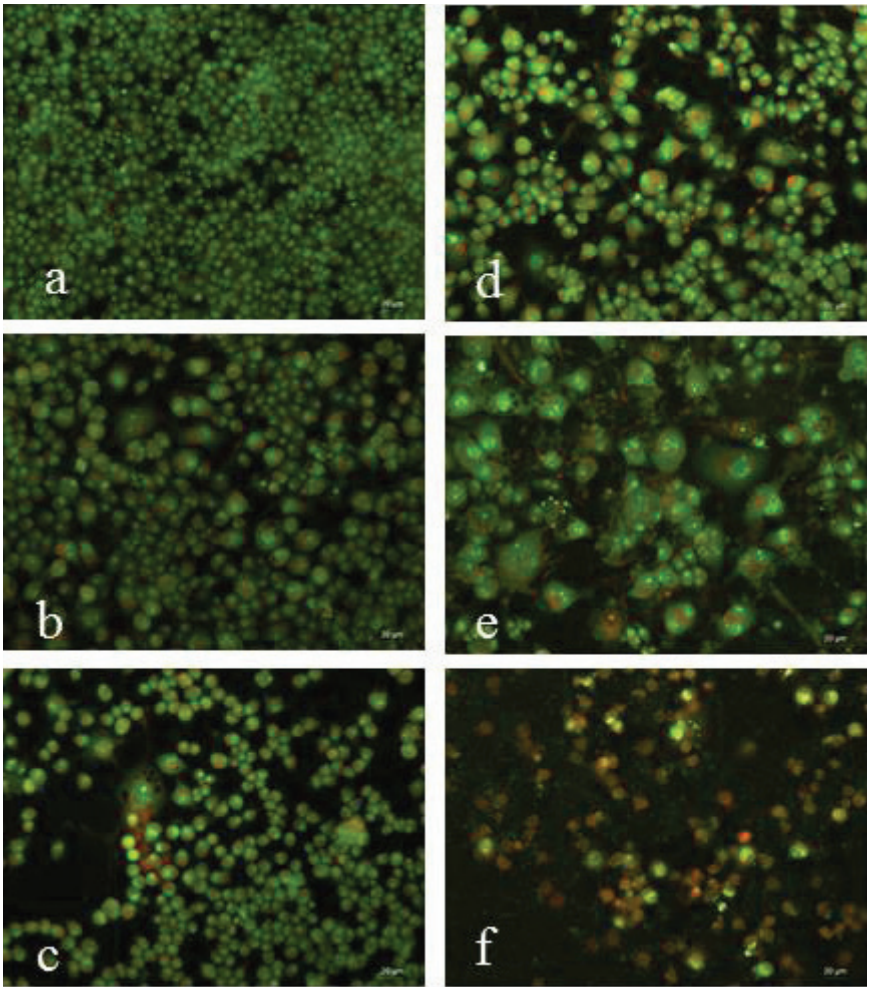

Fig. 2. Non-treated (Control) LSR-SF-SR rat sarcoma cells (a) and cells cultured in the presence of disulfiram applied for 72h at a concentration of 0.39 (b), 3.12 (c), 6.25 (d), 12.5 (e) and 25(f) μg/ml. Double staining with acridine orange and propidium iodide.

and thiuram structure has been proved to be indispensable for the anticancer activity of DS [3]. In this study we report for the first time that DS decreases 2D- and 3D-growth of retrovirus transformed rat sarcoma cells containing *v-src* gene. Src family kinases are known to play an important role in tumor development / progression being involved in cell adhesion, invasion, proliferation, survival, and angiogenesis and have been recognized as promising therapeutic targets for cancer [9].

Conclusion

The promising antitumor properties of disulfiram as well as its well known pharmacokinetics, pharmacodynamics and toxicity profile make it a suitable candidate for

the so called “drug repurposing” – a promising strategy for cancer therapy. Additional studies are needed to clarify better the antitumor activity of disulfiram and to establish the most appropriate form of its application.

Acknowledgements: The work was supported by National Science Fund, Bulgarian Ministry of Education and Science, Grant № DFNI Б 02 30 from 12.12.2014 and Operational Programme “Science and Education for Smart Growth” 2014-2020, co-financed by the European Union through the European Structural and Investment Funds, Grant BG05M2OP001-2.009-0019-C01 from 02.06.2017.

References

1. **Alexandrov, I**. Immunobiological characterization of transplantable sarcoma in rats. – *Compt. Rend. Bulg. Acad. Sci*., **46**, 1993, 97 – 100.
2. **Alexandrova, R., T. Zhivkova, L. Dyakova, R. Kalfin, R. Tudose, E.-M. Mosoarca, O. Azmi, O. Costisor**. Effect of Ni(II) complexes with Mannich bases on viability and proliferation of human cancer cells. – *Acta Morphol. Anthropol*., **25**(1-2), 2018, 3-10.
3. **Butcher, K., V. Kannappan, R. S. Kilari, M. R. Morris, C. McConville, A. L. Armesilla, W. Wang.** Investigation of the key chemical structures involved in the anticancer activity of disulfiram in A549 non-small cell lung cancer cell line. – *BMC Cancer*, **18**(1), 2018, doi: 10.1186/s12885-018-4617-x.
4. **Dyakova, L., D.-C. Culita, G. Marinescu, M. Alexandrov, R. Kalfin, L. Patron, R. Alexandrova**. Metal (ZnII, CuII, NiII) complexes of Ursodeoxycholic acid as putative anticancer agent. – *B&BE*, **28**(3), 2014, 543-551.
5. **Feoktistova, M, P. Geserick, M. Leverkus.** Crystal violet assay for determining viability of cultured cells. – *Cold Spring Harb Protoc*., **4**, 2016, doi: 10.1101/pdb.prot087379.
6. **Han, D., G. Wu, C. Chang, F. Zhu, Y. Xiao, Q. Li, T. Zhang, L. Zhang**. Disulfiram inhibits TGF-β-induced epithelial-mesenchymal transition and stem-like features in breast cancer via ERK/NF-κB/Snail pathway. – *Carcinogenesis*, **35**(3), 2014, 692-702.
7. **Jiao,Y., B. N. Hannafon, W. Q. Ding.** Disulfiram‘s anticancer activity: evidence and mechanisms. – *Anticancer Agents Med. Chem*., **16**(11), 2016, 1378-1384.
8. **Kim, Y. J., J. Y. Kim, N. Lee, E. Oh, D. Sung, T. M. Cho, J. H. Seo.** Disulfiram suppresses cancer stem-like properties and STAT3 signaling in triple-negative breast cancer cells. – *Biochem. Biophys. Res. Commun*., **486**(4), 2017, 1069-1076.
9. **Kim, L. C., L. Song, E. B. Haura**. Src kinases as therapeutic targets for cancer. – *Nat. Rev. Clin. Oncol*., **6**(10), 2009, 587-595.
10. **Kona, F. R., D. Buac, A. M. Burger**. Disulfiram, and disulfiram derivatives as novel potential anticancer drugs targeting the ubiquitin-proteasome system in both preclinical and clinical studies. – *Curr Cancer Drug Targets*., **11**(3), 2011, 338-46.
11. **Martin, G. S.** The road to Src. – *Oncogene*, **23**(48), 2004, 7910-7917.
12. **Paranjpe, A., R. Zhang, F. Ali-Osman, G. C. Bobustuc, K. S. Srivenugopal.** Disulfiram is a direct and potent inhibitor of human O6-methylguanine-DNA methyltransferase (MGMT) in brain tumor cells and mouse brain and markedly increases the alkylating DNA damage. – *Oncotarget*, 6(38), 2015, 40907-40919.
13. **Sonawane, V. K., U. B. Mahajan, S. D. Shinde, S. Chatterjee, S. S. Chaudhari, H. A. Bhangale, S. Ojha, S. N. Goyal, C. N. Kundu, C. R. Patil. A Chemosensitizer** Drug: Disulfiram prevents Doxorubicin-induced cardiac dysfunction and oxidative stress in rats. – *Cardiovasc. Toxicol*., 2018, doi: 10.1007/s12012-018-9458-y.
14. **van Tonder, A., A. M. Joubert, A. D. Cromarty**. Limitations of the 3-(4,5-dimethylthiazol-2-yl)-2,5-diphenyl-2H-tetrazolium bromide (MTT) assay when compared to three commonly used cell enumeration assays. - *BMC Res. Notes*. 8, 2015, doi: 10.1186/s13104-015-1000-8.

Institute of Experimental Morphology, Pathology and Anthropology with Museum
Bulgarian Anatomical Society

Acta morphologica et anthropologica, 25 (3-4)
Sofia ● 2018

The Significance of Anticardiolipin Antibodies in Patients with Vasculitis

Mary Gantcheva

Institute of Experimental Morphology, Pathology and Anthropology with Museum, Bulgarian Academy of Science, Sofia, Bulgaria

* Corresponding author e-mail: mary_gant@yahoo.com

We evaluate the incidence of serum anticardiolipin antibodies in patients with different types of vasculitides and vasculopathies and describe clinical, histological and laboratory specificity and disease course in correlation with their positivity. We conclude that they activate endothelial cells in both occlusive and inflammatory vascular diseases, aggravate skin symptoms, but are not related to advanced systemic involvement and poor prognosis. They represent skin ulcerations on acral sites in lupus erythematosus and have a predictive role for thrombosis. Livedo vasculitis may be a clinical sign of antiphospholipid syndrome.

Key words: Anticardiolipin antibodies, vasculitis, vasculopathy, antiphospholipid syndrome, livedo vasculitis.

Introduction

Anticardiolipin antibodies (aCL) are one of the most prominent members of antiphospholipid family. They bind to immobilize cardiolipin in an ELISA and cross-react with phosphotidylserin, phosphatidylinositol, and phosphatidic acid. Their assays are isotype-specific, but of different isotypes: IgG, IgM and IgA. ACL are detectable in up to 2% of the normal population with no definite association with either age or sex. They are revealed also in autoimmune diseases - systemic lupus erythematosus (SLE) and other, infection diseases, malignancies and drug-induced conditions. ACL in patients with autoimmune diseases are completely different from those occurring in patients with nonautoimmune diseases, which confer little risk of thrombosis and are inhibited by cofactor. Autoimmune-related antibodies are suspected to be IgG. They bind with high avidity with high correlation between the presence of aCL and lupus anticoagulant. The pathogenecity of aCL is tend to be due to activation of proinflammatory and procoagulant phenotype sustain by the up-regulation of adhesion molecules, synthesis and secretion of cytokines, chemokines, endothelin-1 and tissue factor [1]. Plasma beta$_2$–GPI is always needed to inhibit the contact activation of the intrinsic coagulation pathway, factor XII, factor Xa generating activity, ADP-induced platelet aggregation, and protein C [9].

Materials and Methods

The total number of 90 patients of both sex aged 18-77 years were enrolled in the study. Several patient groups were differentiated in accordance with the clinical entities: cutaneous necrotizing vasculitis (CNV) – 15 patients, Henoch Schonlein purpura (HSP)-7, Morbus Behcet (MB)-7, cutaneous polyarteritis nodosa (cPAN)–4, systemic lupus erythematosus (SLE) – 25, systemic scleroderma (SSc) – 12, livedoid vasculitis (LiV)–18 and gangrene – 2 (Fig. 1). Antibodies to cardiolipin IgG, IgM, IgA and to beta$_2$–GPI IgG were tithred by solid-phase enzyme immunoassay on the first visit of each patient. A conformation of aCL-ELISA (chromogenic) positivity in 12 weeks interval was needed. Histology samples were taken with a routine punch 4-mm technique. Clinical observations assessing skin changes and concomitant systemic symptoms were made on the day of the first visit, and at follow-up visits at the end of the first month, sixth month and after one year period.

Results

Anticardiolipin antibodies were detected in 30 of our patients (**Table 1**).

We found that 4 of the investigated 15 patients with CNV were positive for IgG and IgMaCL. No IgAaCL were detected. One of these cases was a 71-year old man. He developed hemorrhagic, bullous and ulcerative lesions on the skin on his left leg and on the stump of the right one (**Fig. 1**). He was amputated one year before because of thrombosis of a. tibialis posterior dextra. He had high titters of IgGaCL and leucocytoclastic vasculitis on histopathology. We put the diagnosis antiphospholipid syndrome (APS) considering aCL responsible for the thrombosis. We think that vasculopathy has thrombotic origin and vasculitis is concomitant. Another interesting case was that of a young man with wide spread necrosis on the testes and thigh (**Fig. 2**), aCL and leucocytoclastic vasculitis. We achieved improvement with therapy with corticosteroids and anticoagulants. The other two cases with positive aCL and CNV were women who like the previous ones had stormy course of the disease with deep painful bleeding ulcerations.

We had two patients with aCL from our series of 7 patients with HSP (**Fig. 3**), and all of them had only positive IgAaCL, neither IgG nor IgM.

Table 1. Clinical entities, number of the investigated patients and number of the positive ones for aCL

Vasculitidis		**Vasculopathies**
Leucocytoclastic V	**Lymphocytic V**	
CNV- 15/ **4 aCL**	SLE- 25/ **7 aCL**	Livedo vascul- 18/ **7 aCL**
HSP- 7/ **2 aCL**	SSc- 12/ **4 aCL**	Gangrene-2/ **1 aCL**
M. Behcet- 7/ **2 aCL**		
cPAN- 4/ **3 aCL**		

Fig.1. Hemorrhagic lesion on the skin of the stump in a patient with CNV and aCL

Fig.2. Necrotic ulcer on the skin of the thigh in a patient with CNV and aCL

Fig.3. Patient with HSP and aCL

Fig.4. Painful nodules and purpuric plaqes in a patient with cPAN and aCL

We investigated 7 patients with MB and found that two of them had high titters aCL but only of IgM isotype.

Our patients with elevated aCL with cPAN were three. They had no systemic involvement and therapy with prednisone was successful (**Fig. 4**). The majority of patients with vascular endothelial damage demonstrate aCL with positive correlation between aCL and livedo reticularis.

We observed 7 patients with SLE and positive aCL. This is not uncommon as aCL

are positive in 40% in SLE. All our patients had ulcerations on the extremities and one of them had it on the ear, which is rarely seen.

We tested 12 cases with SSc for aCL and found elevated levels in 4 of them. An amputation of the thumb was required in one patient because of a digital gangrene (**Fig. 5**).

We followed 18 patients with LiV and found that 7 had positive aCL. Two of them developed thromboses years after they had been diagnosed as having LiV (thrombosis of the femoral vein and cerebral thromboembolism). We put the diagnosis APS in 5 of these patients (including the 2 cases above). However, ulcerations and scarring are recognized cutaneous manifestations of aCL and occlusion of the smaller dermal vessels in APS may result in the clinical picture of LiV.

We had 2 other cases with digital gangrene and one of them had high titters of IgGaCL and not reversible ischemic changes (**Fig. 6**). An amputation of the gangrenous digits was necessary. The combination of thrombotic and inflammatory defects compromise tissue perfusion and lead to tissue necrosis.

Fig.5. Amputated thumb in a patient with SSc and aCL

Fig.6. Gangrenous digits in a patient with positive aCL

Discussion

Clinical observations showed that high serum levels of aCL aggravates skin symptoms, but are not related to advanced systemic involvement and poor prognosis for our patients with vasculitides and vasculopathies. ACL activate endothelial cells in both occlusive and inflammatory vascular diseases by inducing a proinflammatory and procoagulantphenotype resulting in high thrombogenetic activation.

The association of aCL and cutaneous necrotizing vasculitis demonstrates significant tissue ischemia and necrosis (uncommon in vasculitis alone) and lead to dramatic and complicated course of the disease. ACL possibly favor the diminution of blood flow and thrombi form more easily at the site of vasculitis-induced endothelial injury when a coagulopathy exists [3].

The aCL pathogenetic role in Henoch Schonlein purpura is quite controversial. Based on earlier observations it is suggested that aCL are often co-incidentally associated with HSP with no pathogenetic events of occlusive vasculopathy [6]. The presence of IgAaCL may be used as an indicator of adult HSP thus being an indicator of its activity [2]

The frequency of aCL in Morbus Behcet ranges between 8 and 50% in different publications. ACL are pointed as markers of endothelial damage in MB associated with retinal vasculitis [10] and are linked to the risk of development of cutaneous vasculitis and erythema nodosum. According to a study including 128 patients with MB, aCL have not a primary role in MB and regional determinants - environmental or genetic, might also play a role in controlling aCL production [8]. We suppose aCL may cause inflammatory tissue reaction in MB due to acute infection or hypersensitivity to bacterial antigens.

The presence of aCL in systemic lupus erythematosus patients is not uncommon as aCL are positive in 40% in SLE. Having in mind our cases we may say aCL in SLE represent significant tissue ischemia and necrosis with deep skin ulcerations on acral sites. Although vasculitis is not considered to be a common manifestation in systemic sclerosis, it is suggested that vasculitis involving small vessels is present histologically if not always clinically in the SSc patients with severe ischaemia [4]. It is still unclear wheather aCL could after a certain period of time lead to vasculopathy or these are the vasculitic changes that lead to the formation of aCL. Or it is possible that aCL in such cases do not have a pathogenetic role but should be interpreted as a marker of vasculopathy. ACL may have a role in the genesis of vascular involvement related to SSc - pulmonary arterial hypertension and digital infarcts.

Livedo vasculitis-like ulcers may be a clinical sign of APS and should raise suspicion for it [7]. We can also speculate of a predictive importance of aCL in LiV for development of thrombosis. It would seem that LiV may represent a clinical sign of a heterogeneous group of diseases that cause an occlusive vasclopathy such as APS or that may occur as a sole entity [5].

Conclusions

The aCL antibodies are found to activate endothelial cells by inducing a proinflammatory and procoagulantphenotype resulting in high thrombogenetic activation in both occlusive and inflammatory vascular diseases. Clinical observations showed that high levels of aCL aggravate skin symptoms, but are not related to advanced systemic involvement and poor prognosis. The presence of IgAaCLmay be used as an indicator of adult HSP activity due to their positive correlation with some clinical and laboratory markers of inflammation in the initial phase of the disease. All positive SLE patients represent skin ulcerations and necrosis on acral sites. Occlusion of the smaller dermal vessels in APS may result in the clinical picture of LiV and the suspicions of LiV as a manifestation of APS might be easily adopted.

References:

1. **Favaloro, E. J., R. Silvestrini**. Assessing the usefulness of anticardiolipin antibody assays: a cautious approach is suggested by high variation and limited consensus in multilaboratory testing. – *Am. J. Clin. Pathol*., **118**, 2002, 548–557.
2. **Gantcheva, M., I. Angelova**. Antiphospholipids in vasculitic patients. – *Clin. Dermatol.*, **17**, 1999, 619-24.
3. **Goeser, M. R., V. Laniosz, D. A. Wetter**. Practical approach to the diagnosis, evaluation, and management of cutaneous small-vessel vasculitis. – *Am. J. Clin. Dermatol.*, **15**, 2014, 299-306
4. **Herrik, A., P. K. Oogarah, A. J. Freemont, R. Marcuson, M. Haeney, M. Jayson.** Vasculitis in patients with Ssc and severe digital ischemia requiring amputation. – *Ann. Rheum. Dis*., **53**, 1994, 323-326.

5. **Hughes G. R.V.** Hughes syndrome/APS. 30 years on, what have we learnt? Opening talk at the 14th international congress on antiphospholipid antibodies Rio de Janeiro, October 2013. – *Lupus*, **23**, 2014,400–406.
6. **Monastiri, K., H. Selmi, B. Tabarki, M.Yacoub, T. Mahjoub T, A. S. Essoussi.** Primarily antiphospholipid syndrome presenting as complicated Henoch-Schonlein purpura. – *Arch. Dis. Child*, **86**, 2002, 132-133.
7. **Papi, M., B. Didona, M. Gantcheva**. PURPLE (atrophie blanche): clinical, histological and immunological study of twelve patients. – *J. Eur. Acad. Derm. Venereol.*, **9**, 1997, 129-133.
8. **Tokay, S., H. Direskeneli, S. Yardakul, T. Akoglu**. Anticardiolipin antibodies in Behcet diseases: a reassessment. – *Rheumatology*, **40**, 2001, 192-195.
9. **Wong, R. C**. Consensus guidelines for anticardiolipin antibody testing. – *Thromb. Res*., **114**, 2004, 559-571.
10. **Zivkovic, M., M. Zlatanovic, G. Zlatanovic, J. Djordjevic-Jocic, S. Cekic**. Anticardiolipin antibodies in patients with Behcet's disease. – *Bosn. J. Basic. Med. Sci*., **11**, 2011, 58-61

Institute of Experimental Morphology, Pathology and Anthropology with Museum
Bulgarian Anatomical Society

Acta morphologica et anthropologica, 25 (3-4)
Sofia ● 2018

Cytomorphological Alterations Induced by Simvastatin in Graffi Tumor Cells

Ani Georgieva[1], Reneta Toshkova[1], Veselina Uzunova[2], Rumiana Tzoneva[2]*

[1] *Institute of Experimental Morphology, Pathology and Anthropology with Museum, Bulgarian Academy of Sciences, Sofia, Bulgaria*
[2] *Institute of Biophysics and Biomedical Engineering, Bulgarian Academy of Sciences, Sofia, Bulgaria*

***** Corresponding author e-mail: georgieva_any@abv.bg

Statins are a group of lipid-lowering drugs widely used for treatment of hypercholesterolemia and known to reduce the risk of cardiovascular diseases. Recently, the statins have been gaining an increasing scientific interest due to their anti-inflammatory, immuno-modulatory, neuroprotective and anticancer effects. The present study aims to assess the antitumor activity of simvastatin on Graffi myeloid tumor cells. The effect of simvastatin on the viability of the tumor cells was studied by MTT assay. The alterations in the tumor cell morphology induced by the statin were analyzed by fluorescent microscopy after staining with acridine orange/ethidium bromide, DAPI and annexin V/propidium iodide. The results of the MTT test showed a significant and dose-dependent reduction of the viability of simvastatin-treated cells. Fluorescent microscopic analysis of Graffi myeloid cells exposed to simvastatin revealed morphological alterations typical for the apoptosis. These findings are in accordance with previous data indicating significant *in vitro* antitumor and proapoptotic activity of simvastatin and suggests that it is a promising drug candidate for cancer treatment.

Key words: statins, simvastatin, tumor, antitumor activity, apoptosis

Introduction

Statins are effective and safe cholesterol-lowering drugs, widely used for the treatment of dyslipidemia [1]. The statin family consists of eight members, some of which (mevastatine, lovastatin, simvastatin, pravastatin) are natural products derived from *Penicillium* and *Aspergillus* filamentous fungi and others (fluvastatin, rosuvastatin, atorvastatin, and pitavastatin) are chemically synthesized [6, 21]. The introduction of the statins into medical practice led to a significant reduction of morbidity and mortality associated with cardiovascular diseases [19, 21]. The molecular mechanism by which statins reduce cholesterol is well understood. It is known that statins decrease cholesterol concentrations by blocking the enzyme 3-hydroxy-3-methylglytaryl-coenzyme A (HMG-CoA) reductase. This enzyme catalyzes the conversion of HMG-CoA into mevalonate that is the rate-limiting step in the cholesterol biosynthesis pathway [8, 18].

Besides the cholesterol-lowering properties, statins exhibit many other beneficial pharmacological activities including anti-inflammatory and immuno-modulatory, neuroprotective and anticancer effects [9, 10]. The increasing interest in statins as potential anticancer agents has originated from several studies demonstrating a decreased cancer incidence in patients treated with statins [1, 10, 16, 17]. Consequently, a wide variety of experimental studies, as well as some clinical trials, has confirmed the noticeable antitumor effect of statins [3, 7, 13, 20]. Statins have been reported to exert antineoplastic activity by inhibition of tumor cell growth, induction of apoptosis, suppression of angiogenesis, repression of metastatic potential and stimulation of antitumor immunity [2, 17]. The exact molecular mechanism by which these drugs elicit their antitumor activity still remains unclear. It has been suggested that the changes in lipid metabolism initiated by the statins lead to inhibition of intracellular proliferative and survival signaling pathways and induction of apoptosis [2, 15].

The present study aims to assess the antiproliferative and proapoptotic activity of simvastatin on cell cultures derived from Graffi myeloid tumor in hamsters (GMTH). The tumor was originally induced by Graffi murine leukemia virus and adapted to grow in a solid form after subcutaneous inoculation in Syrian golden hamsters. GMTH is a transplantable, rapidly growing tumor with very aggressive behavior that never show a spontaneous regression. This experimental tumor and the cell cultures derived from it are reliable model systems for studying the antitumor effects of natural and synthetic chemical substances, showing precise and reproducible results [22].

Materials and Methods

Simvastatin. A stock solution of simvastatin (Sigma-Alrich) in DMSO was prepared and stored at 4ºC. Serial dilutions of the stock solution with cell culture growth medium were made and solutions with concentrations ranging from 1 to 100 μM were used in the experiments.

Cell cultures and cultivation. Cell cultures of Graffi myeloid cells were isolated from the solid tumor tissue of Syrian golden hamsters under aseptic conditions. The cells were grown as monolayers in 25cm^2 tissue culture flasks in RPMI-1640 medium containing 10% fetal bovine serum, 2 mM glutamine, 100 U mL^{-1} penicillin and 100 μg mL^{-1} streptomycin. The cultures were maintained in an incubator at 37ºC in a humidified atmosphere with 5% CO_2.

MTT-dye reduction assay. The *in vitro* antitumor activity of simvastatin was studied on Graffi myeloid tumor cells using the standard MTT-dye reduction assay, described by Mosmann [14]. Tumor cells in a density of 1×10^5 cells/mL RPMI-1640 containing 10% FBS were plated (100 μL/well) in 96-well microplates and allowed to adhere for 24 h. The cells were then treated with simvastatin at concentrations of 0.8, 1.6, 3.2, 6.4, 12.5 25, 50 and 100 μM for 24, and 48 h. Untreated tumor cells were used as negative controls. After simvastatin treatment, the culture medium was discarded and 100 μL of MTT solution with a concentration of 0.5 mg/mL were added to each well. The plates were incubated for 3h at 37.5°C in a humidified atmosphere and 5% CO_2. Formazan crystals were dissolved by adding 100 μL/well of an absolute ethanol/DMSO (1:1 v/v) solution and the absorption was measured using a microplate reader (TECAN, Sunrise TM, Groedig/Salzburg, Austria) at 540 nm.

Acridine orange/ethidium bromide double staining. Apoptotic cell morphology was assessed using acridine orange and ethidium bromide double staining according to standard procedures [11] with a minor modification [22]. Briefly, Graffi cells cultured on 13-mm-diameter cover glasses in 24-well plates were treated with 25μM simvastatin.

After 24 h of incubation, the glass coverslips were washed with phosphate buffer saline (PBS), equal volumes of fluorescent dyes AO (10 µg/mL) and EtBr (10 µg/mL) were added and the cells were immediately examined under fluorescent microscope (Leica DM 500B, Wetzlar, Germany).

DAPI staining. The alterations in the nuclear morphology of the Graffi cells induced by simvastatin were studied by fluorescent microscopy after staining with DNA binding dye 4′,6-Diamidine-2′-phenylindole dihydrochloride (DAPI). The tumor cells were seeded on glass coverslips in 24-well tissue culture plates at a concentration of 1×10^5/well, incubated overnight at 37°C and 5% CO_2 and then treated with 25µM simvastatin for 24 hours. The culture medium was poured off and the coverslips were fixed with methanol. The cells were incubated for 15 minutes in 1 µg/mL DAPI in methanol in the dark, mounted with glycerol on microscope slides and examined under a fluorescence microscope (Leica DM 5000B, Wetzlar, Germany).

Annexin V and pripidium iodide (PI) double staining. Apoptosis-inducing ability of simvastatin was assessed using annexin V Apoptosis Detection Kit: sc-4252 AK (Santa Cruz Biotechnology, Inc. USA) according to manufacturer's instructions. Briefly, glass cover slips were placed on the bottom of each well in 24-well plates. Graffi cells were seeded on glass coverslips (1×10^5 cells/well), incubated overnight and treated with 25µM simvastatin for 24 h. The culture medium was removed, the glass coverslips were washed twice with PBS (pH 7.4) and fixed with 3% paraformaldehyde. The cells were washed with distilled water and incubated in a solution containing 1 µg/ml PI and 1 µg/ml annexin V-FITC for 10 min, in the dark, at room temperature. After staining the coverslips were mounted with glycerol on slides and analyzed using fluorescence microscope Leica DM 5000B.

Statistical analysis. Statistical analysis was performed by One-way ANOVA followed by Bonferroni's post hoc test (GraphPad Prism software package). $p<0.05$ was accepted as the lowest level of statistical significance. All results are presented as a mean ± SD.

Results and Discussion

The *in vitro* antiproliferative activity of simvastatin on the Graffi myeloid tumor cells was evaluated by MTT test after 24 and 48 hours of exposure. The results from the assay showed that the tested statin induce a concentration-dependent decrease of the tumor cell growth and viability (**Fig. 1**).

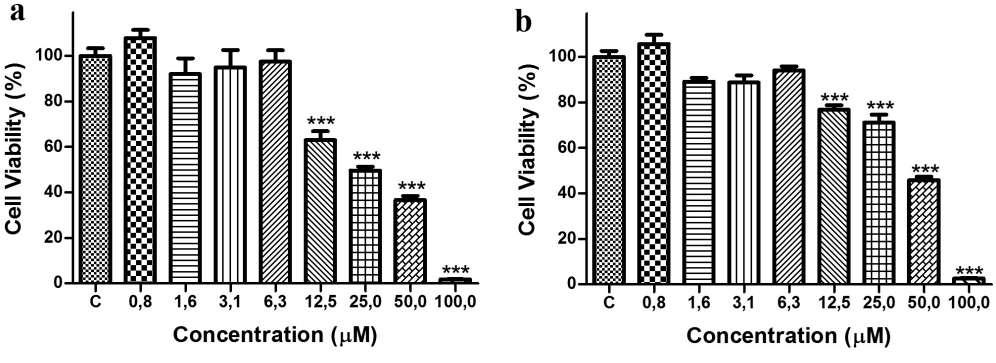

Fig. 1. Antiproliferative effect of simvastatin on Graffi myeloid tumor cells after 24 (a) and 48 (b) hours of treatment. MTT-dye reduction assay; ***$p<0.001$, compared to the untreated control.

As evident from the presented data, statistically significant reduction of the cell viability of simvastatin-treated cells ($p < 0.001$) as compared to the untreated control was established at all concentrations higher than 10 μM. The inhibition of the tumor cell growth was more clearly expressed after 24h as compared to 48h exposure. The IC_{50} values of simvastatin, determined after 24 and 48 hours of treatment were 24.67 μM and 36.90 μM, respectively.

Fluorescent microscopy of acridine orange/ethidium bromide stained cells showed that simvastatin induced cytopathic alterations such as shrinkage, rounding up and detachment of the cells and loss of monolayer integrity. In contrast to the untreated cell that were uniformly green stained (**Fig. 2a**), some of the simvastatin-treated cells showed granular yellow-green fluorescence or orange staining (**Fig. 2b**) that are characteristic for the early and late apoptosis, respectively.

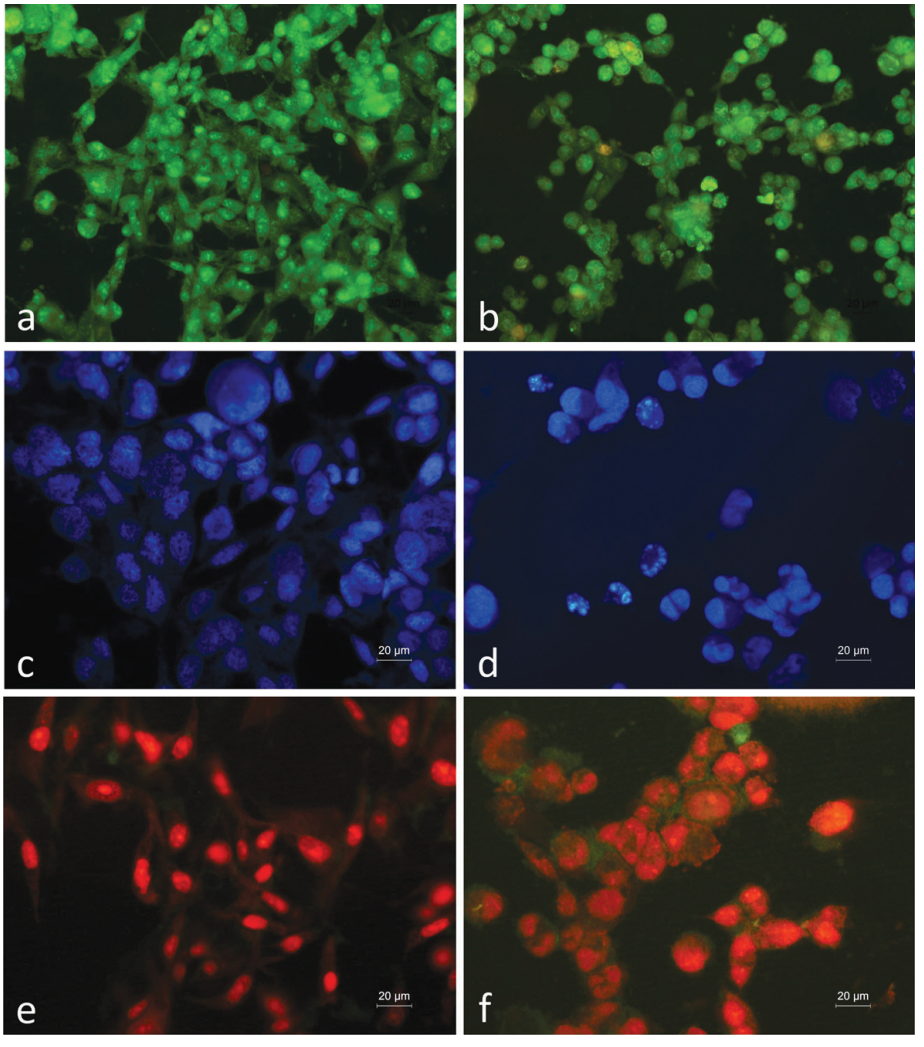

Fig. 2. Fluorescent microscopy images of the morphological alterations induced by simvastatin in Graffi myeloid tumor cells.
a-, c-, d- control cell cultures; b- ,d-, f- cell cultures exposed to 25 μM simvastatin for 24h; a-, b- Acridine orange/ethidium bromide staining**;** c-,d- DAPI staining; e-, f- Annexin V-FITC and propidium iodide staining.

Simvastatin-induced alterations in the nuclear morphology of the tumor cells were analyzed after DAPI staining. The nuclei of the control cells were homogenously stained with DAPI (**Fig. 2c**), whereas cancer cells treated with simvastatin showed an altered nuclear staining pattern with condensed chromatin, fragmented nuclei and apoptotic bodies (**Fig. 2d**) that are hallmarks of the apoptotic cell death.

The apoptosis-inducing ability of simvastatin was confirmed by Annexin V-FITC/PI staining. One of the earlier events of apoptosis includes translocation of membrane phosphatidylserine from the inner side of the plasma membrane to the surface. The green fluorescence observed in simvastatin-treated cells (**Fig. 2f**), but not in controls (**Fig. 2e**) indicates the binding of FITC-labeled Annexin V to the exposed phosphatidylserine and is an evidence for apoptosis.

A number of reports have shown that simvastanin inhibits proliferation and induces apoptosis in various cancer cell types including leukemic cells [23], breast [13], cervical [5], prostate [13], colon [4, 13], liver [13], pancreatic [13], renal [7], lung [12, 13] and skin [13] cancer cells. Our results complement and confirm the previous findings and indicate that this statin exhibits pronounced antineoplastic effect against myeloid tumor cells.

Conclusion

Simvastatin induced a significant and dose-dependent reduction of cell viability of Graffi myeloid tumor cells. Apoptotic cell death is one of the main mechanisms of the antineoplastic activity of simvastatin. Presented results indicate that simvastatin is a promising drug candidate for treatment of hematologic malignances.

Acknowledgements: This work was supported by Grant DFNI BO2/5-2014 from the Bulgarian National Science Fund of Ministry of Education and Science and Grant No BG05M2OP001-2.009-0019-C01/02.06.2017 by the Operational Programme "Science and Education for Smart Growth" 2014-2020, co-financed by the European Union through the European Structural and Investment Funds.

References

1. **Ahern, T. P., T. L. Lash, P. Damkier, P. M. Christiansen, D. P. Cronin-Fenton.** Statins and breast cancer prognosis: evidence and opportunitie. – *Lancet Oncol.,* **15**(10), 2014, 461-468.
2. **Apostolova, S., R. Toshkova, A. Momchilova, R. Tzoneva.** Statins and alkylphospholipids as new anticancer agents targeting lipid metabolism. – *Anti-Cancer Agents Med. Chem.*, **16**(12), 2016, 1512-1522.
3. **Cardwell, C. R., B. M. Hicks, C. Hughes, L. J. Murray.** Statin use after colorectal cancer diagnosis and survival: A population-based cohort study. – *J. Clin. Oncol.*, **32** 2014, 1-11.
4. **Cho, S. J., J. S. Kim, J. M. Kim, J. Y .Lee, H. C. Jung, I. S. Song.** Simvastatin induces apoptosis in human colon cancer cells and in tumor xenografts,and attenuates colitis-associated colon cancer in mice. – *Int. J. Cancer.*, **123**(4), 2008, 951-957.
5. **Crescencio, M. E., E. Rodríguez, A. Páez, F. A. Masso, L. F. Montaño, R. López-Marure.** Statins inhibit the proliferation and induce cell death of human papilloma virus positive and negative cervical cancer cells. – *Int. J. Biomed. Sci.*, **5**(4), 2009, 411.
6. **Dulak, J., A. Jozkowicz.** Anti-angiogenic and anti-inflammatory effects of statins: relevance to anti-cancer therapy. – *Curr. Cancer Drug Targets*, **5**(8), 2005, 579-594.
7. **Fang, Z., Y. Tang, J. Fang, Z. Zhou, Z. Xing, Z. Guo, X. Guo, W. Wang, W. Jiao, Z. Xu, Z. Liu.** Simvastatin inhibits renal cancer cell growth and metastasis via AKT/mTOR, ERK and JAK2/STAT3 pathway. – *PLoS One*, **8**(5), 2013, 1-13.

8. **García-Ruiz, C., A. Morales, J. C. Fernández-Checa.** Statins and protein prenylation in cancer cell biology and therapy. – *Anticancer Agents Med. Chem.,* **12**(4), 2012, 303-315.
9. **Goldstein, L. B.** Statin therapy should be discontinued in patients with intracerebral hemorrhage. – *Stroke*, **44**, 2013, 2058-2059.
10. **Hindler, K., C. S. Cleeland, E. Rivera, C. D. Collard.** The role of statins in cancer therapy. – *Oncologist*, **11**(3), 2006, 306-315.
11. **Ibrahim, S., A. Wahab, A. B. Abdul, A. S. Alzubairi, M. M. Elhassan, S. Mohan.** In vitro ultramorphological assessment of apoptosis induced by zerumbone on (HeLa). – *J. Biomed. Biotechnol.*, 2009, Article ID 769568.
12. **Khanzada, U. K., O. E. Pardo, C. Meier, J. Downward, M. J. Seckl, A. Arcaro.** Potent inhibition of small-cell lung cancer cell growth by simvastatin reveals selective functions of Ras isoforms in growth factor signalling. – *Oncogene*, **25**(6), 2006, 877-887.
13. **Menter, D. G., V. P .Ramsauer, S. Harirforoosh, K. Chakraborty, P. Yang, L. Hsi, R. A. Newman, K. Krishnan.** Differential effects of pravastatin and simvastatin on the growth of tumor cells from different organ sites. – *PLoS One*, **6**(12), 2011, 1-13.
14. **Mossman, T.** Rapid colorimetric assay for cellular growth and survival: application to proliferation and cytotoxicity assays. – *J. Immunol. Meths.,* **65**(1-2), 1983; 55-63.
15. **Sassano, A., L. C. Platanias.** Statins in tumor suppression. – *Cancer Lett.*, **260**(1-2), 2007, 11-19.
16. **Singh, S., P. Lewis, R. Roberts.** Chemopreventive strategies in hepatocellular carcinoma. – *Nat. Rev. Gastroenterol Hepatol.,* **11**(1), 2013, 45-54.
17. **Sleijfer, S., A. van der Gaast, A. S. Planting, G. Stoter, J. Verweij.** The potential of statins as part of anti-cancer treatment. – *Eur. J. Cancer*, 2005, **41**(4), 516-522.
18. **Stancu, C., A. Sima.** Statins: mechanism of action and effects. – *J. Cell. Mol. Med.,* **5**(4), 2001, 378-387.
19. **Stossel, T. P.** The discovery of statins. – *Cell*, **134**(6), 2008, 903-905.
20. **Sun, L., M. C. Lin, C. L. Lin, S. N. Chang, J. A. Liang, I. C. Lin, C. H. Kao.** Statin use reduces prostate cancer all-cause mortalitya nationwide population-based cohort study. – *Medicine*, **94**(39), 2015, 1-6.
21. **Tobert, J. A.** Lovastatin and beyond: The history of the HMG-CoA reductase inhibitors. – *Nat. rev. drug discovery*, **2**, 2003, 517-526.
22. **Toshkova, R., N. Manolova, E. Gardeva, M. Ignatova, L. Yossifova, I. Rashkov, M. Alexandrov.** Antitumor activity of quaternized chitosan-based electrospun implants against Graffi myeloid tumor. – *Int. J. Pharm.*, **400**(1-2), 2010, 221-233.
23. **Van der Weide, K., P. M. Korthuis, F. Kuipers, E. G. de Vries, E. Vellenga.**. Heterogeneity in simvastatin-induced cytotoxicity in AML is caused by differences in Ras-isoprenylation. – *Leukemia*, **26**(4), 2012, 845-848.

Institute of Experimental Morphology, Pathology and Anthropology with Museum
Bulgarian Anatomical Society

Acta morphologica et anthropologica, 25 (3-4)
Sofia ● 2018

Zinc Salivary Levels in Healthy Individuals of Bulgarian Population

Irena Ivanova[1], Vlayko Vodenicharov[2], Bisera Atanasova[3], Konstantin Mitov[4]*

[1] *Department of Clinical Laboratory, St. Ivan Rilski University Hospital, Medical University of Sofia, Bulgaria*
[2] *Department of Hygiene, Medical Ecology and Nutrition, Medical Universityof Sofia, Bulgaria*
[3] *Department of Clinical Laboratory and Clinical Immunology, Alexandrovska Hospital, Medical University of Sofia, Bulgaria*
[4] *Departments of Organization and Economics of Pharmacy, Medical University of Sofia, Bulgaria*

*Corresponding author e-mail: irena.dimitrova@gmail.com

The main goal of this study is to assess zinc (Zn) salivary levels in healthy Bulgarian individuals. Totally 40 healthy volunteers have been investigated – 31 males and 9 females. Zn is measured in morning saliva collected in Saliveti tubes, Sarstedt. After centrifugation, the saliva is diluted 1: 2 with 1%HNO_3 and Zn is measured by flame atomic absorption spectrometry (AAnalyst 400, Perkin-Elmer, with deuterium correction). Mean Zn salivary levels are 1.43 ± 0.57μmol/ L for all studied individuals and higher levels in females (1.76 ± 0.56 μmol / L) than males (1.36 ± 0.55 μmol/L) with no significant difference (p = 0.076). Our previous studies establish significantly higher serum Zn levels in females (13.09 ± 2.25 μmol/l) than in males (12.45 ± 3.58 μmol/l). It seems likely that salivary Zn levels follow similar biological gender variation, as serum levels do.

Key words: saliva, zinc, salivary omics

Introduction

Saliva is composed of salivary glands secrets, cellular debris, upper respiratory tract fluid and microorganisms in the oral cavity [3]. Saliva testing for monitoring and diagnosis of both oral and systemic disorders is a challenge in accordance with the contemporary development of "omics" sciences. Research applications are directed to dental diseases and evaluation of hormonal, neurological and emotional status, and human behavior [2, 3]. Essential micronutrients copper (Cu) and zinc (Zn), simultaneously with salivary cortisol and other laboratory findings as adrenocorticotropic hormone, catecholamines and various cytokines, could be useful stress biomarkers [3]. Zn with neurotransmission and receptor functions is involved in mental health [2]. Cu and Zn are suggestive to participate in sleep durations due to the fact that they are antagonists of the sleep-mediated N-methyl-D-aspartate glutamate (NMDA) receptor [12]. Systemic zinc supplementation may alter salivary stress hormone levels, particularly these of cortisol [2].

The interest on saliva as a biological specimen is provoked by non-invasive way of collection and large enough sample volume [3]. Analysing of salivary samples could serve as an aspect in laboratory assessment of hormonal, emotional and immunological status and also dental health. Knowledge on the metabolic relations of trace elements in different body fluids could be of benefit in medicine. Specific salivary pathological findings could be compared to those in other fluid matrixes. "Omics" development of science and, in particular salivary omics (genomics, proteomics and metabolomics) is associated with the introduction of new biomarkers in clinical practice [9]. In this sense, salivary metallomics is definitely a modern perspective.

Zinc has a dual nature in human body. It is essential for life as component of various metalloenzymes with physiological significance for immune system, cell division and growth processes, reproductive system, etc. From the other hand, the element is cytotoxic when accumulated in high concentrations [6, 8]. Data about salivary levels of Cu, Zn and Fe as biomarkers in oral carcinogenesis are provided [11]. Recent observations underline the significance of trace elements in saliva, particularly Cu, Zn and Fe, as markers for the effects of the social stress [10].

The main goal of this study is to evaluate salivary zinc levels in healthy individuals of Bulgarian population.

Materials and Methods

The study comprises 40 volunteers (males:females = 31:9) with no evidence of anemia and impaired glucose tolerance. A signed informed consent form of all participants has been obtained. Non-stimulated salivary samples are collected in Salivette tubes-Sarstedt, after 2-hours pause in food and liquid intake and cigarette smoking prior to the saliva release. The samples are centrifuged at 2500 rpm for 10 min at room temperature and the supernatants are stored at -80°C until the analyses. Saliva samples are diluted 1:2 with 1% nitric acid immediately before the measurement. Zn levels are measured by flame atomic absorption spectrophotometry (AAnalyst 400, Perkin-Elmer) with a deuterium background corrector. All samples are determined in one run to minimize the analytical variation. The analyses are performed in Clinical Laboratory of St. Ivan Rilski University Hospital, Medical University of Sofia, in 2017. The results are statistically processed by MED CALC program.

Results and Discussion

Zn levels in saliva are presented in **Table 1**. Data are not normally distributed in both groups of males and females.

Table 1. Descriptive statistics and distribution analyses

Zn Saliva µmol/L	**Gender**								**Total**			
	Males				**Females**							
	n	Mean	SD	Distribution	n	Mean	SD	Distribution	n	Mean	SD	Distribution
	31	1.36	0.55	0.0038	9	1.76	0.56	<0.0001	40	1.43	0.57	0.0345

The established mean values for zinc in saliva are 1.43±0.57 μmol/L. Comparing to previously published results of other authors, zinc concentrations in the present study are the lowest (**Table 2**). The reasons for this observation could be multifactorial: diets, soil contents, age of participants or analytical variations.

Table 2. Salivary Zn concentration in comparison to the data of other studies

	Present study, 2017	**Wang, D. et al., 2008 [13]**	**Erkekoglu, P. et al, 2016 [2]**	**Mehmetoğlu, I. et al., 2013 [7]**	**Jassim A. M. N. etal., 2016 [5]**
Zn Saliva μmol/L	1.43±0.57	3.97±2.019	2.57±1.90	4.36±3.36	16.24±0.73
Method for determination	AAS	ICP-MS	Colorimetric	AAS	AAS

- AAS – Atomic absorption spectrophotometry
- ICP-MS – Inductive Coupled plasma mass spectrometry

The Mann-Whitney test points no statistically significant difference between the levels of salivary Zn depending on gender: p=0.0776. Higher levels are established in females than in males. One limitation of the present study is the limited numbers of the included individuals. In any case, eventual gender variation must be confirmed by enough numbers of individuals in both studied groups. Gender and age are widely known biological factors for variation of trace element levels in human body [8]. Our previous observations for Bulgarian population reveal higher serum Zn levels in women (13.09±2.25 μmol/l) than in men (12.45±3.58 μmol/l) with significant statistical difference ($p < 0.01$) [4]. It seems likely that the salivary levels follow the same model for gender distribution.

Salivary diagnostics becomes more and more a reality nowadays. But it must face to certain challenges: standardization of preanalytical phase; measurement with acceptable sensitivity, establishment of factors for variability that define biochemical profile of saliva with potential for clinical use.

Conclusion

Saliva as a specimen in clinical laboratory practice might complement and enrich the disease management.

***Acknowledgements*:** This study is funded by Medical University of Sofia, Project № 311/ 15.01. 2015.

References

1. **Alghadir, A. H., S. A. Gabr, E. Al-Eisa.** Effects of physical activity on trace elements and depression related biomarkers in children and adolescents. – *Biol. Trace Elem. Res*., **172**(2), 2016, 299-306.
2. **Erkekoglu, P., Y. Üçkardeş, E. N. Özmert, B. K. Gumusel, K. Yurdakök**. The effect of zinc supplementation on salivary cortisol levels and salivary amylase activity in primary school children with low socioeconomic status. – *MOJ. Toxicol*., **2**(2), 2016, 00032.

3. **Humphrey, S. P., R. T. Williamson**. A review of saliva: normal composition, flow, and function. – *J. Prosthet. Dent*., **85*(2)***, 2001, 162-169.
4. **Ivanova, I., B. Atanasova, A. Ilieva, K. Tzatchev**. Serum copper and zinc concentrations in healthy individuals of Bulgarian population. – *Clin. Chem. Lab. Med.*, **52**, 2014, Special Suppl, pp S1 – S1760 2014.
5. **Jassim, A**. **M. N., M.T. Mohammed, S. A. Farhan, O. M. Ahmed.** Investigation of zinc concentrations in serum and saliva of obese. – *Int. J. Chem. Sci.,* **14**(4), 2016, 1857 – 1864.
6. **McClain, C. J., M. L. McClain, M. G. Boosalis., B. Henning**. Zinc and the stress response. – *Scand. J. Work Enviorn. Health*, **1**, 1993, suppl. 132-133.
7. **Mehmetoğlu, I., F. H. Yerlikaya, S. Gönen**. Investigation of zinc concentrations in saliva of patients with thyroid diseases. – *Turk. J. Endocrinol. Metab.,* **17**, 2013, 1 – 4.
8. **Mocchegiani, E., R. Javier, M. Malavolta, L. Costarelli, R. Giacconi, L. E. Diaz, A. Marcos.** Zinc: dietary intake and impact of supplementation on immune function in elderly. – *AGE*, **35**, 2013, 839-860.
9. **Nunes, L. A., S. Mussavira, O. S. Bindhu**. Clinical and diagnostic utility of saliva as a non-invasive diagnostic fluid: a systematic review. – *Biochem. Med*., **25**(2), 2015, 177-192.
10. **Sheibaninia, A**. The effect of social stress on salivary trace elements. – *Biol. Trace Elem. Res*., **162**(1-3), 2014, 58-63.
11. **Shetty, S. R., S. Babu, S. Kumari, P. Shetty, S. Hegde, A. Karikal.** Status of trace elements in saliva of oral precancer and oral cancer patients. – J. *Cancer Res. Ther.,* **11**(1), 2015, 146-149.
12. **Song, C.H., Y. H. Kim, K. I. Jung.** Associations of zinc and copper levels in serum and hair with sleep duration in adult women. – *Biol. Trace Elem. Res.,* **149**(1), 2012, 16-21.
13. **Wang, D., X. Du, W. Zheng.** Alteration of saliva and serum concentrations of manganese, copper, zinc, cadmium and lead among career welders. – *Toxicol. Lett.,* **176**(1), 2008, 40-47.

Institute of Experimental Morphology, Pathology and Anthropology with Museum
Bulgarian Anatomical Society

Acta morphologica et anthropologica, 25 (3-4)
Sofia ● 2018

Mast Cells in the Intrapulmonary Airways in Rats of Different Age

Ivelina Ivanova[1], Ivaylo Stefanov[1], Dimitrinka Atanasova[1,2]*

[1] *Department of Anatomy, Medical Faculty, Trakia University, Stara Zagora, Bulgaria*
[2] *Institute of Neurobiology, Bulgarian Academy of Sciences, Sofia, Bulgaria*

*Corresponding author e-mail: ivcho_84@abv.bg

The rat is one of the most frequently used species in experimental models regarding pulmonary fibrotic and allergic processes. The lack of data about the comparison between mast cell distribution in the different layers of intrapulmonary airways, interalveolar septa and pulmonary pleura in normalleft lung and that in right lung of rats at different ages motivated us to perform this study. Eighteen rats at the age of 20 days, 3 months and 1 year were used in the study. Tissue pieces were taken from both left and right lung. Sections were stained with Toluidine blue and Bismarck brown. Mast cell number, estimated per field (x200 with area of 0.163 mm^2), were specified for different layers of the intrapulmonary large and small bronchi, terminal and respiratory bronchioles, interalveolar septa and pulmonary pleura in both left and right lungs and age dependent peculiarities were identified.

Key words: lung, mast cell, rat

Introduction

The rat is widely used in experimental models regarding pulmonary fibrotic processes, hypoxia and allergic bronchoreactivity [9, 12, 13]. Mast cells (MCs) are one of the main cells involved in the pathophysiology of the mentioned processes, accompanied by increased number of these cells.

It is important to notice that the data about the MC distribution in rat lung are controversial. Some authors reported that in rat, the mast cell number decreased from large to small bronchi,and were not detected in the interalveolar septa [1, 2, 5]. In contrast, other authors established mast cell distribution in the alveolar septa in the same species [3, 6, 13].

Detailed information about the distribution of both metachromatic and serotonin positive mast cells in the intrapulmonary airways, interalveolar septa and pulmonary pleura of cranial lobe in rat right lunghas been reported in our previous study [6]. Metachromatic cytoplasmic granules of mast cells together with the histamine-producing capacity and the existence of membrane IgE receptors are fundamental properties of these cells. The metachromatic staining with cationic dyes,for example Toluidine Blue, at low pH enables the identification of glycosaminoglycans such as galactosaminoglycan and heparin, produced by mucosal mast cells (MMCs) and connective tissue mast cells

(CTMCs) [4].Enerback et al. [4],reported that the granules of the rat MMCs, like those of the few CTMCs in the subserosal layer of the organs, stained strongly with Toluidine Blue.

The aim of the study was to compare the number of mast cells in the different layers of intrapulmonary airways, interalveolar septa and pulmonary pleura in both left and right lungs of normal rats at different ages.

Materials and Methods

Animals

In this study we used six male Wistar rats for each age group (20 day-old, 3 month-old and 1 year old), housed under a 12/12 h light/dark cycle and given a standard diet and tap water *ad libitum*. The procedures were performed according to the Bulgarian laws about the animal care (Ordinance 20 of 01.11.2012 on the minimum requirements for the protection and welfare of experimental animals and requirements to objects for use, cultivation and/or delivery) and the Directive 2010/63/EU of the European Parliament and of the Council of 22 September 2010 on the protection of animals used for scientific purposes.The animals were anesthetized with ketamine and xylasine (90 mg/kg + 10 mg/kg, IP), then transcardially perfused with4% paraformaldehyde in phosphate-buffered saline (PBS).

The cranial and caudal lobes of right lung as well as cranial part of left lung from each animal were removed, immersed in the same fixative for 24 h, washed in PBS, dehydrated, cleared in xylene and embedded in paraffin.

Histochemistry for detection of metachromatic mast cells using Toluidine blue

Cross sections of 5 μm thickness from the tissue specimens were cut and mounted on gelatin-coated glass slides, deparaffinised in two changes of xylene, and rehydrated through descending ethanol concentrations. The sections were immersed in buffered solution of Toluidine blue (pH=3).

After Toluidine blue staining additional Bismarck brown staining was performed on serial sections in order to confirm the mast cell presence. The adjacent sections were deparaffinised, rehydrated through descending ethanol concentrations and immersed in a staining solution of 500 mg Bismarck brown in 80 ml 96% ethanol and 10 ml 1N HCL for two hours at room temperature. After three changes of 70% ethanol for differentiation, the sections were counterstained by immersion in Mayer`s haematoxylin, then rinsed in tap water, cleared in xylene and coverslipped in Entelan [10].

Statistical analysis

The number of mast cells was estimated on two microscopic fields (X200 with area of 0.163 mm^2) from the sections of the three lung lobes from each animal using a light microscope (LEICA DM1000) equipped with a digital camera (LEICA DFC 290). The data for mast cells density (number per field) were processed using GraphPad Prism 6 for Windows (GraphPad Software, Inc., USA) via one-way ANOVA followed by Tukey-Kramer's post-hoc test. P-values of less than 0.05 were considered statistically significant. The data are presented as mean ± SD.

Results

In this study toluidine blue staining enabled to mark and count metachromatic MCs in the different layers of intrapulmonary airways as well as in pulmonary pleura from

the left lung (LL), cranial (CrLRL) and caudal lobes of right lung (CaLRL) in rats at different ages (**Fig 1**). To confirm the presence of MCs, Bismarck brown staining was performed (**Fig 2**). In this regard, adjacent sections were used, where the same MCs were demonstrated by both methods (**Fig.1** and **Fig. 2**).

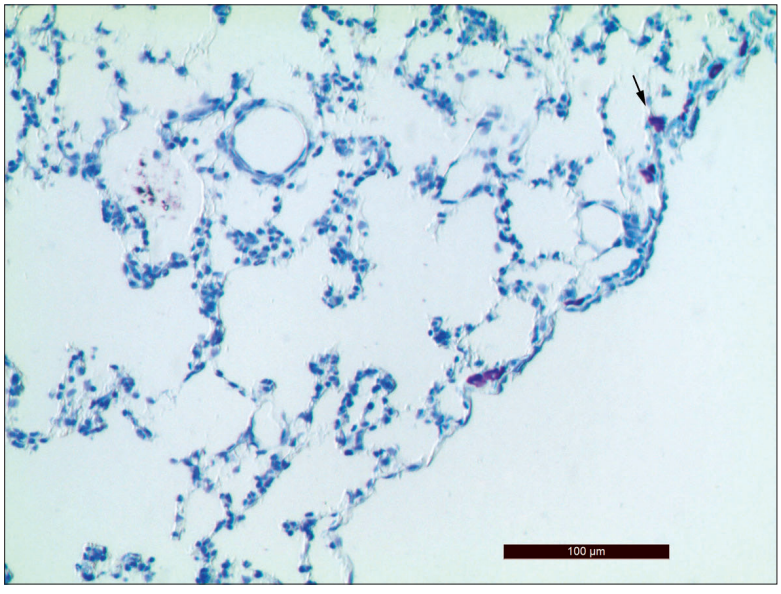

Fig. 1. Metachromatic MCs (arrow) in the visceral pleura of cranial lung lobe in rats at the age of 3 months.Toluidine blue staining. Bar = 100µm.

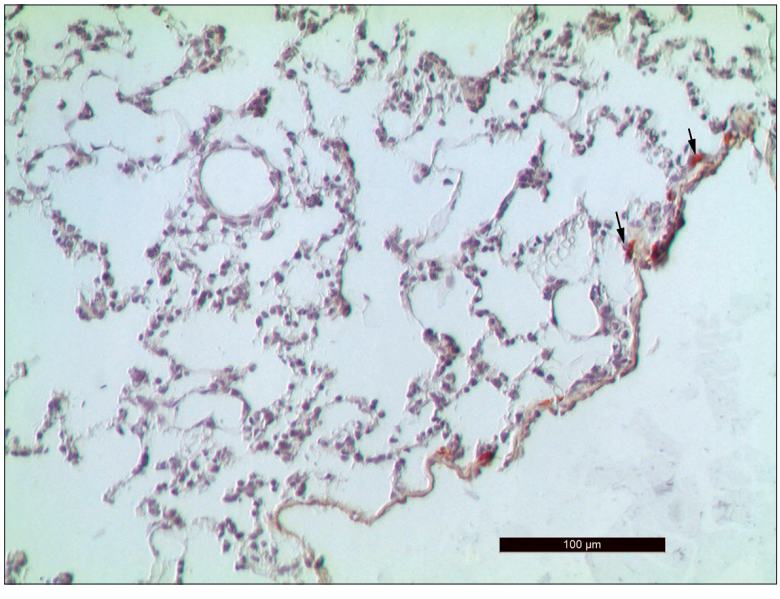

Fig. 2. MCs visualized by Bismarck brown staining (arrows) in the visceral pleura of cranial lung lobe in rats at the age of 3 months. Bar = 100µm.

In the rat, the intrapulmonary airways are devoid of cartilaginous structures; large bronchi represented those of the first bronchial generation and the others were considered to be small bronchi (second generation) which continue with the terminal and respiratory bronchioles. Mast cells were counted in the airways propria bordered by the base of the epithelium and muscular layer, also in the muscular and adventitial layer. In general, mast cells were located in lamina propria predominantly of large and small bronchi, but rarely in propria of bronchioles, near blood vessels in the adventitia. The most MCs were found in the adventitial and muscle layers of the airways, than in the propria. The least MCs were found in the respiratory bronchioles and interalveolar septa.

However some differences in the distribution of lung MCs were detected according to both: the place – left lung or cranial and caudal lobes of right lung and the age of animals.

I. Comparing the mast cell number in the wall of airways with different diameters, alveolar septa and pulmonary pleura in cranial lobe of rat right lung

I.1. In rats at the age of 20 days

After comparing the mast cell number in the airways with different diameters, alveoli and pulmonary pleura, the following results were detected:

In the whole wall of the airways of CrLRL from 20-day-old rats, the highest MC number was estimated in large bronchi (LBr) (14.50±2.6), followed by small bronchi (SBr) (2.9±0.5), interalveolar septa (1.5±0.52) and pleura (1.2±0.39). In terminal (TBol) and respiratory bronchioles (RBol), MCs were not detected. Significant difference between alveolar septa and pleura was not found.

In the different layers of LBr wall, the MC number observed in the propria (3.5±0.52) was significantly lower than in the adventitial (6.5±0.52) and muscular layer(5.5±0.52). MC amount in muscular layer was equal to that in adventitial layer.

In contrast to LBr, in the wall of SBr, MCs were not detected in the propria. Their number in muscular layer (1.17± 0.39) was equal to that in the adventitial layer (1.75±0.45) but was smaller than in the same layers of LBr.

I.2. In rats at the age of 3 months

Unlike 20-day-old rats, in the whole wall of the airways of cranial lobe of right lung from 3-month-old rats, the highest MC number was estimated in pleura (8.5±0.52), followed by LBr (6.08±0.51), SBr(3.75±0.45) and alveolar septa(1.25±045). Similar to 20-day-old rats, in terminal and respiratory bronchioles MCs were not observed. MC number in the muscle layer (4.83± 0.39) of LBr was significantly higher than in the same layer (1.17± 0.39) of small bronchi, but in adventitial layer (1.25± 0.45) of LBr their number was lower than in the small bronchi (2.5±0.51).

I.3. In rats at the age of 1 year

In this group of animals, like 3-month-old rats, MC number was highest in the pleura (10.50 ±0.52). MC amount in the whole wall of LBr(4.5±0.67) and SBr(4.0±0.42) as well as in terminal bronchioles(4.5±0.52) was similar but higher than in respiratory bronchioles(1.83± 0.39) and alveolar septa (1.83± 0.39). In the respiratory bronchiole wall and alveolar septa equal number of MCs was detected.

II. Comparing the mast cell number in the wall of airways with different diameters, alveoli and pulmonary pleura in caudal lobe of right lung

II.1. In rats at the age of 20 days

In the whole wall of the airways of caudal lobe of right lung from 20-day-old rats, the most MCs were estimated in LBr (5.5±0.52), but less – in the alveolar septa (1.5±0.52) and pleura (1.5±0.52) (with the same number of mast cell). We found more MCs in the muscle layer (4.00± 1.04) than in adventitial one (1.5±0.52). In SBr, terminal and respiratory bronchioles MCs were not detected.

II.2. In rats at the age of 3 month

The most MCs were estimated in pleura (10.50±0.52), followed by LBr (7.00±1.04) and SBr (4.67±1.16), terminal bronchioles (1.17±0.39) and alveolar septa (1.50± 0.52). In the propria of all airways and in the whole wall of respiratory bronchioles MCs were not observed. In the wall of LBr and SBr, the MC number was highest in the adventitial layer (5.50±0.52 and 3.08± 0.90,respectively),followed by that in muscle layer (1.5±0.52and 1.58±0.51, respectively). In terminal bronchioles these cells were located in the muscle layer (1.17±0.39) only.

II.3. In rats at the age of 1 year

MC number was highest in the pleura (9.00±1.04). MC amount in the wall of LBr (4.67± 0.49) and SBr(5.00±0.43) was similar but higher than alveolar septa (1.25±0.45). In the terminal and respiratory bronchioles`wall, MCs were not observed.

III. Comparing the mast cell number in the wall of airways with different diameters, alveoli and pulmonary pleura in left lung in rats

III.1. In rats at the age of 20 days

In the whole wall of the airways the highest MC number was estimated in LBr (10.08± 0.99), followed by SBr (2.17±0.38), alveolar septa (1.50±0.52) and pleura (1.08±0.29). In the alveolar septa and pleura the MC amount was almost the same. In the wall of terminal and respiratory bronchioles MCs were not detected. In the adventitial layer of LBr (5.50±0.52) MCs were lower than in propria (1.08±0.29) and muscle layer (3.5±0.52) but significantly more than in the adventitial layer of SBr (1.08±0.29).

III.2. In rats at the age of 3 month

The most MCs were estimated in pleura (8.5±0.52), followed by LBr (4.42±0.51) and SBr (3.50±1.57), terminal bronchioles (2.58±0.67) and alveolar septa (1.17±0.39). Like the caudal right lung lobe, in the propria of all airways and in the whole wall of respiratory bronchioles MCs were not observed.

Unlike the caudal right lung lobe, in the wall of LBr, the MC number was highest in the muscular layer (2.92±0.51), but in SBr and terminal bronchioles similar MC number was observed in the muscle (1.50±0.52 and 1.08±0.29, respectively) and adventitial layers (2.00± 1.04 and 1.50±0.52, respectively). The highest amount of MC was observed in the muscle layer of LBr than in the same layer of SBr and terminal bronchioles.

III.3. In rats at the age of 1 year

MC number was highest in the pleura (8.92±2.43), followed by the wall of LBr (6.50± 2.61) and SBr (3.42±0.67), terminal (1.33±0.65) and respiratory bronchioles (1.17±0.39), alveolar septa (1.58±0.51). There is not significant difference between the amount of MCs in the terminal and respiratory bronchioles, and alveolar septa as well. In the terminal bronchioles MCs were located in their adventitial layer only, but in the respiratory ones – in the muscle layer only.

Discussion

In this study, toluidine blue staining was successfully used for demonstration of metachromasia and identification of lung mast cells which is in agreement with the findings of Enerback et al. [4].The distribution of toluidine blue stained MCs in the wall of intrapulmonal airways as well as in the interalveolar septa and pulmonary pleura was compared between left lung and cranial and caudal lobes of the right lungs in rats at different ages, for the first time. To confirm the presence of MCs Bismarck brown staining was used, known as an alternative to the Toluidine blue staining [10]. For

that purpose, serial sections were used, where the same MCs were identified by both methods.

The localization of rat lung cells predominantly in the muscular and near the blood vessels of adventitial layer can be explained with the ability of these cells to synthesize mediators such as serotonin [6, 7]and nitric oxide [8], responsible for smooth muscle cell contraction and relaxation. This means that mast cells may regulate the function of the smooth muscle layer of airways with different diameters and the same layer of blood vessels.

Rat lung mast cells and their mediators are widely studied in experimental models regarding pulmonary fibrotic and allergic processes associated with increasing mast cell density [1, 2, 5]. But the information about the normal rat mast cell distribution in the left and right lugs and also in different lung lobes is scarce. In this regard, we undertook this study to establish the MC density in the different lobes of normal rat lungs that can be used as reference values. In general, we agree with the authors reported that in the rat, the mast cell number decreased from large to small bronchi [1, 2, 5].

The data about the mast cell distribution in rat lung are controversial, for example, some authors did not describe mast cell in the interalveolar septa [1, 2, 5]. The current study showed that single mast cells are located in the interalveolar septa in lungs of rats at different ages which confirm the results of other studies where the same mast cell distribution was described [3, 6, 13].

Based on both the results of studies above and our findings we tried to give more detailed data regarding the distribution of lung mast cells in normal rat. Firstly, the normal distribution of mast cells in the different layers of the airways` wall, pulmonary parenchyma and visceral pleura in left and right lungs was elucidated; secondly, lung MC distribution in rats at different ages was established; thirdly, it was clarified whether MCs localize in the interalveolar septa of normal rat lungs or not.

Conclusions

The mast cell populations in the left and right lung of the rat are different in terms of both their distribution along the bronchial tree and visceral pleura, and their distribution during the ages. Our findings could be very useful in planning experimental morphological studies using rat lungs. The results showed that in such studies the same parts of lungs should be collected from the control and experimental animals to be sure that the accurate results will be received.

Acknowledgements: I would like to thank to scientific project number 13/2017, Medical Faculty, Trakia University, Stara Zagora, for delivering of animals for this study.

References

1. **Ahlstedt, S., G. Smedegard, H. Nygren, B. Bjorksten.** Immune responses in rats senitized with aerosolized antigen. – *Int. Arch. Allergy Immunol.*, **72**, 1983, 71-78.
2. **Bachelet, C. M., J. F. Bernaudin, J. Fleury-Feith.** Distribution and histochemical characterization of pulmonary mast cells in the rat and guinea pig. – *Int. Arch. Allergy Immunol*, **87**, 1983, 225-229.
3. **Bienenstock, J., D. Befus, J. Denburg, T. Goto, T. Lee, H. Ot-suka, F. Shanahan.** Comparative aspects of mast cell heterogeneity in different species and sites. – *Int. Arch. Allergy Appl. Immunol.,***77**, 1985, 126-129.

4. **Enerback, L., S. O. Kolset, M. Kusche, A. Hjerpe, U. Lindahl.** Glycosaminoglycans in rat mucosal mast cells.– *J. Biochem.*, **227**, 1985, 661-668.
5. **Goto, T., D. Befus, R. Low, J. Bienenstock.** Mast cell heterogeneity and hyperplasia in bleomycin-induced pulmonary fibrosis of rats. – *Am. Rev. Resp. Dis*., **130**, 1984, 797-802.
6. **Ivanova, I., N. S. Tomov, N. D. Dimitrov, D. Y. Atanasova, D. Sivrev, I. S. Stefanov.** Distribution of serotonin positive mast cells in the intrapulmonary airways of rats. – *Compt. Rend. Bulg. Acad. Sci*.,(in press).
7. **Keith, I., R. Day, S. Lemaire, I. Lemaire.** Asbestos-induced fibrosis in rats: increase in lung mast cells and autacoid contents. – *Exp. Lung Res*., **13**, 1987, 311-327.
8. **McCauleys, S. D., M. Gilchrist, A. D. Befus.** Nitricoxide: a major determinant of mast cell phenotype and function. – *Mem. Inst. Oswaldo Cruz, Rio deJ aneiro*, **100**(1)**,** 2005, 11-14.
9. **Pearce, F. L., H. Ali, K. E. Barrett, A. D. Befus, J. Bienenstock, J. Brostoff, M. Ennis, K. C. Flint, B. Hudspith, N. M. Johnson, K. B. P. Leung, P. T. Peachell.** Functional characteristics of mucosal and connective tissue mast cells of man, the rat and other animals. – *Int. Arch. Allergy Immunol*, **77**, 1985, 274-276.
10. **Tomov, N., N. Dimitrov.** Modified bismarckbrown staining for demonstration of soft tissue mast cells. – *Trakia Journal of Sciences*, **15** (3), 2017, 195-197.
11. **Uslu, S., M. Yörük.** A morphological and histometric study on the distribution and heterogeneity of mast cells found in lungs and trachea of van cats. – *AnkaraÜniv. Vet. Fak. Derg.*, **62**, 2015, 87-91.
12. **Veerappan, A., N. J. O'Connor, J.Brazin, A. C. Reid, A. Jung, D. McGee, B. Summers, D. Branch-Elliman, B. Stiles, S.Worgall,R. J. Kaner,** R. **B. Silver.** Mast cells: A pivotal role in pulmonary fibrosis.– *DNA and Cell Biology*, **32** (4), 2013.
13. **Williams, D., J. M. Kay Heath, P. Smith.** Lung mast cells in rats exposed to acute hypoxia, and chronic hypoxia with recovery. – *Thorax*, **32**, 1977, 287-295.

Institute of Experimental Morphology, Pathology and Anthropology with Museum
Bulgarian Anatomical Society

Acta morphologica et anthropologica, 25 (3-4)
Sofia ● 2018

Protein YKL-40 in Cerebrospinal Fluid in Traumatic Brain Injury

Maria Kazakova[1], Georgi Pavlov[2,5], Dorian Dikov[3], Kiril Simitchiev[4], Valentin Dichev[1,6], Chavdar Stefanov[2,5], Victoria Sarafian[1,6]*

[1] *Department of Medical Biology, Medical Faculty, Medical University – Plovdiv*
[2] *Department of Anesthesiology, Emergency and Intensive Care Medicine, Medical Faculty, Medical University – Plovdiv*
[3] *Department of General and Clinical Pathology, Medical Faculty, Medical University – Plovdiv*
[4] *Department of Analytical Chemistry and Computer Chemistry, Faculty of Chemistry, University of Plovdiv*
[5] *University Hospital "St. George" Plovdiv*
[6] *Technological Center for Emergency Medicine, Plovdiv*

* Corresponding author e-mail: kazakova25@abv.bg

Traumatic brain injury (TBI) is one of the leading causes of non-natural death in younger adults. High levels of YKL-40 are discussed to serve as a biomarker in acute and chronic inflammatory diseases. The aim of our study was to examine the expression and dynamics of YKL-40 secretion in TBI patients. Cerebrospinal fluid (CSF) and plasma samples were collected from nineteen patients with TBI – on the 24th and 96th hour after injury. ELISA and immunocytochemical methods were performed.
We determined that the CSF levels of YKL-40 were significantly lower compared to plasma concentrations on the 24th and 96th hour. No significant change between CSF levels of YKL-40 on the 24th h after TBI compared to the control group was found. The presence of YKL-40 protein in the cytoplasm of polymorphonuclear leukocytes was detected as a strong diffuse reaction. We suggest that YKL-40 levels reflect the inflammatory process and could provide new information about its dynamics in patients with TBI.

Key words: traumatic brain injury, YKL-40, biomarker

Introduction

Traumatic brain injury (TBI) is a global health problem, characterized by high frequency of occurrence, high mortality rate, severe and long lasting disability in patients who have survived [12]. There is a lack of accurate and standardized panel of biomarkers for assessment of progression and disease outcome. Severety of TBI is defined by clinical prognostic models. Brain damage following head injury may occur as a direct physical effect at the moment of action of the traumatic agent (skull fractures, hematoma, cerebral

contusion). It is referred to primary brain injury and leads to deformation and damage of brain tissue due to exceeding its structural tolerance [19].

Complications after the trauma are defined as a secondary brain damage. They happen within hours to days and are performed as brain-barrier alteration, oxidative stress [5], exocytotoxicity [13], mitochondrial dysfunction [14]. Inflammation is also an accompanying process [10]. The inflammatory process is mediated by the activation of cells (astrocytes, glial cells, macrophages and lymphocytes) and production of pro- and anti-inflammatory cytokines and chemokines [1].

YKL-40, also known as CHI3L1, is an extracellular glycoprotein with a molecular weight of 40 kDa. It is a member of the glycosyl hydrolase family 18 and has no enzymatic activity [4]. Protein expression was detected in neutrophils, activated macrophages, T cells, chondrocytes, synovial cells, endothelial cells, stelate liver cells, activated astrocytes, oligodendrocytes [16]. There is evidence that YKL-40 is involved in the immune response by inhibiting oxidant injury, apoptosis and pyroptosis [7]. It was proved that YKL-40 was associated with T cell activation and proliferation [9]. Participation in neoangiogenesis, tissue remodeling, fibrosis, cell migration and proliferation was reported [11].

However, the particular mechanism of YKL-40 function remains unclear. Elevated YKL-40 in acute and chronic inflammatory diseases was determined [6, 8, 18]. There are few investigations focused on YKL-40 levels in TBI pathology which suggested that the protein expression correlated to the local neuroinflammation [3].

The aim of our study was to examine the expression and dynamics of YKL-40 production in TBI patients.

Material and Methods

Cerebrospinal fluid (CSF) and plasma samples were collected from nineteen patients with TBI – on the 24th and 96th hour after the trauma. The age distribution of the patients assessed as mean ± standard deviation was 50 ± 15 years. Seventeen of the patients were males and two were females. CSF samples were isolated also from forensic autopsies of 15 adult cadavers (healthy individuals before death) and served as an age-matched (63 ± 18 years) and gender-matched (13 males and 2 females) control group. Concentrations of YKL-40 in biological fluids were analyzed by ELISA using MicroVue™YKL-40 kit (QUIDEL, Cat. №8020) according to manufacturer's instructions.

Immunocytochemical staining of YKL-40 in lumbar punctuate was performed by the indirect immunoperoxidase method. The avidin-biotin system was applied (VectastainElite ABC Kit, Vector Laboratories, Burlingname,CA). The sections were incubated at 37 °C for 1 h with primary goat anti-human chitinase 3-like antibody (YKL-40) (R&D Systems, Minneapolis, MN) and anti-goat IgG secondary antibody. The final detection was performed by freshly prepared DAB as a chromogen. Nuclei were counterstained with haemotoxylin. A morphological analysis was performed by standard hematoxylin and eosin (H&E) staining.

The cytopathological examination was verified by two independent observers. The study was approved by the University Ethics Committee (Protocol№3/31.05.2018). Informed consent was signed by all examined individuals according to the Helsinki Declaration.

Statistical analysis. The Wilcoxon signed rank test was used to compare the concentrations of YKL-40 in plasma and CSF on the 24th and 96th hour after TBI. The levels of YKL-40 in the group of patients were compared with the ones in the control group by the Mann-Whitney test. Boxplot diagrams were used for graphical visualization of

YKL-40 concentrations - the criteria 1.5 of the interquartile range have been accepted to distinguish outliers. The significance level was set at 5%.

Results and Discussion

Inflammatory processes after TBI induce time-dependent cascades of acute phase response [15]. Proteins secreted into the systemic circulation and CSF are able to reflect the severity of the inflammation and the disease course [1]. We found no significant change between CSF levels of YKL-40 on the 24th h after TBI compared to the control group (mean ± standard deviation: 269±165 *vs* 153±51 ng/ml) (**Fig.1**). However, the interquartile range (25–75 percentiles) of YKL-40 concentrations for the control group was much narrower than the one of TBI patients (**Fig. 1**). Our results are in accordance with earlier investigations [3] suggesting that the level of the glycoprotein illustrates the inflammatory process.

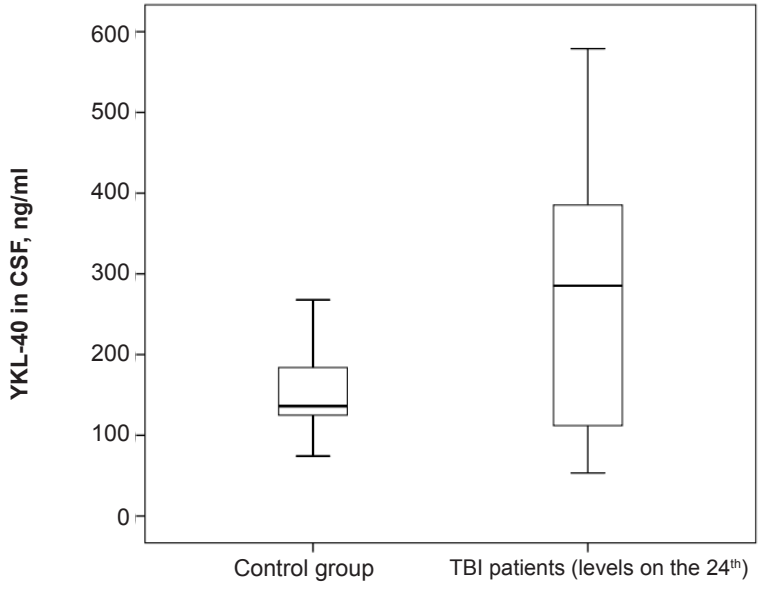

Fig. 1. YKL-40 concentrations in CSF of TBI patients and the control group.

We showed that CSF levels of YKL-40 were significantly lower compared to plasma concentrations on the 24th (p=0,027) and 96th hour (p=0,044) (**Fig. 2**). A recent study revealed increased CSF concentrations of YKL-40 in athletes with postconcussion syndrome due to repetitive concussive TBI. YKL-40 concentration correlated with lifetime concussion events. The authors claimed that head trauma was associated with biomarker evidence of astroglial activation but they did not report plasma YKL-40 values [17].

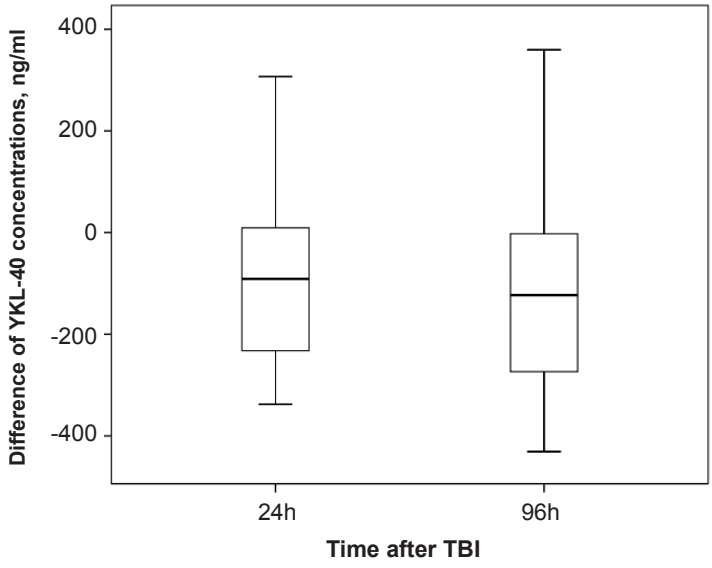

Fig. 2. Time-dependent differences of YKL-40 concentrations in CSF and plasma in TBI patients; the distributions of the differences $CSF_{concentration}$ – $Plasma_{concentration}$ calculated for each individual patient are visualized, ng/ml

Another clinical study following neuroinflammation and CSF YKL-40 levels in Huntington's disease showed that the concentration of the protein was not suitable as an early marker in this pathology but might have a possible role as a marker for glia activation [20].

Monocytes, phagocytes and polymorphonuclear cells were observed by morphological examination (**Fig. 3 A, B**). The results are in accordance with the findings of other researchers in CSF cytology who reported that lymphocytes and macrophages/monocytes were the cells frequently seen in nonspecific reactive conditions [2].

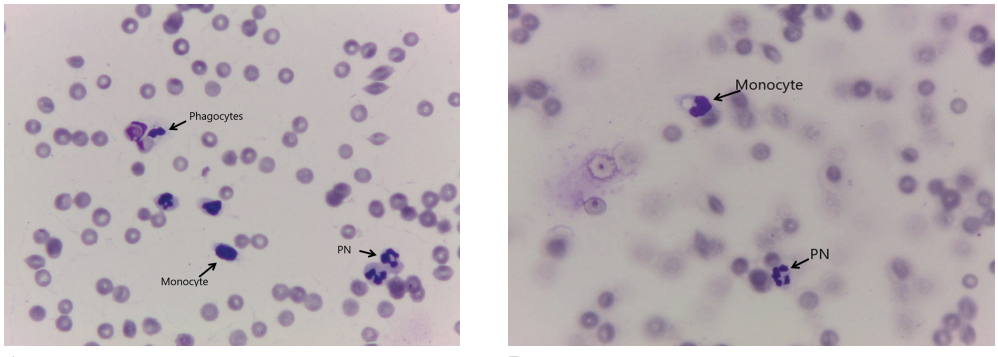

A **B**

Fig. 3. Cytology of CSF in TBI patients (hematoxylin and eosin staining).
Monocytes, phagocytes and polymorphonuclear (PN) cells are observed (3A, B). (magn × 630).

The immunocytochemical examination determined the presence of the YKL-40 protein in the cytoplasm of polymorphonuclear leukocytes. A strong diffuse staining was recorded (**Fig. 4**).

Another study suggested that YKL-40 expression at the perimeter of contusions might be an important feature of the astrocytic response to modulate neuroinflammation[21].

Therefore, CSF and plasma YKL-40 measurements are useful tools to analyze the course of inflammation and the time of lethal outcome in TBI. Higher plasma concentrations of the glycoprotein seem to be a part of the acute phase response as an immediate reaction after injury. The biomarker value and its dependency on trauma survival times are in prospect examination.

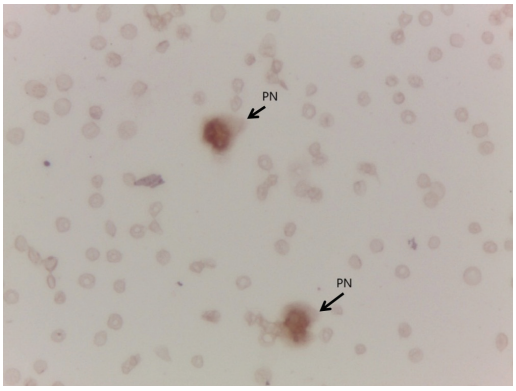

Fig. 4. Immunocytochemical expression of YKL-40 in a smear of CSF (indirect immunoperoxidase reaction). A strong diffuse cytoplasmic expression with perinuclear accentuation in two polymorphonuclear (PN) cells is observed (magn × 630).

Conclusion

Our study is the first to show time-dependent change of YKL-40 levels in TBI. We assume that plasma and CSF YKL-40 levels reflect the inflammatory process and would provide new information about its dynamics in TBI patients.

Acknowledgements: The financial support by the National Science Fund of Bulgaria (Contract DM 03/2 12.12.2016) is acknowledged.

References

1. **Alawieh, A.** Neuro-proteomics and neuro-systems biology in the quest of TBI biomarker discovery. – *Biomarkers of Brain Injury and Neurological Disorders* (Eds. K Kevin.), 2014, https://www.taylorfrancis.com/
2. **Bigner, S.** Cerebrospinal fluid (CSF) cytology: Current status and diagnostic applications. – *J. Neuropathol. Exp. Neurol*., **51,** 1992, 235-245.
3. **Bonneh-Barkay D., P. Zagadailov, H. Zou, C. Niyonkuru, M. Figley, A. Starkey, G. Wang, S., J. Bissel, C. A. Wiley, A. K. Wagner.** YKL-40 expression in traumatic brain injury: an initial analysis. – *J. Neurotrauma*., **27,** 2010, 1215–1223.
4. **Bussink, A. P., D. Speijer, M. F. Johannes, G. Aerts, R. G. Boot.** Evolution of mammalian chitinase (-like) members of family 18 glycosyl hydrolases. **–** *Genetics.,* **177,** 2007, 959–970.
5. **Cernak, I., L. J. Noble-Haeusslein.** Traumatic brain injury: an overview of pathobiology with emphasis on military populations. **–** *J. Cereb. Blood Flow Metab*., **30**, 2010, 255-266.
6. **Guan, J., Z. Liu, F. Li, J. S. Feng, H. J. Wang, J. G. Chu, Y. Z. Song, L. Xie, L. B. Ding.** Increased synovial fluid YKL-40 levels are linked with symptomatic severity in knee osteoarthritis patients. – *Clin. Lab.,***61,** 2015, 991-997.
7. **He, C. H., C. G. Lee, C. S. Dela Cruz, C. M. Lee, Y. Zhou, F. Ahangari, B. Ma, E. L. Herzog, S. A. Rosenberg, Y. Li, A. M. Nour, C. R. Parikh, I. Schmidt, Y. Modis, L. Cantley, J. A. Elias.** Chitinase 3-like 1 regulates cellular and tissue responses via IL-13 receptor α2. – *Cell. Rep.,* **29,** 2013, 830-41.

8. **Kazakova, M. H., A. Z. Batalov, N. G. Mateva, Z. G. Kolarov, V. S. Sarafian.** YKL-40 and cytokines a new diagnostic constellation in rheumatoid arthritis? – *Folia Med. (Plovdiv)*., **59,** 2017, 37-42.
9. **Kim, D. H., H. J. Park, S. Lim, J. H. Koo, H. G. Lee, J. O. Choi, J. H. Oh, S. J. Ha, M. J. Kang, C.M. Lee, C. G. Lee, J. A. Elias, J. M. Choi.** Regulation of chitinase-3-like-1 in T cell elicits Th1 and cytotoxic responses to inhibit lung metastasis. – *Nat. Commun.,* **9,** 2018, 503.
10. **Kokiko-Cochran, O. N., J. P. Godbout.** The inflammatory continuum of traumatic brain injury and Alzheimer's disease. – *Front. Immunol.,* **9,** 2018, 672.
11. **Lee, C. G., C. A. Da Silva, C. S. Dela Cruz, F. Ahangari, B. Ma, M. J. Kang, C. H. He, S. Takyar, J. A. Elias.** Role of Chitin and Chitinase/Chitinase-Like proteins in inflammation, tissue remodeling, and injury. **–** *Annu. Rey Physiol.,***73,** 2011, 479-501.
12. **Leibson, C. L., A. W. Brown, J. E. Ransom, N. N. Diehl, P. K. Perkins, J. Mandrekar, J. F. Malec.** Incidence of traumatic brain injury across the full disease spectrum: a population-based medical record review study. – *Epidemiology*, **22,** 2011, 836-844.
13. **Maas, A., N. Stocchetti, R. Bullock.** Moderate and severe traumatic brain injury in adults. – *Lancet Neurol*., **7,** 2008, 728-741.
14. **Mazzeo, A. T., A. Beat, A. Singh, M. R. Bullock.** The role of mitochondrial transition pore, and its modulation, in traumatic brain injury and delayed neurodegeneration after TBI. – *Exp. Neurol*., **8,** 2009, 363-370.
15. **Ondruschka, B., S. Schuch, D. Pohlers, H. Franke, J. Dreßler.** Acute phase response after fatal traumatic brain injury**.** – *Int. J. Legal Med.,* **132,** 2018, 531-539.
16. **Ringsholt, M., E. V. Høgdall, J. S. Johansen, P. A. Price, L. H. Christensen.** YKL-40 protein expression in normal adult human tissues-an immunohistochemical study. **–** *J. Mol. Histol.,* **38,** 2007, 33-43.
17. **Shahim, P.,Y. Tegner, N. Marklund, K. Höglund, E. Portelius, D. L. Brody, K. Blennow, H. Zetterberg.** Astroglial activation and altered amyloid metabolism in human repetitive concussion. – *Neurology,* **88,** 2017, 1400-1407.
18. **Spoorenberg, S. M. C., S. M. T. Vestjens, G. P. Voorn, C. H. M. van Moorsel, B. Meek, P. Zanen, G. T. Rijkers, W. J. W. Bos, J. C. Grutters.** Course of SP-D, YKL-40, CCL18 and CA 15-3 in adult patients hospitalised with community-acquired pneumonia and their association with disease severity and aetiology: A post-hoc analysis. – *PLoS One,* **13,** 2018, e0190575.
19. **Stergiou-Kita, M., S. Rappolt, D. Dawson.** Towards developing a guideline for vocational evaluation following traumatic brain injury: the qualitative synthesis of clients' perspectives. – *Disabil. Rehabil.,* **34,** 2012, 179-88.
20. **Vinther-Jensen, T., E. Budtz-Jørgensen, A. H. Simonsen, J. E. Nielsen, L. E. Hjermind.** YKL-40 in cerebrospinal fluid in Huntington's disease -a role in pathology or a nonspecific response to inflammation? – *Parkinsonism Relat. Disord*., **20,** 2014, 1301-1303.
21. **Wiley, C.A., D. Bonneh-Barkay, C. E. Dixon, A. Lesniak, G. Wang, S. J. Bissel, P. M. Kochanek.** Role for mammalian chitinase 3-like protein 1 in traumatic brain injury. – *Neuropathology*, **35**, 2015, 95-106.

Institute of Experimental Morphology, Pathology and Anthropology with Museum
Bulgarian Anatomical Society

Acta morphologica et anthropologica, 25 (3-4)
Sofia ● 2018

Evidence of Neuronal Damage in Elderly

Vera Kolyovska

Institute of Experimental Morphology, Pathology and Anthropology with Museum, Bulgarian Academy of Sciences, Sofia, Bulgaria

* Corresponding author e-mail: verakol@abv.bg

Blood sera from 13 psychologically and neurologically healthy volunteers from Sofia aged 90-95 years were investigated. Our previous studies have shown that GD1a antibodies can be considered as biomarkers for neurodegenerative changes. According to the performed ELISA technique, no elevated IgG titers of these antibodies were detected. This shows that the neurons of this people are healthy independently of the ageing.

Key words: GD1a, old elderly people, neurodegeneration

Introduction

Health is the ability of a biological system to acquire, convert, allocate, distribute, and utilize energy sustainably. The World Health Organization (WHO) defined human he-alth in a broader sense in its 1948 constitution as "a state of complete physical, mental and social well-being and not merely the absence of disease or infirmity" [12].

Over the last 150 years, life expectancy has increased by 2 years for every decade. Today in the developed countries it is 75-80 years, but the duration of health increases by about 1.7 per decade. More people suffer from age-related illnesses – cancer, cardiovascular disease, diabetes, hypertension, dementia, osteoporosis, eye and hearing problems and others. Life time duration over the years is: 1850-40 years; 1900-47 years; 1950-68 years; 2000-78 years; 2050-88 years. The solution is: moderate sports and exercise, nutrition – excessive intake of carbohydrates definitely shortens life (and in what form it is taken), it is good not to eat as many hours as possible, repairing the damage to the body from outside [11]. Our studies since 2002 have convincingly demonstrated that the titer of GD1a gangliosides may be a marker for neuronal damage. We have found in our experimental model of multiple sclerosis (MS) – chronic remitting experimental allergic encephalomyelitis (CREAE) that before the destruction of the myelin sheath, there is an increased titer of GD1a gangliosides, which is a sign of neuronal damage [5].

Materials and Methods

The health status of 76 randomly chosen volunteers between 90 and 104 years of age from all parts of Bulgaria is described. The illnesses that appear on our list are just like those described by prof. E. Verdin as diseases of the elderly all over the world [11]. A group of all 13 persons who are from Sofia are presented. Their sera were estimated by enzyme-linked immunosorbent assay (ELISA) technique for detecting IgG anti-GD1a antibodies [6]. People are selected one at a time and they do not have any neurological or psychiatric indications – their neurons are healthy.

All these 13 patients were without any neurological or mental illness. The ELISA protocol was selected by slight modifications of the method of Mitzutamari et al [6].

Results

Blood sera from 13 psychologically and neurologically healthy volunteers from Sofia aged 90-95 years were studied. In the ELISA technique, no elevated IgG titers of anti-GD1a antibodies were detected. It is important to note that in all 13 blood samples, there was no need for centrifugation because the serum was self-excreted. This is because all healthy old people who were tested take preparations for decrease of blood viscosity and thus they are in great condition **(Table 1)**.

Table 1. Titers of anti-GD1a antibodies in sera from elderly (90-95 years old)

Age / **OD Optical density**	90-95 year old n=13
IgG anti – GD1a Mean ± SEM	(-) ≤ 0.06 ± 0.02

Data are presented as a mean value x± standard error of mean (SEM)
Legend: OD – optical density; SEM – standard error of mean; n – number of patients

Discussion

Screening at the level of anti-GD1a antibodies indicates that neuronal damage can be traced in many patients. The mechanism by which ganglioside GD1a participates in the cell cohesion is not known. So we decided to study elderly with different diagnoses but without dementia. When there is no evidence for dementia, for impaired function of the neuron, the elderly are mentally healthy no matter how old they are. In all 13 elderly there was no increase in the antibody titers against GD1a meaning that there were no neuronal damages.

The production of fibrinolytic enzyme plasmin, produced by vascular endothelial cells, decreases with the age. This is the main reason for increased coagulation (blood clotting). On the other hand, fibrinogen increases with the age. This causes increased platelet aggregation, which increases the risk of stroke and heart attack. The elevated fibrinogen is a more significant risk factor for strokes than high blood cholesterol levels. To this should be added the combination of risk factors with different relative weight [7].

Plasma lipids could increase the cerebrovascular risk through alteration of the hemorheological profile [9]. Parallel with whole blood viscosity (WBV) many hematological parameters, including the erythrocyte morphology have also been evaluated [3].

Nicotinamide adenine dinucleotide (NAD(+)) is a coenzyme found in all living cells. Here we review factors that regulate NAD(+) and discuss how supplementation with NAD(+) precursors may represent a new therapeutic opportunity against aging and associated disorders, particularly neurodegenerative diseases [10]. The ketone body β-hydroxybutyrate (βOHB) is a convenient source of energy from adipocytes to peripheral tissues during fasting or exercise. These regulatory functions of βOHB serve to link the outside environment to cellular function and gene expression, and have important implications for the pathogenesis and treatment of metabolic diseases including diabetes type 2 [8].

Factors that support human health are: income and social status; social support network; education and literacy; work conditions; social environment; physical environment; personal health practices and coping skills; healthy development in childhood; biology and genetics; health services; culture. Longevity is a side effect of health [12].

The causes of stroke have been tested in 47 countries and are described as follows: 1. Hypertension – 24%; 2. Lack of regular physical activity – 18%; 3. Not administering statins – ratio of apolipoproteins B/A1 – 13%; 4. Harmful feeding habits – 12%; 5. Waist to hip ratio – 9%; 6. Psychosocial factors – stress, bullying at the workplace – 8.5%; 7. Smoking – 6%; 8. Cardiovascular diseases – 4.5%; 9. Alcohol consumption – 3%; 10. Diabetes mellitus – 2% [7].

Global grey matter volume decreases linearly with age, with a significantly steeper decline in males. Local areas of accelerated loss were observed bilaterally in the insula, superior parietal gyri, central sulci, and cingulate sulci. Areas exhibiting little or no age effect (relative preservation) were noted in the amygdala, hippocampi, and endorhinal cortex. Global white matter does not decline with age, but local areas of relative accelerated loss and preservation were seen [4]. From the brain regions affected by ageing, the hippocampus and the prefrontal cortex (PFC) seem to be particularly vulnerable, but even within and between these regions the impact of ageing on the neuronal function can differ. The morphology of neurons in the PFC is more susceptible to age-related changes, as these cells show a decrease in dendritic branching in rats and humans [1].

In 2017 David Cundiff reports 19 different relative risk factors for cardiovascular disease in 168 countries. They include: consumption of products of animal origin; refined carbohydrates; alcohol; tobacco; vitamin K2 intake; level of exercise; body mass index; blood sugar/hemoglobin A1c; problems with the blood pressure; medicines for hypertension; cholesterol/HDL ratio; the incomes of individuals; level of education; gender; age; ethnic origin; vitamin D level; air pollution; fetal, baby and childhood stress [2].

There is no evidence of neuronal damage in elderly who are born in 1924 to 1928 and are in good mental and psychological health.

Acknowledgements: I would like to express my gratitude to Svetlana Vladova, Ivayla Ivanova-Pandourska and Irina Evstatieva for provided excellent technical assistance.

References

1. **Burke, S. N., C. A. Barnes.** Neural plasticity in the ageing brain. – *Nature Reviews Neuroscience,* **7**(1), 2006, 30–40.
2. **Cundiff, D. K., P. S. Agutter.** Cardiovascular disease death before age 65 in 168 countries correlated statistically with biometrics, socioeconomic status, tobacco, gender, exercise, macronutrients, and vitamin K**.** – *Cureus,* **8(**8), 2016, e748.

3. **Gluhcheva, Y., I. Ivanov, V. Atanasov, N. Antonova, J. Ivanova, M. Mitewa.** Hematological changes in case of chronic cadmium intoxication and monensin detoxication. Relationship with rheological variables. – *Clin. Hemorheol. Microcirc.,* **49**(1-4), 2011, 417-422.
4. **Good, D., I. S. Johnsrude, J. Ashburner, R. N. A. Henson, K. J. Friston, R. S. J. Frackowiak.** A voxel-based morphometric study of ageing in 465 normal adult human brains catriona. – *Neuro-Image*, **14**, 2001, 21–36.
5. **Kolyovska, V., D. Deleva**. Serum IgG and IgM antibodies to GD1a ganglioside in adults – preliminary data. – *Acta morphol et anthropol.,* **19**, 2012, 114-117.
6. **Kolyovska, V.** Serum IgG antibodies to GD1a and GM1 gangliosides in elderly people. – *Biomed. Khim.*, **62**(1), 2016, 93-95.
7. **Maslarov, D.** Cerebrovascular diseases – current assessments and ideas for improving public health. – *DSci Thesis* Sofia, 2017.
8. **Newman, J. C., E. Verdin.** β-hydroxybutyrate: much more than a metabolite. – *Diabetes Res. Clin. Pract.,* **106**(2), 2014, 173-181.
9. **Velcheva, I., N. Antonova, V. Dimitrova, N. Dimitrov, I. Ivanov**. Plasma lipids and blood viscosity in patients with cerebrovascular disease – *Clin. Hemorheol. Microcirc.*, **35(**1-2), 2006, 155-157.
10. **Verdin, E**. NAD^+ in aging, metabolism, and neurodegeneration. – *Science*, **350**(6265), 2015, 1208-1213.
11. **Verdin, E.** How aging research is changing our lives: http://aging.nautil.us/feature/226/how-aging-research-is-changing-our-lives, 2017.
12. **World Health Organization.** *Constitution of the World Health Organization – Basic Documents*, Forty-fifth edition, Supplement, October 2006.

Institute of Experimental Morphology, Pathology and Anthropology with Museum
Bulgarian Anatomical Society

Acta morphologica et anthropologica, 25 (3-4)
Sofia ● 2018

The Effect of Salinomycin on Ganglioside Production in Lead-Intoxicated Mice. An Immunological Study.

Vera Kolyovska[1], Juliana Ivanova[2], Emilia Petrova[1], Yordanka Gluhcheva[1], Ekaterina Pavlova[1]*

[1] Institute of Experimental Morphology, Pathology and Anthropology with Museum, Bulgarian Academy of Sciences, Sofia, Bulgaria
[2] Faculty of Medicine, Sofia University "St. Kliment Ohridski", Sofia, Bulgaria

* Corresponding author e-mail: verakol@abv.bg

GM3 gangliosides have been described as biomarkers for oncogenic tissue changes. Anti-GM3 antibodies in mouse sera were tested in a lead intoxication model, followed by treatment with the polyether ionophorous antibiotic salinomycin. The results show abiding high titer of IgG antibodies against the GM3 gangliosides only in sera from salinomycin-treated mice. It could be concluded that the high titer of anti-GM3 antibodies is associated with signs of oncogenity.

Key words: salinomycin, anti-GM3 ganglioside antibodies, lead intoxication

Introduction

Lead (Pb) is a heavy toxic metal and a major environmental pollutant. Pb-poisoning in humans is possible by the consumption of contaminated food and water, inhalation or absorption through the skin [1]. Entering in the body, lead induces damages in the brain and kidneys, in the cardiovascular, nervous and reproductive system [2, 7, 15, 16, 17].

Chelation therapy is used to treat metal ion poisoning. Among the polyether ionophorous antibiotics, salinomycin is the representative with the lowest *in vivo* toxicity [12] and it has a potential application as antitumor agent for treatment of cancer stem cells [13]. In our previous study we demonstrated that the polyether ionophorous antibiotic salinomycin reduced significantly the concentration of Pb in the organs of Pb-exposed mice [14].

Numerous studies have recognized gangliosides as promising biomarkers for different disorders. Gangliosides are acidic glycosphingolipids. They occur not only in cells and tissues but also in tissue fluids. Over the last decades many studies have shown that gangliosides are immunogenic [9, 10] and their potential for cancer immunotherapies has been discussed.

The aim of the present work is to explore the effect of salinomycin on the presence of anti-ganglioside GM3 antibodies in a mouse model of lead intoxication.

Materials and Methods

Experimental design. Mature 60-days old male ICR mice weighting 25-30 g were obtained from Experimental and Breeding Base for Laboratory Animals (EBBLA) – Slivnitza, Bulgaria. The animals were housed at the Institute of Experimental Morphology, Pathology and Anthropology with Museum, Bulgarian Academy of Sciences at standard conditions: 12:12 h light/dark cycle, 25°C temperature and constant humidity. Each animal was accommodated in a single cage with polypropylene bottom. The animals were divided into four experimental groups as follow:

– Control group (untreated control animals; n =10) – the mice from this group obtained distilled water – **A** group.

– Toxic control group (n = 10) – the mice from this group were exposed to $Pb(NO_3)_2$ treatment for 14 days. The compound was dissolved in distilled water and administrated *per os* in an average daily dose of 80 mg/kg body weight (b.w.). From the 15th to 28th day the mice obtained distilled water – **B** group.

– Lead and Salinomycin treated group (n = 10) – animals from this group were intoxicated with $Pb(NO_3)_2$ in an average daily dose of 80 mg/kg b.w. Next two weeks animals obtained tetraethylammonium salt of salinomycinic acid dissolved in drinking water in an average daily dose of 20 mg/kg b.w. – **C** group.

– Salinomycin-treated group (n =10) – the mice from this group obtained tetraethylammonium salt of salinomycinic acid dissolved in drinking water in an average daily dose of 20 mg/kg b.w. for 14 days – **D** group.

On the 29th day of the experimental protocol the animals were anesthetized and sacrificed. The samples were collected for analysis. Blood was collected and centrifuged (for 10 min at 1500 rpm). Pool samples were prepared from the separated sera and stored at -20 °C prior to analysis. The protocol was approved by Ethics committee of the Institute of Experimental Morphology, Pathology and Anthropology with Museum of Bulgarian Academy of Sciences.

Titers of antibodies to GM3 gangliosides served as biomarkers. Immunoglobulin G (IgG) is used for chronic disorders. The serum anti-GM3 antibodies were estimated by the enzyme-linked immunosorbent assay (ELISA) with slight modifications of the method [10].

Results

Our observations in salinomycin-treated animals show strongly elevated titer of anti-GM3 antibodies **(Table 1)**. More than a 4-fold increase in the antibody titer was measured in the pool sample of animals treated only with salinomycin, compared to the untreated control mice. In the Pb-intoxicated group elevated titer was not observed. Subsequent treatment with salinomycin though, induced a 4-fold and a 6-fold increase in the anti-GM3 titer compared to the untreated control and the intoxicated group, respectively. The highest antibody titer was measured in the pool sera sample of Pb-intoxicated mice with subsequent administration of the ionophorous antibiotic. The results found confirmation in 5 of 6 repeats, although the capriciousity of the method (relative to pH, temperature and other parameters). High titer of antibodies was not measured in only one of the pools which could be explained by the possibility gangliosides to be linked to each other in micelles.

There are many literature data on the increased levels of GM3 molecules in different pathological conditions with various interpretations of these findings. The high titer of anti-GM3 antibodies may be a marker for common metabolic disorders and/or diabetes.

Table 1. Numeric values of the anti-ganglioside GM3 antibodies titers in sera in lead intoxication model mice treated with the polyether ionophorous antibiotic salinomycin

Probe (n =10)	Numerical value of the IgG titre of anti-GM3 antibodies	Symbol
A group, Control	0.0175 ± 0.01	-
B group, Pb	0.0244 ± 0.02	-
C group, Pb+Sal	0.1105 ± 0.03	++
D group, Ctrl+Sal	0.0825 ± 0.02	+

Legend:
A group – Control group (untreated control animals; Ctrl, n =10); **B** group – Toxic control group (only Pb, n = 10); **C** group – Lead and salinomycin-treated group (Pb+Sal, n = 10); **D** group – Salinomycin-treated group (treated control animals; Ctrl+Sal, n =10)

Numerical value of the titre:
- ≤ 0.047; Normal 0.047; ± 0.062; + 0.077; ++ 0.107

According to literature data, elevated anti-GM3 antibody levels are also reported in malignant cells as a neoplastic marker, including their protective functions. Similarly, our results could be indicative for the relevance of salinomycin to cancer therapy.

Discussion

Gangliosides perform different biological functions. They are involved as membrane regulatory molecules in the cell growth, differentiation and axon-oligodendrocyte interaction formation in myelinogenesis. Ganglioside composition in the serum is very constant and shows no significant variations in healthy individuals associated with age and gender. However, in pathological conditions, the serum ganglioside spectrum undergoes significant alterations. Our long-term research has shown that it is of critical importance to establish the clinical significance of serum IgG anti-GD1a and anti-GM1 ganglioside antibodies as potential biomarkers for neuronal damage in neurodegenerative diseases, immuno-mediated neuropathies and demyelination [9, 10].

The antibiotic salinomycin (E716) is a carboxylic polyether ionophore, produced by *Streptomyces albus*. Salinomycin, due to its lipophilic properties, easily penetrates through the plasma membrane into the cell and through intracellular membranes into various cellular organelles. In 2009 Gupta et al. discovered that salinomycin is able to kill cancer stem cells, as well as to inhibit breast cancer growth and metastasis in mice [4]. Cancer stem-like cells (CSCs) in different types of cancers may account for the failure of treatments because they are resistant to many current anticancer therapies. Therefore Gupta's discovery could be very important for cancer therapy in the future [4, 6]. Salinomycin induces apoptosis of human prostate cancer cells owing to accumulation of reactive oxygen species, DNA damage and mitochondrial membrane depolarization. This drug also inhibits chemoresistant cancer cells and sensitizes DOX- or ETO-treated or irradiated cancer cells by increasing apoptosis causing DNA damage and reducing p21 protein levels. Salinomycin inhibits Wnt-signalling and selectively induces apoptosis in

tumor cells [13]. Therefore, at present salinomycin is considered to be a potential anti-neoplastic drug for cancer therapy. It has been shown that T-lymphocytes with CD4+ phenotype, obtained from patients with leukemia (malignant cells), are significantly more sensitive to the action of this drug than CD4+ T-lymphocytes of healthy people [13].

The ionophore antibiotics can disrupt the intracellular balance of cations and ultimately can lead to cell death. The neurotoxicity of salinomycin appears to be primarily due to disturbances in the cell ionic balance [13, 14]. It has been shown that salinomycin can inhibit mitochondrial respiration and disrupt the transmembrane potential. This can cause the release of cytochrome C from the intermembrane space of the mitochondria, activation of caspase-9 and the development of apoptosis.

There are evidences that a synthetic derivative of salinomycin exhibits a more potent and selective activity against breast CSCs *in vitro* and *in vivo*, by accumulating and sequestering iron in lysosomes. In response to the ensuing cytoplasmic depletion of iron, cells triggered the degradation of ferritin in lysosomes, leading to further iron loading in these organelles. Iron-mediated production of reactive oxygen species (ROS) promoted lysosomal membrane permeabilization, activating a cell death pathway consistent with ferroptosis. These findings reveal the prevalence of iron homeostasis in breast CSCs, pointing towards iron and iron-mediated processes as potential targets against these cells [11]. Salinomycin is able to kill different types of non-stem tumor cells that usually are resistant to common therapeutic approaches, but the mechanism of action of this molecule remains largely unknown [12]. Since salinomycin has been suggested to act as a K(+) ionophore, Managò et al. explored its impact on mitochondrial bioenergetic performance at an early time point following drug application [12]. In addition, mitochondrial matrix acidification and significant decrease of respiration were observed in intact mouse embryonic fibroblasts (MEFs) and in cancer stem cell-like HMLE cells within ten minutes, while increased production of ROS was not detected [12]. Compatible with its direct modulation of mitochondrial function, salinomycin was able to induce cell death also in Bax/Bak-less double-knockout MEF cells [12]. Since at the concentration range used in most studies (around 10 μM) salinomycin exerts its effect at the level of mitochondria and alters bioenergetic performance [12]. The specificity of its action on pathologic B cells isolated from patients with chronic lymphocytic leukemia versus B cells from healthy subjects was investigated [12]. The results indicate that salinomycin, when used above μM concentrations, exerts direct mitochondrial effects, thus compromising cell survival [12]. Jiang et al. present evidence that a dual role of salinomycin involving in autophagy may account for its unique anticancer effects with preference for cancer cells [8]. GM3 regulates cell adhesion, growth and motility by changing molecular organization in glycosynaptic microdomains. GM3 may change the activation levels of co-localized signaling molecules, which are involved in cancer pathogenesis [5]. B16 melanoma cells showed GM3 on the cell surface and GM3-dependent *in vitro* growth. Depletion of sialic acid residues from the cell surface completely abolished antibody response against melanoma cells [3]. These data indicate that the antitumor activity of GM3 is associated with GM3 expression on tumor cell surface and demonstrate a major role of sialic acid in the humoral response [3].

In conclusion, the results of the present study show that salinomycin treatment following lead intoxication increases the titer of anti-GM3 antibodies. Our findings suggest that GM3 gangliosides can serve as cancer biomarker and provide evidence for the potential application of salinomycin in oncotherapy.

References

1. **Flora, G, D. Gupta, A. Tiwari.** Toxicity of lead: A review with recent updates. – *Interdisc. Toxicol,*. 2012, **5**(2), 47-58.
2. **Flora, S. J. S., V. Pachauri, G. Saxena.** Arsenic, cadmium and lead. – In Gupta R. C. (ed.) *Reproductive and Developmental Toxicology*, *Academic New York, NY,* **33**, 2011, 415-438.
3. **Gabri, M. R., G. V. Ripoll, D. F. Alonso, D. E. Gómez.** Role of cell surface GM3 ganglioside and sialic acid in the antitumor activity of aGM3-based vaccine in the murine B16 melanoma model. – *J. Cancer Res. Clin. Oncol*., **128**, 2002, 12, 669-677.
4. **Gupta, P. B., T. T. Onder, G. Jiang, K. Tao, C. Kuperwasser, R. A. Weinberg, E. S. Lander.** Identification of selective inhibitors of cancer stem cells by high-throughput screening. – *Cell*, **138**, 2009, 4, 645-659.
5. **Hakomori, S. I., K. Handa.** GM3 and cancer. – *Glycoconj. J.*, **32**, 2015, 1-2, 1-8.
6. **Huczyński, A.** Polyether ionophores – promising bioactive molecules for cancer therapy. – *Bioorg. Med. Chem. Lett.*, **22**, 2012, 7002-7010.
7. **Ivanova, J., Y. Gluhcheva, D. Dimova, E. Pavlova, S. Arpadjan.** Comparative assessment of the effects of salinomycin and monensin on the biodistribution of lead and some essential metal ions in mice, subjected to subacute lead intoxication. – *J. Trace Elem. Med. Biol.,* 2016, **33,** 31-36.
8. **Jiang, J., H. Li, E. Qaed, J. Zhang, Y. Song, R. Wu, X. Bu, Q. Wang, Z. Tang.** Salinomycin, as an autophagy modulator – a new avenue to anticancer: a review. – *J. Exp. Clin. Cancer Res.,* 37, 2018, (1), 26.
9. **Kolyovska, V**. – *PhD Thesis*, 2006, 120p.
10. **Kolyovska, V.** Serum IgG antibodies to GD1a and GM1 gangliosides in elderly people. – *Biomed. Khim.*¸ **62**, 2016, 1, 93-95.
11. **Mai, T. T., A. Hamaï, A. Hienzsch, T. Cañeque, S. Müller, J. Wicinski, O. Cabaud, C. Leroy, A. David, V. Acevedo, A. Ryo, C. Ginestier, D. Birnbaum, E. Charafe-Jauffret, P. Codogno, M. Mehrpour, R. Rodriguez.** Salinomycin kills cancer stem cells by sequestering iron in lysosomes. – *Nat. Chem.,* **9**, 2017, 10, 1025-1033.
12. **Managò, A.., L. Leanza, L. Carraretto, N. Sassi, S. Grancara, R. Quintana-Cabrera, V. Trimarco, A. Toninello, L. Scorrano, L. Trentin, G. Semenzato, E. Gulbins, M. Zoratti, I. Szabò.** Early effects of the antineoplastic agent salinomycin on mitochondrial function. – *Cell Death Dis.*, **22**(6), 2015, e1930.
13. **Moskaleva, E. Yu., S. E. Severin**. Antitumor activity of ionophore antibiotic salinomycin: the target – cancer stem cells. National Research Centre «Kurchatov Institute» NBICS-Centre. – *Molekuliarnaya medicina*, **6,** 2012. [in Russian]
14. **Pressman, B.** Ionophorous antibiotics as model for biological transport. – *Fed. Proc.,* **27**, 1968, 1283–1288.
15. **Saleh, H. A., G. A. El-Aziz, M. M. El-Fark, M. El-Gohary.** Effect of maternal lead exposure on craniofacial ossification in rat fetuses and the role of antioxidant therapy. – *Anat. Histol. Embryol.,* 38, 2009, 5, 392-399.
16. **Sanders, T., Y. Liu, V. Buchner, P. B. Tchounwou.** Neurotoxic effects and biomarkers of lead exposure: a review. – *Res. Environ. Health*, **24,** 2009, 1, 15-45.
17. **Vaziri, N. D.** Mechanisms of lead-induced hypertension and cardiovascular disease. – *Am. J. Physiol. Heart Circ. Physiol.,* 295, 2008, 2, 454-465.

Institute of Experimental Morphology, Pathology and Anthropology with Museum
Bulgarian Anatomical Society

Acta morphologica et anthropologica, 25 (3-4)
Sofia ● 2018

The Muscle Phase of Trichinellosis in Mice is Associated with Increased ST6GalNAc-1 Sialyltransferase Activity in Skeletal Muscle Fibers

Rositsa Milcheva, Katerina Todorova, Svetlozara Petkova, Ivelin Vladov, Valeria Dilcheva, Ani Georgieva, Dimitar Ivanov, Ivan Iliev, Ludmil Kirazov

Institute of Experimental Morphology, Pathology and Anthropology with Museum, Bulgarian Academy of Sciences, Sofia, Bulgaria

* Corresponding author e-mail: rosicamilcheva@abv.bg

We previously showed that the de-differentiation of the occupied portion of muscle fibers toward Nurse cell after invasion by *Trichinella spiralis* is associated with increased intracellular accumulation of α-2,6-sialylated glycoproteins and novel gene activation of ST6GalNAc1. With this work we demonstrate ST6GalNAc1 expression in mouse skeletal muscles invaded by *T. spiralis*. Muscle samples were collected at certain time points after invasion. Immunochistochemistry was performed using rabbit polyclonal antibody against ST6GalNAc1 sialyltransferase. We found short up-regulation of the enzyme ST6GalNac1 that faded within the transformation of the occupied area into a Nurse cell. The enzyme ST6GalNAc1 is not synthesized in healthy mouse muscle tissue and is rarely expressed in normal tissues. It is responsible for the formation of the cancer-associated sialyl-Tn antigen in variety of carcinomas, blocking regular carbohydrate chain elongation. The functional role of this enzyme for the Nurse cell formation of T. spiralis in muscles has to be elucidated.

Key words: sialic acids, skeletal muscle *Trichinella*

Introduction

Sialic acids are called over than 40 modifications of the Neuraminic acid that occupy terminal position on the oligosaccharide chains of glycoproteins and glycolipids, and are thus involved in almost all types of recognition phenomena and adhesion mechanisms [10].

In skeletal muscles the sialic acids are important for the functional maintenance of glycoproteins involved in fiber structure and neuromuscular junctions [3, 7], for the development and regeneration [1], muscle excitability [6] and exercise performance [5]. However, even if sialylation in skeletal muscles is not as abundant as in other tissues, the muscles are very sensitive to losses of sialic acid due to mutations, which result in severe and progressive loss of motility [2, 11].

Among all known myopathies, the establishment of a Nurse cell-parasite complex resulting from infestation by the parasitic nematode *Trichinella* is a unique event.

This structure derives from a portion of the striated skeletal muscle fiber and develops within 15 to 20 days after a larva of *Trichinella* invades the fiber. After penetrating the skeletal muscle fiber, the larva induces morphological, functional and enzymatic changes. The occupied portion of the muscle fiber transforms into a structure called Nurse cell, capable of supporting the parasite for years [4]. During this process of de-differentiation, at least 53 genes associated with apoptosis, satellite cell activation and proliferation, cell differentiation, cell proliferation and cycle regulation, myogenesis and muscle development change in expression [13]. The affected areas lose their contractile properties but the membranes of the newly developing Nurse cells remain adherent within the construction of the contractile fiber. Considering the role of the sialic acids in cell adhesion we assumed that this process of transformation is associated with changes in sialylation of the occupied skeletal muscle fiber.

Our previous studies showed that the occupation of skeletal muscle fibers by *Trichinella spiralis* is associated with intracellular accumulation of α-2,3- and α-2,6-sialylated glycoconjugates, as well as elevated levels of free sialic acid, sialylated glycoproteins and total sialyltransfrase activity [8]. Further, up-regulation of sialyltransferase ST6GalNAc2 and a novel gene activation of sialyltransferase ST6GalNAc1 were found, too [9].

With this short report, by means of immunohistochemistry, we demonstrate a transient protein expression of the enzyme ST6GalNAc1 (ST6 [alpha-N-acetyl-neuraminyl-2,3-beta-galactosyl-1,3]-N-acetylgalactosaminide alpha-2,6-sialyltransfrase 1, Mouse Genome Informatics Database) in mouse skeletal muscles, invaded by infectious larvae of the parasitic nematode *T. spiralis*.

Material and Methods

Ethical procedures

All animal experiments were performed in compliance with the Institutional Guidelines for Animal Experiments of the Institute of Experimental Morphology, Pathology and Anthropology with Museum, Bulgarian Academy of Sciences, following the EU and locally established norms and procedures.

Parasites, invasion, sample collection and tissue preparation for basic pathomorphology

Infective *T. spiralis* larvae were isolated from previously invaded mice, between days 30 and 40 day post infection (d.p.i.) according to a routine protocol. ICR mice, 6-8 weeks old, were inoculated with 500 infective *T. spiralis* larvae *per os*. The animals (five per group) were sacrificed at day 0, 10, 14, 18, 24 and 35 post invasion (d.p.i.). Tissue specimens were excised from the femoral, pectoral and gluteal muscles and fixed with 10% neutral buffered formaldehyde. After processing, the specimens were embedded in paraffin. Tissue sections, 5 μm thick, from all experimental groups were submitted for staining with hematoxylin and eosin (H&E) for basic morphological evaluation and immunohistochemistry.

Immunohistochemistry

Selected tissue sections from all experimental groups were heated for 5 min in 10 mM Tris-1.25mM EDTA revitalizing buffer at pH 9.2. The endogenous peroxidase activity was blocked by 0.3% solution of H2O2, then 2.5% normal goat serum (Vector Laboratories Ltd, Burlingame, CA, USA) was used to prevent non-specific antigen activity. Polyclonal antibody against ST6GalNAc1 (Aviva Systems Biology Cor., San Diego, CA, USA) was applied overnight at 4°C in dilution 1:50. The sections were then treated with a secondary antibody (ImmPress HRP anti-rabbit IgG polymer detection kit, Vector Laboratories) for 30 min, a color reaction was developed with DAB Peroxidase

(HRP) Substrate Kit (Vector Laboratories) and the sections were counterstained with hematoxylin. The immunohistochemical staining was evaluated as negative (-) and positive (+).

Results and Discussion

The results are shown in **Figure 1**.

The occupied sites in skeletal muscle specimens from day 10 p.i. were distinguished by the enlargement and centralisation of the fiber nuclei. Following the time course of muscle invasion, the affected area of the sarcoplasm disintegrated progressively and by the day 35 p.i. the de-differentiation of the occupied fiber resulted in a Nurse cell completion. During this period the affected sarcoplasm changed from eosinophilic to basophilic and then back to light eosinophilic. The enlarged nuclei persisted also in the mature Nurse cell containing coiled larvae. Between days 18 and 24 p.i. the developing Nurse cells were surrounded by cells of inflammatory response. Protein expression of the sialyltransferase ST6GalNAc1 was observed within the invaded sarcoplasm only at day 14 p.i.

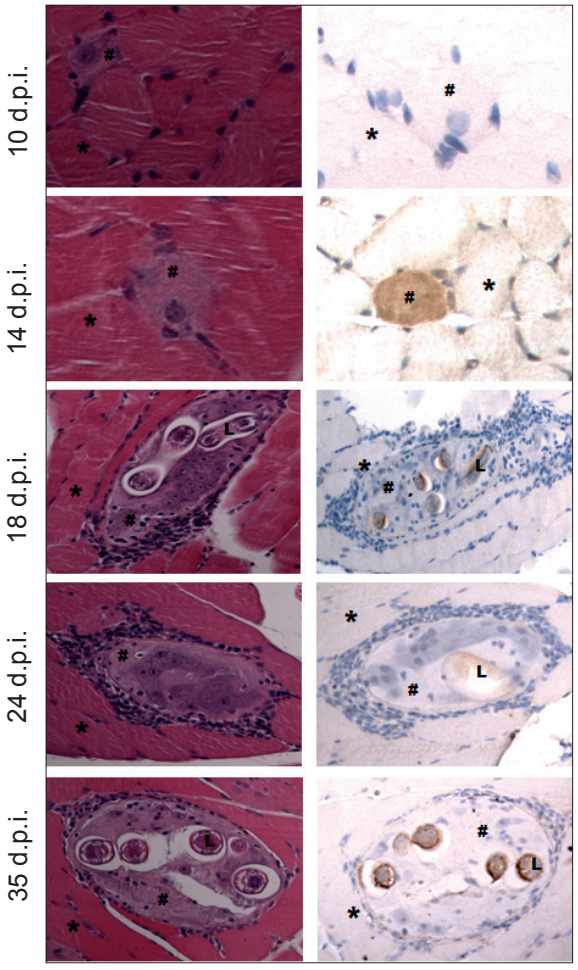

The enzyme ST6GalNAc1 catalyzes the transfer of a sialic acid in an alpha-2,6 linkage to O-linked N-acetylgalactosamine (GalNAc) residues and is responsible for the formation of the cancer-associated sialyl-Tn antigen (SiA-α-2,6-GalNAc-α-1-Ser/Thr) [12]. According to the Mouse Genome Informatics database and our molecular studies [9] expression of this enzyme is absent in healthy skeletal muscles. It is typical however for the alimentary system and its expression is considered as a prognostic marker for many cancer diseases characterized by increased levels of the sialyl-Tn antigen [12]. The biological function of the short expression of ST6GalNAc1in the developing Nurse cell of *T. spiralis* should be further elucidated.

Fig. 1. Immunohistochemistry of mouse skeletal muscles with Trichinella spiralis at days 10, 14, 18, 24 and 35 post invasion (d.p.i.) with polyclonal Ab against ST6GalNAc1. Star – non-occupied skeletal muscle fibre, hashtag – occupied sarcoplasm, L – larva. Obj. magn. 40×.

Acknowledgments: This study was financially supported by grant DN01/16 funded by the National Science Fund of Republic of Bulgaria.

References

1. **Broccolini, A., T. Gidaro, R. De Cristofaro, R. Morosetti, C. Gliubizzi, E. Ricci, P.A. Tonali, M. Mirabella.** Hyposialylation of neprilysin possibly affects its expression and enzymatic activity in hereditary inclusion-body myopathy muscle. – *J. Neurochem*., **105**, 2008, 971–981.
2. **Broccolini, A., T. Gidaro, R. Morosetti, M. Mirabella.** Hereditary inclusion-body myopathy: clues on pathogenesis and possible therapy. – *Muscle Nerve*, **40**, 2009, 340-349.
3. **Combs, A.C., J. M. Ervasti.** Enhanced laminin binding by alpha-dystroglycan after enzymatic deglycosylation. – *Biochem. J*., **390**, 2005, 303-309.
4. **Despommier, D. D.** How does *Trichinella spiralis* make itself at home? – *Parasitol. Today*, **14**, 1998, 318-323.
5. **Hanisch, F., W. Weidemann, M. Großmann, P. R. Joshi, H. J. Holzhausen, G. Stoltenburg, J. Weis, S. Zierz, R. Horstkorte.** Sialylation and muscle performance: Sialic acid is a marker of muscle ageing. – *PLOS One*., **8**, 2013, e80520. Doi: 10.1371/journal.pone.0080520.
6. **Johnson, D., M. L. Montpetit, P. J. Stocker, E. S. Bennett.** The sialic acid component of the β_1 subunit modulates voltage-gated sodium channel function. – *J. Biol. Chem*., **279**, 2004, 44303-44310.
7. **McDearmon, E. L., A. C. Combs, J. M. Ervasti.** Core 1 glycans on α-dystroglycan mediate laminin-induced acetylcholine receptor clustering but not laminin binding. – *J. Biol. Chem*., **278**, 2003, 44868-44873.
8. **Milcheva, R., D. Ivanov, I. Iliev, R. Russev, S. Petkova, P. Babál.** Increased sialylation as a phenomenon in the accommodation of the parasitic nematode *Trichinella spiralis* (Owen, 1835) in skeletal muscle fibres. – *Folia parasitol*., 2015, Doi: 10 14411/fp.2015.049.
9. **Milcheva, R., P. Janega, P. Celec, R. Morphew, Z. Hurnikova, S. Petkova, B. Izrael-Vlkova, K. Todorova, P. Babál.** An increased expression of cytosolic α-2,6-sialylated glycoproteins in the sarcoplasm is associated with the skeletal muscle fiber stage of Trichinella spiralis. (under review).
10. **Schauer, R.** Sialic acids as regulators of molecular and cellular interactions. – *Curr. Opin. Struct. Biol*., **19**, 2009, 507-514.
11. **Tajima, Y., E. Uyama, S. Go, C. Sato, N. Tao, M. Kotani, H. Hino, A. Suzuki, Y. Sanai, K. Kitajima, H. Sakuraba.** Distal myopathy with rimmed vacuoles: Impaired O-glycan formation in muscular glycoproteins. – *Am. J. Pathol*., **166**, 2005, 1121-1130.
12. **Varki, A. Structure and biosynthesis.** – In: *Essentials of Glycobiology*, 2nd edition (Eds. A. Varki, R. Cummings, J. Esko, H. Freeze, P. Stanley, C. Bertozzi, G. Hart, M. Etzler), Cold Spring Harbor (NY) Laboratory Press, 2009. Available at https://www.ncbi.nlm.nih.gov/books/NBK1908/.
13. **Wu, Z., I. Nagano, Y. Takahashi.** Candidate genes responsible for common and different pathology of infected muscle tissues between *Trichinella spiralis* and *T. pseudospiralis* infection. – *Parasitol. Int*., **57**, 2008, 368-378.

Mouse Genome Informatics Database. Available at http://www.informatics.jax.org/.

Institute of Experimental Morphology, Pathology and Anthropology with Museum
Bulgarian Anatomical Society

Acta morphologica et anthropologica, 25 (3-4)
Sofia ● 2018

Biological Activity of a Newly Synthesized Specific Inhibitor of Aminopeptidase A: A Preliminary Study

Vessela Petrova[1], Donka Tasheva[2], Ivan Iliev[1], Mashenka Dimitrova[1], Ivaylo Ivanov[3]*

[1] *Institute of Experimental Morphology, Pathology and Anthropology with Museum – Bulgarian Academy of Sciences, Sofia, Bulgaria*
[2] *Faculty of Chemistry and Pharmacy, Sofia University "St. Kl. Ohridski", Sofia, Bulgaria*
[3] *Department of Medical Chemistry and Biochemistry, Medical University, Sofia, Bulgaria*

*Corresponding author e-mail: mashadim@abv.bg

According to the recent studies, aminopeptidase A (APA) activity is very low in the tumor tissue of human mammary gland carcinoma, whereas the enzyme is well expressed in the normal breast tissue. In order to elucidate if this is a secondary phenomenon or part of the tumor phenotype of the cells, we determined (MTT test) the effect of the newly synthesized APA inhibitor α-glutamylhydroxamate (GH) on the proliferative activity and survival rate of three types of human cells: MCF-10A (epithelial cells of mammary gland), MCF-7 (luminal adenocarcinoma type A) and MDA-MB-231 (triple negative carcinoma). The results show that the inhibitor is not toxic to all three cell lines, but its application enhances the proliferation of normal MCF-10A cells. According to these results, the decrease of APA activity may increase the survival and division of normal cells (tumor phenotype).

Key words: aminopeptidase A, enzyme inhibitor, cultured cells, MTT test, mammary gland carcinoma

Introduction

Aminopeptidase A (APA, EC 3.4.11.7) is a plasma membrane-associated enzyme, catalyzing the hydrolysis of glutamic (Glu) or aspartic (Asp) acidfrom the N-terminal of natural peptides and synthetic substrates ($pH_{opt} \approx 7.6$) [7]. The enzyme is a part of the systemic and local renin-angiotensin systems (RAS), where it hydrolyzes angiotensin II to angiotensin III (AngII to AngIII) thus participating in the regulation of blood pressure [3]. APA has been also found in the invasive front of different types of tumors [e.g. 2, 8] where it participates in the opening of free spaces for tumor growth, together with matrix metallopeptidases. On the other hand, in AngII-mediated cancers (like breast cancer) the enzyme may act as a tumor-suppressor by minimizing the cell migration and angiogenesis, induced by AngII [1]. Biochemical studies of biopsies from patients with mammary gland carcinoma have shown a lower activity of APA in the tumor tissue in comparison to the adjacent normal tissue [4, 5]. We obtained similar results in Erlich's

model of breast carcinoma of mice and in a model system of three types of human mammary gland cells [unpublished results]. Since APA is a tumor suppressor in breast carcinoma, it would be valuable to test whether the inhibition of the enzyme may result in a promotion of tumor phenotype in normal breast epithelial cells, which is the aim of the present study.

Materials and Methods

Three types of human cells were used in the study: MCF-10A (immortalized epithelial cells of mammary gland), MCF-7 (luminal adenocarcinoma type A) and MDA-MB-231 (triple negative carcinoma). The tumor cells were cultured in DMEM high glucose medium with 10% FBS and 100 µg/ml penicillin/streptomycin in a humidified atmosphere with 5% CO_2 at 37ºC. The normal cells were grown in the same conditions but with the addition of 20 µg/ml hEGF, 0.5µg/ml hydrocortisone, 0.1µg/ml cholera toxin and 10 µg/ml insulin. Cell viability and proliferative activity were measured (MTT-test [6]) after the incubation of the cells with the APA inhibitor GH in the concentrations range from 0.001 to 10 mg/ml for 72 hours. Cells were also cultivated with the inhibitor on cover slips for 72 hours, stained with acridine orange /propidium iodide and studied under a fluorescent microscope.

Results and Discussion

AngII is well known to act not only as a vasoconstrictor but also as a stimulator of cell migration, invasiveness and angiogenesis in AngII-mediated carcinomas [1]. On the other hand, AngII is the main natural substrate of APA. Thus, the lower APA activity in AngII-mediated tumors is expected to favor the tumor growth. In the present study, we test the effect of a recently synthesized specific APA inhibitor GH on cell viability and proliferation potential in a model system of three types of human mammary gland cells: normal (MCF-10A), luminal breast cancer of low invasiveness (MCF-7) and triple negative (highly invasive) cancer of the mammary gland. According to our results, GH affects the cells growth in a concentration-dependent manner with IC_{50} in all the three cell lines being above 6 mg/ml (**Fig. 1** and **2**). Since these IC_{50} are high, we concluded

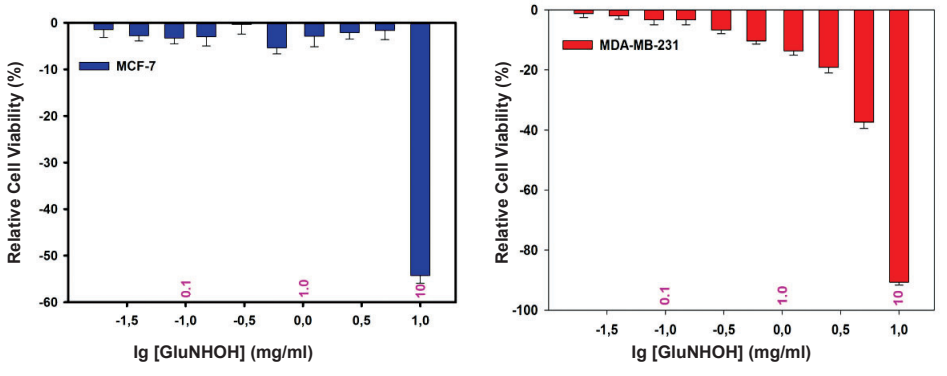

Fig. 1. Effect of the inhibitor GH on the tumor cell lines. Left – MCF-7 (IC_{50} = 9.0 mg/ml); Right – MDA-MB-231 (IC_{50} = 6.5 mg/ml).

that GH is not toxic to the three types of cells. Additionally, the inhibition of APA in the normal mammary gland epithelial cells (MCF-10A) led to an increase of cells viability by 30% (effective concentration EC_{50} = 0.150 mg/ml) in comparison to the non-treated control (**Fig. 2**). Furthermore, the number of mitotic figures under the fluorescent microscope was substantially higher than the control cells (**Fig. 3**).

Thus, it can be concluded that the suppression of APA activity leads to a considerable increase of the survival rate and proliferative capacity of the normal mammary gland epithelial cells, which corresponds to the tumor phenotype. According to our results, the inhibition of APA is part of the tumor phenotype of the cells.

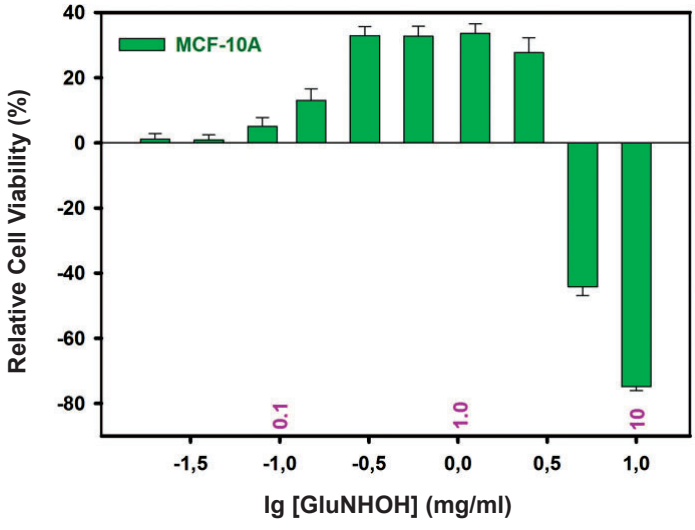

Fig. 2. Effect of GH on the normal cell line MCF-10A (IC50 = 6.0 mg/ml; EC50 = 0.15 mg/ml).

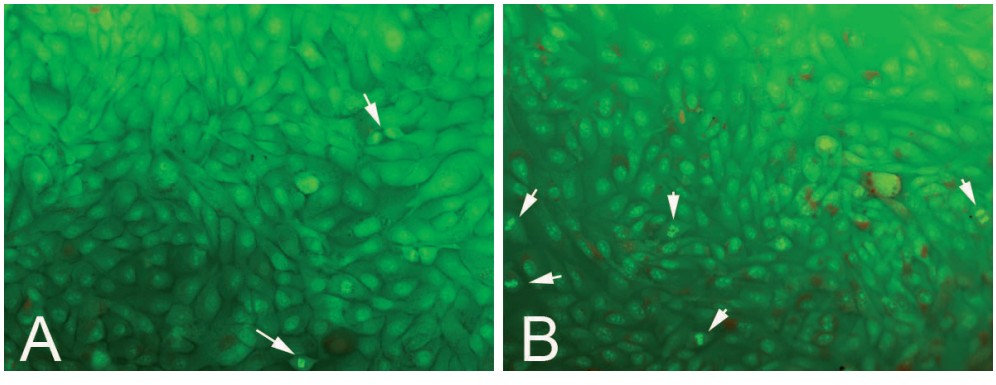

Fig. 3. Increased number of mitotic figures (arrows) in the cells, treated with GH (B) in comparison to the non-treated cells (A). 200X

References

1. **Andrade, S. P., C. C. Cardoso, R. D. P. Machado, W. T. Beraldo**. Angiotensin II-induced angiogenesis in sponge implant in mice. – *Int. J. Microcirc. Clin. Exp.*, **16**, 1996, 302-307.
2. **Fujimura, H., K. Ino, T. Nagasaka, N. Nagashima, H. Nakazato, F. Kikkawa, S. Mitzutani.** Aminopeptidase A expression in cervical neoplasia and its relationship to neoplastic transformation and progression. – *Oncology*, **58**, 2000, 342-352.
3. **Marc, Y., C.Llorens-Cortes**. The role of the brain renin–angiotensin system in hypertension: Implications for new treatment. – *Progress in Neurobiology*, **95**, 2011, 89–103.
4. **Martinez, J. M., I. Prieto, M. J. Ramirez, C. Cueva, F. Alba, M. Ramirez**. Aminopeptidase activities in breast cancer tissue. – *Clin. Chem.*, **45**, 1999, 1797–1802.
5. **Martinez-Martos J-M, Carrera-Gonzalez MP, Duenas B, Mayas M-D, Garcia MJ, Ramirez-Exposito, M. J**. Renin angiotensin system-regulating aminopeptidase activities in serum of pre- and postmenopausal women with breast cancer. – *The Breast*, **20**, 2011, 444-447.
6. **Mosmann, T.** Rapid colorimetric assay for cellular growth and survival: Application to proliferation and cytotoxicity assays. – *J. Immunol. Methods*, **65**, 1983, 55-63.
7. **O-Wang, J., M. D. Cooper, X. Iturrioz, C. Llorens-Cortes**. Glutamyl Aminopeptidase. – In: *Handbook of proteolytic enzy*mes (Eds. N. D. Rawlings, G. Salvesen), Academic Press Elsevier, 2013, 410-414.
8. **Suganuma, T., K. Ino, K. Shibata, S. Nomura, H. Kajiyama, E. Kikkawa, N. Tsuruoka, S. Mizutsni.** Regulation of aminopeptidaseA expression in cervical carcinoma: role of tumor-stromal interaction and vascular endothelial growth factor. – *Lab. Invest.*, **84**, 2004, 639-648.

Institute of Experimental Morphology, Pathology and Anthropology with Museum
Bulgarian Anatomical Society

Acta morphologica et anthropologica, 25 (3-4)
Sofia ● 2018

Mast Cells in the Rat Tongue

Nikola Pirovski[1], Nikola Tomov[2], Dimitrinka Atanasova[2,3], Nikolay Dimitrov[2]*

[1] *Medical College, Faculty of Medicine, Trakia University, Stara Zagora, Bulgaria*
[2] *Department of Anatomy, Faculty of Medicine, Trakia University, Stara Zagora, Bulgaria*
[3] *Institute of Neurobiology, Bulgarian Academy of Sciences, Sofia, Bulgaria*

* Corresponding author e-mail: pirovsky@abv.bg

The aim of the present study is to determine the quantity, distribution and age differences of the mast cells in rat tongue (in lamina propria and muscle layer). The experiments were carried out on rats of different ages - 20 days, 3 months and 1 year. We used toluidine blue and Bismarck brown staining for visualization of mast cells. We observed more mast cells around nerve bundles and blood vessels. In 20 days and 3 months old rats we observed more mast cells in the deep muscular layer of the tongue compared to lamina propria. The density of mast cells in 1 year old rats was equal in lamina propria and muscle layers. Distribution of mast cells in rat tongue was different in rats of different ages. The total number of mast cells was constant during lifetime; only the distribution changed. Furthermore, we show that staining with Bismarck brown demonstrates more reliable results.

Key words: rat, tongue, mast cells

Introduction

The tongue is an interesting structure in many ways. Substances are commonly administered sublingually, its observation has an important diagnostic value, it is a frequent trauma spot, as well as a target of reflexology manipulation. Mast cells distribution and involvement in processes involving the tongue are therefore interesting to study. The data regarding their normal distribution in the tongue are scarce. Even though rat mast cells differ from human ones, they are still suitable for preliminary testing and control group for experiments with other animals.

It has been previously established, that in the tongue, the mast cell concentration was the same both along its length and in the symmetrical parts of the organ. The concentration of mast cells diminished considerably from the tongue, the duodenum and down to the stomach [14]. Researchers have observed that numerous mast cells were scattered throughout the submucosal region, adjacent to nerve bundles, blood vessels, and skeletal muscle. Mast cells occurred within bundles containing both myelinated and unmyelinated nerves in the rat tongue. Despite this data, no clear evidence for the existence of any specific mast cell distribution in other parts of the animal body has been provided [2].

In mice, mast cells were present in abundance in the tongue, and there was no clear evidence of a difference between numbers of mast cells in animals of different age or

sex [6]. Considerable mast cell heterogeneity exists within the gastrointestinal mucosa of the mouse and indicates that there are both similarities and differences between mouse and rat in the distribution of mast cells and of their granule proteinases [10].

In healthy rats, mast cells were present in abundance in mesenteric lymph nodes and tongue. There was no clear evidence of a difference between numbers of mast cells in young and older animals. There were more mast cells in rats than in mice. Mast cells appear to be more abundant in Wistar rats than in Sprague Dawley rats. Mast cells were hardly seen in dogs and primates except for a few in tongue and sciatic nerve [7].

Mast cell populations in mammals have been recognized as morphologically and functionally heterogeneous. It is currently accepted that mast cell heterogeneity occurs not only in different species but also within the same organ in the same species. Mast cells in the nasal mucosa are essentially unaffected by the polyamine compound 48/80, indicating that they are functionally dissimilar to the connective tissue type mast cells exemplified by those present in the rat tongue [3]. In the rat, the individual mast cell secretory granules may be divided into three subpopulations based on the presence of the specific proteases RMCP-1, RMCP-2, or a variable combination of these two proteases. Mast cells in the tongue only express RMCP-1, both in normal and infected animals [5].

The aim of the present study is to determine the quantity, distribution and age differences of the mast cells in rat tongue, comparing lamina propria and muscle layer.

Materials and Methods

The experiments were carried out on six male and female Wistar rats from each age – 20 days (65-80 g body weight), 3 months (220-350 g) and 1 year (400-450 g). The experimental design was approved by the Research Ethics Committee at the Faculty of Medicine of Trakia University (TrU project number: 1317/2017 MF). All efforts were made to minimize the number of animals used and their suffering. For the histological preparations, the rats were deeply anaesthetized with Ketamine-Xylazine with the usual dosage, and perfused first with 0.05 M PBS followed by 4% PFA in 0.1 M phosphate buffer, pH 7.36. Tongues were dissected, and postfixed in the same fixative overnight at 4 °C. Tissue was paraffin-embedded and sectioned on a conventional microtome in 5 μm sections. We used classical histological staining techniques: H&E, Toluidine Blue and Bismarck Brown [13]. Cells were counted per viewfield at x200 (0,163 m^2) using LAS v.4.12 (Leica, Germany). Mast cell density was expressed as mean number of cells per viewfield. For the statistic evaluation, we counted the cells on 5 different sections per animal, 5 viewfields per slice, for each staining. Raw data were analyzed using GraphPad Prism 6 (GraphPad Inc, USA) with one-way analysis of variance (ANOVA) followed by Tukey's post-hoc test for multiple comparisons. P values < 0.05 were considered statistically significant.

Results

The results show interesting trends in the mean count of mast cells in different ages, layers, and stains. We observed that numerous mast cells in rats were scattered throughout the lamina propria (**Fig.1**) and in the deep muscular layer (**Fig. 2**). We observed more mast cells in the loose connective tissue around nerve bundles and blood vessels. Mast cells were observed as solitary cells or in groups of several cells.

Distribution of mast cells was different between 20 days, 3 months and 1 year old rats. In 20 days and 3 months old rats we observed more mast cells in the deep muscular

layer of the tongue compared to lamina propria. The density of the mast cells in 1 year old rats was equal in lamina propria and muscle layers. At the age of 1 year the quantity of the mast cells in both layers was without statistical difference (**Fig. 3**). The mean number of mast cells per viewfield was around 8 (8,45-8,77) in all ages (**Table 1**). The total number of mast cells does not change during lifetime, it remains the same, however the distribution changes.

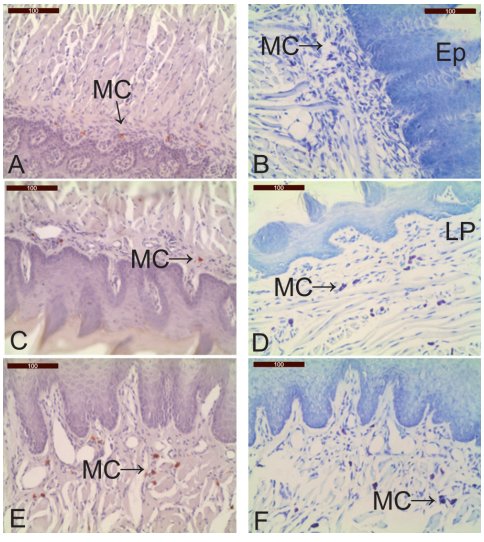

Fig. 1. Mast cells in lamina propria of rat tongues stained with Toluidine Blue (B, D, F) and Bismarck Brown (A, C, E) form 20d, 3m, 1y rats. MC - mast cells, Ep- epithelium, LP- lamina propria. Scale bar = 100 μm.

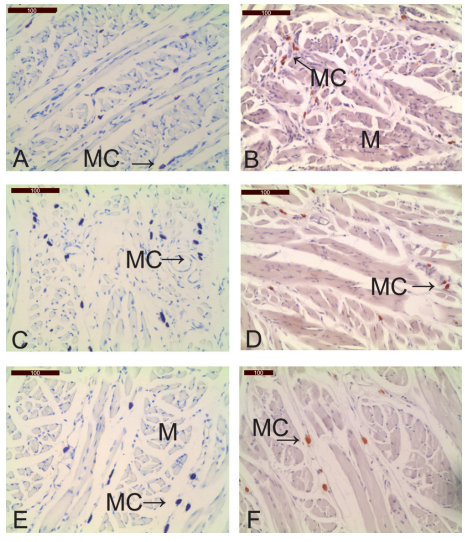

Fig. 2. Mast cells in muscle layer of rat tongues stained with Toluidine Blue (A, C, E) and Bismarck Brown (B, D, F) form 20d, 3m, 1y rats. MC – mast cells, M - muscle layer. Scale bar = 100 μm.

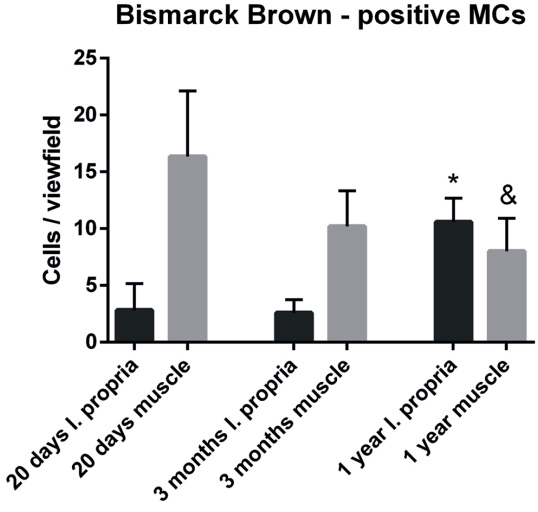

Fig. 3. One-way analysis of variance (ANOVA) with Tukey's post-hoc test for multiple comparisons of mast cell counts of different ages (data from analysis of Bismarck brown staining only). *$p<0.01$ (3 months lamina propria vs. 1 year submucosa); &$p<0.01$ (20 days muscle vs. 1 year muscle)

The different stains used showed some difference in the demonstrated numbers of mast cells. Toluidine blue staining produced a great variability of the numbers of mast cells in lamina propria and muscle layer (**Table 1**). Bismarck Brown staining, on the other hand, demonstrated more reliable results compared to Toluidine blue staining, mainly because of the more consistent results obtained.

Table 1. Mean count of mast cells in different ages (20d, 3m, 1y rats) and layers (lamina propria and muscle layer) and stains (Toluidine Blue and Bismarck Brown).

Numb. of mast cells in one visual area, mag. X20							
stain	Bismark Braun		Toluidin Blue				
layer	lam.pr.	muscl.	lam.pr.	muscl	maen lam.pr.	mean muscl.	mean all
age							
20 d	2,833333		7,4285714		5,130952381		
		16,33333		8,5		12,41666667	8,77381
3 m	2,6		5,2857143		3,942857143		
		10,2		15,375		12,7875	8,365179
1 y	10,6		6,5714286		8,585714286		
		8		7,7143		7,857142857	8,221429
mean quantity of mast cells in one visual area at x20 during lifetime							8,453472

Discussion

It has been previously described, that the total number of mast cells was similar in the superficial layers of all oral tissues studied. There were more mast cells in the deeper than in the superficial portions of the tongue. Mast cells with staining characteristics and size similar to those observed in the intestinal mucosa (MMCs) were found together with 'classical' connective tissue mast cells (CTMCs). The results suggest that the mast cell population of oral mucosal tissues of the rat contains both CTMC- and MMC-like cells [8]. The mast cell population is very dynamic and can respond to different stimuli – a considerable increase of density of mast cells in rat mucosae was reported after photodynamic therapy [11].

The close anatomical associations suggest communication between nerve fibers and immune cells, which can be crucial for maintaining mucosal homeostasis and for ensuring an appropriate response to injury [4]. That could be part of the morphological substrate of the reflexogenic response after tongue manipulations (like acupuncture). Also the involvement of mast cells with branches of the trigeminal nerve is not to be ignored. TN stimulation has been shown to result in MC activation and oral vascular permeability, suggesting that MC inhibitors may be used for the treatment of oral inflammatory diseases [1].

Some age differences in the distribution of oral mast cells have been previously reported. It has been demonstrated that the total number of mast cells in the tongue, buccal mucosa, and gingival mucosa was significantly higher in the juvenile than in the adult rats. In the buccal and gingival mucosa, more than twice as many mast cells were found in the young animals [9].

The results obtained in our study indicate that both staining used by us (Toluidine blue and Bismarck brown) were suitable for visualizing the mast cells, however the Bismarck brown showed better grouping of the results, which could be due to lower specificity of the Toluidine Blue for mast cells and the staining of eosinophil and plasmatic cells alongside mast cells. The quantity of mast cells per visual area was constant in all samples but the distribution changed with age. Young animals have lower number of mast cells in lamina propria than in the muscle layer. This distribution could be a normal feature for the growing organism. The older animals have equal distribution as their structural development is completed.

A comparative characterization of the oral mucosa in various animals is needed to identify the best animal model(s) for nonclinical evaluation of sublingual immunotherapy products. The oral mucosae of minipigs and monkeys are closest to that of humans, and the immune networks are quite similar between all rodents and non-rodents. That data also support the use of rats and minipigs to perform biodistribution and safety studies of sublingual products [12]. Interesting area for our future work could be studying the effects of the acupuncture on the rat tongue.

Conclusions

Distribution of mast cells in rat tongue was different in rats of different ages. The total number of mast cells does not change during lifetime; however, the distribution in lamina propria and the muscle layer changes significantly. The staining with Bismarck brown demonstrated more reliable results.

References

1. **Alhelal, M. A., I. Palaska, S. Panagiotidou, R. Letourneau, TC. Theoharides** Trigeminal nerve stimulation triggers oral mast cell activation and vascular permeability. – *Ann. Allergy Asthma Immunol*., **112**(1), 2014, 40-45.
2. **Chapman, G. B.** Occurrence of mast cells within bundles of myelinated and unmyelinated nerves in the rat tongue. – *Anat. Rec*. **256**(4), 1999, 347-353.
3. **Gomez, E., O. J, Corrado, R.J. Davies.** Histochemical and functional characteristics of the human nasal mast cell. – *Int. Arch. Allergy Appl. Immunol*., **83**(1), 1987, 52-56.
4. **Kispélyi, B., Z. Lohinai, K. Altdorfer, E. Fehér**. Neuropeptide analysis of oral mucosa in diabetic rats. – *Neuroimmunomodulation*, **21**(4), 2014, 213-220.
5. **Krüger, P. G., J. F. Huntley, A. MacKellar, J. Røli, G.F. Newlands**. Mast cell and mast cell granule phenotypes in normal and Nippostrongylus-infected rats. Aqualitative laser confocal microscopic study. – *APMIS,* **105**(3), 1997, 229-237.
6. **Majeed, S. K.** Mast cell distribution in mice. – *Arzneimittelforschung*, **44**(10), 1994, 1170-1173.
7. **Majeed, S. K**. Mast cell distribution in rats. – *Arzneimittelforschung,* **44**(3), 1994, 370-374.
8. **Matsson, L.** Mast cell heterogeneity in various oral mucosal sites in the rat. – *Arch. Oral Biol*., **37**(6), 1992, 445-450.
9. **Matsson, L.** Presence of mast cells in various oral mucosal sites in juvenile and adult rats. – *Scand. J. Dent. Res*., **101**(5), 1993, 292-298.
10. **Miller, H. R., J. F. Huntley, G. F. Newlands, A. Mackellar, D. A. Lammas, D. Wakelin D.** Granule proteinases define mast cell heterogeneity in the serosa and the gastrointestinal mucosa of the mouse. – *Immunology*, 65(4), 1988, 559-566.
11. **Rosin, F. C., A. R. Barcessat, G. G. Borges, L. Corrêa.** Effect of 5-ALA-mediated photodynamic therapy on mast cell and microvessels densities present in oral premalignant lesions induced in rats. – *J. Photochem. Photobiol. B*., **153,** 2015, 429-434.

12. **Thirion-Delalande, C., F. Gervais, C. Fisch, J. Cuiné, V. Baron-Bodo, P. Moingeon, L. Mascarell.** Comparative analysis of the oral mucosae from rodents and non-rodents: Application to the nonclinical evaluation of sublingual immunotherapy products. – *PLoS One*, **12**(9), 2017, e0183398.
13. **Tomov, N., N. Dimitrov.** Modified Bismarck brown staining for demonstration of soft tissue mast cells. – *Trakia Journal of Sciences,* **3**, 2017, 195-197.
14. **Zakharov, M. K., V. V. Bogach**. Assessment of the quantity of mast cells in the organs of the gastrointestinal tract of rats and frogs. – *Biull. Eksp. Biol. Med*., **81**(1), 1976, 94-95.

Institute of Experimental Morphology, Pathology and Anthropology with Museum
Bulgarian Anatomical Society

Acta morphologica et anthropologica, 25 (3-4)
Sofia ● 2018

Morphology of Mesenchymal Stem Cells in 3D spheroids

*Radko Sotirov, Milena Kostadinova, Shina Pashova, Snejana Kestendjieva, Kameliya Vinketova, Desislava Abadjieva, Elena Stoyanova, Tsvetelina Oreshkova, Elena Kistanova, Milena Mourdjeva**

Institute of Biology and Immunology of Reproduction, Bulgarian Academy of Sciences, Sofia, Bulgaria

* Corresponding author e-mail: milena_mourdjeva@abv.bg

The conventional method of cell cultivation in plasticware leads to the formation of a monolayer of cells with changed morphology and intercellular communications. Here, the method of the hanging drop is used as a technique for 3D cultivation of adipose tissue-derived mesenchymal stem cells to study the morphological changes of cells, which compose the spheroids. Three cell lines were investigated and were shown to form spheroids in hanging drops after 24 hours. A time-dependent decrease of x and y dimensions of the spheroids and a simultaneous increase of z dimension were observed. Changes in morphology and the nuclei volume of the cells at day 3 and day 5 in 3D culture compared to monolayer cell culture were observed indicating the importance of the type of culture conditions (2D and 3D) for the communications and physiology of the cells.

Key words: Mesenchymal stem cells, 3D, Spheroids, Spheroid size, Nuclei size

Introduction

Mesenchymal stem cells (MSC) are multipotent stem cells which exist in different tissues of adult organisms. They are self-renewable, and can easily be isolated and expanded for long periods *in vitro*, without losing their major biological characteristics. Initially, MSC have been isolated from bone marrow, but later on techniques have been elaborated for isolation of MSCs from almost all other tissues. To date, there are no MSC-specific markers known; therefore, the International Society for Cellular Therapy has defined three criteria, which should be fulfilled in order to assign a cells to MSC type. These criteria are: (a) ability of adherence to lab plasticware; (b) expression of specific surface antigens ($CD73^+$, $CD90^+$ and $CD105^+$) and lack of expression of hematopoietic antigens, such as ($CD45^-$, $CD34^-$, $CD11b^-$ and HLA class II); and (c) potential for differentiation in different cell types, such as osteoblasts, adipocytes and chondrocytes [5]. Due to their multipotency, MSC are a promising candidate for vast applications in regenerative medicine. Moreover, this type of stem cells has the ability to migrate to the sites of injured tissues in the organism where they help tissue recovery by secreting various growth factors and cytokines. Other significant biological property of MSC is their participation as immunomodulators in the places of inflammation [summarized in 8].

In vitro, MSC are usually maintained in long-term 2D condition without undergoing any significant abnormalities. MSC adhere to plastic labware, proliferate and form monolayer during cultivation. This artificial condition of maintenance of MSC is different from the natural microenvironment in the organism and leads to atypical morphology of some cell types, when they are cultured in a monolayer. Furthermore, this way of cell culturing limits cell-to-cell contacts and the opportunities of the cells to form natural structures specific for organisms. The three-dimensional (3D) cell culture creates an environment in which the cells grow and interact among them in the space [4]. There are different techniques for 3D culturing but the hanging drop method is the easiest and the most commonly used. A cell suspension with a defined concentration is placed on the lid of a Petri dish. This prevents the cells from adherence to the lab plasticware and leads to the formation of three-dimensional structure called spheroid. These 3D cell structures provide closer to the natural environment for the cell maintenance compared to the 2D monolayer culturing, and are a better model for studies in regenerative medicine, cell therapies, drug testing, tumor biology and stem cell research [3].

The purpose of this work is to investigate the process of formation of 3D cell structures (spheroids) by adipose tissue-derived mesenchymal stem cells (ASC) as well as to study the occurring morphological changes of the cells when they are cultured in 3D condition.

Material and Methods

Cell Cultures. Human mesenchymal stem cells from adipose tissue (ASC) have been isolated, characterized and cultured in DMEM supplemented with 10% fetal calf serum and 1% Penicillin, Streptomycin, Amphotericin B (Sigma) in 2D culture condition to achieve a confluent monolayer. The method of the hanging drop was used for spheroid formation. Thirty-five µl cell suspension drops (25 000 cells/drop) were placed and cultured on the lid of Petri dishes at 37°C, 5%CO_2.

Light microscopy. The spheroids were taken on pictures every 24 hours from day 1 to day 6 of cultivation via LeicaDMI 3000B. The spheroids' dimensions (x; y) have been measured [µm] by LAS version 3.4.0 software. The data was analysed by Excel.

Confocal microscopy. Spheroids in hanging drops have been prepared for confocal microscopy on day 3 and day 5. Nuclei staining was performed by 20 µg/ml Hoechst 33258 (Sigma) in 1xPBS for 1h at room temperature. The spheroids were washed three times in 1xPBS and mounted on slides with Eukitt® quick hardening mounting medium (Sigma). 3D structures have been scanned: 1) whole spheroids and 2) the periphery and the center area of the spheroids. The size (x; y; z) of the nucleus of each cell was measured by ImageJ in different parts of the spheroids. The data was analyzed in Excel.

Statistical analysis. Standard data deviations were calculated in Excel and are shown on figures.

Results

Spheroids in hanging drops in 35 µl culture medium and concentration 25 000 cells/drop were prepared from three primary cell cultures of adipose tissue-derived mesenchymal stem cells (ASC07, ASC08 and ASC10). The formation of spheroid-like structures from each cell line was detected after 24 hours via light microscopy. One spheroid was formed in each

drop and its morphology and structure were observed till day 6 (**Fig. 1A**). All spheroids were organized in compact, round structure with smooth edges. The size of the spheroids (x; y) was measured every 24 hours from day 1 to day 6 (**Fig. 1B, C and D**). All spheroids decreased in size (x; y) during the 6 day period of culturing showing changes in the range from 450-500 µm/diameter at day 1 to 290-350 µm at day 6. The change of the size was different for the spheroids formed by different cell lines. ASC07 spheroids decreased the most showing a reduction of 30%: from ~450µm/diameter at day 2 to ~290µm/diameter at day 6, while the spheroids from the other two ASC primary cultures shrank to lesser extent.

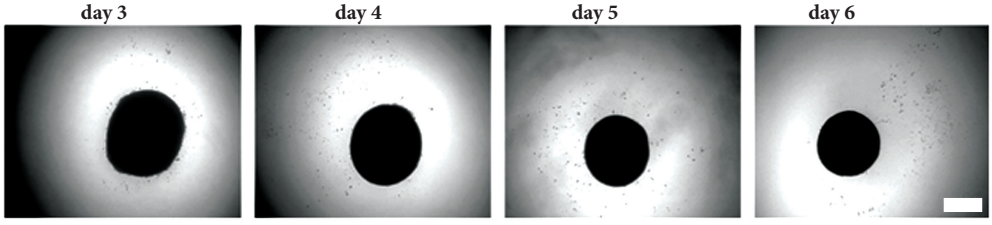

Fig. 1A

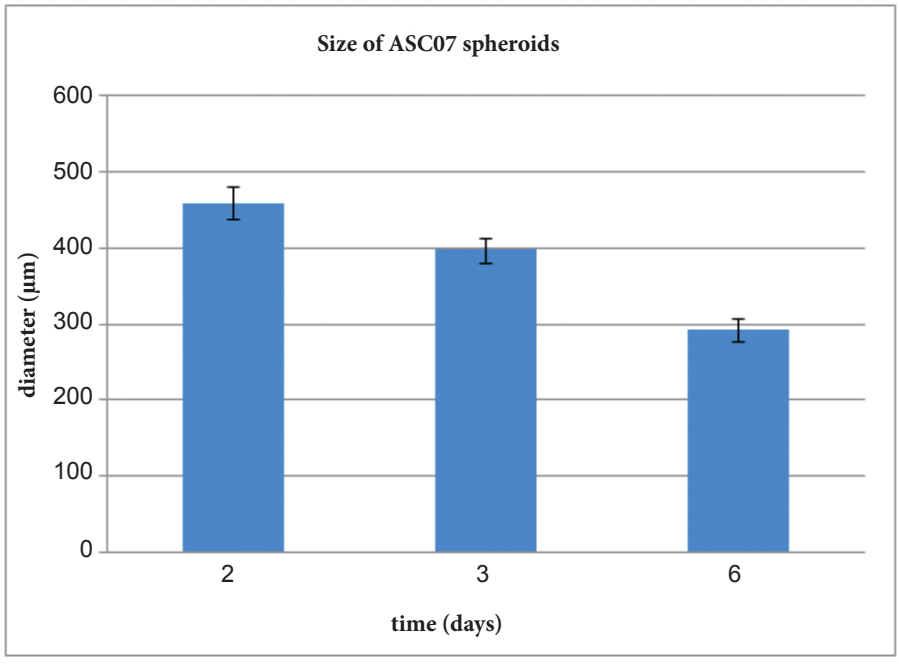

Fig. 1B

Fig. 1C

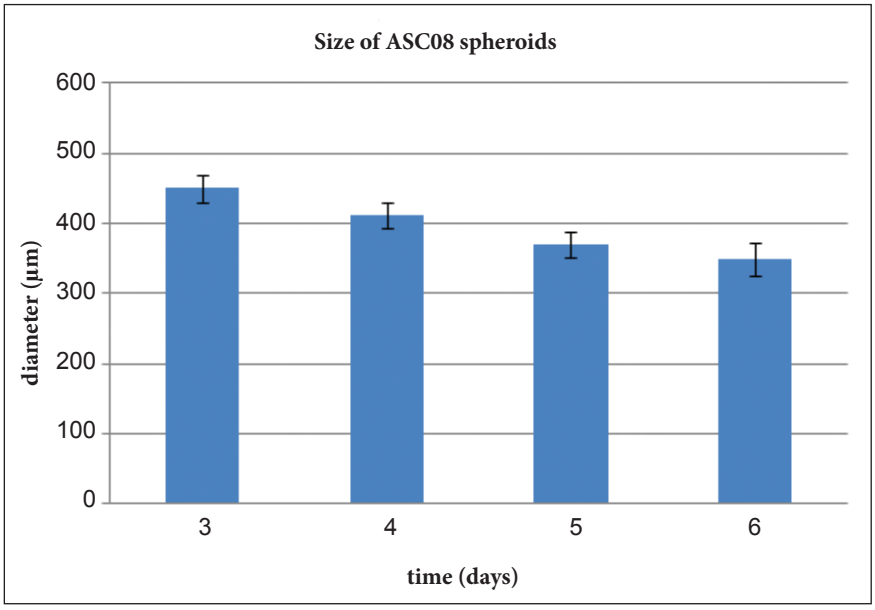

Fig. 1D

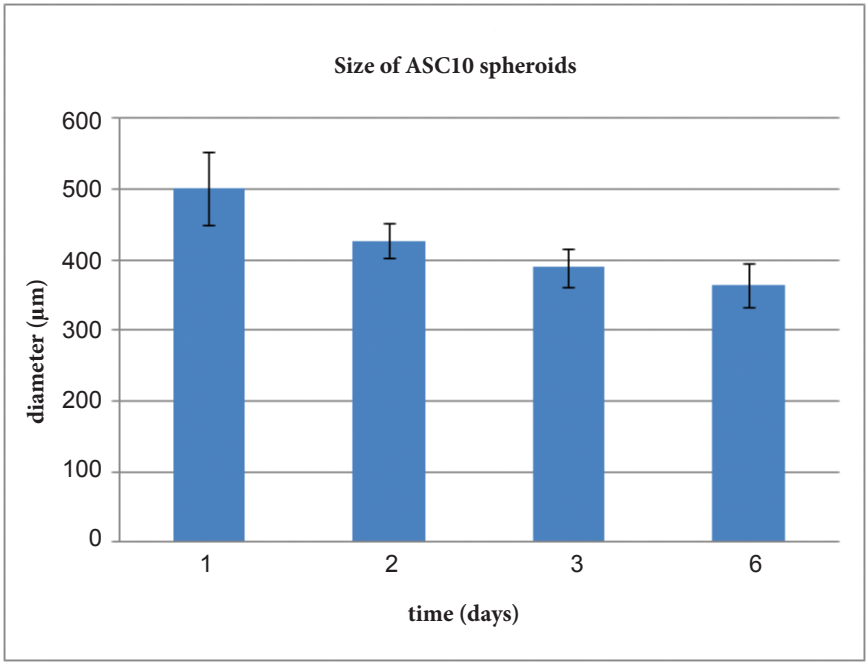

Fig. 1. Morphology of ASC spheroids. (A) Light microscopy of ASC08 spheroids from day 3 to day 6; Charts of average diameter (µm) of ASC07 spheroids, n = 20 (B); ASC08 spheroids, n = 58, at day 2 and day 3; n = 18, at day 5 and day 6 (C); and ASC10 spheroids, n = 22 (D) measured every 24 hours from day 1 to day 6. Scale bar = 200 µm

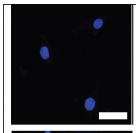

2D single cells	Nuclei diameter (µm)	Cell area diameter (µm)
Mean	12.974	38.151
SD	3.316	20.433
Min	7.488	11.264
Max	22.645	86.72

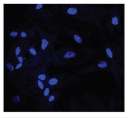

2D monolayer	Nuclei diameter (µm)	Cell area diameter (µm)
Mean	12.09	36.731
SD	2.618	9.676
Min	6.671	16.682
Max	18.333	64.262

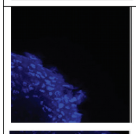

3D day 3 - periphery	Nuclei diameter (µm)	Cell area diameter (µm)
Mean	5.841	8.905
SD	1.232	1.74
Min	2.641	5.213
Max	9.712	14.296

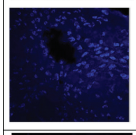

3D day 3 - core	Nuclei diameter (µm)	Cell area diameter (µm)
Mean	6.25	8.096
SD	1.337	1.394
Min	3.597	4.195
Max	10.792	10.937

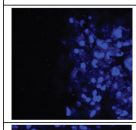

3D day 5 - periphery	Nuclei diameter (µm)	Cell area diameter (µm)
Mean	7.146	9.403
SD	1.299	1.69
Min	4.438	6.014
Max	10.671	15.541

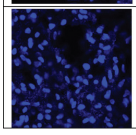

3D day 5 - core	Nuclei diameter (µm)	Cell area diameter (µm)
Mean	7.959	11.413
SD	1.164	1.921
Min	5.276	6.479
Max	11.151	16.069

Fig.2. Comparison between dimensions of ASC10 cell nuclei in 2D and 3D culture conditions. Left panel: confocal microscopy of cells in 2D conditions compared to cells in 3D spheroids (nuclei staining – Hoechst 33258). Right panel: Table of average diameter (µm) of nuclei and cell area in 2D and 3D conditions. Scale bar = 50 µm

Furthermore, a comparison of cell morphology between 2D and 3D culture conditions was performed. The dimensions of nuclei and cytoplasm (**Fig. 2**) were studied. First, ASC10 cell line was used to compare the size of nuclei and cytoplasm of non-confluent to confluent ASC grown in 2D conditions. The results showed no significant difference of nuclei and cytoplasm in both culture conditions. In average the size of nuclei was ~12-13 µm/diameter and cell area ~36-38µm in diameter independent of the confluence of ASC. Nevertheless, a distinctive difference in the morphology of ASC nuclei was observed. In the non-confluent cultures the nuclei had more rounded shape unlike the elongated nuclei of ASC in confluent state of culture. Moreover, we measured the size of ASC nuclei in the 3D spheroids and compared the results with 2D culture. At day 3 and day 5 the size of ASC nuclei in the periphery and the center of spheroids were compared. The results showed a significant decrease of the nuclei dimensions (x; y), which changed from ~12-13 µm in 2D to ~6-8µm in 3D. Also taking into account the z dimention, the volumes of nuclei showed even more significant decrease: from 310-360 μm^3 in 2D to 134 μm^3 in the center and 109 μm^3 in the periphery of 3D spheroids on day 3. On day 5, the nuclei doubled their volumes in 3D cultures becoming 273 μm^3 in the center and 197 μm^3 in the periphery of the spheroids. Similar results were also observed for the cells size (**Fig. 2**).

The morphology of the spheroids is presented by confocal microscopy on **Fig. 3**. While the light microscopy revealed decrease in x and y dimensions of 3D spheroids during the culturing, the measurement of z dimention by confocal microscopy showed an increase of the spheroids from 40-50 µm at day 2 and day 3 to 150 µm at day 6. In addition the confocal imaging revealed the formation of cavities in the center of some spheroids.

Discussion

Hanging drop method for spheroid formation eliminates surface attachment by placing the cell suspension in a drop, allowing gravity to facilitate cellular aggregation at the bottom of the drop [6]. Here, our results showed that ASC aggregated at the bottom of the drop in the first day of spheroids formation. Confocal imaging revealed a sheet-like aggregation of ASC in the spheroids when investigated in z dimention at day 3. At day 6 the structures significantly increased in z axis. Corresponding to this result, the nuclear

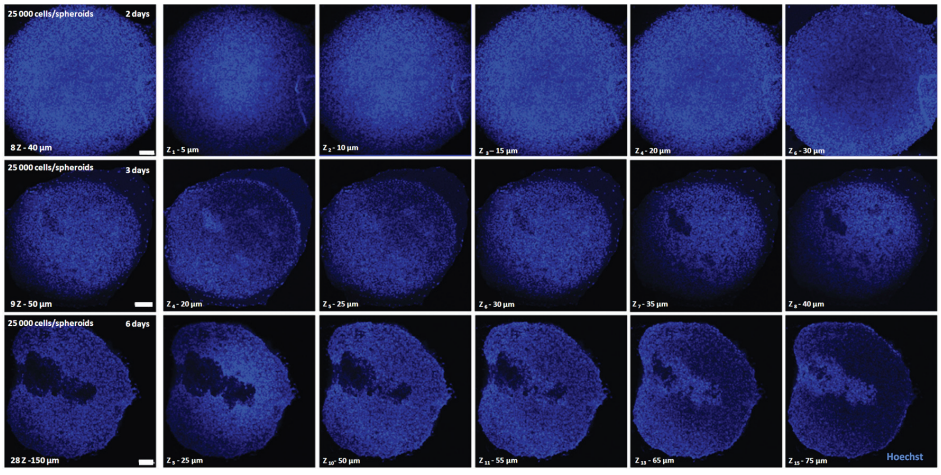

Fig. 3. Confocal microscopy of ASC07 spheroids (nuclei staining – Hoechst 33258): Changes of structure and thickness (on z axis) of spheroids on day 2, day 3 and day 6. Scale bar = 100 µm

volumes initially decreased by 72% till day 3, and thereafter doubled their volume by day 5, when compared to 2D culturing. A significant 75% reduction of the size of MSCs in spheroids compared to cells in 2D monolayer was reported by others [1, 2, 10, 11]. Our observation that nuclei volume reduces to the same extend confirms the data from the literature. We have not observed more elongated cells in the periphery of the spheroids, reported by Zhang Q [11], but the nuclei dimensions in the center and in the periphery of the spheroids are slightly different. The nuclei of the cells in the center are larger than those in the edges of the spheroids. Additionally, the shape of the nuclei changed and the cells in the spheroids showed sphere-like shape of nuclei, while the cells in the monolayer had ellipsoid-like nuclei. In MSC biology cellular morphology is a key characteristic used to determine cellular phenotypes, ability for differentiation and fates of MSC. Cytoskeletal reorganization and drastic changes in cell morphology in MSC spheroids indicate a major difference in mechanophysical properties compared with 2D culture [3].

Now it is well known that conventional methods of cell cultivation provide conditions which are very different from the natural environment of the cells. The necessity of adding a third dimention to the cell culture system, more closely resembles the natural environment and might generate significant differences in MSCs phenotype, behavior and therapeutic potential, which is increasingly recognized in the literature [7, 9].

Conclusion

The main observations in this work are the reduction of x and y dimensions of ASC spheroids during the culturing and simultaneous enlargement in z direction; nuclei volumes in 3D on day 3 lessening to 38%, compared to 2D, but doubled between day 3 and 5.

Acknowledgement: This research was supported by grant DCOST01/18, NSF, Bulgaria.

References

1. **Baraniak, P. R., M. T. Cooke, R. Saeed, M. A. Kinney, K. M. Fridley, T. C. McDevitt.** Stiffening of human mesenchymal stem cell spheroid microenvironments induced by incorporation of gelatin microparticles. – *J. Mech. Behav. Biomed. Mater*., **11**, 2012, 63-71.
2. **Bartosh, T. J., J. H. Ylostalo, A. Mohammadipoor, N. Bazhanov, K. Coble, K. Claypool, R. H. Lee, H. Choi, D.J . Prockop**. Aggregation of human mesenchymal stromal cells (MSCs) into 3D spheroids enhances their antiinflammatory properties. – *Proc. Natl Acad. Sci. U S A*, **107**, 2010, 13724-13729.
3. **Cesarz, Z., K. Tamama**. Spheroid culture of mesenchymal stem cells. – *Stem Cells Int*., 2016, 9176357.
4. **Delphine, A., H. Burckel, E. Josset, G. Noel.** Three-dimensional cell culture: a breakthrough in vivo. – *Int. J. Mol. Sci*., **16**, 2015, 5517-5527.
5. **Dominici, M., K. Le Blanc, I. Mueller, I. Slaper-Cortenbach, F. C. Marini, D. S. Krause, R. J. Deans, A. Keating, D. J. Prockop, E. M. Horwitz.** Minimal criteria for defining multipotent mesenchymal stromal cells. The International Society for Cellular Therapy position statement – *Cytotherapy*, **8**, 2006, 315-317.
6. **Foty, R**. A simple hanging drop cell culture protocol for generation of 3D spheroids. – *J. Vis. Exp*., 51, 2011, Article ID e2720.
7. **Mueller-Klieser, W**. Three-dimensional cell cultures: from molecular mechanisms to clinical applications. – *Am. J. Physiol*., **273**, 1997, C1109-Cl123.
8. **Nayoun, K., S.-G. Cho**. Clinical applications of mesenchymal stem cells. – *Korean J. Intern. Med.*, **28**, 2013, 387-402.
9. **Saleh, F. A., J. E. Frith, J. A. Lee, P. G. Genever**. Three-dimensional in vitro culture techniques for mesenchymal stem cells. – *Methods Mol. Biol*., **916**, 2012, 31-45.
10. **Tsai, A.C., Y. Liu, X. Yuan, T. Ma.** Compaction, fusion, and functional activation of three-dimensional human mesenchymal stem cell aggregate. – *Tissue Eng. Part A*, **21**, 2015, 1705-1719.
11. **Zhang,** Q., **A. L. Nguyen, S. Shi, C. Hill, P. Wilder-Smith, T. B. Krasieva, A. D. Le.** Three-dimensional spheroid culture of human gingiva-derived mesenchymal stem cells enhances mitigation of chemotherapy-induced oral mucositis. – *Stem Cells Dev*., **21**, 2012, 937-947.

Institute of Experimental Morphology, Pathology and Anthropology with Museum
Bulgarian Anatomical Society

Acta morphologica et anthropologica, 25 (3-4)
Sofia ● 2018

Anthropology and Anatomy

Anthropological Investigations of Necropolis from the Ottoman Period Revealed during the Excavations of Archaeological Site "Trayanovi Vrata", Located in the Kapiyata Locality, Kostenets Municipality

Nadezhda Atanassova

Institute of Experimental Morphology, Pathology and Anthropology with Museum, Bulgarian Academy of Sciences, Sofia, Bulgaria

* Corresponding author e-mail: naditimeva@gmail.com

In 2016 were carried out excavations of archaeological site "Trayanovi vrata", located in the Kapiyata locality, Kostenets municipality (Sofia Province). In one of the trenches was excavated a Christian necropolis with 15 graves (15th-17th c.) of civilian population. The burial ritual was inhumation. The aim of the present study is to provide generalized anthropological information about the skeletons in this necropolis: age-at-death and sex distribution, stature, body mass and paleopathological changes. During the anthropological investigation have been identified remains from 19 individuals. In this skeletal series predominate the subadults in a ratio of 1:0.73, as the most numerous group is this of the infants up to the age of 7 (47.37%). The identification of porous skull lesions in subadult and adult individuals is indicative of anaemic conditions in the population.

Key words: Christian necropolis, Ottoman period, paleoanthropological analysis, paleopathology

Introduction

The excavations of archaeological site "Trayanovi vrata", located in the Kapiyata locality, Kostenets municipality (Sofia Province), were carried out in 2016 under the leadership of Gergana Kabakchieva and Vladislav Todorov. The main purpose of this research was to reveal the remains of the famous "Trayan's gate" in the ancient pass "*Suki*". In one of the trenches was excavated a Christian necropolis with 15 graves of civilian population. The burials were marked with stones and orientated West-East. In three of the burial structures have been found jewellery, by which the archaeologists

dated the necropolis in the 15th-17th c. [9]. The burial ritual was inhumation. During the field anthropological investigation have been identified bone remains from 19 individuals. **The aim** of the present study is to provide generalized anthropological information about the skeletons in this necropolis: age-at-death and sex distribution, stature, body mass and paleopathological bone changes.

Material and Methods

This paper includes results of detailed anthropological investigation of 19 inhumated skeletons from Christian necropolis at archaeological site "Trayanovi vrata", Kapiyata locality, Kostenets municipality (Sofia Province). The human bone material is in poor condition. The skeletons are fragmented and incompletely represented. A fully preserved skull was found only in one case (grave No. 9).

Using well established anthropological methods [1, 3, 4, 5, 6, 7, 8, 10, 11, 16, 18], metric and scopical analyzes of the osteological materials were made in order to determine the age-at-death and sex of the investigated individuals. The reconstruction of the height (by Pearson-Lee [14] and Trotter-Gleser [17]) and the evaluation of the body mass (by Ruff et al. [15]) of adults were carried out depending on the condition of the presented bones. The health status of the studied population was assessed by age and sex distribution of the identified morphological bone changes by Aufderheide, Rodriguez-Martin [2], Ortner, Putschar [13] and Ortner [12].

Results and Discussion

Age-at-death and sex distribution (**Table 1**)

The age and sex distribution of the investigated buried individuals is as follows: one fetus (38-40 gestational week) and eight children in *Infans I*; two female juveniles; only one male in the age group *Adultus* (20-40 years); four men in *Maturus* (40-60 years); two males and one female in the group *Adultus+* (>18/20 years). In this skeletal series predominate the subadults in a ratio of 1:0.73, as the most numerous group is this of the infants up to the age of 7 years (47.37%). Concerning adults, males from the age group *Maturus* prevail and only one female was defined at the age over 18/20 years. None individual from both sexes was identified in the elderly (>60 years).

Table 1. Age-at-death and sex distribution of the investigated individuals from the necropolis at archaeological site "Trayanovi vrata" (Sofia Province).

Age group																					
Fetus	***Inf I***	***Inf II***	***Juvenis***			***Adultus***					***Maturus***			***Senilis***		***Adultus+***					**Total**
			♂	♀	♂♀	♂	♂**?**	♀	♀**?**	♂♀	♂	♀	♂♀	♂	♀	♂	♂**?**	♀	♀**?**	♂♀	
1	8	0	0	2	0	1	0	0	0	0	**4**	0	0	0	0	2	0	1	0	0	**19**

Stature and body mass estimation (Fig. 1)

The height and body mass have been reconstructed in only one adult female individual (grave No. 1) who was with "middle" stature and 63.39 kg body weight. Concerning the male sex, the height varies from 161.69 cm to 168.31 cm by the formula of Pearson-Lee [14] and from 166.59 cm to 173.33±3.71 cm by the formula of Trotter-Gleser [17]. It is established that most of the male individuals were with "above middle" and "high" stature. The body mass is estimated in three males and the values are as follows: 62.83 kg (grave No. 5); 66.53 kg (grave No. 7) and 78.87 kg (grave No. 12).

Fig. 1. Reconstruction of stature and body mass of the investigated individuals from the necropolis at archaeological site "Trayanovi vrata" (Sofia Province).

Paleopathological analysis

In the series have not been identified jaw and tooth pathology in children, except for one child in *Infans I* (grave No. 4) with localized hypoplastic pit (BP) on the buccal enamel surface of the lower second deciduous molars. Despite the small number (6) of studied individuals with permanent dentition, in five of them (only males) a large number (57) of intravital teeth loss is observed.

Traumatic cranial traces are registered only in a mature man (Grave No. 9) – on nasal bones (**Fig. 2**) and right parietal bone. The largest number of cases have been identified with secondary skull morphological changes resulting from slightly expressed form of *cribra orbitalia* (two children in *Infans I* and one male individual in age group *Adultus*) and *porotic hyperostosis* (a male in *Maturus*). The identification of these porous skull lesions in subadult and adult individuals is indicative of anaemic conditions in the population.

Morphological changes of the postcranial skeleton were not identified in subadults from the series. Pathology of the postcranial bones is observed in seven (87.5%) of the adults buried in the necropolis. In the series mainly males in age group *Maturus*

(40-60 years) are affected. It is established only one case with *spina bifida occulta* in an adult female (grave No. 1). Another type of malformation of *os sacrum* (sacralization of the fifth lumbar vertebra), was found in the skeleton (grave No. 11) of a male individual in *Adultus*. Most common in the series are degenerative joint diseases (DJD) of the spine moreover in their severe forms. Ankylosing spondylitis is diagnosed in the lumbar region of a male individual in age group *Adultus* (grave No. 11) and in the thoracic vertebrae of a male in *Maturus* (grave No. 9). A mild form of spondylosis and spondyloarthrosis in all sections of the spine is found in one of the buried men in group *Maturus* (grave No. 12). Slightly pronounced DJD of the upper and lower limbs are recorded in two males (graves No. 2 and 5) – on both shoulder and knee joints. In one of these individuals (grave No. 5) is identified and *myositis ossificans* on the left *humerus* and *tibia*, with a probable etiology of chronic trauma, resulting from intense physical activity. Bilateral epicondylitis of the shoulder bones and a trace of healed fracture on a fragment of left rib were diagnosed in a male from age group *Maturus* (grave No. 12). In one of the buried male individuals is registered also benign bone tumor formation (*osteoma*) on the right *tibia* (grave No. 7).

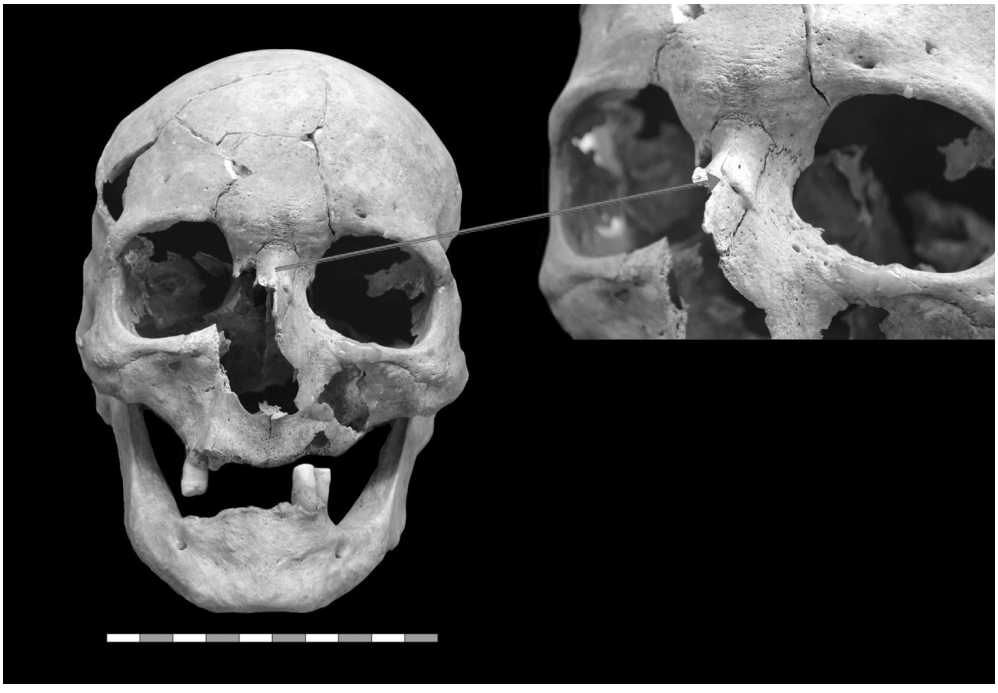

Fig. 2. Grave No 9. Male (50-55 years). Traumatic traces on nasal bone.

Conclusions

Most of the pathological bone changes (mainly degenerative joint diseases) of the postcranial skeleton are registered in male individuals, even in the age group *Maturus*, which suggests a premature and rapid aging of bone-joint apparatus, probably due to intensive and heavy physical works.

R e f e r e n c e s:

1. **Alekseev, V.** *Osteometry, methods of anthropological study*. Moscow, Nauka, 1966, 249 pp. [in Russian].
2. **Aufderheide, C., C. Rodriguez-Martin.** *The Cambridge encyclopedia of human paleopathology*. Cambridge University Press, 1998, 478 pp.
3. **Bass, W.** *Human osteology: a laboratory and field manual of the human skeleton.* University of Missoury, Special publication no. 2 of the Missouri Archaeological Society, 2005, 365 pp.
4. **Brothwell, D.** *Digging up bones*. London, British Museum of Natural History, 1965, 196 pp.
5. **Buikstra, J., D. Ubelaker.** *Standards for data collection from human skeletal remains: Proceedings of a seminar at the field museum of natural history*. Fayetteville, AK, Arkansas Archaeological Survey, 1994, 272 pp.
6. **Fazekas, I. Gy., F. Kósa, E. Kerner**. *Forensic fetal osteology*. Budapest, Akademiai Kiado, 1978, 413 pp.
7. **Ferembach, D., I. Schwidetzky, M. Stloukal.** Recommendations for age and sex diagnosis of skeletons. – *J. Hum. Evol*., **9**, 1980, 517-549.
8. **Gerasimov, M.** *Reconstruction of the face by the skull*. Moscow. Nauka, 1955, 586 pp. [in Russian].
9. **Kabakchieva, G.** Excavation of the "Trayanovi vrata" ("Trajan's gate") in Kapiyata locality, Kostenets municipality, Sofia province. – Archaeological discoveries and excavations in 2016, 2017, 441-444 [in Bulgarian].
10. **Maresh, M.** Measurements from roentgenograms**.** – In: *Human growth and development* (Ed. R.W. McCammon), Springfield IL: C.C. Thomas, 1970, 157–200.
11. **Meindl, R., C. Lovejoy.** Ectocranial suture closure: a revised method for the termination of skeletal age-at-death based on lateral-anterior sutures. – *Am. J. Phys. Anthropol*., **68**, 1985, 57-66.
12. **Ortner, D. J.** *Identification of pathological conditions in human skeletal remains*. 2nd Edition. San Diego, Academic Press, 2003, 647 pp.
13. **Ortner, D.J., J. Putschar.** *Identification of pathological conditions in human skeletal remains.* Washington, Smithsonian Institution Press, 1981, 499 pp.
14. **Pearson, K.** Mathematical contributions to the theory of evolution. V. On the reconstruction of the stature of prehistoric races. – *Philosophical Transactions of the Royal Society of London*. Series A, Containing Papers of Math. or Phys. Character (1896-1934), **192**, 1899, 169–244.
15. **Ruff, C. B., W. W. Scott, A. Y. Liu.** Articular and diaphyseal remodeling of the proximal femur with changes in body mass in adults. – *Am. J. Phys. Anthropol*., **86(3)**, 1991, 397–413.
16. **Tood, T.W.** Age changes in the pubic bone I: the male white pubic. – *Am. J. Phys. Anthropol,* **3**, 1920, 285-334.
17. **Trotter, M., G. Gleser.** Estimation of Stature from Long Bones of American Whites and Negroes. – *Am. J. Phys. Anthropol*, **10**, 1952, 463-514.
18. **Zubov, A.** Odontology. *Methods of anthropological investigations.* Moscow, Nauka, 1968, 200 pp. [in Russian].

Institute of Experimental Morphology, Pathology and Anthropology with Museum
Bulgarian Anatomical Society

Acta morphologica et anthropologica, 25 (3-4)
Sofia ● 2018

Use of High Pressure for Retrograde Forced Impregnation of Lung

*Antoaneta Georgieva, Jordan Stoyanov, Ivelina Ivanova, Dimitar Sivrev**

Department of Anatomy, Faculty of Medicine, Trakia University, Stara Zagora, Bulgaria

*Corresponding author e-mail: dsivrev@abv.bg

We offer an improved method for forced lung impregnation. In this case, the organ is not placed under low pressure, but the silicone is injected retrograde by means of pressurized air that is fed into the bronchial tree. The results are good and the method is economical compared to the classic impregnation techniques.

Key words: plastination, Biodur S_{10}, impregnation, lung, bronchial tree

Introduction

There are many modifications in the classical S_{10} technique, but the next four processing phases are always used:

- ✓ Fixing and preparation;
- ✓ Dehydration;
- ✓ Forsed impregnation;
- ✓ Gas curing.

Material and methods

Fixing is done with traditional fixing fluids: formaldehyde or alcohol.

We use the perfusion method and inject the fixator into the femoral vein. Routine preparatory techniques are the basis for the preliminary preparation of the biological material.

For dehydration, acetone is used as the most effective means [3]. It provides complete removal of water from tissues and is safe for fire or explosion. The water content of acetone is measured periodically, and when it is below the critical minimum, we replace it with a new one. Usually this happens once a week. Dehydration occurs at a temperature minus 27 degrees celsius [1].

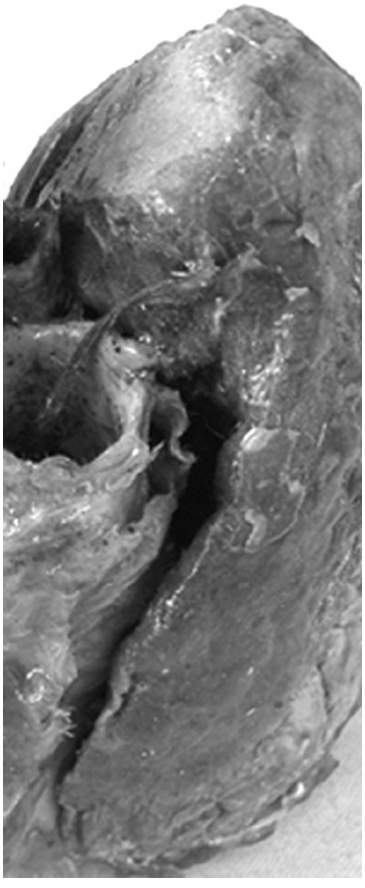

The water content of acetone is measured periodically, and when it is below the critical minimum, we replace it with a new one. Usually this happens once a week [6].

The classical impregnation is carried out at a gradual decreasing pressure, as the organ is immersed in Biodur S_{10} [6]. Experiments were made to impregnate at room temperature as well as to combine platelets with blood vessels [2, 4].

We put the lung in chilled Biodur medium for 24 hours, filling the bronchial tree with silicone.

According to our modification, we put the lungs in chilled Biodur S_{10} for 24 hours, filling the bronchial tree with silicone and connect it to a compressor that supplies atmospheric air at a pressure of 98.00-100.00 kPa. (**Fig. 1**).

The air pushes Biodur S_{10} through the bronchial and alveolar walls together with dust particles, impregnating the lung tissue.

Results and Discussion

Lung treatment is not one of the difficult procedures in the plastination. It is also applied when this unique conservation method is put into practice [5]. Application of classical techniques gives good results but it is not economical if applied to a small number of organs.

Fig. 1. Lung preparation.

After processing, a high-quality preparation of lung is obtained which can be used in student training in the internal organ education cycle. The lung tissue is white or light pink, the consistency is soft, and the organ is life like. These results are corresponding to the publications of other authors [4, 7].

Conclusions

Retrograde forced impregnation is a very economical method – suitable for our conditions.

The most valuable quality of the lung preparation is that it is completely safe for human health.

References

1. **de Jong, K., R. Henry**. Silicone plastination of biological tissue: cold temperature technique – Biodur™ S10/S15 technique and products. – *J. Int. Soc. Plast.*, **22**, 2007, 2-14.
2. **Henry, R., J. Butler**. Room-temperature "forced air" impregnation of dried lungs with S10/S3-xylene mix. – *J. Int. Soc. Plast.*, **4**, 1990, 23.

3. **Henry, R. Plastination**. Dehydration of specimens. – *J. Int. Soc. Plast.*, **6**, 1992, 4.
4. **Henry, R.** Silicone pulmonary vascular casts with attached tracheobronchial casts. – *J. Int. Soc. Plast.*, **6**, 1993, 41-44.
5. **Poterski, R., A. J. S. Summerlee and G. C. Miller**. A new method for preservation of lungs. – *J. Int. Soc. Plast.*, **7**, 1993, 13-15.
6. **von Hagens, G. Heidelberg**. Plastination folder: Collection of all technical leaflets for plastination. Anatomische Institut 1, Universitat Heidelberg, Heidelberg, Germany, 1985/86.
7. **Yoon, S., R. Henry, D. Bouley, N. Bennett, R. Fahrig**. Characterization of a novel anthropomorphic plastinated lung phantom. – *Med. Phys*., 35(12), 2008, 5934-43.

Institute of Experimental Morphology, Pathology and Anthropology with Museum
Bulgarian Anatomical Society

Acta morphologica et anthropologica, 25 (3-4)
Sofia ● 2018

Traumatic Axonal Injury – a Clinical-Pathological Correlation

Natasha Davceva[1], Atanas Sivevski[2]

[1] Institute of Forensic Medicine, Criminology and Medical Deontology. Medical Faculty, Ss. Cyril and Methodius University, Skopje, Republic of Macedonia; Faculty of Medical Sciences, University Goce Delchev, Shtip, Republic of Macedonia
[2] University Clinic for Gynecology and Obstetrics, Medical Faculty, Ss. Cyril and Methodius University, Skopje, Republic of Macedonia.

* Corresponding autor e-mail: drdavcevamk@yahoo.com; drdavceva2012@yahoo.com

Traumatic axonal injury (TAI) is a distinct clinico-pathological entity that can cause serious impairment of the brain function and can sometimes be found as a concrete cause of death. It has been discussed from the perspective of its biomechanical importance, and also from the standpoint of certain criteria for the pathological diagnosis of TAI. However, since the time when DAI (diffuse axonal injury) was initially described, there have been few, if any, discussions about the clinical-pathological correlation in TAI. This paper is an attempt to address this issue.
For the purpose of certain pathological diagnoses of TAI, 63 cases with closed head injuries have been subjected to the complete forensic-neuropathological examination, involving immunohistochemistry with antibody against β-APP. In the diagnosis of TAI strict criteria have been followed. Then, retrograde analysis of the clinical parameters has been performed in order to determine some clinical-pathological correlation. The following two most reliable parameters of the impairment of the brain function have been analyzed: the impairment of the consciousness and the time of survival. Comparing the two groups, the one with TAI and the other without TAI, and using appropriate statistical evaluation, our results show that TAI is not a significant contributing factor to the lethal outcome in the early post injury period (24 hours), but it is undoubtedly a contributing factor for the severe impairment of the brain function indicated through the status of the consciousness.

Key words: traumatic axonal injury, diffuse axonal injury, closed head injury, β-amyloid precursor protein

Introduction

Diffuse axonal injury (DAI), as classically named, is a distinct clinico-pathological entity that is found in closed head injuries can cause a serious impairment of the brain function. Much of the attention so far has been paid to the definition of DAI and the criteria for its pathological diagnosis.

In the initial and very profound descriptions of Adams, DAI has been understood as a clinico-pathological entity of traumatic origin, clinically [1,3,10] defined with im-

mediate and prolonged unconsciousness leading to death or severe disability, typically in the absence of any mass lesion, and pathologically by the widespread and diffuse damage of the axonal fibers. Later, with the introduction of the immunohistohemistry in the process of diagnosing of DAI, there were found series of other conditions but trauma that can cause axonal damage. Soon thereafter prominent authors reported certain differences in the findings (appearance, pattern and distribution of damaged axons) that are indicative of the origin of the axonal damage, traumatic or ischemic. The term traumatic axonal injury (TAI) was preferred instead of DAI to describe axonal damage of traumatic origin and by analogy, the term ischemic axonal injury was introduced. Certain criteria for the pathological diagnosis of TAI have been specified, paying particular attention to distinguishing traumatic axonal damage from secondarily occurring ischemic axonal damage [6, 11, 12, 16, 19].

The medico-legal importance of TAI lies in the fact that sometimes it is the sole reason for the impairment of the brain function and in a forensic medicine setting it can be found as a concrete cause of death [6]. With the purpose of establishing the diagnosis of TAI, a complete forensic neuropathological examination of the brain must be undertaken [6, 8, 11, 12], so it certain criteria have to be met before it is interpreted as a cause of death [6, 11, 12]. Another significant aspect of TAI in forensic medicine is its biomechanical importance. TAI occurs as a result of acceleration forces of longer duration [13-15, 23], and is mostly found in road traffic accidents (RTA), but can be found in other events associated with acceleration, such as in cases of falling from a considerable height. DAI is very rare in cases of a simple fall, and in cases of a blow to the head [3, 7, 9].

Since the time when Adams made the initial descriptions of DAI [1, 2], there have been few, if any, discussion about its clinico-pathological correlation. Previously, most of the efforts were focused on a certain post-mortem diagnosis of TAI, and nowadays efforts are also being made for its clinical and radiological diagnosis***. In order to identify some clinico-pathological correlation of TAI and its diagnosis on a pathological level, a retrograde analysis of the clinical parameters should be performed. This paper is an attempt to address this issue. The impairment of consciousness and the time of survival have been analyzed as the two most reliable indicators of the impairment of the brain function. The hypothesis under consideration is that TAI is constantly accompanied with the state of coma and can be found as a significant contributing factor to death in the first 24 hours after the closed head injury.

Two crucial questions to be answered are:

1. Is the impairment of consciousness (state of coma) a constant accompanying element of TAI, as classically defined?
2. Is TAI a significant contributing factor to the fatal outcome in the early post injury period (24 hours post injury).

Materials and Methods

A total of 63 cases with fatal closed head injuries have been investigated by performing a forensic-medicine autopsy and a forensic-neuropathological examination (age ranged from 5 to 94 years, 48 males and 15 females). In all 63 cases, a fatal closed head injury was found to be the cause of death. All open head injury and polytrauma cases have been excluded, to avoid the possibility of any other cause of death. The post-mortal interval had to be up to 24 hours and the time of survival between two hours (long enough to be admitted to hospital and also for pathological evidence of axonal damage)

and 1.5 month. The clinical information, as well as the information about the traumatic event, had to be available for all the cases included. Table 1 displays the information about the type of traumatic event where the closed head injury occurred.

The injury mechanism was analyzed, based on the injuries of the scalp, skull, intracranial structures (epidural, subdural and subarachnoidal hemorrhage) and the brain tissue (focal and diffuse brain injuries). Then a complete forensic-neuropathological examination of the fixed brain was performed (fixed in a 10% buffered formalin solution). Macroscopic examination of 1cm thick coronal sections has been documented in photographs. Samples for microscopic examination were taken from brain areas already known as predilection for the occurrence of TAI: the body and the splenium of corpus callosum including parasagittal white brain matter; posterior limb of the internal capsule; pons and cerebellar peduncles.

For the purpose of visualization of damaged axons, additionally to the conventional haematoxylin and eosin staining, immunohistochemical staining was performed with the application of antibodies to β–APP, by the method of Sheriff et al. [20]: antigen retrieval in citrate buffer (pH 5.0), incubation with antibody against β–APP (Mouse anti-Alzheimer precursor protein A4 monoclonal antibody, clone 22°C 11, diluted 1:200, Chemicon International, Temecula, CA) overnight at 4°C. The enzyme complex used was ABC (Universal VECTASTAIN ABC-Peroxidase kit, Vector Labs, Burlingame, CA) with a secondary antibody - biotinylated anti-mouse IgG (Biotinylated Anti-mouse IgG, produced in horse, Vector Labs). Diaminobenzidine (Peroxidase Substrate Kit (DAB) Vector Labs) was used for visualization.

In the process of TAI diagnosing, the pathological criterion was based on the grading system of Adams et al. [1] according to which the presence of a focal lesion in the corpus callosum was regarded as DAI 2, while a focal lesion in the rostral brainstem was regarded as DAI 3. The diagnosis of DAI 1 had to be established by a microscopic finding of widespread axonal damage with traumatic pattern in the absence of any macroscopic feature [18].

In the histological determination of TAI, damaged axons with a typical traumatic appearance and distribution had to be seen in at least three different brain regions, of which at least one located above and one below the tentorium [11, 12]. We regarded the "typical traumatic appearance and distribution of damaged axons" as the occurrence of single or small groups of swollen "varicosity"-like β-APP-positive axons or torn axons seen as "retraction balls" diffusely distributed throughout the white matter and particularly present in the white matter bundles [6, 11, 12, 16, 19] (**Fig. 1**).

The feature of circumscribed foci or a linear pattern of β-APP positive axons, frequently described as a "zig-zag" or "Z-shaped" pattern, which are densely distributed in one or two brain regions (most often in the pons) was considered a predominantly hypoxic-ischemic finding and was not taken into consideration in the diagnosing of TAI [6, 11, 12, 16, 19] (**Fig. 2**).

The degrees of the Glasgow Coma Scale (GCS, 3-15) have been taken as the indicator of the impairment of consciousness. In accordance with this scale, the head injury has been classified as severe with GCS $\leq$ 8 manifested clinically with coma or stupor; moderate with GCS = 9-12, manifested as somnolence; and minor GCS $\geq$ 13 [22].

In order to analyzee the clinical-pathological correlation of TAI, comparative statistics has been performed between these three groups:

1. Cases with diagnosed TAI – TAI cases;
2. Cases without TAI – no TAI cases;
3. Cases with Axonal Injury (AI), where the appearance, pattern and distribution of the β-APP immunoreactivity suggested its ischemic origin.

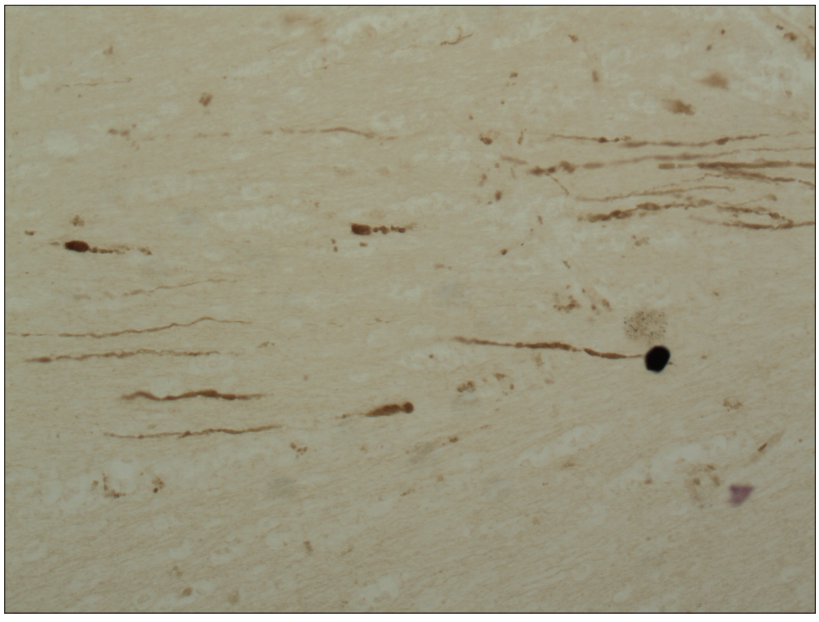

Fig.1. Typically traumatic pattern and distribution of β-APP-positive axons are seen in Corpus calosum, in a case with a time of survival of 8 days. Single or small groups of swollen "varicosity"-like or torn axons seen as "retraction balls" are diffusely distributed throughout the white matter and particularly present in the white matter bundles.

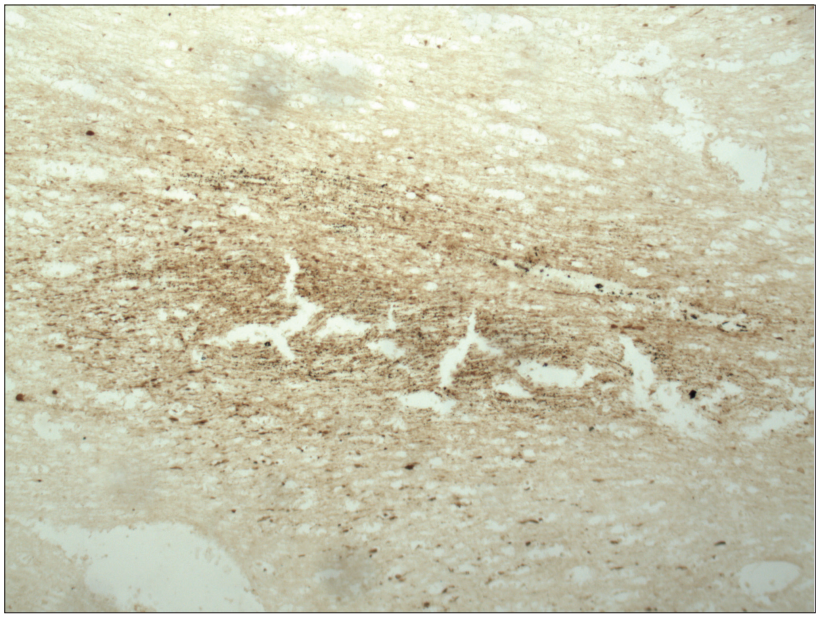

Fig.2. Axonal injury of hypoxic-ischemic origin, in a case who survived 3 days after injury. There is a feature of linear and geographical pattern of β-APP positive axons, which are densely distributed on wide planes. The positive axons are rather with a granular appearance than neatly shaped axons which can be seen in traumatically damaged tissue.

Statistical evaluation was performed using the Pearson Chi-Square test of independence with the significance level used is a = 0.05.

Results

TAI has been diagnosed in 47,6% of the examined cases as shown in **Table 1** [9]. Table 1 also shows the correlation between the occurrence of TAI and the type of the traumatic event that caused the head trauma.

Table 1. Cases with diagnosed TAI

Type of traumatic event	Total	TAI	%	no TAI	AI-ish
Traffic accident	49	26	53	17	6
Pedestrian	26	13	50	12	1
Cyclist	10	3	30	3	4
Motorist	4	3	75	1	0
Driver	5	5	100	0	0
Passenger	2	1	50	0	1
Railroad accident	2	1	50	1	0
Fall	11	4	36	4	3
Simple fall (<2m)	6	0	0	4	2
Fall of a height (>2m)	5	4	80	0	1
Blow-assault	3	0	0	2	1
Total	63	30	48	23	10

* TAI – cases diagnosed with diffuse axonal injury; no TAI – cases without diffuse axonal injury; AI ish – axonal injury of ischemic origin.

The frequencies of the major autopsy findings, such as skull fractures, intracranial hemorrhages, contusions and the frequency of TAI are presented on **Table 2**.

Table 2. Frequencies of the major autopsy findings

Fractures	37	59%
ICH, SDH, EDH, SAH	46	73%
FBI-contusions	23	36,50%
TAI	30	47,60%

* Fractures - fractures of the skull; ICH – intracranial haemorrhage (SAH – subarachnoidal haemorrhage, EDH – epidural haematoma, SDH – subdural haematoma); FBI – focal brain injury – contusion; TAI – diffuse axonal injury.

The pathological findings of 30 cases with diagnosed TAI, along with the clinical information about their state of consciousness and the time of survival were presented on **Table 3**. Results show that 80% of them have been in primary coma, and in the rest of the cases, 6 of them, moderate disturbances of consciousness have been observed.

Table 3. Presentation of the cases diagnosed with TAI.

F 13	TA-ped	9 d	Coma, GCS=7	Fr,EDH, SDH	Cont	TAI 2, Swell, ISH
M 17	TA-motor	3 w	Coma, GCS=6	SDH, SAH		TAI2, Swell, ISH
M 33	TA-driver	3 d	Coma	Fr, EDH, SAH	Cont	TAI3
F 73	TA-ped	24 h	Coma	SDH, SAH,		TAI2, Swell, ISH
M 39	TA-driver	4-5 h	Coma, GCS=3	Fr, SAH, IVH	Cont	DVI, TAI 1
M 75	TA-ped	5d	Stupor, Coma	SDH, SAH, ICH	Cont c-c	TAI2,
M 89	TA-ped	3 h	Coma	SAH		TAI 1
M 23	TA-driver	2 d	Coma, GCS=3	SAH, SDH		TAI 3,
M 40	TA-ped	11 d	Coma	Fr, SAH		TAI 1, Swell
M 33	TA-driver	3 d	Coma, GCS=3	Fr, SAH		TAI3,Swell,ISH
M 26	F-hight	12 d	Coma, GCS=3	Fr, EDH, SDH, SAH	Cont c-c	TAI3,Swell,ISH
M 30	TA-motor	10 d	Coma, GCS=5	Fr, SAH, SDH	Cont c-c	TAI1, Swell, ISH
M 55	F-hight	1,5 m	Coma, GCS=3	EDH, SAH	Cont	TAI1,Swell, ISH
F~70	TA-ped	3 d	Stupor	Fr,SDH, SAH,IVH	ICH	TAI2/3,Swell, ISH
M 10	TA-ped	8 d	Coma, GCS=4			TAI1,Swell, ISH
M 81	TA-cyc	15 d	Coma	Fr, SDH, SAH	Cont c-c	TAI1, Swell,
F 64	TA-ped	4 d	Coma, GCS=3	Fr, SDH, SAH	Cont	TAI2/3,Swell, ISH
M 61	TA-cyc	5 d	Coma	Fr, SAH, IVH	Cont, ICH	TAI 2, Swell, ISH
M~30	TA-pass	4 h	Coma			TAI2, Swell, ISH
M 60	TA-ped	1 m	Coma, GCS=8	SDH, SAH, IVH		TAI 2, Swell, ISH
M 30	TA-driver	2-3h	Coma	Fr, SAH		TAI3, Swell, ISH
F 46	TA-ped	24 h	Coma	SAH		TAI 1, Swell, ISH
M 25	TA-motor	4 d	Stupor			TAI 1, ISH
M 67	TA-ped	2,5 d	Stupor	Fr, SDH, SAH	Cont c-c	TAI1, Swell, ISH
F 72	TA-ped	6d	Coma, GCS=6	Fr, SDH, SAH	Cont	TAI2/3, Swell,ISH
M 58	F-hight	6 d	Coma	Fr, SDH, SAH	Cont c-c	TAI1, Swell, ISH
F 20	TA-ped	7 d	Coma	Fr, EDH, SDH, SAH	Cont	TAI 2, Swell, ISH
M 50	RA	2 d	Stupor	Fr, SAH		TAI1, Swell
F 24	F-hight	3 d	Stupor	SAH		TAI1, Swell
M 78	TA-cyc	8 d	Coma, GCS=3	Fr, EDH, SDH, SAH	Cont	TAI 2, ISH, edem

* A-G – age and gender; Trauma – type of traumatic event where closed head injury occurred: TA – traffic accident (ped-pedestrian, cyc-cyclist, mcyc-motorcyclist; pass-passenger; RA-railway accident), F – fall (F-simple – fall from one's own height, F-height – fall from a height of more than 2 metres), B-F – blow and fall; TS – time of survival (imm-immediate death; h -hour; d -day, w -week, m -month); Consciousness – state of consciousness immediately after the impact (GCS – Glasgow Coma Score); Fr – fractures of the skull, ICH – intracranial haemorrhage (SAH – subarachnoidal haemorrhage, EDH – epidural haematoma, SDH – subdural haematoma, IVH – intraventricular haemorrhage); FBI – focal brain injury (cont-contusion, cont c-c – contusion coup-contra-coup, ICH – intracerebral haemorrhage); DBI – diffuse brain injury (TAI 1, 2, 3 – diffuse axonal injury - Adams grading system (Adams 1989); DVI – diffuse vascular injury; ISH – ischemia; Swell – brain swelling.

Analyzing the group of cases without TAI, shown on **Table 4**, a primary coma was present in 7 cases (30% of the total of 23 cases). In the rest of the cases, moderate or mild disturbances of consciousness occurred.

Table 4. Cases without TAI

A-G	Trauma	TS	Consiousness	Fr and ICH	FBI	DBI
M 48	TA-ped	3-4h	Concussion	SAH		Swell
F 23	TA-cyc	10 d	GCS=8	SDH	Cont	Swell, ISH
M 61	TA-cyc	14 d	Concussion	Fr, SDH, SAH	Cont	Swell
M 70	TA-ped	1 d	Concussion	Fr, SAH		Swell
M 52	TA-ped	2-4 h	Concussion			Swell
M 41	TA-ped	6 h	Coma, GCS=3	Fr, SAH		Swell, ISH
M 60	TA-motor	5 d	Somnolency	SDH, SAH	Cont	Swell
M~60	F-hight	3,5 w	Stupor	Fr, SDH, SAH	Cont	Swell
M 15	TA-ped	10 d	Somnolency GCS=14	Fr, EDH	Cont c-c	Swell, ISH
M~50	RA	10 d	Coma	Fr		Swell
F 80	TA-ped	8 d	Consciousness			Swell, ISH
M 57	TA-ped	2d	Consciousness			Swell
F 40-50	TA-ped	1,5 m	Concussion			Swell
M 37	F-simple	5 d	Stupor		Cont	Swell
F 74	TA-ped	3-4h	Stupor	SAH		Swell, ISH
M 70	TA-ped	4 h	Coma	Fr, SAH		Swell, ISH
M 33	TA-cyc	2-4 h	Coma	Fr, SDH, SAH	Cont	Swell, ISH
M 88	TA-ped	8 h	Concussion			Swell, ISH
M 74	TA-ped	2 h	Stupor			Swell
F 94	Blow	1-2h	Stupor	Fr, SAH, IVH		
M 55	B-F	5d	Coma	Fr, SDH, SAH	Cont	Swell
F 66	F-simple	3-5h	Stupor	SAH		

*A-G – age and gender; Trauma – type of traumatic event where closed head injury occurred: TA – traffic accident (ped-pedestrian, cyc-cyclist, mcyc-motorcyclist; pass-passenger; RA – railway accident), F – fall (F-simple – fall from one's own height, F-height – fall from a height of more than 2 metres), B-F – blow and fall; TS – time of survival (imm-immediate death; h -hour; d -day, w -week, m -month); Consciousness – state of consciousness immediately after the impact (GCS – Glasgow Coma Score); Fr – fractures of the skull, ICH – intracranial haemorrhage (SAH – subarachnoidal haemorrhage, EDH – epidural haematoma, SDH – subdural haematoma, IVH – intraventricular haemorrhage); FBI – focal brain injury (cont-contusion); DBI – diffuse brain injury; ISH – ischemia; Swell – brain swelling.

Cases diagnosed with ischemic axonal injury were presented on **Table 5.** All these cases died in a state of coma.

Table 5. Group of cases diagnosed with ischemic axonal injury.

A-G	Trauma	TS	Consiousness	Fr and ICH	FBI	DBI
M 59	TA-cyc	2 d	Coma	Fr, EDH, SDH, SAH,	Cont c-c	AI-ish, Swell, ISH
M 5	TA-ped	15 d	Coma, GCS=3	Fr		AI-ish, Swell, ISH
M~35	F-hight	2 d	Coma, GCS=4	Fr, EDH, SDH, SAH, IVH	Cont c-c	AI-ish, Swell, ISH
M 69	TA-cyc	3 w	Coma	Fr, SDH, SAH	Cont c-c	AI-ish, Swell, ISH
M 60	F-simple	7 d	Coma	SDH, SAH	Cont c-c	AI-ish, Swell, ISH
M~50	Blow	3-5h	Coma, GCS=3	Fr, SDH, SAH, IVH	Cont	AI-ish, Swell, ISH
F 20	TA-pass	10 d	Coma	Fr, SAH	Cont	AI-ish, Swell, ISH
M~50	TA-cyc	7 h	Coma, GCS=4	Fr, SAH	Cont c-c	AI-ish, Swell, ISH
M 63	F-simple	10 d	Coma, GCS=7	Fr, EDH, SAH	Cont c-c	AI-ish, Swell, ISH
M43	TA-cyc	2d	Coma, GCS=3	Fr, EDH, SDH, SAH,		AI-ish, Swell, ISH

* A-G – age and gender; Trauma – type of traumatic event where closed head injury occurred: TA – traffic accident (ped-pedestrian, cyc-cyclist, mcyc-motorcyclist; pass-passenger; RA – railway accident), F – fall (F-simple – fall from one's own height, F-height – fall from a height of more than 2 metres), B-F – blow and fall; TS – time of survival (imm – immediate death; h -hour; d -day, w -week, m -month); Consciousness – state of consciousness immediately after the impact (GCS – Glasgow Coma Score); Fr – fractures of the skull; ICH – intracranial haemorrhage (SAH – subarachnoidal haemorrhage, EDH – epidural haematoma, SDH – subdural haematoma, IVH – intraventricular haemorrhage); FBI – focal brain injury (cont - contusion, cont c-c – contusion coup-contra-coup); DBI– diffuse brain injury; Ai-ish – axonal injury of ischemic origin; ISH – ischemia; Swell – brain swelling.

Statistical evaluation explored the interdependence between the occurrence of TAI and the state of consciousness. Three groups of cases have been investigated comparatively (**Table 6**). Statistically, a significant interdependence was shown between the occurrence of TAI and the occurrence of primary coma (Chi square = 29, 99; df=2, p<0, 00001). Also, as perceived before, the analysis shows the presence of coma in all AI cases.

Table 6. Association between the occurrence of TAI and the occurrence of the primary coma.

	Coma, Stupor	Concussson, Somnolency	Total
TAI cases	28 (44,43%)	2 (3,17%)	30 (47,61%)
No TAI cases	7 (11,10%)	16 (25,39%)	23 (36,50%)
AI cases	10 (15,87%)	0	10 (15,87%)
Total	45 (71,42%)	18 (28,57%)	63 (100%)

* TAI – cases diagnosed with diffuse axonal injury; no TAI – cases without diffuse axonal injury; AI ish – axonal injury of ischemic origin.

As a next step, an additional investigation was conducted into the correlation between the state of coma and the post-mortem β-APP positive immunoreactivity found on pathological substrate, as a specific and direct indicator of the damage of the axonal fibers (**Table 7**). Statistically significant association has been shown (Chi – square = 29, 83; df=2, p<0, 00001).

Table 7. Association between the state of the coma and the post-mortem β-APP positive immunoreactivity

	Coma, Stupor	**Concuss, Somnolency**	**Total**
ß -APP +	38 (60,31%)	2 (3,17%)	40 (63,49%)
ß -APP -	7 (11,10%)	16 (25,39%)	23 (36,50%)
Total	45 (71,42%)	18 (28,57%)	63 (100%)

* ß -APP + – cases who show ß -APP positivity on pathological substrate; ß -APP - – cases who don't show ß -APP positivity on pathological substrate.

As another indicator of the severe impairment of brain function, the two groups of cases, the one with diagnosed TAI and the other without TAI, have been analyzed comparatively in terms of the time of survival. The time of survival ranged: until 24 hours, until 1 week, and until 1.5 months, as shown on **Table 8**. The statistical evaluation did not show any significant association between the occurrence of TAI and the time of survival (Chi square = 4, 75; df = 2; p = 0, 0929>0.01).

Table 8. Association between occurrence of the TAI and time of survival.

TAI*Time of survival	**24 h**	**1 week**	**1,5 months**	**Total**
TAI cases	6	14	10	30
No TAI cases	14	8	11	33
Total	20	22	21	63

* TAI – cases diagnosed with diffuse axonal injury; no TAI – cases without diffuse axonal injury.

Discussion

The results of the present study demonstrate that the impairment of consciousness (state of coma) is a constant accompanying element of TAI, as classically defined [1, 3, 14, 15]. 80% of the cases with TAI were in primary coma, and the remainder showed a moderate disturbance of consciousness. In comparison, primary or immediate coma was observed in 30% of the cases that did not show TAI in the neuropathological examination.

The results in the third group of cases diagnosed with axonal injury of ischemic origin were particularly revealing, as all of them were in coma. Since the differences in the appearance, pattern and distribution of the damaged axons have been widely discussed before [6, 11, 12, 16, 19], it should be pointed out that the occurrence of β-APP immunoreactivity to one or two samples, of which at least one is from a brain stem and with a predominantly granular deposition on wide "geographic" planes, is a characteristic ischemic feature. If the ischemic feature is found next to a traumatic

axonal damage, then it can be interpreted as a case of TAI with secondarily occurring ischemia.

Hence, the analysis indicated significant statistical interdependence between the axonal damage (regardless of whether they showed a traumatic pattern, as in the TAI cases, or an ischemic feature as in AI cases) and the occurrence of primary coma. This association triggered another statistical evaluation which revealed the strong interdependence between β-APP immunoreactivity found on a pathological substrate and the state of coma. One of the advantages of this study is that, all cases in coma demonstrated clear β-APP immunoreactivity on a pathological substrate, implying that axonal damage indicated by β-APP disposition, from traumatic or ischemic origin, is in clear correlation with the state of coma. This correlation has been noted by other authors as well [4,5] but more profound studies are needed in order to establish more definite observations that can shed a new light to the neurophysiology of coma. In a previous study [8] we investigated the correlation between different pathological grades of TAI and the depth of the coma. The majority of the cases in deep coma (GCS=3-5), demonstrated pathological grade 3 of TAI, and two cases that clinically showed somnolence (GCS 11-14) had grade 1 of TAI. Also, in other study has been shown that the prognosis worsens in direct relationship to the extent of injury, especially to the injury of the brainstem [17].

The time of survival has been analyzed here as another indicator of the severity of the brain impairment as a result of the head injury. It has been shown that only 6 subjects (20% of all the cases with diagnosed TAI) died within the first 24 hours, in comparison with 14 subjects (42% of the cases where TAI was not diagnosed) who died in the first 24 hours. Furthermore, from the total of 20 cases that died in the first 24 hours, only 6 (30% of them) were diagnosed with TAI. Comparatively, in the group of cases that had survived for one week, there were 14 (64% of 22) with a TAI diagnosis. These considerations demonstrate that the presence of TAI is not the factor which contributes to the fatal outcome in the first 24 hours. Finally, this correlation of TAI with the time of survival has been explored statistically and no significant association has been found. In one of the aforementioned studies [7] the survival time in a correlation with the grade of TAI has also been explored and no significance has been found, but it has been observed that the lower survival time values are more typical of cases with grade 3 of TAI.

Conclusion

In this study TAI has not been found to be a significant contributing factor to the lethal outcome from closed head injuries in the early post injury period (24 hours), but undoubtedly is a contributing factor for the severe impairment of the brain function indicated through the status of the consciousness.

Presumably, the most contributing factors for lethal outcome in the early post injury period in closed head injuries should be found among the sequels of the raised intracranial pressure which develops as a result of the edema or intracranial hemorrhage.

References

1. **Adams, J. H., D. Doyle, I. Ford, T. A. Gennarelli, D. I. Graham**. Diffuse axonal injury: definition, diagnosis and grading. – *Histopathology*, **15**, 1989, 49-59.
2. **Adams, J. H., D. Doyle, D. I. Graham, A. E. Lawrence, D. R. McLellan**. Diffuse axonal injuries caused by fall. – *Lancet*, **2** (8417-18), 1984, 1420-1422.

3. **Adams, J. H., D. I. Graham, L. S. Muray, G. Scott.** Diffuse axonal injury due to nonmissile head injury in humans: an analysis of 45 cases. – *Ann. Neurol.,* **12,** 1982, 557-563.
4. **Adams, J. H., D. I. Graham, B. Jennett.** The structural basis of moderate disability after traumatic brain damage. - *J. Neurol. Neurosurg. Psychiatry,* **71**(4), 2001, 521-524.
5. **Adams, J. H., B. Jannet, L. S. Murray, G. M. Teasdale, T. A. Gennarelli, D. I. Graham.** Neuropathological findings in disabled survivors of a head injury. – *J. Neurotrauma*, **28**, 2011, 701-709.
6. **Davceva, N., N. Basheska, J. Balazic.** Diffuse axonal injury - a clinicopathological entity in closed head injuries. – *Am. J. Forensic. Med. Pathol.,* **36**, 2015, 3, 127-133.
7. **Davceva, N., V. Janevska, B. Ilievski, L. Spasevska, Z. Popeska**. Dilemmas concerning the diffuse axonal injury as a clinicopathological entity in forensic medical practice. – *J. Forensic. Leg. Med.,* **19,** 2012, 413-418.
8. **Davceva, N., V. Janevska, B. Ilievski, L. Spasevska, R. Jovanovic**. The importance of the detail forensic-neuropathological examination in the determination of the diffuse brain injuries. – *Soud. Lek.*, **57**, 2012, 1, 2-6.
9. **Davceva, N., V. Janevska, B. Ilievski, G. Petrushevska, Z. Popeska.** The occurrence of acute subdural haematoma and diffuse axonal injury as two typical acceleration injuries. – *J. Forensic. Leg. Med.,* **19,** 2012, 480-484.
10. Di Mayo, V. S., D. Di Mayo. Forensic pathology. CRC Press, NY, 2001.
11. **Geddes, J. F., G. H. Vowles, T. W. Beer, D. W. Ellison**. The diagnosis of diffuse axonal injury: implications for forensic practice. – *Neuropath. Appl. Nevrobiol.*, **23**, 1997, 339-347.
12. **Geddes, J. F., H. L. Whitwell, D. I. Graham.** Traumatic axonal injury: practical issues for diagnosis in medicolegal cases. – *Neuropath. Appl. Nevrobiol.*, **26**, 2000, 105-116.
13. **Gennarelli, T. A**. Head injury in man and experimental animals: clinical aspects. - *Acta Neurochir. Suppl. (Wien)* 1983; 32:1-13.
14. **Gennarelli, T. A.** Mechanisms of brain injury. – *J. Emerg. Med.*, **11**, 1993, Suppl 1, 5-11.
15. **Gennarelli, T. A., L. E. Thibault, J. H. Adams, D. I. Graham, C. J. Thompson, R. P. Marcincin**. Diffuse traumatic injury and traumatic coma in the primate. - *Ann. Neurol.*, **12**, 1982, 564-574.
16. **Graham, D. I., C. Smith, R. Reichard, P. D. Leclercq, S. M. Gentleman.** Trials and tribulations of using β-amyloid precursor protein immunohistochemistry to evaluate traumatic brain injury in adults. - *Forensic Sci. Int.,* **146**, 2004, 89-96.
17. **Hilario, A., A. Ramos, J. M. Millan, E. Salvador, P. A. Gomez, M. Cicuendez, R. Diez-Lobato, A. Lagares**. Severe traumatic head injury: prognostic value of brain stem injuries detected at MRI. – *AJNR Am. J. Neuroradiol.*, **33**, 2012, 10, 1925-1931.
18. **Omalu, B. I.** Diagnosis of traumatic diffuse axonal injury. Letter to the editor. – *Am. J. Forensic Med. Pathol.*, **25**, 2004, 3, 270-272.
19. **Reichard, R. R., C. Smith, D. I. Graham.** The significance of B-APP immunoreactivity in forensic practice. – *Neuropath. Appl. Nevrobiol.*, **31**, 2005, 304-313.
20. **Sheriff, F. E., L. R. Bridges, S. Sivaloganatham**. Early detection of axonal injury after human head trauma using immunocytochemistry for β-amyloid precursor protein. – *Acta Neuropathol.*, **87**, 1994, 55-62.
21. **Smith, C., D. I. Graham, J. F. Geddes, H. L. Whitwell**. The interpretation of β-APP immunoreactivity: a response to C. Neiss et al., *Acta Neuropathol* (2002) 104:79. – *Acta Neuropathol.*, **106**, 2003, 97-98.
22. **Teasdale, G., B. Jennett**. Assessment of coma and impaired consciousness. A practical scale. – *Lancet*, **2**, 1974, 7872, 81-84.
23. **Zhang, J., N. Yoganandan, F. A. Pintar, T. A. Gennarelli.** Role of translational and rotational accelerations on the brain strain in lateral head impact. – *Biomed. Sci. Instrum.*, **42**, 2006, 501-506.

Institute of Experimental Morphology, Pathology and Anthropology with Museum
Bulgarian Anatomical Society

Acta morphologica et anthropologica, 25 (3-4)
Sofia ● 2018

Morphological Characteristics of the Types of Os Lunatum and their Relation to Kienbock's Disease

Karim Ibrahim[1], Plamen Panchev[1], Alexandar Iliev[1], Boycho Landzhov[1], Georgi P. Georgiev[2]*

[1] *Department of Anatomy, Histology and Embryology, Medical University of Sofia, Bulgaria*
[2] *Department of Orthopaedics and Traumatology, University Hospital Queen Giovanna – ISUL, Medical University of Sofia, Bulgaria*

* Corresponding author e-mail: dralexiliev@abv.bg

The lunate bone is a carpal bone which can be easily distinguished by its crescent outline. The bone has its role in orthopedics and the related pathologies are difficult for diagnostics. The aim of our work was to overview the morphological characteristics of the bone which have significant role in pathological conditions of the wrist, like Kienbock's disease and carpal coalition. In our research we included 40 lunate bones of unknown sex and age. As a result, we specified 4 types of lunate bone based on its relation to the surrounding bones. Type II+ was the most commonly observed type. People with this type of bone suffer from different pathological conditions significantly less often as opposed to people with the other types of lunate (type I+, I- and II-). Knowledge of the morphology of the bone plays a crucial role in the treatment of the discussed pathological conditions.

Key words: os lunatum, morphology, types, Kienbock's disease

Introduction

The wrist represents one of the most complex joints in the human organism that performs numerous movements and plays an important role in the everyday activities of every individual [3, 5, 6, 8]. The etymology of the word comes from the Greek word "luna" meaning moon, because of the crescent shape of the bone [8]. It can be easily distinguished from the other carpal bones by its deep concavity on the distal surface. Os lunatum is located in the proximal row of the carpal joint complex between os scaphoideum and os triquetrum. The bone has both intrinsic and extrinsic ligaments for attachment with the surrounding bones, such as the scapholunate ligament, lunotriquetral ligament, radiolunotriquetral, radioscapholunate and ulnolunate ligaments. The arterial blood supply comes from the branches of the dorsal radiocarpal arch and the intercarpal arch [3, 5, 6, 8].

There are 4 types of os lunatum based on its communication with the surrounding bones [1, 4]. Type I+ has two proximal facets for connection with the radius and discus articularis and one distally located facet for connection with the capitate bone. Type

I- has one proximal facet and one distal. Type II+ has two proximally located and two distally located facets for connection with os hamatum and os capitatum. Finally, type II- has one proximal and two distal facets [4]. The possible variations of the bone could cause different pathologies which very often create difficulties for diagnostics. The most common disorder of the lunate bone is its avascular necrosis, termed Kienbock's disease, characterized by death and fracture of bone due to interruption of blood supply with fragmentation and collapse of the lunate [9].

The aim of our study was to overview the possible variations of os lunatum and its role in the pathological conditions of the hand.

Materials and Methods

In the present study we examined 40 unselected human lunate bones collected at the Department of Anatomy, Histology and Embryology of the Medical University of Sofia. These bones came exclusively from Bulgarian individuals and their sex was unknown. The study was approved by the Medical Legal Office and Local Ethics Committee. The specimens were distributed in groups based on the number of facets on each surface of the bone and its communication with the surrounding bones. Ten different measurements of each type of the bone were established. Measurements were made using a digital ruler micrometer caliper 0.01 mm. The mean values and the SD for all parameters were calculated. The obtained quantitative data were demonstrated with tables. Microsoft Office Excel 2010 was used to process the data and to demonstrate the obtained results in an adequate way.

Results

From the examined specimens, 5% were type I - (**Fig. 1a, 1b**) with one facet proximally and distally and 25% were type I+ (**Fig. 1c, 1d**) with two facets proximally and one distally. The majority of the bones (53%) were type II+ **(Fig. 2a, 2b**) with two proximally and two distally located facets. Type II- (**Fig. 2 c, 2d**) with one proximal and two distal located facets was detected in 17% of cases. From the conducted measurements, we noted that only the length, the greatest width and the greatest height differed, while the other measurements remained constant (**Tables 1-4**). Furthermore, we observed that the average height of type I- was bigger than type I+ by approximately 3 mm. The average length of both types differed by approximately 1 mm and the width – by 1.25 mm. We also observed that the average length of type II+ was approximately 3 mm longer than type II-. The greatest width of type II+

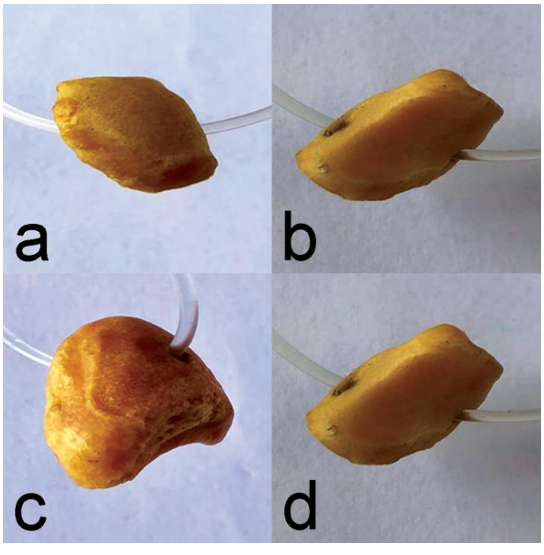

Fig. 1. Photographs of the types of os lunatum, as follows: type I- (a, b); type I+ (c, d)

was approximately 2 mm wider than that of type II-, while its greatest height was 3 mm longer than that of type II-.

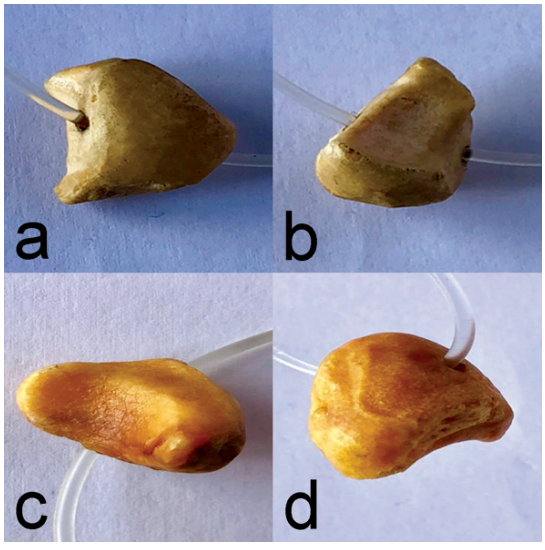

Fig. 2. Photographs of the types of os lunatum, as follows: type II+ (a, b); type II- (c, d)

Discussion

Our observations of the lunate bones revealed similar results compared to Dyankova [4], although there were some differences in the measurements. The greatest width of our specimens from each type of the bone; the greatest height of type I+ and II+; the greatest width of the proximal surface of types II+ and II- and the greatest height of the distal surface in types I+ and II- were less, compared to the measurement of those types of bones by Dyankova [4].

It appears that the number of facets on each surface has its role in the pathology. Type II+ has two facets on each side so the pressure is distributed better between them. In type I- there is one facet proximally and one distally. This type is most rarely seen and the risk of a pathological condition is bigger than the other types. In addition, the gender has its role in os lunatum's pathology as well. It is well known that men usually apply more stress on their hands than women. Thus, after years of constant pressure on the wrist, it may get damaged, which in turn may lead to development of Kienbock's disease – death and fracture of bone tissue due to interruption of blood supply with fragmentation and collapse of the lunate [3, 5, 6, 8].

Kienbock's disease was first described by Austrian radiologist Robert Kienbock in 1910 and is also called osteonecrosis, lunatomalacia, and aseptic or ischemic necrosis of the lunate [10]. The disease is more often seen in people at age 20-40 years. The symptoms include severe wrist pain, inability of wrist movement and often edema [9].

Table 1. Basic metrical characteristics and indices of os lunatum type I+

Indicators and indices	***Mean value (mm)***
Length of os lunatum	16.07
Greatest width of os lunatum	9.00
Greatest height of os lunatum	13.64
Greatest height of the proximal surface	13.28
Greatest width of the proximal surface	11.17
Greatest height of the distal surface	10.52
Width of the distal surface in the middle	5.47
Width of the joint facet for os capitatum	5.88
Width of the joint facet for os hamatum	0
Greatest depth of distal surface	1.88

Table 2. Basic metrical characteristics and indices of os lunatum type I-

Indicators and indices	*Mean value (mm)*
Length of os lunatum	15.25
Greatest width of os lunatum	10.50
Greatest height of os lunatum	16.75
Greatest height of the proximal surface	14.53
Greatest width of the proximal surface	10.36
Greatest height of the distal surface	13.58
Width of the distal surface in the middle	6.00
Width of the joint facet for os capitatum	6.00
Width of the joint facet for os hamatum	0
Greatest depth of distal surface	2.00

Table 3. Basic metrical characteristics and indices of os lunatum type II+

Indicators and indices	*Mean value (mm)*
Length of os lunatum	16.72
Greatest width of os lunatum	12.18
Greatest height of os lunatum	15.90
Greatest height of the proximal surface	14.36
Greatest width of the proximal surface	11.00
Greatest height of the distal surface	11.21
Width of the distal surface in the middle	9.71
Width of the joint facet for os capitatum	6.11
Width of the joint facet for os hamatum	2.44
Greatest depth of distal surface	2.10

Table 4. Basic metrical characteristics and indices of os lunatum type II-

Indicators and indices	*Mean value (mm)*
Length of os lunatum	14.00
Greatest width of os lunatum	10.00
Greatest height of os lunatum	13.00
Greatest height of the proximal surface	14.23
Greatest width of the proximal surface	11.88
Greatest height of the distal surface	10.00
Width of the distal surface in the middle	6.75
Width of the joint facet for os capitatum	4.57
Width of the joint facet for os hamatum	1.93
Greatest depth of distal surface	2.30

The disease is a big challenge for diagnostics not only because it is rarely observed, but also because of its unclear etymology [11]. Early diagnostics is very important for the proper treatment of the condition and may prevent progression of the necrosis and bone collapse [9]. Another condition associated with the lunate bone is the so called carpal coalition – abnormal fusion of two or more carpal bones during the embryonal development. This is a congenital disease seen in otherwise healthy people and may occur as part of a syndrome, such as Turner's and Holt-Oram syndromes [2]. This disease is often found after radiographic evaluation following trauma [7].

Conclusion

Pathological conditions of the lunate bone are commonly seen in the dominant wrist. People with type II+ suffer significantly less often, because of the two proximally and two distally located facets between which the pressure is distributed better. The anatomical features, the age relation and gender are all associated with os lunatum pathology.

References

1. **Bain, G. I., S. B. M. MacLean, C. J. Yeo, E. Perilli, D. M. Lichtman.** The etiology and pathogenesis of Kienböck disease. – *J. Wrist Surg.*, **5,** 2016, 248-254.
2. **DeFazio, M. V., B. J Cousins, R. A. Miversuski, R. Cardoso.** Carpal coalition: a review of current knowledge and report of a single institution's experience with asymptomatic intercarpal fusion. – *Hand (New York)*, **8,** 2013, 157-163.
3. **Dyankova, S.** Anthropometric characteristics of wrists joint surfaces depending on lunate types. – *Surg. Radiol. Anat*., **29,** 2007, 551-559.
4. **Dyankova, S.** Lunate bone-types and morphological characteristics. – *Acta Morphol. Anthropol.,* **10,** 2005, 304-308.
5. **Dyankova, S., G. Marinov.** Basic anthropometric characteristics of wrist bones in the wrist joint complex with lunatum types I and II. – *Acta. Morphol. Anthropol.*, **12,** 2007, 193–198.
6. **Dyankova, S., G. Marinov.** Comments about the hamate facet of the lunate: a radiographic study in an Arab population from Bahrain. – *Surg. Radiol. Anat.*, **29,** 2007, 181.
7. **Gottschalk, M. B., M. Danilevich, H. P. Gottschalk.** Carpal coalitions and metacarpal synostoses: a review. – *Hand (New York)*, **11,** 2016, 271-277.
8. **Kamburov, D. G. Marinov, S. Dyankova.** Anatomical features of os lunatum: significance in the wrist joint statics and mechanics. – *Scr. Sci. Med.,* **30**, 1998, 49-55.
9. **Kulhawik, D., T. Szałaj, M. Grabowska.** Avascular necrosis of the lunate bone (Kienböck's disease) secondary to scapholunate ligament tear as a consequence of trauma – a case study. – *Pol. J. Rad.*, **79,** 2014, 24-26.
10. **Omor, Y., I. Nassar, A. Ajana, N. Moatassimbillah.** Kienböck's disease: a case report. – *Pan. Afr. Med. J.*, **22,** 2015, 246.
11. **Squitieri, L., E. Petruska, K. C. Chung.** Publication bias in Kienbock's disease: a systematic review. – *J. Hand Surg.*, **35,** 2010, 359-367.

Institute of Experimental Morphology, Pathology and Anthropology with Museum
Bulgarian Anatomical Society

Acta morphologica et anthropologica, 25 (3-4)
Sofia ● 2018

Anatomical Study of Arterial Plantar Arch and its Clinical Significance

Elena Krasteva[1], Stoyan Novakov[2]*

[1] Department of Propaedeutics of Surgical Diseases, [1]Clinic of Plastic, Reconstructive and Aesthetic Surgery, Clinic of General and Operative Surgery, University Hospital "St. George" Plovdiv
[2] Department of Anatomy, Histology and Embryology, Medical Faculty, Medical University – Plovdiv

* Corresponding author e-mail: elinko6@gmail.com

The study aimed to examine the morphology of the plantar arterial archand determine the dominant variants of the plantar arch. On twenty-two dissected lower limbs the origin, course, and branches of the arteries in the plantar part of foot were examined. The plantar arterial arch was observed to be fully developed in all specimens with variations found in 5 (22.7%) of the limbs. The plantar arterial arch was mostly located in the anterior middle in 18 (81.8%) cases, in the junction between the anterior middle and intermediate middle in four (18.2%) cases. Normal course of lateral and medial plantar arteries was found in 17 cases (77.3%). In one case (4.5%) the deep plantar arch originated from dorsalis pedis artery and partly lateral plantar artery. In one case (4.5%) the lateral plantar artery gave origin to the third and fourth metatarsal arteries andin three cases (13,6%) the lateral planar artery gave off the second, third and fourth metatarsal arteries. The data from the study indicate that the plantar arch is a regular finding, but variants in terms of origin, formation and branching are not an unusual finding.Thorough knowledge of the blood supply to the foot is essential for surgeons in the mobilization and application of plantar flaps.

Key words: plantar arterial arch, morphology, variations, plastic surgery

Introduction

Reconstruction of the arteries of the foot in patients with severe chronic arterial occlusive disease has become a routine and valuable procedure. However, it is frequently difficult to select the optimal site for the distal arterial anastomosis [7]. Hence, accurate knowledge of the arterial patterns and variations becomes necessary in reconstructive surgery. The origin, course and branching of the plantar arch is essential as it forms the stem of one of the major musculo-cutaneous flaps used in reconstructive foot surgery.

Although the arterial anatomy of the foot has been addressed in literature, more comprehensive studies of the plantar arch and its branches in terms of morphological and morphometric variations, are still insufficient [2, 4, 5, 6]. More recently Ozer et al. and Gabrielli et al. [2, 6], have shown the contributing arteries and the positioning of the plantar arch within the foot, documenting a few anatomical variations in this region. In 2008, Anupama investigated the plantar arterial arch in 50 formalin fixed cadavers, and

confirmed the findings of the above mentioned authors [5] and had not noted any further differences. Farlex (2014) confirmed the position of the plantar arterial arch within the foot as described by Ozer et al. and Gabrielli et al. [2, 6], but further refined it by stating that it lies on the transverse arch of the foot.

In order to determine the most important anatomic variations of the plantar arteries providing greater anatomical detail to vascular surgery, the anatomy and constitution of the deep plantar arch was studied.

Therefore, the aims of the study were to: a) re-examine and describe the morphology of the plantar arterial arch, and b) determine the dominant contributors to the plantar arch.

Material and Methods

On twenty-two dissected lower limbs the origin, course, and branches of the arteries in the plantar part of foot were examined.

The anatomy of the plantar arteries, their variations,origins, courses, and distributing branches were examined. The relations of the plantar arch were noted, and the entire plantar arterial arch was clearly defined. The plantar arch and its branches were exposed and photographed (iPhone6).

To determine the location of the plantar the sole of the foot was divided into three regions: anterior; middle; and posterior [3]. The middle was further divided into three parts: middle anterior; intermediate middle; and middle posterior (**Fig. 1**). The predominant blood supply to the plantar arch was determined by measuring each commissure along the plantar archcourse [1]. The diameter measurement as compared to the previous one determined the artery contributing to the dominating arterial supply.

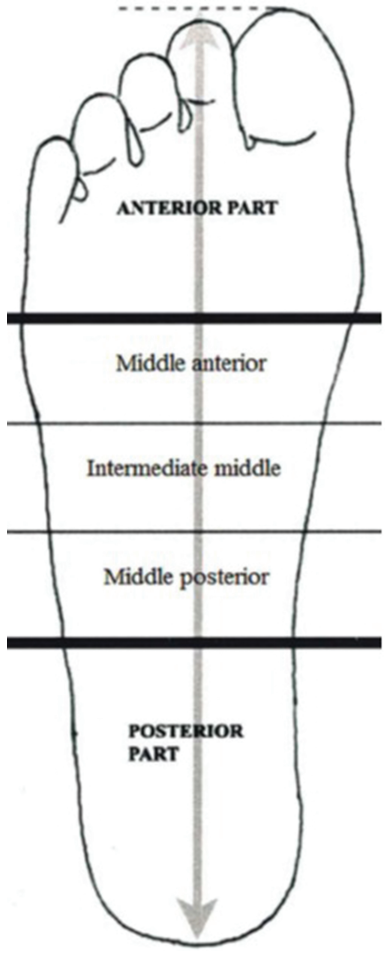

Results

Posterior tibial artery

The posterior tibial artery runs between the superficial and deep muscles in the rear section of the lower leg. In downward direction it moves medially and can be palpable behind the medial malleolus. (**Fig. 2**)

The anatomy of the plantar arteries, their variations, origins, courses, and distributing branches were examined. The relations of the plantar arch were noted, and the entire plantar arterial arch was clearly defined. Once the entire course of the plantar arch was visible *in situ,* it was recorded and photographed (Samsung Galaxy Note 10.1 5 megapixel).

Fig. 1. Schematic representation of the different quadrants the plantar side of the right foot. (Adapted from Ozer *et al*., 2005).

Fig. 2. Normal course of a. tibialis posterior behind the medial malleolus**.**

The location of the plantar arterial arch was determined by dividing the foot into three compartments: anterior; middle and posterior. The middle was further divided into three parts: middle anterior; intermediate middle; and middle posterior (**Fig. 1**). The length of the plantar arterial arch was measured from the point of anastomoses between the lateral plantar artery and the deep branch of the dorsalis pedis artery (**Fig. 2**). Predominant blood supply to the plantar arch was determined by measuring each commissure of the entire course of the plantar arch. A larger or smaller diameter as compared to the previous measurement determined which of the closest contributing artery, i.e the deep branch of dorsalis pedis artery, lateral plantar artery, or both, was responsible for the dominating arterial supply.

Branches in the ankle area

• Posterior medial malleolar artery- forms arterial network around the medial ankle
• Calcaneal rami – arterial network of the heel area
• Artery of tarsal canal - blood supply to the body of the talus

Branches in the foot

Below the sustentaculumtali posterior tibial artery divides intolateral and medial plantar arteries (**Fig. 3**)

On its course the lateral plantar artery gives of

• medial calcaneal branch (first clone) for the heel pad. Avulsio on the heel is a severe injury associated with high energy trauma and often with poor prognosis because of the possibility of heel pad necrosis
• branch to adductor digitiminimimuscles (second branch)
• digitiminimiartery (third branch)
• plantar arch (terminal branch). Plantar metatarsal arteries arise from the arch (**Fig. 4**)

Fig. 3. Tibialis posterior artery branching into lateral plantar and medial plantar arteries.

Fig. 4. Deep plantar arch – a terminal branch of lateral plantar artery.

Medial plantar artery runs along the medial edge of the foot and at the scaphoid / medial cuneiform bone divides into superficial and deep branch. The deep branch anastomoses with the first plantar metatarsal artery.

The Plantar Arterial Arch and Variations. The plantar arterial arch was observed in all of the specimens. It was found to be fully developed in all of the specimens as well (**Fig. 3**) with variations in 5 (22.7%) of the specimens.

Shape. In 3 (13.6%) of the specimens, a variation with the shape of the plantar arterial arch was observed. These variations were grouped as follows: a) Type A - Sharp irregular curve: observed on the left foot in one (4.5%) of the sample of variations (**Fig. 4**); b) Type B - Obtuse shaped curve: observed in six (4.5%) of the specimens, four right feet and two left feet (**Fig. 5**); and c) Type C - Spiral shaped arch: observed in one (4.5%) of the specimens (**Fig. 6**).

Location. The location of the plantar arterial arch was in the anterior middle in 18 (81.8%) cases, in the junction between the anterior middle and intermediate middle in four (18.2%) cases [3].

Formation. The results of this study are grouped as follows: Normal course of lateral and medial plantar arteries was found in 17 cases (77.3%) (**Fig. 3**). In one case (4.5%) the deep plantar arch originated from dorsalis pedis artery and partly lateral plantar artery (**Fig. 5**). In one case (4.5%) the lateral plantar artery gave off the third and fourth metatarsal arteries (**Fig. 6**). In three cases (13,6%) the lateral planar artery gave off the second, third and fourth metatarsal arteries. (**Fig. 7**).

By changing lifestyle and increasing stress, people suffer more often from diseases such as diabetes and hypertension. Diabetic neuropathy leads to foot infections and ischemia, resulting in the risk of large amputations. In the effort to rescue the ischemic limb, the arterial bypass plays a major role. A. dorsalis pedis with the main and clones is preferentially used as a receptacle. A lumbar arthritis arterialized by a. dorsalis pedis can safely be used as an island flap to cover ankle or heel defects and as a free flap for palm defects. Therefore, a. A. dorsalis pedis.

Because variations in the plantar arch are not unusual, it is important to have in-depth anatomical knowledge of the arteries. Preoperative angiography for each anomaly is recommended to prevent risks during surgical intervention.

Fig. 5. Deep plantar arch formed by dorsalispedis artery and partly from lateral plantar artery.

Fig. 6. Division of a. tibialis posterior artery – plantar arch, medial plantar; plantar metatarsal arteries, lateral plantar arteries.

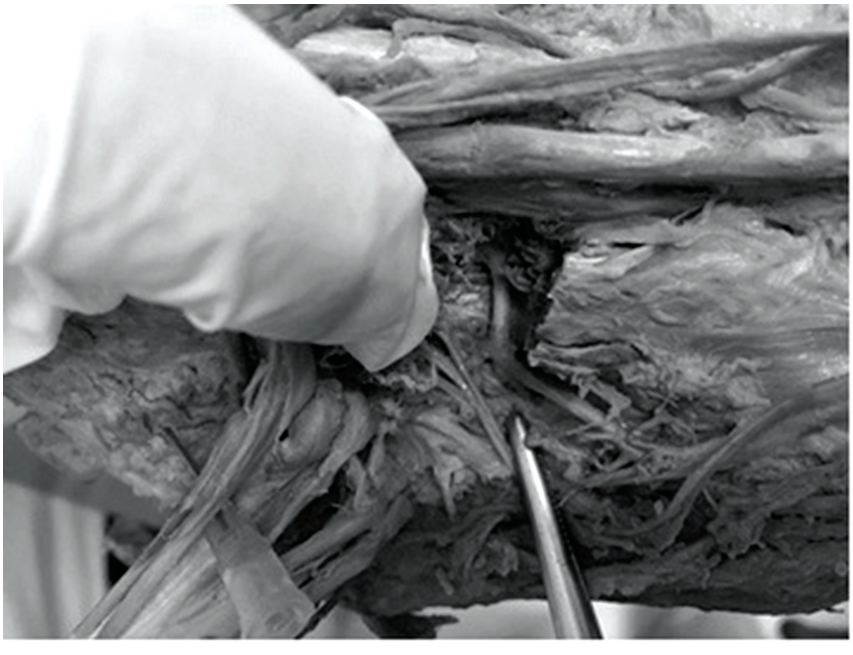

Fig. 7. Deep plantar arch giving off the second, third and fourth metatarsal arteries.

Conclusion

This study was designed to improve the understanding of the plantar arterial arch and its variations. Thorough knowledge of the blood supply to the foot is essential for surgeons in the mobilization and application of plantar flaps. The study findings complement the existing descriptions of the plantar arch with regard to morphology and variations in the formation.

The data from the study indicate that there is asymmetry in the plantar arch, which is largely related to its formation. On the other hand, the distances between plantar metatarsal arteries arising from arcus plantaris are variable. Some are close and others are at a greater distance; some arteries may arise even from the same point of the arch.

References

1. **Bergman, R. A., A. K. Afifi, M. S. R. Miyauchi.** Various arterial patterns on dorsum of foot and in the plantar arch. *Anatomy atlases. An anatomy digital library. Illustrated encyclopedia of human anatomic variation: Opus II: Cardiovascular system.* Availabe at https://www.anatomyatlases.org/AnatomicVariants /Cardiovascular/ Text/Arteries/DorsalisPedis.shtml
2. **Gabrielli, C., E. Olave, E. Mandiola, C. F. Rodrigues, J. C. Prates.**The deep plantar arch in humans: constitution and topography. – *Surg. Radiol. Anat.*, **23**, 2001, 253-258.
3. **Kalicharan, A., P. Pillay, C. Rennie, M. R. Haffajeeh.** The anatomy of the plantar arterial arch. – *Int. J. Morphol.,* **33**, 2015, 36-42.
4. **Kelikian, A. S., S. K. Sarrafian.** *Sarrafian's anatomy of the foot and ankle: Descriptive, topographic, functional.* 3rd ed. Philadelphia, Lippincott Williams &Wilkins, 2011, pp.321.
5. **Moore, K. L., A. F. Dalley, A. M. R. Agur,** *Clinically Orientated Anatomy*. 6th ed. Philadelphia, Wolters Kluwer Health/Lippincott Williams & Wilkins, 2010. pp.610.
6. **Ozer, M. A., F. Govsa, O. Bilge.** Anatomic study of the deep plantar arch. – *Clin. Anat.*, **18**, 2005, 434-42.
7. **Yamada, T., P. Gloviczki, T. C. Bower, J. M. Naessens, S. W. Carmichael.** Variations of the arterial anatomy of the foot. – *Am. J. Surg.*, **166**, 1993,130-5.

Institute of Experimental Morphology, Pathology and Anthropology with Museum
Bulgarian Anatomical Society

Acta morphologica et anthropologica, 25 (3-4)
Sofia ● 2018

Morphological Classification and Significance of the Acromion for the Shoulder Pathology

Sonya Mersinkova[1], Stefan Milev[1], Alexandar Iliev[1], Boycho Landzhov[1], Georgi P. Georgiev[2]*

[1] Department of Anatomy, Histology and Embryology, Medical University of Sofia, Bulgaria
[2] Department of Orthopaedics and Traumatology, University Hospital Queen Giovanna – ISUL, Medical University of Sofia, Bulgaria

* Corresponding author e-mail: dralexiliev@abv.bg

The acromion is one of the two processes of the scapula. It plays a role in the field of orthopedics by having a correlation with some diseases. The morphology of this process has a significant role in upper limb pathology. The aim of the present study was to describe the different types of acromion process based on its morphology and to discuss its relation to some orthopedics diseases. We carried out a research which included 30 scapulae of unknown sex and age, provided by the Medical University of Sofia. Digital Vernier caliper and goniometer were used to calibrate the parameters (length, width etc.) of the process. We established three types of acromion process: type 1 – flat, type 2 – curved and type 3 – hooked. Our study showed that type 2 (curved) was the most commonly observed – around 80 % of the fixed materials; type 1 (flat) was seen in 11% and type 3 (hooked) – in 9%. People with type 3 (hooked) acromion process tend to suffer more often from the subacromial impingement syndrome. Knowledge of the morphology of the acromion process may help with the diagnosis and treatment of various diseases discussed in the present study and may supplement the work of shoulder surgeons and people occupied with this field of work.

Key words: acromion, morphology, scapula, orthopedics

Introduction

The scapula is a large flat bone with triangular shape that has three processes – spine, acromion and coracoid process [9]. The anatomy term "process" itself means a prominence on a bone. The acromion process projects forward from the lateral end of the spine of scapula at an approximately right angle [9]. It is larger than the other processes and articulates with the lateral end of the clavicle. The tendon of supraspinatus muscle passes under the process; furthermore, these two structures are separated by the subacromial bursa [8].

There are three main structures that create the so-called coraco-acromial arch - the anterior part of acromion process, the coraco-acromial ligament and the coracoid process [8]. The morphometry of the acromion and the measurements of the arch

have a significant role in the field of orthopedics, by having a correlation with some diseases [7]. In addition, it contributes to the medical treatment of the upper limb. The morphology of the acromion is mostly associated with the subacromial impingement syndrome which causes inflammation of the bursa situated under the acromion, thus leading to pain while abducting the upper limb in the shoulder joint [2, 5, 8].

The aim of the present study was to describe the different types of acromion process based on its morphology and to discuss its relation to some orthopedics diseases.

Materials and Methods

The present study was conducted on 30 adult human scapulae of unknown age and sex in the Department of Anatomy, Histology and Embryology, Medical University of Sofia, Bulgaria. The study was approved by the Medical Legal Office and Local Ethics Committee. The materials had been fixed and had undergone chemical processing for this study. Only bones with clear features that were intact were used while the unfit excluded. One structure that we didn't take under consideration was the glenoid notch located in the anterior margin of the glenoid cavity.

The measurements were taken with the help of a caliper and recorded in millimeters (mm). The following parameters were measured: length; width; thickness; acromio-coracoid (A-C) distance, which was the distance between the tip of the coracoid process and the acromion process; acromio-glenoidal (A-G) distance, representing the distance between the supraglenoid tubercle and the tip of the acromion process. The measurements were analysed by means of descriptive statistics including percentage, mean and standard deviation and were statistically evaluated through a T-test.

Results

In the present study, we reported the presence of three types of acromion process – type 1 – flat (**Fig. 1a**), type 2 – curved (**Fig. 1b**) and type 3 – hooked (**Fig. 1c**). These types were distinguished based on the extent of its arch. The obtained data showed that the maximum length of the acromion was 51 mm, the maximum width – 29 mm and the maximum thickness – 11 mm. The A-C distance and the A-G distance were 39 and 30 mm, respectively. We also calculated the mean values: length – 44 mm, width – 24.3 mm, thickness – 7.7 mm, A-C distance – 26.6 mm and A-G distance – 22.9 mm (**Table 1**). As a result, we concluded that type 2 (curved) was most commonly observed – around 80% of the fixed materials, followed by type 1 (flat) which was seen in 11%. Type 3 (hooked) represented only 9% of the scapulae.

Table 1. Numerical representation of the measurements of acromion

Measurements	*Mean values*	*SD*	*Min values*	*Max values*	*t-test*
Length (mm)	44.0	4.15	35	51	0.40
Width (mm)	24.3	2.33	19	29	0.46
Thickness (mm)	7.7	1.37	6	11	0.17
Acromio-coracoid distance (mm)	26.6	4.81	20	39	0.21
Acromio-glenoidal distance (mm)	22.9	3.41	16	30	0.02

Fig. 1. Photograph of different types of acromion: a) type 1 – flat; b) type 2 – curved; c) type 3 – hooked.

Discussion

Many studies have explored the morphometry of the acromion process, the different types of acromion and its correlation with the impingement syndrome [1, 3, 6]. It appears that most data reported in previous studies are comparable to our measurements and evaluations. Anetzberger and Putz observed that the mean acromial length was 47.00 mm [1]. In the present study, this parameter was calculated as 44 mm. Rarely, a fourth type is observed, in which case the acromion is concave in cranio-caudal direction [4]. This classification was proposed by Farley et al. [4] but has not been taken into consideration because of the rare occurrence of type 4 acromion and absence of correlation with rotator cuff pathology.

According to Epstein et al. [3], the acromion morphology appears to affect the success of conservative medical treatment in some cases and surgical procedures to people with orthopedic diseases. It appears that patients with the hooked type of acromion tend to suffer more often from the impingement syndrome [9]. This means that the anatomical features of the process have an effect on the pathology of the rotator in the arm joint. This hooked shape particularly tends to create pressure on the bursa which is situated under the process. This leads to pain while rotating the shoulder joint. Furthermore, the presence of enthesophytes is associated with acromion type III, and together they are mainly associated with subacromial impingement syndrome and injury of the rotator cuff [6]. Some of the parameters we examined vary with sex and age, which also has a clinical significance. Information about sex and age of the examined material, however, was unavailable and could not be assessed in the present study.

Conclusion

In the present study, we described the presence of 3 types of acromion process: flat (type 1), curved (type 2) and hooked (type 3), based on the extent of its arc. We found that the dominant type was type 2 (curved). People with type 3 (hooked) acromion process tend to suffer more from the subacromial impingement syndrome, because this shape tends to create pressure on the bursa which is situated under the process. The morphometric data on the acromion process and types of acromion may be helpful for the field of orthopedics during surgical repair around the shoulder joint.

References

1. **Anetzberger, H, R. Putz.** The scapula: principles of construction and stress. – *Acta Anat. Basel*., **156**, 1996, 70-80.
2. **Bigliani, L. U., J. B. Ticker, E. L. Flatow, L. J. Soslowsky, V. C. Mow.** The relationship of acromial architecture to rotator cuff disease. – *Clin. Sports Med.,* **10**, 1991, 823-838.
3. **Epstein, R. E., M. E. Schweistzer, B. G. Frieman, J. M. Fenlin, D. G**. **Mitchell.** Hooked acromion: prevalence on MR images of painful shoulders. – *Radiology,* **187**, 1993, 479-481,
4. **Farley, T. E., C. H. Neumann, L. S. Steinbach, S. A. Petersen.** The coracoacromial arch: MR evaluation and correlation with rotator cuff pathology. – *Skeletal Radiol.,* **23**, 1994, 641-645.
5. **Iliev, A., G. P. Georgiev, D. Dimitrov, P. Yordanova, B. Landzhov.** An anatomic study of the types of glenoid notch and their distribution among the genders. – *Chr. J. Clin. Case Rep.,* **1**, 2017, 010.
6. **Natsis, K., P. Tsikaras, T. Totlis, I. Gigis, P. Skandalakis, H. J. Appell, J. Koebke.** Correlation between the four types of acromion and the existence of enthesophytes: a study on 423 dried scapulas and review of the literature. – *Clin. Anat*., **20**, 2007, 267-272.
7. **Paraskevas, G., A. Tzaveas, B. Papaziogas, P. Kitsoulis, K. Natsis, S. Spanidou.** Morphological parameters of the acromion. – *Folia Morphol. (Warsz),* **67**, 2008, 255-260.
8. **Singh, J., K. Pahuja, R. Agarwal.** Morphometric parameters of the acromion process in adult human scapulae. – *Indian J. Basic Appl. Med. Res.,* **8**, 2013, 116570.
9. **Vinay, G., S. Sheela.** Morphometric study of the acromion process of scapula and its clinical importance in south Indian population. – *Int. J. Anat. Res.,* **5**, 2017, 4361-4364.

Institute of Experimental Morphology, Pathology and Anthropology with Museum
Bulgarian Anatomical Society

Acta morphologica et anthropologica, 25 (3-4)
Sofia ● 2018

Anatomical Variants in the Termination of the Cephalic Vein

Stoyan Novakov[1], Elena Krasteva[2]*

[1] Department of Anatomy, Histology and Embryology, [2]Department of Propaedeutics of Surgical Diseases, Medical Faculty, Medical University of Plovdiv

* Corresponding author e-mail: stoyan67@gmail.com

Jugulocephalic vein is atavistic structure which is very rare. The low incidence of the variations of the cephalic vein in deltopectoral triangle and its position on the anterior surface of the clavicle and the neck doesn't make it less important for the clinical practice. Phylo- and ontogenesis explain the formation of the above mentioned variations. We followed the pattern of the cephalic vein in its proximal part and termination to describe possible variations. In this long term study on 140 upper limbs of 70 cadavers, 4 or 2,9% of the cephalic veins were variable. The direct empting of the cephalic vein into internal jugular is an exception with few descriptions at the moment. The rareness of this anatomical variation doesn't make it less important for clinical practice. It is described as a possible obstacle in catheter implantation, clavicle fractures and creation of arteriovenous fistula in patients on hemodialysis.

Key words: cadavers, human anatomy variation, cephalic vein, external jugular vein, jugulocephalic vein

Introduction

Cephalic vein (CV) belongs to the group of superficial veins of the upper limb. It usually forms over the anatomical snuff-box on the radial side of the wrist from the radial end of the dorsal venous plexus. Proximally it curves around the lateral side of the forearm collecting tributaries from both radial and ulnar aspects in that area. The CV ascends anterior to the elbow, superficial to a groove between brachioradialis and biceps brachii, crosses superficial to the lateral cutaneous nerve of the forearm, and ascends lateral to biceps and between pectoralis major and deltoid, where it adjoins the deltoid branch of the thoracoacromial artery [15]. At the lateral aspect of the deltopectoral groove, the CV is located superficially in a fat pad lying horizontally and separating the two muscles [7]. In the infraclavicular fossa it passes posterior to pectoralis major and piercing the clavipectoral fascia it crosses the axillary artery and opens in the axillary vein at the level of the lower border of the clavicle [15].

Variations of cephalic vein are rare. They include its total absence and termination into subclavian vein [14].The cephalic vein may end in the internal jugular vein (IJV), the external jugular vein (EJV), or the basilic vein [6, 12]. A more infrequent anastomosis named "jugulocephalic anastomosis", which usually connects the terminal part of the cephalic and

the EJV, appears where cephalic vein goes deep behind the clavicular head of pectoralis major and travels up anterior to the clavicle [12, 17].

The very first thorough description in anatomy by Galen defines cephalic vein (Galen's humeral vein) as arising from the external jugular vein and encircling the clavicle 'ran towards the periphery' [19]. That postulate like all other Galen's anatomy beliefs rules for centuries. The explanation for this misleading information is in the material of his dissection which is animals and non-human primates [16]. So we can define the jugulocephalic vein like an atavistic feature in humans. Phylogenetic and ontogenetic features of the superficial veins of the neck and upper limbs are clarifying the possible anatomical variants found rarely but not meaninglessly.

Study of variations in the superficial veins is important for the anatomists, interventional radiologists, surgeons, and clinical practitioners who carry out procedures like canulations, venegraft harvesting in endarterectomy, implantation and selective venous samplings, as well as traumatologists, plastic surgeons and specialists in centers for hemodialysis [2,9, 14].

The aim of this study was to follow up the incidence of CV variations in its termination and discuss the embryological basis and clinical implications.

Material and methods

During a routine gross anatomy dissection in the Department of Anatomy, Histology and Embryology at the Medical Faculty, Medical University of Plovdiv we made observation for the termination of CV on 140 upper limbs of 70 (52 men and 18 women) embalmed cadavers for a period of 18 years.

Results

Four out of 140 upper limbs showed significant differences from the usual pattern of the CV in its most proximal part.

Case No 1. – An adult male cadaver aged approximately 75 years dissected for educational purposes showed two concomitant variations in the left axilla and on the same side of the neck. The axillary arch of Langer was more common one but the CV draining in EJV was really a rare variety. The vein travelled in the deltopectoral groove and remained superficial after reaching the clavicle where it passed anterior to it. Arching the clavicle the CV after a short course entered the EJV at its terminal part. Its supraclavicular part was 12 mm long. No anastomoses or extra tributaries were found coming out from the CV in the observed area (**Fig.1**).

Case No 2. – During the dissection of an adult male cadaver over age of 70 another variation in the course and position of the terminal part of the left CV was found. At the level of the coracoid process CV divides into a main tributary which arches deep under the pectoralis major muscle to join axillary vein and so called 'jugulocephalic anastomosis' climbing on the anterior surface of the clavicle to the adjacent EJV (**Fig.2**).

Case No 3. – The last case was male cadaver aged 62 years. He was the most recently dissected and with multiple variations. The followed cephalic vein pattern was different on both sides from the standard described in the books.

On the right side CV was positioned lateral out of the deltopectoral groove following the fibers of the deltoid muscle. In the distal portion of the deltoid the CV was 1 cm lateral of its border. It travelled up and medial and crossed the clavicle at the attachment of the medial edge of deltoid muscle. In fossa supraclavicularis major CV received a tributary coming from the fossa supraclavicularis minor which is following the upper border of the clavicle.

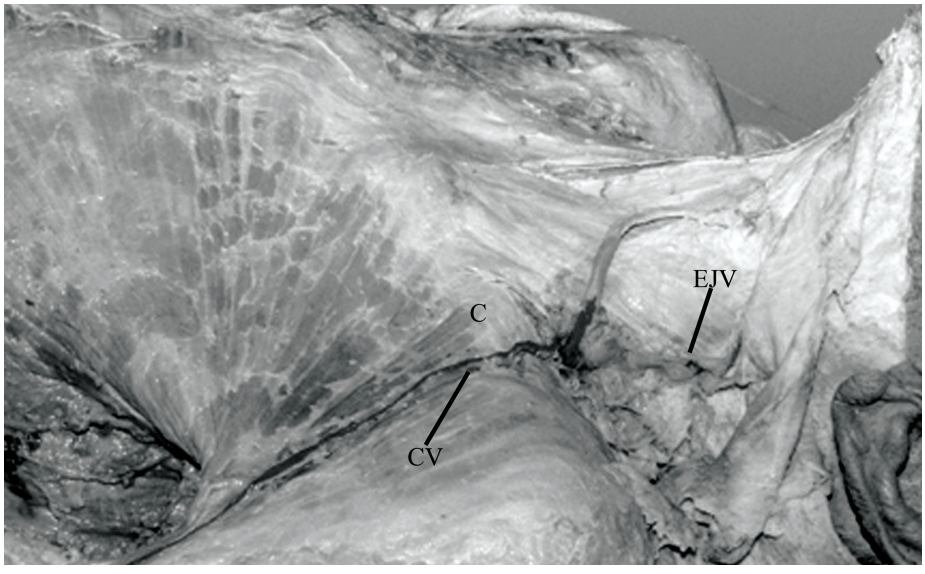

Fig. 1. Left arm, shoulder and neck with cephalic and external jugular veins.
EJV – external jugular vein, CV – cephalic vein, C - clavicle

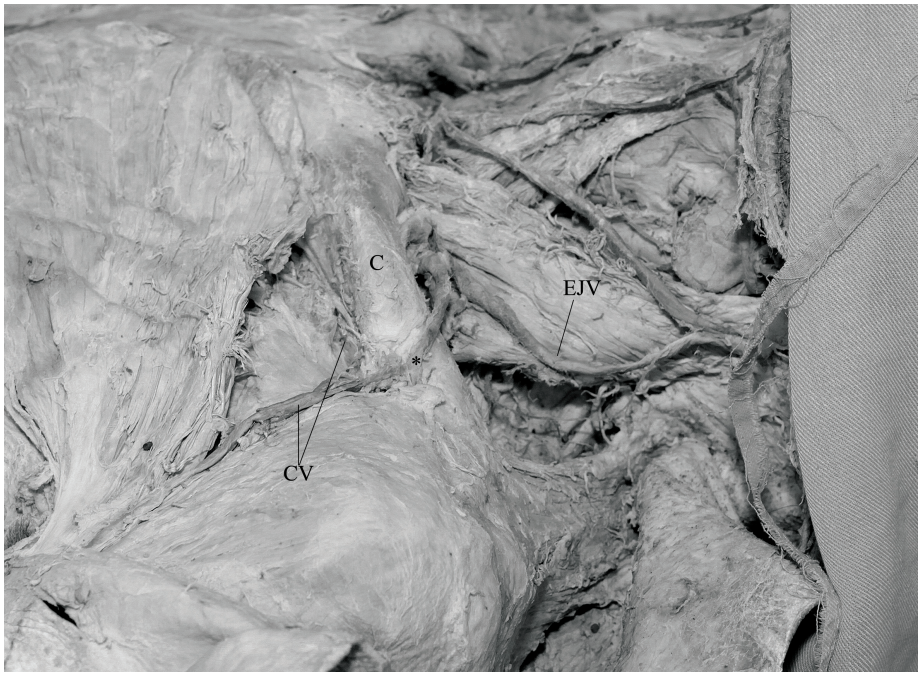

Fig. 2. Left arm, shoulder and neck with cephalic and external jugular veins.
EJV – external jugular vein, CV – cephalic vein, C – clavicle, * - jugulocephalic anastomosis

The main vein continued deep under the sternocleidomastoid to enter the lateral side of the internal jugular vein. The length of the CV from the distal end of deltopectoral groove to IJV was 183 mm. The length from the point of entry to the right venous angle was 59 mm and to the upper end of the superior vena cava it was 95 mm. The diameter of the CV at its end was 5 mm (**Fig. 3**).

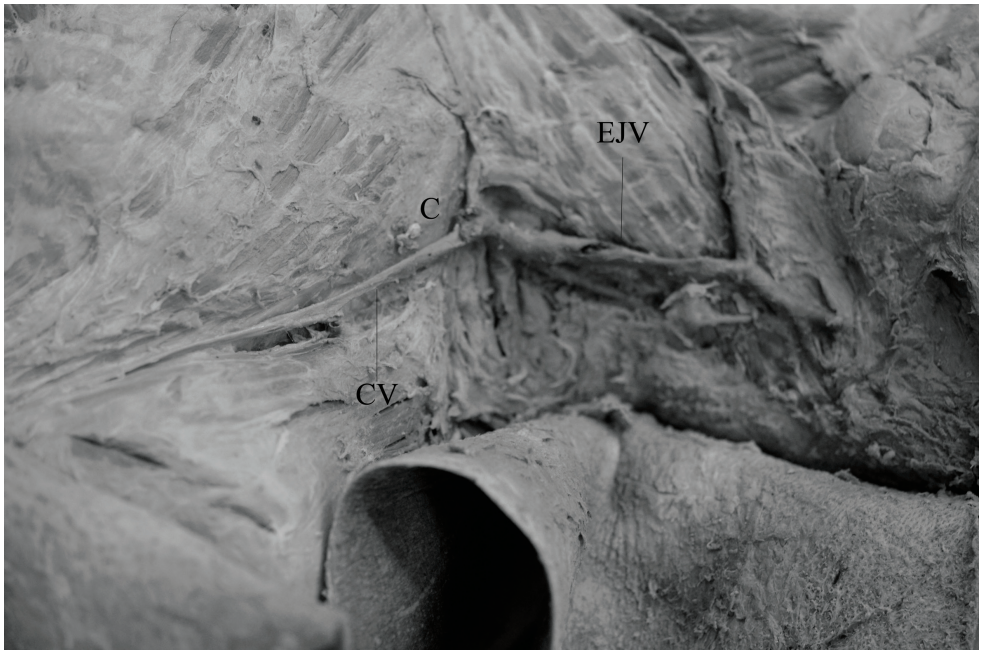

Fig. 3. Left deltopectoral groove and neck.
EJV – external jugular vein, CV – cephalic vein, C – clavicle

The left CV was lying in the deltopectoral groove. Its length from the distal beginning of the groove to the entry into EJV was 149 mm. There were no tributaries to CV in this region. It was crossing anterior the clavicle and medial to the attachment of deltoid. Finally CV entered the EJV (**Fig. 4**).

A concomitant variation related to the thyroid gland was found on the neck of the last case.

The incidence of the variations of the CV, crossing the anterior aspect of the clavicle, is 2,9% of the population in Bulgaria. The incidence of jugulocephalic anastomosis is 0,7%.

Discussion

The cephalic vein is one of the most used veins for a great number of activities, such as venipuctures, arteriovenous fistula creation and for right atrial and ventricular lead placement in patients receiving pacemakers and implantable cardioverter defibrillators [1, 18]. CV is usually anatomical landmark known for its consistent anatomy because of its rare variability. Despite that, its anatomical variations are clinically and surgically significant and healthcare professionals must be aware of the variations of this vessel [1].

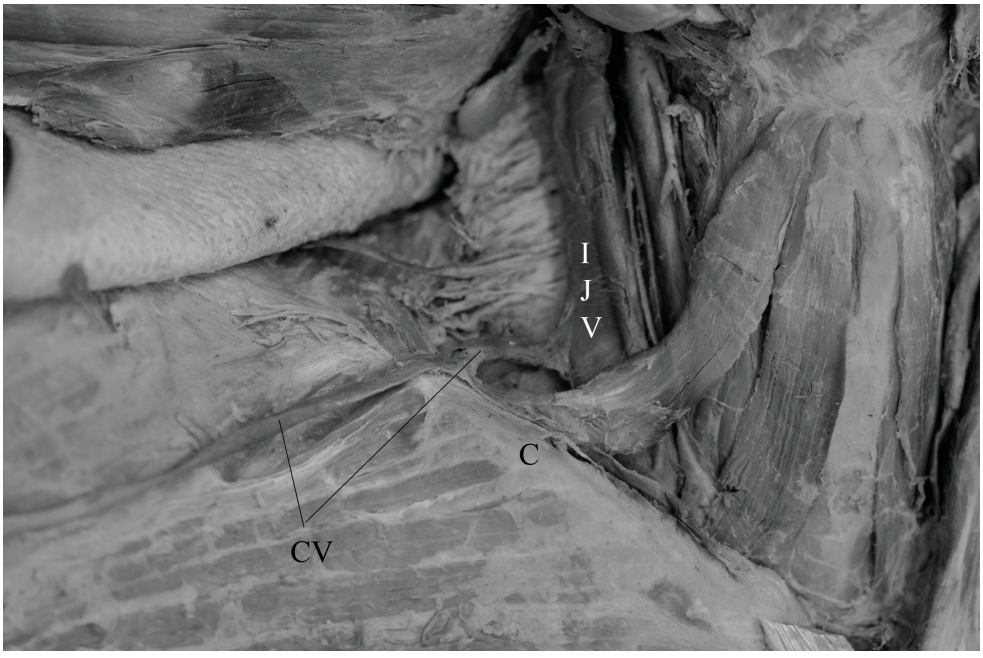

Fig. 4. Right deltopectoral groove and neck.
CV – cephalic vein, C – clavicle, IJV – internal jugular vein

In this article we present some exceptional variations of CV which are considered atavistic and explained by the onto- and phylogenetic development. The superficial veins of the upper limb develop from a superficial plexus of capillaries, then, as they fuse and enlarge, the greater venous trunks are formed. The capillary plexus on the ulnar border develops the subclavian, axillary and basilic veins which emerge from the postaxial primitive vein. The radial border capillary plexus atrophies and CV at further stages of development comes from the preaxial vein [1, 16]. The preaxial vein primarily empties into the venous plexus located within the neck [19]. The CV is developed by a growth of an anastomotic channel of the EJV which initially empties into the IJV and later into the axillary vein [8, 13]. Thus, the CV acquires a new connection with the axillary vein only at a further stage of the ontogeny, while, usually, the part of the CV running over the clavicle (the jugolocephalic vein) gradually atrophies [19]. In our study three of the vessels are persistent jugulocephalic vein which in case No2 occurs as a connecting branch between EJV and CV that normally ends in the axilary vein or it is a typical jugulocephalic anastomosis, while in cases No1 and No3 (left side) the remnant jugulocephalic channel connects directly CV to EJV.

The right CV of the case No 3 is a very rare variation which could be explained by the ontogeny of the superficial veins and a stage of existing connection between CV and IJV. We found just one more case in the available literature which described that unusual end of CV into IJV [8].

The cephalic vein has recently emerged as an alternative to the subclavian and EJVs for the implantation of catheters and artificial cardiac pacemakers [5]. CV cut-down is considered a first choice for venous access [3]. Although variations of CV are rare they should be taken in mind during these manipulations as they can cause some

difficulties [3]. In cases of central venous line insertion that requires critical central venous access from the subclavian vein, the CV cut-down method is employed at the deltopectoral to insert a catheter under visual inspection [10]. Clinically, the CV is preferred for hemodialysis to remove waste products from the blood [9]. The variant anatomy of the cephalic arch is important for arteriovenous fistula creation in patients on hemodialysis and the clinicians caring for vascular access patients may choose to consider alternative vascular access [4]. Orthopedicians treating fractures of the clavicle by either percutaneous intramedullary nailing or open exposure should be very careful to avoid potentially iatrogenic injuries for the patient from an unnoticed anatomic variant [11].

Human anatomy variations are abundantly described in the literature but are not yet well systematized and categorized. Kameda et al. are classifying the CV variations in the deltopectoral region into four types: 1A, 1B, 2A, and 2B [5]. Two of our CVs are Type 1A, one is 1B and the rare case of CV empting in IJV is not included in Kameda's classification. We agree that more studies in the future are needed to evaluate both arms with a larger pool of cadavers and confirm the incidence of unusual jugulocephalic veins and CV termination [5].

Conclusion

Based on the result of 140 upper limbs of 70 embalmed cadavers, from our study 3 out of 70 (4,3%) cadavers are with CV variations, one bilateral and two unilateral on the left side. Four out of 140 (2,9%) cephalic veins pass anterior to the clavicle and follow a course beyond this bone. One CV or 0,7% is registered as jugulocephalic anastomosis and 1 (0,7%) CV terminates in IJV. Knowledge of these anatomical variants could avoid serious complications during catheter implantation, fractures of the clavicle or arteriovenous fistula creation in patients on hemodialysis.

References

1. **Araújo, R. C., L. A. S. Pires, M. L. Andrade, M. C. Perez, C. S. L. Filho, M. A. Babinski.** Embryological and comparative description of the cephalic vein joining the external jugular vein: A case report. – *Morphologie*, **102**, 2018, 44-47.
2. **Darabi, M. R., A. Shams, P. Bayat, M. Bayat, S. Babaee, B. Ghahremani.** A Case report: variation of the cephalic and external jugular veins. – *ASJ*, **12**, 2015, 203-205.
3. **De Maria, E, S.Cappelli.** Cephalic vein with a supraclavicular course: rare, but do not forget it exists! – *J. Cardiovasc. Med. (Hagerstown)*, **18**, 2017, 727-728.
4. **Jun, E. S. W., A. L. Y. Lun, M. Nikam.** A rare anatomic variant of a single-conduit supraclavicular cephalic arch draining into the external jugular vein presenting with recurrent arteriovenous fistula stenosis in a hemodialysis patient. – *J. Vasc. Surg. Cases Innov. Tech.*, **22**, 2017, 20-22.
5. **Kameda, S., O. Tanaka, H.Terayama, T. Kanazawa, R. Sakamoto, S.Tetsu,K. Sakabe.**Variations of the cephalic vein anterior to the clavicle in humans. – *Folia Morphol. (Warsz),* 2018 in press
6. **Kommanda, R. K. S., M. Asif, C. H. Shivarama.** Supraclavicular course of the left cephalic vein: Rare anatomical variant. – *Int. J. Case Rep. Images*, **8**, 2017, 792–795.
7. **Loukas, M., C. S. Myers, C. T.Wartmann, R. S. Tubbs, T. Judge, B. Curry, R.Jordan.**The clinical anatomy of the cephalic vein in the deltopectoral triangle. – *Folia Morphol. (Warsz)*,**67**, 2008, 72-77.
8. **Lum, C., E. D. Ladenheim.** An interesting clinical case: variant of the cephalic vein emptying into the internal jugular vein. – *Seminars in Dialysis*, **26**, 2013, E11-E12.
9. **Maalman, R. S., Y. O. Donkor, A. M. Ayamba, J. K. Abledu.**A Rare anatomical variation of the termination of right and left cephalic veins. – *Case Rep. Vasc. Med.,* **2018**, 2018, 1.

10. **Parsonnet, V., M.Roelke.** The cephalic vein cutdown versus sublcavian puncture for pacemaker/ ICD lead implantation. – *Pacing Clin. Electrophysiol.*, **22**, 1999, 695-697.
11. **Ramírez, J. D., L. C. Sáenz, D. Rodríguez, A. J. Restrepo, F. Villegas.** Supraclavicular course of the cephalic vein. – *Int. J. Case Rep. Images*, **5**, 2014, 281–284.
12. **Saaid, A., I. Drysdale.** Unusual termination of the cephalic vein. – *Clin. Anat.*, **21**, 2008, 786-787.
13. **Schoenwolf, G. C., S. B. Bleyl, P. R. Brauer, P. H. Francis-West.** *Larsen's human embryology.* Churchill Livingstone, 2014.
14. **Shetty, P., S. B. Nayak, R. Thangarajan, M. R. D'Souza.** A rare case of persistent jugulocephalic vein and its clinical implication. – *Anat. Cell Biol.*, **49**, 2006, 210-212.
15. **Standring, S.** *Gray's Anatomy: The Anatomical Basis of Clinical Practice*, Elsevier; 41 edition, 2016, 830.
16. **Thiranagama, R., A. T. Chamberlain, B. A. Wood.** *The comparative anatomy of the forelimb veins of primates. – J. Anat.*, **164**, 1989, 131-144.
17. **Tubbs, R. S., M. M. Shoja, M. Loukas.** *Bergman's Comprehensive Encyclopedia of Human Anatomic Variation,* Wiley-Blackwell; 1 edition, 2016, 829-830.
18. **Watts, T. E., S. Pant, S. Reddy, K. Siddiqui, D. Singh, H. Paydak.** Cephalic vein cutdown for left ventricular lead placement in biventricular device upgrades. – *J. Innov. Cardiac Rhythm Manage.*, **6**, 2015, 1906-1907.
19. **Wysiadecki, G., M. Polguj, M. Topol.** Persistent jugulocephalic vein: case report including commentaries on distribution of valves, blood flow direction and embryology. – *Folia Morphol. (Warsz.)*, **75**, 2016, 72-77.

Institute of Experimental Morphology, Pathology and Anthropology with Museum
Bulgarian Anatomical Society

Acta morphologica et anthropologica, 25 (3-4)
Sofia ● 2018

Application of Left Circular Polarized Light for Polymerization of Biodur P_{40}

*Jordan Stoyanov, Antoaneta Georgieva, Ivelina Ivanova, Dimitar Sivrev**

Department of Anatomy, Faculty of Medicine, Trakia University, Stara Zagora, Bulgaria

* Corresponding author e-mail: dsivrev@abv.bg

Biodur P_{40} is a UV light cured polyester Co-polymer that is used for making of brain slices. Ultraviolet light is the usual factor for curing the polyester. We use a device constructed by us for hardening stage of procedure. There are many worldwide attempts to apply other sources of light. The purpose of this study is to test the effect of left-rotating circular polarized light on polymerization of Biodur P_{40}.

Key words: plastination, left-rotating circular polarized light, Biodur P_{40}, UV

Introduction

Plastination is a new method for durable preservation of anatomical preparations. The plastinators use some basic methods in their work. S_{10}, E_{12}, P_{35} and P_{40} are modern plastination techniques for production of safety and life like anatomical preparations. Biodur P_{40} is a UV light cured polyester co-polymer that is used for making of brain slices [7]. Ultraviolet light is the usual factor for curing the polyester [1]. We use a device constructed by us for hardening stage of procedure (**Fig. 1**). It has four lower and two upper ultraviolet tube manufactured by Phillips.

There are many worldwide attempts to apply other sources of light [3]. They are described by *Robert Henry* [4]. In China, Thailand and Carolina (USA) the materials that are used work at room temperature after being mixed with chemical hardener [5, 6, 8].

Fig. 1. A UV light source used to solidify brain plates.

In our previous studies [9], we had been successful in applying sunlight as the hardener of the polymer. This is an economical method, but the procedure is slow and the process is more difficult to control.

The purpose of this study is to test the effect of left-rotating circular polarized light on polymerization of Biodur P_{40}. The light is an electromagnetic wave, but the polarization light is a state in which the electric field has a constant magnitude [10].

To accomplish this goal, we set out the following main tasks:

- ✓ Detecting the action of circularly polarized light with a yellow filter;
- ✓ Detecting the action of circularly polarized light with a red filter;
- ✓ Detecting the action of circularly polarized light with a green filter;
- ✓ Detecting the action of circularly polarized light with a violet filter;
- ✓ Detecting the action of circularly polarized light without a filter;
- ✓ Control reaction with sunlight.

Material and Methods

We used standard resin Biodur P_{40}, manufactured by *Biodur*^{TM}, *Heidelberg*, *Germany*. For better visualization of the polyester fluid, we added colorants in different versions as follows:

- ✓ Hematoxylin;
- ✓ Eosin;
- ✓ Eosin in acetone;
- ✓ Without coloring.

The source of left-turning circularly polarized light is our construction, made from an old dia-projector with an attachment for removable filters of different color (**Fig. 2**).

We used several filters with different color and different band width.

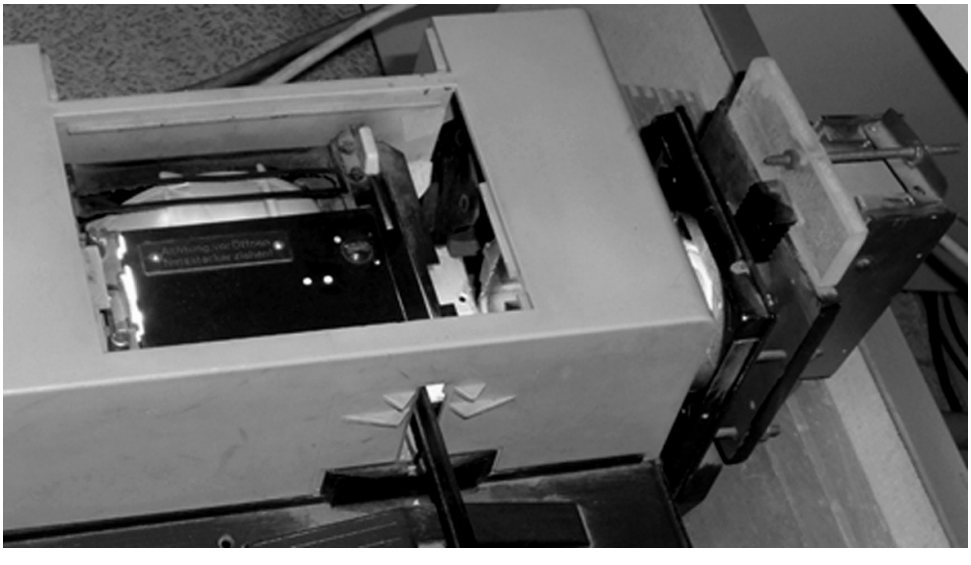

Fig 2. The light source.

Results and Discussion

The first sign of the beginning of the reinforcement is the appearance of a "mesh" in the polyester fluid. The grid appeared first in the polymer without a colorant, and soon after – in this stained with eosin in acetone. The results are presented on **Table 1**.

The results of applying different filters to a colorless polymer are shown in **Table 2**.

We can't compare our results with other authors because there are not similar investigations with circularly polarized light.

Final hardening occurred after 6-7 days. It turns out that the circularly polarized light causes a slow curing of the Biodur P^{40} but it is not enough for the needs of the practice. In the control reaction with sunlight, a network appears after 20 minutes.

Table 1. The grid appearance in the polyester co-polymer (in minutes).

No	**Polyester co-polymer BIODUR P_{40}**	**minutes**
1	Without a colorant	45
2	Tinted with eosin in acetone	60
3	Tinted with eosin	75
4	Tinted with hematoxylin	150

Table 2. The grid appearance in the polyester co-polymer (by filter color).

No	**Polyester co-polymer BIODUR P_{40}**	**minutes**
11	Without filter	30
22	Yellow filter	45
33	Violet filter	45
44	Green filter	135
55	Red filter	180

Conclusions

1. Left circular polarized light is not suitable for curing the Biodur P_{40} polyester co-polymer since the process is running too slowly.

2. The best and quickest cure is obtained by using ultraviolet rays of special lamps, which is suitable for practice (the process is described in another study).

3. The second most effective is the application of sunlight, but it is more suitable for initial polymerization of the material (the process is described in another study).

References

1. **Adds, P. A** low-temperature dehydration/room-temperature impregnation protocol for brain tissue using Biodur S10/S3. – *J. Int. Soc. Plast*., **23**, 2008, 41.
2. **Barnett, R.** Plastination of coronal and horizontal brain slices using the P_{40} technique. – *J. Int. Soc. Plast.*, **12**, 1997, 33-36.
3. **Henry, R**. Polyesterplastination: P_{40} technique. – *J. Int. Soc. Plast.*, **26**, 2014, 31.
4. **Henry, R**. Plastination history. – *J. Int. Soc. Plast.*, **28**, 2016, 20.
5. **Jabarin, S**. Chemistry and physical properties of polymers for plastination. – *J. Int. Soc. Plast.*, **28**, 2016, 24.
6. **Kularbkaew, C., P. Cook, W. Yutanawiboonchal, G. von Hagens**. Plastinated pathology specimens at room temperature in Thailand. – *J. Int. Soc. Plast.*, **11**, 1996, 1, 17-18.
7. **Lozanoff, S., B. Lozanoff, M. Sora, J. Rosenheimer, M. Keep, J. Tregear, L. Saland, J. Jacobs, S. Saiki, D. Alverson**. Anatomy and the access grid: exploiting plastinated brain sections for use in distributed medical education. – *Anat. Rec.*, **270**, 2003, 30-37.
8. **Mandeep, C., P. Adds**. Room temperature plastination of stained brain slices. – *J. Int. Soc. Plast.*, **24**, 2009-2012, 13.
9. **Stoyanov, A. Georgieva, D. Sivrev**. Use of physicval and chemical factors in the development of plastination anatomical preparations. – *Trakia Journal of Sciences*, **13**, 2015, Suppl. 2, 21-22.
10. SPIE – The International Society of Optics and Photonics. The Polarization Ellipse.Optipedia • SPIE Press books opened for your reference.

https://spie.org/publications/fg05_p07-09_polarization_ellipse?SSO=1

Institute of Experimental Morphology, Pathology and Anthropology with Museum
Bulgarian Anatomical Society

Acta morphologica et anthropologica, 25 (3-4)
Sofia ● 2018

Endo-Perio Paleopathology – Antropological and Microbiological Evidences

Georgi Tomov[1], Nadezhda Atanassova[2]

[1] Oral Pathology Department, Faculty of Dental Medicine, Medical University, Plovdiv, Bulgaria
[2] Institute of Experimental Morphology, Pathology and Anthropology with Museum, Bulgarian Academy of Sciences, Sofia, Bulgaria

* Corresponding author e-mail: dr.g.tomov@gmail.com

Diseases of teeth and the surrounding periodontal ligament are important topics in paleopathological investigations because they provide useful information about living conditions and oral health of ancient populations. Since dental diseases can cause periodontal lesions (and vice versa), these two types of pathological conditions are often closely related. In early populations, the main causes of tooth loss were periodontal diseases (periodontitis) and pulpoalveolar diseases (periapical periodontitis), both of which are attributed to oral infections. However, a little is known about endo-perio pathology in ancient time and there is no relevant paleopathological and paleomicrobiological data in the literature. The paper describes two cases (one from Roman period and one from medieval period of Plovdiv) of endo-perio lesions emphasizing on paleopathological and microbiological evidences. The results revealed typical morphological presentation of endo-perio lesions in combination with mixed microbiota, relevant to this pathology.

Key words: endo-perio lesions, paleopathology, paleomicrobiology

Introduction

The prevalence of periodontal diseases in archaeological populations has been a controversial topic in paleoepidemiology [9]. Early studies on periodontal disease supported the idea that ancient populations experienced little periodontal disease, with the prevalence of periodontal disease increasing in populations during recent centuries [2, 3]. More recent studies of periodontal disease have recognized that the prevalence of periodontal disease has been variable between archaeological populations and factors other than diet also influencing the development of periodontal disease [1, 6, 12]. However the tooth-related factors predisposing initiation and further development of periodontal diseases in archaeological populations are poorly understood. The pulp-periodontal interrelationship is a unique one and can consider them as a single continuous system or as one biologic unit in which there are many paths of communication [14]. The interrelationship of these structures influences each other during health, function and disease [14]. They can get affected individually or combined; when both systems are involved they are called true

endo-perio lesions. The relationship between the periodontium and the pulp was first discovered by Simring and Goldberg in 1964 and now is considered as a diagnostic and treatment challenge both in endodontics and periodontology [14]. However, little is known about endo-perio pathology in ancient time and there is no relevant paleopathological and paleomicrobiological data in the literature.

This paper describes two cases (one from the Roman period and one from the medieval period) of endo-perio paleopathology emphasizing on anthropological and microbiological evidences.

Material and Methods

The material used in this study belongs to the paleopathological collection of the Medical University of Plovdiv. The collection had been previously catalogued by the Plovdiv Archeological Museum, including burial details and estimates of age and gender.

The data were collected by the authors. All teeth present in their sockets were recorded. Alveolar bone surrounding the teeth on all surfaces was studied carefully for signs of vertical bony lesions. The criteria for these lesions were a clear vertical loss or destruction of the alveolar bone adjacent to a tooth surface. Both sharp edged ragged lesions and more rounded defects with even and smoother bony surfaces were recorded. Periodontal probes UNC 15 with 1 mm gradations were used for the measurements. The measurement was carried out from the deepest part of the lesion within the alveolar bone up to the surrounding bone crest. Assessment for caries lesions was made by dental probe. Furcation's involvement (according to I. Glickman classification), as well as the presence of calculus, visible periapical lesions and other pathologies were also described.

The heavy deposits of dental calculus provided our study with material for paleo-microbiological analysis. Fragments of calculus around the affected teeth were gently detached and prepared for scanning electron microscopy (SEM) evaluation (JEOL 6390, Institute of Physical Chemistry, Laboratory of Electron Microscopy, Bulgarian Academy of Sciences).

Results

Case #1

The first skeleton originates from archeological excavations dated from the Roman period of Plovdiv (1th-3th century AD) and belongs to a female individual approximately 40-45 years of age. The remains were found in a family tomb (archeological site "Medical University", Vasil Aprilov №3) that belongs to the Western necropolis of the ancient city of Philipopolis (Plovdiv). The anthropological examination revealed right mandibular posterior region exhibiting advanced bone loss, furcation involvement and root approximation of tooth 46. Deep mesial-occlusal caries lesion of 46 with pulp camera exposure was identified (**Fig.1A**) Grade III furcation involvement (3.5 mm) was established by measurement with periodontal probe. The bone loss and furcation involvement were confirmed by periapical radiographs. (**Fig. 1B**).

Case #2

The second skeleton originates from archeological excavations dated from the medieval period of Plovdiv (11th-13th century AD) and belongs to a female individual approximately 35-40 years of age. The remains were found in a nomad necropolis (archeological site "Antique Forum - West"). The anthropological examination revealed asymmetrical deposition of calculus on left side (both upper and lower quadrants) –

(**Fig. 2A, B**). The meticulous checkup revealed deep mesial-occlusal caries lesion of tooth 36 with pulp camera exposure. (**Fig. 2C**) Grade II furcation involvement (1.2 mm) was established by measurement with periodontal probe. The bone loss and furcation involvement were confirmed by periapical radiographs. (**Fig. 2D**).

The SEM observations of detached calculus at different magnifications revealed fossilized microorganisms – cocci in chain, cocci in clusters and bacilli (rods), respectively (**Fig. 3A, B**). The morphological identification was performed in the Department of microbiology using standard SEM pictures of oral pathogens [13]. The morphological analysis revealed Streptococcus mutans, Streptococcus gordonii, Actinomyces naeslundii, Porphyromonas gingivalis and Tannerella forsythia.

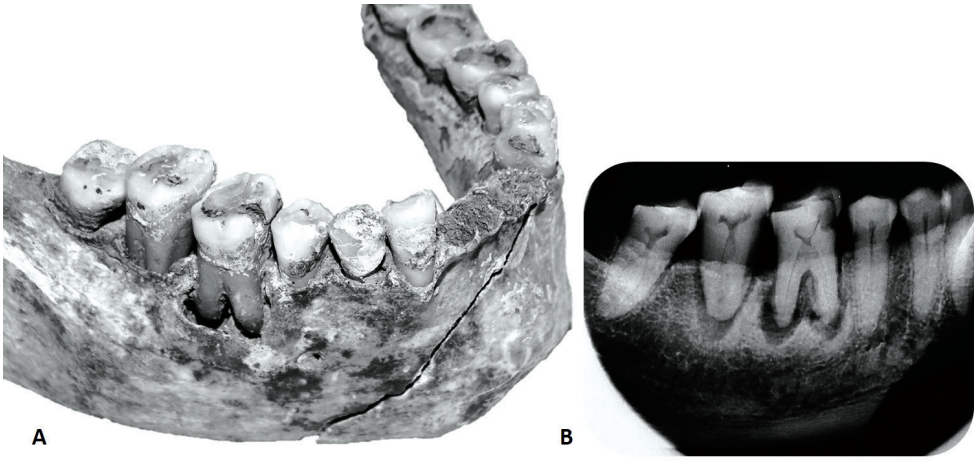

Fig. 1. 40-45 year-old female, buried around 250 AD. Pulpal exposure as a result of deep caries. Note resultant extensive bone loss and full exposure of both mesial and distal roots (**A**). Large apical bony defects on both mesial and distal roots and furcation involvement were verified on X-ray image (**B**).

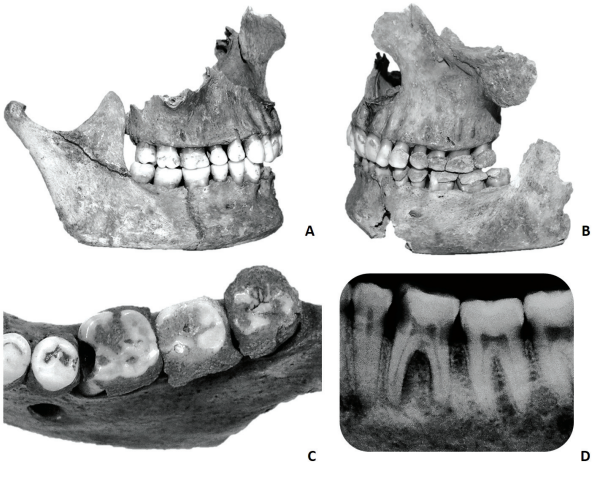

Fig. 2. Right side (**A**) and the affected left side (**B**), showing asymmetrical deposit of calculus. Tooth 36 showed deep MO-carious defect (**C**) X-ray image confirmation of existing endo-periodontal lesion of tooth 36 (**D**).

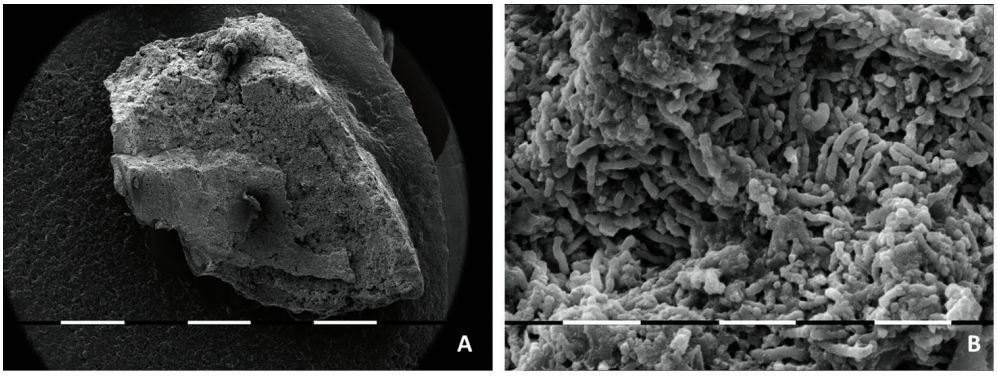

Fig. 3. Dental calculus observed by SEM at different magnification - 40x (**A**) and 200x (**B**) revealed fossilized microorganisms, morphologically identified as oral pathogens.

Discussion

Our findings revealed the typical morphological presentation of the endo-perio lesions in combination with mixed microbiota, relevant to this pathology. Despite the accuracy of anthropological evaluation in cases when the lesions are connected to infection, the microbiological evidences are crucial for the final diagnosis. Nowadays there is a growing recognition of the importance of archaeological dental calculus as a source of oral health information. Early studies of archaeological dental calculus can be traced back nearly a century [7], but it was not until the 1960s and 1970s that dental calculus began to receive serious attention by archaeologists, dental anthropologists and dentists, who described its occurrence in human remains and determined its mineral composition [5, 11]. In addition to macroscopic analysis, scanning electron microscopy (SEM) investigation of dental calculus also greatly advanced during the late 1980s and 1990s. Pioneering work by K. Dobney and D. Brothwell proved a great diversity of well-preserved bacterial forms within dental calculus [4]. The first biomolecular investigation of dental calculus was conducted in 1996 and aimed to identify the oral pathogen Streptococcus mutans (*a causative agent of dental caries!*) through immunohistochemical analysis [8]. In 2011, the preservation of bacterial DNA within dental calculus was confirmed by gold-labelled antibody transmission electron microscopy [10], and this was followed in 2012 by targeted PCR-based genetic approaches, which identified Streptococcus mutans and additional oral taxa, including Fusobacterium nucleatum, Actinomyces israeli, Porphyromonas gingivalis and others.

Microbiology of endo-perio lesions includes bacterial species like Aggregatibacter actinomycetemcomitans, Tannerella forsythia, Eikenella corrodens, Fusobacterium nucleatum, Porphyrominas gingivalis, Prevotella intermedia [14]. Considering the limitation of this study (morphological identification, without genetic confirmation) the microbiota found in the dental calculus (Streptococcus mutans, Streptococcus gordonii, Actinomyces naeslundii, Porphyromonas gingivalis and Tannerella forsythia) confirmed the mixed microbiota involved in endo-perio lesions. Our findings are relevant to data reported by other authors for present populations [14].

Conclusions

This is the first paleopathological report on endo-perio lesions supported by anthropological and paleomicrobiological evidences. Despite the limitations of this study the results revealed typical morphological presentation of endo-perio lesions in combination with mixed microbiota, relevant to this pathology. In ancient times when pulpitis rapidly progressed to periodontitis, and without adequate treatment, every necrotic tooth has been a potential source of oral infection and eventually endo-perio lesion. For this reason, the proper understanding of these coexisting pathologies and the related microbiological status as well as their identification is of primarily importance for human bioarcheology.

References

1. **Bonfigliolo, B., P. Brasili, M. G. Belcastro**. Dento-alveolar lesions and nutritional habits of a Roman imperial age population (1st to 4th century AD): Quadrella (Molise, Italy). HOMO – *J. Comp. Hum. B*iol., **54**, 2003, 36-56.
2. **Brothwell, D. R., H. G. Carr**. Dental health of the Etruscans. – *Br. Dent. J*., **113**, 1962, 207-210.
3. **Clarke, NG., SE. Carey, W. Srikandi, RS. Hirsch, PI. Leppard**. Periodontal disease in ancient populations. – *Am. J. Phys. Anthropol*., **71(2)**, 1986, 173-183.
4. **Dobney, K., D. Brothwell**. A scanning electron microscope study of archaeological dental calculus. – In: Scanning electron microscopy in archaeology. BAR *International Series*, **452**, 1988, 372-385
5. **Dobney, K., D. Brothwell**. Dental calculus: its relevance to ancient diet and oral ecology. – *Teeth Anthropol. BAR Int. Ser.,* **291**, 1986, 55–81.
6. **Kerr, N. W**. The prevalence and natural history of periodontal disease in Britain from prehistoric to modern times. – *Br. Dent. J.,* **185(10)**, 1998, 527-535.
7. **Leigh, R. W**. Dental pathology of Indian tribes of varied environmental and food conditions. – *Am. J. Phys. Anthropol*., **8**, 1925, 179-199.
8. **Linossier, A., M. Gajardo, J. Olavarria**. Paleomicrobiological study in dental calculus: Streptococcus mutans. – *Scanning Microsc.,* **10(4)**, 1996, 1005-1013.
9. **Lukacs, J.R**. Oral health in past populations: Context, concepts and controversy. – In: *Companion to Paleopathology*. (Ed. A. L. Grauer), Chichester, Wiley-Blackwell, 2012, 553-581.
10. **Preus, H.R., OJ. Marvik, KA. Selvig, P. Bennike**. Ancient bacterial DNA (aDNA) in dental calculus from archaeological human remains. – *J. Archaeol. Sci.,* **38**, 2011, 1827-1831.
11. **Rowles, S**. Further studies on the crystalline constituents of oral calculus. – *J. Dent. Res.*, **40**, 1961, 1284-1291.
12. **Whittaker, D**. Quantitative studies on age changes in the teeth and surrounding structures in archaeological material: a review. – *J. R. Soc. Med.*, **85**, 1992, 507-508.
13. **Yoshii, J. Tokunaga, J. Tawara**. *Atlas of scanning electron microscopy in microbiology*. Stuttgart, Georg Thieme Verlag, 1976
14. **Zehnder, M., S. I. Gold, G. Hasselgren**. Pathologic interactions in pulpal and periodontal tissues. – *J. Clin. Periodontol*., **29**, 2002, 663-671.

Institute of Experimental Morphology, Pathology and Anthropology with Museum
Bulgarian Anatomical Society

Acta morphologica et anthropologica, 25 (3-4)
Sofia ● 2018

Novel Optical Method for Visualization of Intracerebral Grafts

Nikola Tomov[1], Lachezar Surchev[1,2]*

[1] *Department of Anatomy, Faculty of Medicine, Trakia University, Stara Zagora, Bulgaria*
[2] *Department of Anatomy, Histology and Embryology, Medical Univeristy of Sofia, Sofia, Bulgaria*

***** Corresponding author email: tomovmd@gmail.com

Experiments with intracerebral grafting studying the processes along the graft-host interface sometimes face a technical difficulty – determining of the exact borders of the graft. Processes of cell migration, decay, and gliosis may obscure the outline of the transplanted tissue. The present report aims to describe a new, simple, yet reliable method for optical demonstration of the graft-host interface. We performed oblique light microscopy using a standard bright field microscope with a built-in the condenser lens diffuser. This method demonstrated good contrast between graft and host brain tissue, regardless of the staining of the otherwise standard specimen. This is the first use of oblique light microscopy in the context of intracerebral transplantation. This method is an easy, replicable, and reliable way to delineate intracerebral grafts without additional histological preparations.

Key words: intracerebral transplantation, grafts, oblique light microscopy

Introduction

In the context of intracerebral transplantation, the graft-host interface is known to be a site of crucial processes of integration between transplanted cells and the recipient's brain [1, 7, 9]. Intensive cell contacts, migration, but also cellular decay and reactive gliosis are known to happen along the border between the graft and the host brain [2, 4, 11, 13]. Histological evaluation of the relationship between the transplanted cells and the nervous tissue of the host requires the exact determination of the graft-host interface. Sometimes, however, this poses a significant difficulty for the investigator, due to accumulation of reactive cells [3, 11] and the resulting intensive staining. Therefore, a method for reliable visualization of this interface is needed, in order to facilitate the evaluation of the processes around grafts.

Dark field microscopy has been previously used with CNS histological preparations to demonstrate white and grey matter structures based on their different refractive properties [10]. It was also used with intracerebral grafts, but only to visualize the fluorescent nerve fibres growing out from them, and not for the graft tissue itself [5].

The aim of the present report is to give an account of a method involving oblique light microscopy for visualization of intracerebral grafts.

Materials and Methods

Intracerebral grafting was performed in the standard unilateral 6-hydroxydopamine model of Parkinson's disease, using single cell suspension of E14 ventral mesencephalic tissue. Details regarding the experimental setting are given in detail elsewhere [12].

The resulting 40 μm sections were stained immunohistochemically for GFAP and processed according to a standard protocol. Transparency of the dehydrated sections was achieved with immersion in xylene, and they were subsequently coverslipped with Histofluid (Marienfeld, Germany). Slides were observed using a standard bright field microscope (Leica DX1000). A diffusing element built in the condenser lens was used to direct the light beam in an oblique direction through the slide. A low power objective lens was implemented to observe and photograph the specimen with a standard camera. Same sections were observed using a dark field microscope in order to visually compare the structures demonstrated using both methods. Furthermore, serial sections processed according a different staining protocol (immunohistochemistry for tyrosine hydroxylase, a marker for the grafted neurons) were also observed for confirmation of the exact site of the graft-host interface.

Results

Observation of the histological preparations confirmed the presence of intracerebral grafts in the expected coordinates. The grafts were ovoid in shape, however their exact outlines could not be always demonstrated easily, as seen on **Fig. 1A.** Especially when observing grafts in later time points of the experiment (as the case with the depicted on the figure graft) the astroglial envelope around the transplant was seen as a dense meshwork, which completely obscured the view of the graft-host interface. In cases of TH staining, the graft cores themselves were not contrasted against the background of the host striatum and their outlines could be only roughly traced thanks to the presence of stained cellular elements.

The observation using oblique light microscopy revealed that the graft cores possessed significantly different light scattering properties. The grafts appeared as uniformly darker objects, contrasted against the silvery, lighter but heterogeneous striatal tissue (**Fig. 1B**). The contrast between graft and host tissue was especially superb in sites of

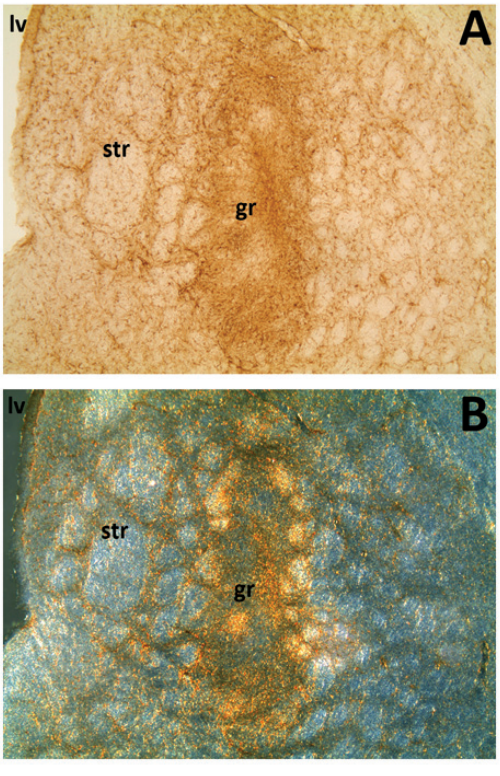

Fig. 1. Low-power microphotographs (4x) of the same GFAP-stained intracerebral graft, observed using bright field microscopy (A) and oblique light microscopy (B). gr – graft, str – striatum, lv – lateral ventricle.

contact between the transplants and the fibers of the internal capsule. In the same time, the DAB-stained (immunopositive) elements did not obscure the picture in any way, merely casting a shadow, as demonstrated on **Fig. 1B**.

Discussion and Conclusions

The present report is the first one to describe the use of oblique light microcopy for demonstration of intracerebral grafts. The differences of the light-scattering properties of gray and white matter of the CNS have been demonstrated before. The property of white matter tracts to appear differently in dark field microscopy depending on their direction relative to the plain of histological section is also known [10]. However, neither dark field microscopy, nor oblique light microscopy have been used to demonstrate the very outlines of intracerebral grafts.

We attribute our observations to the considerable differences of the extracellular matrix in the grafted tissue and in the native brain parenchyma [6]. The preparation of the cell suspension used for transplantation involves intensive washing, which causes considerable dissociation of the tissue and loss of extracellular matter [8]. It is possible that in a later time point following transplantation the consolidation of the graft might lead to a change in the appearance of the transplanted tissue. We, however, could not demonstrate this in the relatively early moment (28 days) following grafting

The proposed method for visualization of intracerebral grafts is fast, easy to apply and reproduce, and does not require any special equipment or histological preparations. This microscopy technique is particularly useful in studies focused on the graft-host interface, because its application allows for uncomplicated determining of its course. A limitation of the method might be the fact that only low-power objective lenses can be used with it; however, we did not find this to be of any practical disadvantage. Validation of the method is needed for studies involving longer follow-ups following grafting, as well as such with different transplantation sites.

References

1. **Barker, R., S. B. Dunnett.** Ibotenic acid lesions of the striatum reduce drug-induced rotation in the 6-hydroxydopamine-lesioned rat. – *Exp. Brain Res.,* **101**, 1994, 365-374.
2. **Barker, R. A., S. B. Dunnett, A. Faissner, J. W. Fawcett**. Time course of loss of dopaminergic neurons and the gliotic reaction surrounding grafts of embryonic mesencephalon to the striatum. – *Exp. Neurol.,* **141**, 1996, 79-93.
3. **Barrett, C. P., L. Guth, E. J. Donati, J. R. Krikorian.** Astroglial reaction in the graymatter of lumbar segments after midthoracic transection of the adult rat spinal cord. – *Exp. Neurol.,* **73**, 1981, 365-377.
4. **Brundin, P., J. Karlsson, M. Emgård, G.S. Schierle, O. Hansson, A. Petersén, R. F. Castilho.** Improving the survival of grafted dopaminergic neurons: a review over current approaches. – *Cell. Transplant*., **9**, 2000, 179-195.
5. **Denham, M., C. L. Parish, B. Leaw, J. Wright, C. A. Reid, S. Petrou, M. Dottori, L. H. Thompson.** Neurons derived from human embryonic stem cells extend long-distance axonal projections through growth along host white matter tracts after intra-cerebral transplantation. – *Front. Cell. Neurosci*., **6**, 2012, 11.http://doi.org/10.3389/fncel.2012.00011
6. **Gates, M. A., E. D. Laywell, H. Fillmore, D. A. Steindler.** Astro cytesandex trace llularma trixfollo wingintra cerebral transplantation of embryonic ventralmesence phalonorlateral ganglioni ceminence. – *Neurosci.*, **74**, 1996, 579-597.
7. **Perlow, M. J., W. J. Freed, B. J. Hoffer, A. Seiger, L. Olson, R. J. Wyatt.** Brain grafts reduce motor abnormalities produced by destruction of nigrostriatal dopamine system. – *Science*, **204**, 1979, 643-647.

8. **Pruszak, J., L. Just, O. Isacson, G. Nikkhah.** Isolation and culture of ventral mesencephalic precursor cells and dopaminergic neurons from rodent brains. – *In: Current protocols in stem cell biology*. New Jersey, Wiley, 2009, 2D.5.1-2D.5.21
9. **Saltykow, S.** Versuche über gehirnplantation, zugleich ein beitrag zur kenntniss der vorgänge an den zelligen gehimeelementen. – *Arch. Psychiatr. Nervenkr*., **40**, 1905, 329-388.
10. **Senatorov, V. V. Dark-field microscopy visualization of unstained axonal pathways using oil of wintergreen. –** *J. Neurosci. Methods*, **113**, 2002, 59-62.
11. **Shinoda, M., J. L. Hudson, I. Strömberg, B. J. Hoffer, J. W. Moorhead, L. Olson.** Microglial cell responses to fetal ventral mesencephalic tissue grafting and to active and adoptive immunizations. – *Exp. Neurol*., **141**, 1999, 173-180.
12. **Tomov, N., L. Surchev, C. Wiedenmann, M. D. Döbrössy, G. Nikkhah.** Astrogliosis has different dynamics after cell transplantation and mechanical impact in the rodent model of Parkinson's disease. – *Balkan Med. J*., **35**, 2018, 141-147. https://dx.doi.org/10.4274%2Fbalkanmedj.2016.1911
13. **Zawada, W. M., D. J. Zastrow, E. D. Clarkson, F. S. Adams, K. P. Bell, C. R. Freed.** Growth factors improve immediate survival of embryonic dopamine neurons after transplantation into rats. – *Brain Res*., **786**, 1998, 96-103.

Institute of Experimental Morphology, Pathology and Anthropology with Museum
Bulgarian Anatomical Society

Acta morphologica et anthropologica, 25 (3-4)
Sofia ● 2018

Anthropological Characteristics of Skeletal Remains from Medieval Vratsa Necropolis

Kaloyan Vassilev[1], Maria Christova-Penkova

Institute of Experimental Morphology, Pathology and Anthropology with Museum, Bulgarian Academy of Sciences, Sofia, Bulgaria

*Corresponding author e-mail: vasilev.kaloian@abv.bg

The article presents anthropological survey of the excavated skeletal remains from the medieval necropolis at T. Balabanov 1 str. in Vratsa. The physical characteristics of the population (height and body mass) were obtained for some of the individuals as well as variations and pathologies that provide information about the hereditary relationships and the health status of some individuals were examined too. The state of the material and its limitation in quantitative terms do not allow for general conclusion on the demographic picture of the Middle Age. But the addition of data from a paleo-anthropological unexplored area is necessary for the creation of empirical material to allow the detailed anthropological characterization of the population of medieval Bulgaria.

Key words: Anthropology, Archaeology, Necropolis, Vratsa, Anthropological characteristic

Introduction

Medieval Vratitsa* is well known in epigraphic and written sources. Since 2007 regular archaeological excavation has been carried out in its fortified part, but the realization of investor intentions in the central part of the modern city has led to the partial study of one of the medieval necropolis, probably linked to the suburb.

Within the area planned for construction 39 graves were revealed, 38 of which can be assigned to the broad chronological terms from the end of the 12th–14th century [8]. A huge part of the necropolis was destroyed before the intervention of the archaeologists. The compromised layer has a thickness of more than 1.20 m and includes the tombs dating back to the second half of the 13th and the 14th centuries. Only half-broken grave 22, dated with John Alexander's coin (1337-1371), was studied only in the western periphery.

The circumstances described above for the discovery and exploration of the necropolis have also precluded the inability of comprehensive anthropological analysis of the population. The good date of the graves based on the imitation of the Bulgarian and Latin coins from the first half of the 13th century allows us to present in this communication the data on the population inhabiting the suburb of Vratsa in that period.

* Vratitsa is the medieval name of present town of Vratsa

Material and Methods

A bone material of 39 individuals was provided for an examination at the National Anthropological Museum. The anthropological analysis was carried out according to the classical methodology [5]. Its results are used to calculate the height of individuals by the formulas of Pirson and Lee, summarized in Alekseev [1]. For the determination of sex, the data obtained from the pelvic marks [3] and the skull [6] were used. In cases where they are too fragmented, the sex is determined using metric scars - lengths of long bones, head diameters and bicondial diameters of shoulder and hip bones [2, 3]. Determining the age at the onset of death of the grown-up individuals is based on the degree of cranial sutures on the Olivier-Simpson scales and summarized by Alekseev-Debets. The age at onset of death in unrelated individuals is determined by the perforation and growth of permanent teeth [11]. The more detailed feature of the individuals buried in the medieval necropolis in Vratsa were supplemented by taking into account the body mass, taking into account the diameters of the femoral heads [9].

Results and Discussion

This paper about the necropolis at "T. Balabanov "1 str. in Vratsa gave for the first time an opportunity to illuminate (albeit partially) the anthropological characteristics of the medieval population of the town. Archaeological excavations were carried out between August and October, 2016 by a team led by A. Petrova – archaeologist at the Regional History Museum – Vratsa, and the results were published in "Contributions to Bulgarian Archeology", vol. VII [8].

Out of the 39 subjects, a detailed anthropological analysis of 38 of them was carried out. The individual of the conditionally designated grave 16 falls chronologically outside the 12th-14th centuries, so the data obtained are not included in this study.

In the skeletal remains studied, the sex of 30 individuals was determined. The proportion of the buried men is equivalent to the proportion of buried women, their percentage being 42% men and 43% women, respectively (**Fig. 1**). Those buried in childhood in which the sex markings did not appear on the bone remains were 7 (15%).

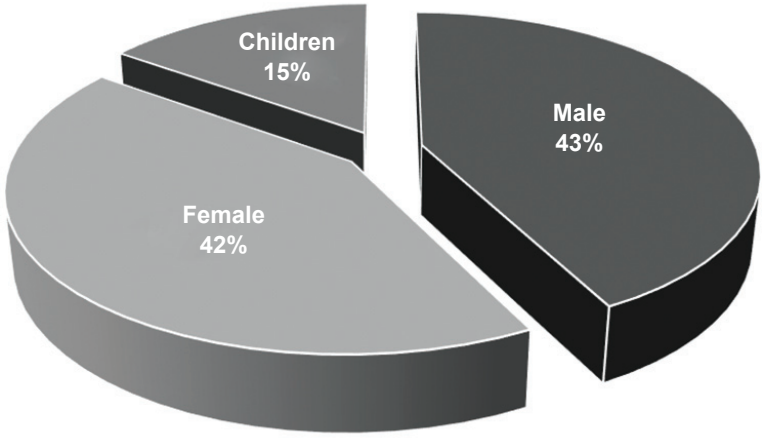

Fig. 1. Sexual distribution of buried individuals

In the age distribution of burials the highest proportion of mature individuals is found – maturus (35/40 to 60 years) (**Table 1; Fig. 2**). The mortality rate of infants I and infans II (7 to 14 years old) reached 30%, showing similar parameters with other necropolises. A similar distribution with a high proportion of the buried in these age groups is also observed in other medieval necropolises (12th–14thcenturies), which indirectly confirms its representativeness [4].

The characteristic peculiarity of the inter-industrial societies for increased mortality of young women is also observed among the buried in the Vratsa necropolis. In the adultus group (20-30/35), women's mortality is twice as great as that of men. This is most often attributable to the risks of pregnancy and childbirth [10].

Table 1. Sex-age distribution of the buried

	Inf. I	Inf. II	Juvenilis	Adult.			Matur.			all
				M	F	all	M	F	all	
N	3	3	3	1	2	3	3	5	8	20
%	15	15	15	5	10	15	15	25	40	100

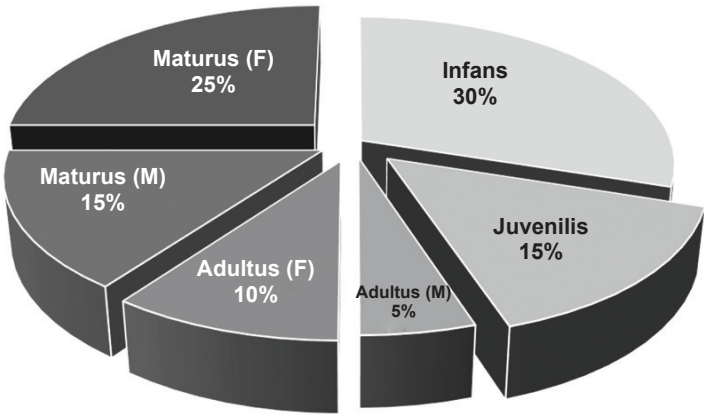

Fig. 2. Distribution of buried by sex and age

Physical development of the buried in the necropolis in Vratsa

The height was calculated for a total of 14 individuals (nine women and five men). The figures show that men's height varies from 160.57 cm to 177.98 cm and for women – from 154.30 cm to 169.56 cm. The average height is respectively 168.61 cm for men and 161.84 cm for women. The average body mass for men is 67.16 kg and ranges from 62.85 to 72.70 kg while the estimated body mass in females ranges from 55.75 kg to 64.50 kg, averaging 61.02 kg (**Fig. 3**).

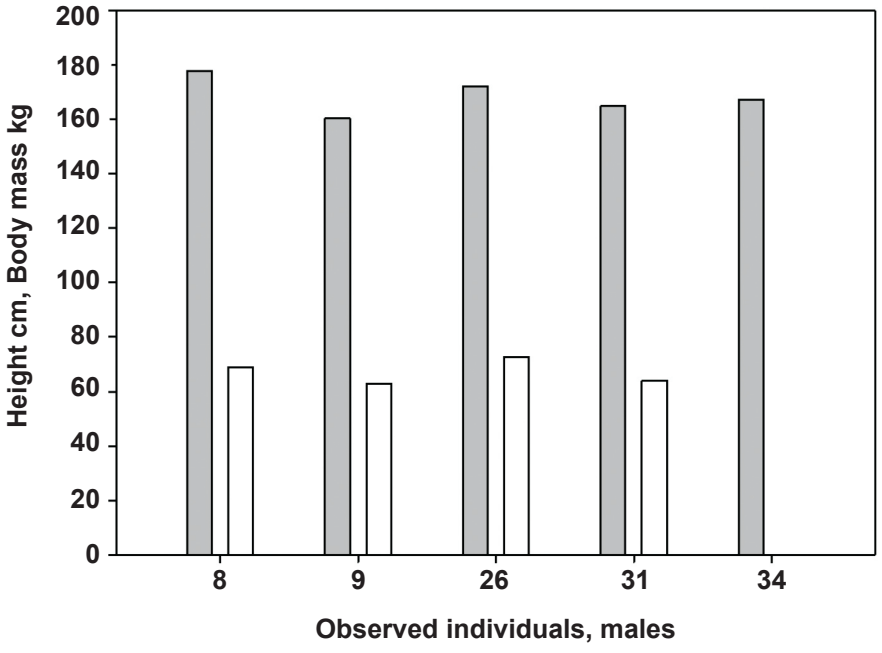

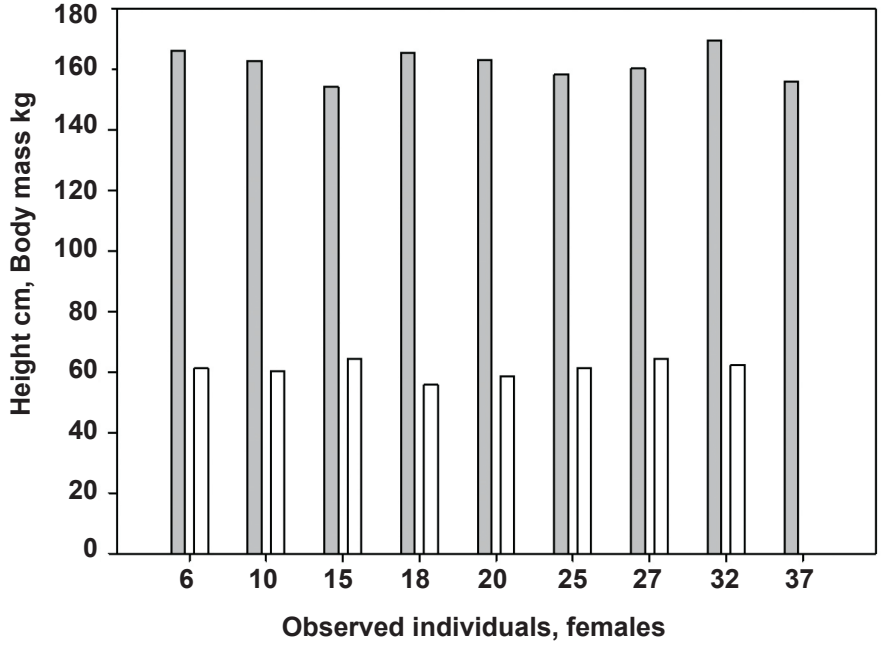

Fig. 3. Correlation of height/body mass in the buried women and men in Vratsa necropolis

Interest is attributed to the ossification of the left blade observed in the buried man (50-60 years) in grave 22 – *ligamentum transversumsuperius scapulae*. This resulted in the closure of the incisura scapularis and turning it into an aperture (**Fig. 4**). The same is another variation fixed on the left shoulder bone – foramen supratrochlearishumeri. In the literature, such variations are considered in connection with heredity as well as a consequence of mechanical joint load [7]. The same variation is observed in the woman buried in grave 37, 30-40 years. In two individuals (female and male buried in grave 10 and 31) there was fixed variation on the sternum – foramen corpus sterni (**Fig. 5**).

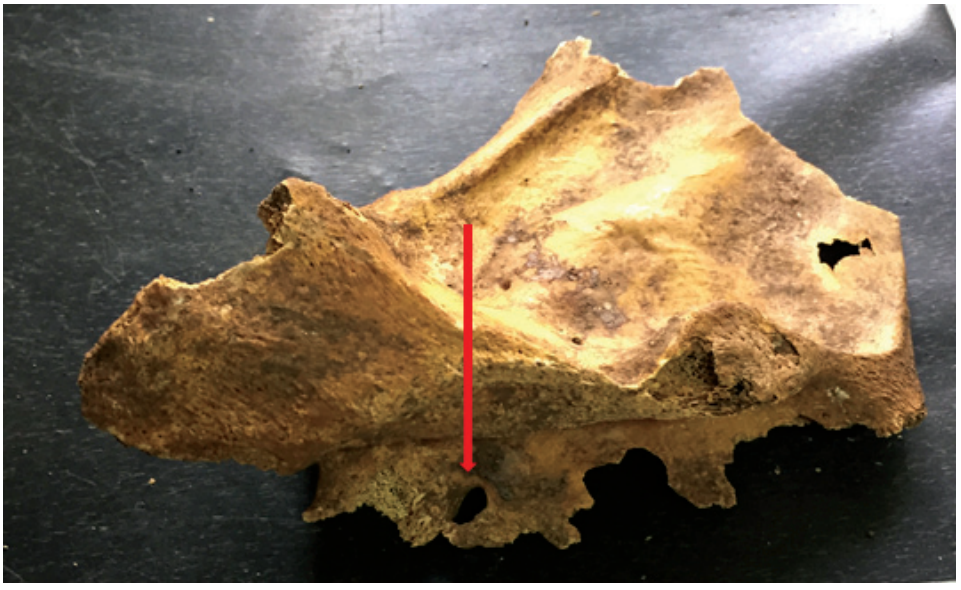

Fig. 4. Ligamentum transversum superius scapulae. Grave 22, male.

Fig. 5. Foramen corpus sterni: a. grave 10, female; b.grave 31, male

In two individuals, buried in grave 31, 35-40 years, and in grave 32, 25-35 years - are found inner bones localized around the lambdoid suture (**Fig. 6**).

The odontological analysis was performed on 26 individuals, with eight of them carious processes was shown. According to the World Health Organization (WHO) main findings, it was found that 3% of the individuals surveyed had an ongoing carious process at the time of death. The relative share of diseased teeth of the studied individuals is 6.97%, with the most infected teeth belonging to the woman buried in grave 20. It has been found that out of the 30 tooth affected by the caries process are 12 of them or 40% of the available teeth. The smallest number of teeth affected by a carious process are observed in the grave 37 (female, 30-40 years) - in the 30 available teeth, a carious process was found in only one.

The high relative frequency of caries and their lack of treatment found in the person buried in grave 20 may have led to worsening nutrition and the development of iron deficiency anemia. The impact of this disease is seen in the cripples in the eyebrows – cribraorbitalia (**Fig. 7**).

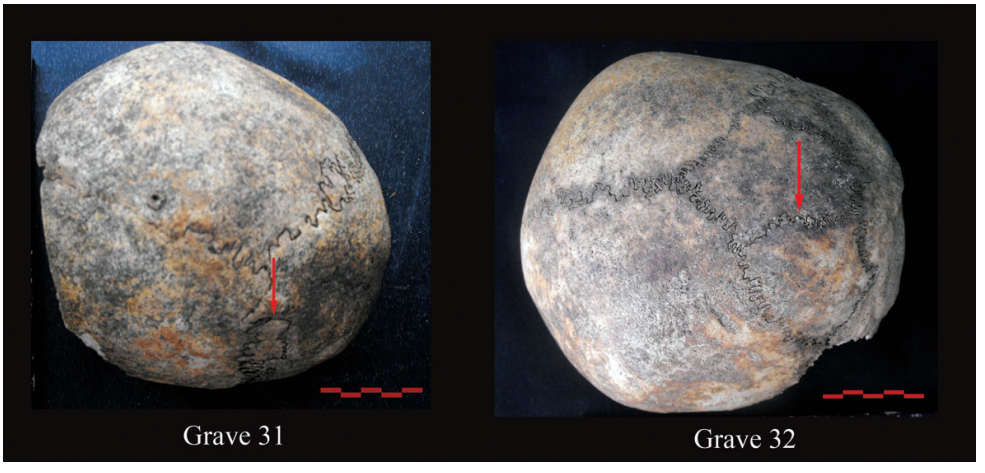

Fig. 6. Wormian bones: a. grave 31, male; b. grave 32, female

Fig. 7. Grave 20: a. abscess around the tooth root; b. carious process; c. cribra orbitalia

In the 31-year-old man buried in grave 31 (35-40 years), fracture was found in the proximal third of the right radius diaphysis, healed without bone fragments. In the same individual, arthrosis changes occurred in the wrist joint (**Fig. 8**).

Osteophyte changes in the vertebrae are observed in most of the buried grown individuals (**Fig.9**).

Conclusion

The presented results of the anthropological survey of the buried in the necropolis on "T. Balabanov "1 in Vratsa are distinguished by a fragmentation that does not allow general conclusions for the population living in the medieval city in the 12th–14th

Fig. 8. Grave 31, male: a. improperly healed fracture of right radius; b. artrosis changes in the wrist joint

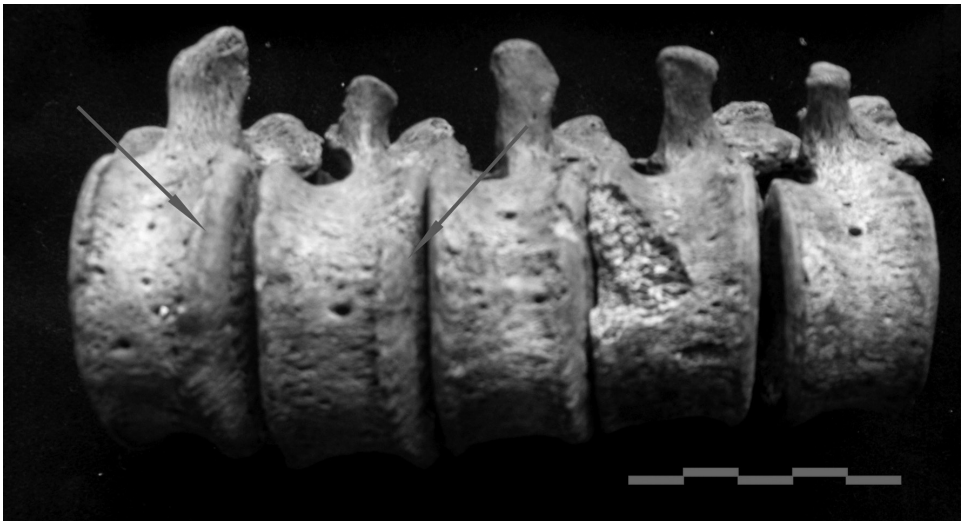

Fig. 9. Grave 10, female, 35-40 years. Osteophite changes on the edges of the lumbar vertebrae

century. However, given the scanty data for this period, the addition of new facts is necessary for the accumulation of an empiric material, allowed the presentation of a detailed anthropological feature of the population of medieval Bulgaria.

References

1. **Alekseev, V., G. Debets**. *Craniometry, methods of anthropological study*. Moscow, Nauka, 1964 [in Russian].
2. **Alekseev, V.** *Osteometry, methods of anthropological study*. Moscow., 1966.[in Russian].
3. **Bass, W. M.** *Human osteology. Special publication № 2 of the Missouri archeological society*, Third ed. 1987.
4. **Cholakov, Sl.** Demographic data about a mediaeval population from Kabile. In: *Interdisciplinary researsches*, III – IV. C., 1979, 111-117. [in Bulgarian].
5. **Martin, R., K. Saller**. *Lehrbuch der anthropologie*. Bd. I-IV, 3 Aufl. Stuttgart, Gustav Fischer Verlag, 1956-1966.
6. **Morse, D., R. Deiley.** *Hand book of forensic archeology*. (Eds. D. Morse, J. Duncan, J. Soutamire) Tallahassee, FL, 1984
7. **Ndou, R., P. Smith, R. Gemell, O. Mohatla.** The supratrochlear foramen of the humerus in a South African dry bone sapmle. – *In: Clinical anatomy*, 26, 2013, pp. 870-874.
8. **Petrova, A, M. Christova.** Medieval cemetery situated on 1 Todor Balabanov Street in Vratsa. – *In: Contributions to the Bulgarian archeology series* Vol. VIII. S., 2018. [in Bulgarian].
9. **Ruff, Ch., W. Scott, Y.-C. Allie.** Articular and diaphyseal remodelling of the proximal femur with changes in body mass in adults. – *Am. J. Phys. Anthropol*., **86**, 1991, 3, 397-413.
10. **Russeva, V.** Buried in the necropolis-Anthropological evidences. – *In: The Proto-Bulgarian necropolis near Balchik*., Prof. Marin Drinov Publishing House of the Bulgarian Academy of Sciences, Sofia, Bulgaria, 2016.[in Bulgarian].
11. **Ubelaker, D. H.** *Human skeletal remains*. Taracsacum, Washington, 1984.

Institute of Experimental Morphology, Pathology and Anthropology with Museum
Bulgarian Anatomical Society

Acta morphologica et anthropologica, 25 (3-4)
Sofia ● 2018

Rare variations of ansa cervicalis

*Iskren B. Velikov, Irina I. Stoyanova**

Department of Anatomy and Cell Biology, Faculty of Medicine, Medical University of Varna, Bulgaria

* Corresponding author e-mail: stoyanovai@yahoo.co.uk

Ansa cervicalis is a loop of nerve fibres, arising from the anterior branches of the cervical spinal nerves C_1, C_2 and C_3, which provides innervation of the infrahyoid muscles. Usually, ansa cervicalis is formed by two roots: superior, originating from C_1, and following the hypoglossal nerve; and inferior root, originating from C_2 and C_3. Different variations in the ansa formation were found during routine dissections on 15 cadavers: lack of inferior root; a loop formed by junction of fibres from C_1, C_2 and C_3 at one point; a nerve bundle, originating from C_1 gave rise of two separated branches, which formed the superior root; the superior root aroused as a branch of the vagus nerve; and the inferior root composed by nerve fibres, coming from the vagus nerve. These variations are important for the invasive medical procedures on the neck.

Key words: ansa cervicalis, variations, infrahyoid muscles, nerve grafting, neck surgery

Introduction

Ansa cervicalis is abundle of nerve fibers, arising from the anterior branches of the first, second and third cervical spinal nerves (C_1,C_2 and C_3), which provides motor innervation of the infrahyoid muscles. In most of the cases, the ansa is formed by two roots: superior and inferior. Fibers of the superior root originate from C_1, ascend to the level of external opening of hypoglossal canal and join the hypoglossal nerve (HN). At the level of the superior margin of the thyroid cartilage, they separate HN and descend as a superior root of ansa cervicalis. The fibers arising from C_2 and C_3 join together and form the inferior root. Usually, it runs antero-laterally to the internal jugular vein. In front of the common carotid artery the two roots join together and form the ansa [13]. However, sometimes the nerve fibers are situated medially to the internal jugular vein [2]. Ansa cervicalis provides motor innervation to the infrahyoid muscles, which depress the hyoid bone [6]. It also plays a role in the phonation and deglutition [11]. In addition, some authors describe ansa cervicalis superficialis, which is formed by anastomosis between r. colli of n. facialis and n. transversus cervicis. It innervates m. platysma and the skin of the neck [15]. Quite often there are variations of ansa cervicalis, which are of great importance for the invasive clinical practice: skull base surgery, thyreoplasty, oesophageal cancer surgery, etc. Therefore, herein we report some rare patterns of the ansa topographic anatomy.

Material and Methods

Ansa cervicalis was studied on 15 cadavers (8 male and 7 female), used for the routine dissection course for medical students in our department, during the period 2014-2017. There were no signs of any traumas in the head and neck area. The skin and the cervical fascia were removed systematically. The muscles, nerves and blood vessels were cleaned and exposed on both sides, with particular attention to the roots of ansa cervicalis.

Results

In most of the cases, in ten cadavers, bilaterally (66.7%) and in five cadavers unilaterally (16.7%), ansa cervicalis was formed in a classical way (**Fig. 1**). In one of the cadavers, unilaterally (3.3%), the superior root was formed as usually, however there was no inferior root: the loop was formed by junction of fibres from C_1, C_2 and C_3 at one point (**Fig. 2**). Another variation was observed in one cadaver, also unilaterally (3.3 %): the nerve bundle, originating from C_1 and following the HN, gave rise of two separated branches, which, after course of 1cm joined together and formed the superior root of the ansa. The inferior root was formed in a classical way (**Fig. 3**). In two cadavers, unilaterally (6.7%), the superior root aroused as a branch of the vagus nerve, while the fibres of the inferior root had a standard pattern of origin (**Fig. 4**).The opposite was also observed in one cadaver, unilaterally (3.3%): the superior root was formed in a classical way, whereas the inferior one was composed by nerve fibers, coming from the vagus nerve (**Fig.5**). Contralateral, the ansa was formed as usually. In ten cadavers (6 male and 4 female) there was superficial ansa cervicalis: anastomosis between fibers of n. transversus colli and r. colli of n. facialis. In 8 cases it was bilaterally (53.3%) and in two of them (6.7%) – unilaterally.

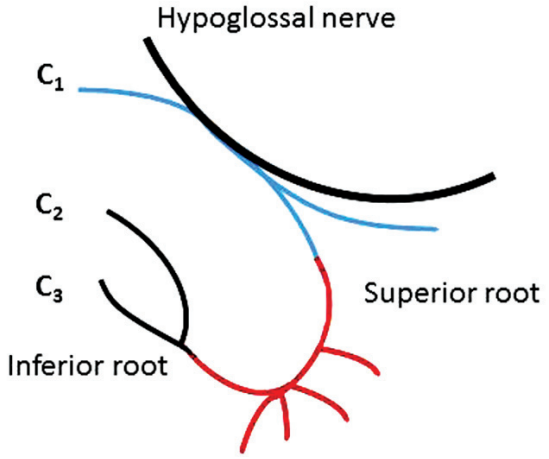

Fig.1. A classical ansa cervicalis.

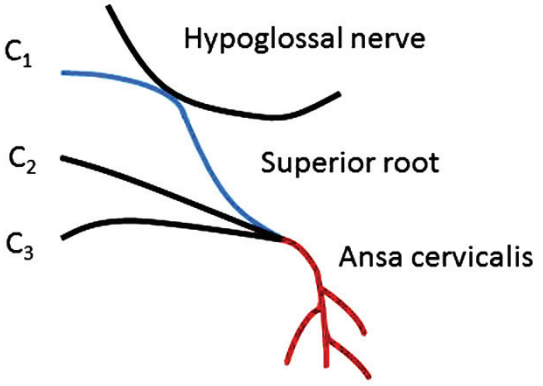

Fig. 2. Fibers, arising from C_1, C_2 and C_3 join in one point.

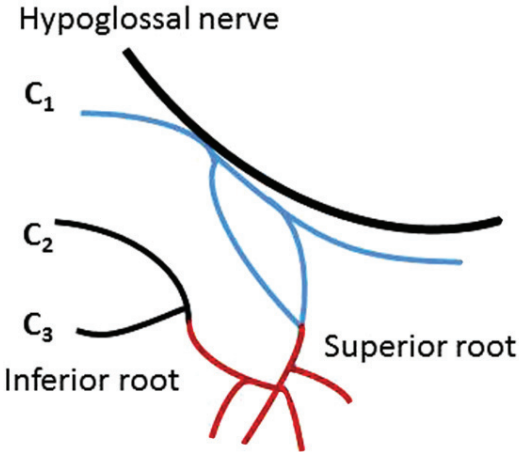

Fig. 3. Two bundles derived from C_1 and following the HN, gave rise of two separated branches, which, after course of 1cm joined together and formed the superior root of the ansa.

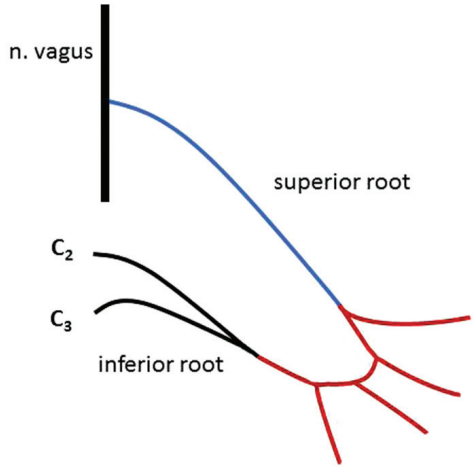

Fig. 4. The superior root aroused as a branch of the vagus nerve.

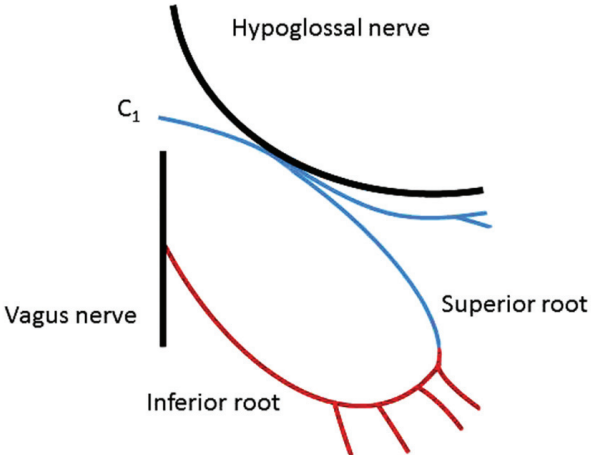

Fig. 5. The inferior root originates from the vagus nerve.

Discussion

Variations of ansa cervicalis are not so rare. It could be even absent bilaterally, and replaced by vagocervical plexus, formed by fibres from the vagus nerve and branches, coming from C_1 and C_2 [1]. Absence of the inferior root of ansa cervicalis was reported by Challa and collaborators [3]. They found double looping of the ansa: fibres from C_2 join the superior root, and below this primary loop, fibres from C_3 form a second loop. One of our finding is similar; however, the three bundles joined at one point and formed a single trunk, providing nerve supply to the infrahyoid muscles. In addition, in one cadaver unilaterally we observed analogous double looping, though related to the superior root: two consecutive bundles branch from the C_1 nerve along the HN at a distance of 1 cm from each other and form the superior root. It further merges with the inferior root to form the ansa.

The formation of the inferior loop varies considerably compared to the superior one, in respect to the source of its fibres. In a comparative study on 160 cadavers, the inferior root was found deriving from the fibres of C_1 to C_4 with a major contributor C_3 [12]. Fibres of spinal accessory nerve also could form the inferior root [10]. As previously reported, the inferior root could arise from the trunk of the vagus nerve [9], and that is the case we observed unilaterally in one cadaver.

The superior root could originate not only from C_1 but also from the HN and the vagus nerve [7, 14]. Origin solely from the vagus nerve, as we report here, is a rare variation of ansa cervicalis, but nevertheless, already described by D'Souza and Ray [5]. Thus, a better knowledge of the origin, formation, and variations of the ansa cervicalis may benefit the surgical practice: to use it as an autograft for reconstruction of the recurrent laryngeal nerve [8] or to prevent injuries of the ansa during different invasive procedures at that area.

References

1. **Abu-Hijleh, M. F.** Bilateral absence of ansa cervicalis replaced by vagocervical plexus: case report and literature review. – *Ann. Anat.,* **187** (2), 2005, 121-125.
2. **Banneheka, S.** Anatomy of the ansa cervicalis: nerve fiber analysis. – *Anat. Sci. Int.,* **83** (2), 2008, 61-67.
3. **Challa, R. G., R. Veeramani, A. Karuppusamy.** Bilateral double looped ansa cervicalis with absence of inferior root-a case report. – *EJPMR,* **4** (6), 2017, 589-592.
4. **Chhetri, D. K., G. S. Berke.** Ansa cervicalis nerve: review of the topographic anatomy and morphology. – *Laryngoscope,* **107** (10), 1997, 1366-1372.
5. **D'Souza, A. S., B. Ray.** Study of the formation and distribution of the ansa cervicalis and its clinical significance. – *Eur. J. Anat.,* **14** (3), 2010, 240-243.
6. **Galabov, G., V. Vankov. Human Anatomy.** – In: *Peripheral nervous system*, Sofia, Medicine and Physical Culture, 1982, 561-563.
7. **Jyothi, S. R., K. R. Dakshayani.** Variation in the formation of Ansa cervicalis on rightside. – *Anat. Karnataka,* (**7**), 2010, 1-3.
8. **Loukas, M., A. Thorsell, R. S. Tubbs, T. Kapos, R. G. Louis, Jr., M. Vulis, R. Hage, R. Jordan.** The ansa cervicalis revisited. – *Folia Morphol. (Warsz),* **66** (2) ,2007, 120-125.
9. **Manjunath, K. Y.** Vagal origin of the ANSA cervicalis nerve-report of two cases. – *Indian J. Otolaryngol Head Neck Surg.,* **52** (3), 2000, 257-258.
10. **Mwachaka, P. M., S. S. Ranketi, H. Elbusaidy, J. Ogeng'o.**Variations in the anatomy of ansa cervicalis. – *Folia Morphol. (Warsz),* **69** (3), 2010, 160-163.
11. **Nayak, S. R., R. Rai, A. Krishnamurthy, L. V. Prabhu, B. K. Potu.** An anomalous belly of sternothyroid muscle and its significance. – *Rom. J. Morphol. Embryol.,* **50** (2), 2009, 307-308.

12. **Poviraev, N. P., Y. F. Chernikov.** Anatomy of the Ansa cervicalis. – *Exerpta Medicu,* **21**, 1967, 219.
13. **Quadros, L. S., L. C. Prasanna, A. S. D'Souza, A. Singh, S. G. Kalthur.** Unilateral anatomical variation of the ansa cervicalis. – *Australas Med. J.,* **8** (5), 2015, 170-173.
14. **Ranajna, V., S. Das, S. Rajesh.** Unusual organization of the Ansa cervicalis-A case report. – *Braz. J. Morphol. Sci.,* **22**, 2005, 175-177.
15. **Schünke, M., S. E. Schumacher, U. Kopf.** *Hals und Neuroanatomie*, Stuttgart-New York Prometeus, 2015.

Institute of Experimental Morphology, Pathology and Anthropology with Museum
Bulgarian Anatomical Society

Acta morphologica et anthropologica, 25 (3-4)
Sofia ● 2018

Palmar Dermatoglyphic Traits on Hypothenar and Thenar in Breast Cancer Patients

G. Yaneva[1], I. Maslarski[2]*

[1] Department of Biology, Faculty of Pharmacy, Medical University of Varna, Bulgaria
[2] Department of Human Anatomy, Histology and Pathology, Faculty of Medicine, University of Sofia, St. Kliment Ohridski, Sofia Bulgaria

*Corresponding author e-mail: galina_yanevaa@abv.bg

Some dermatoglyphic palmar traits such as hypotenar and thenar are relatively rarely investigated in cancer patients. During the period from January 1, 2014 till December 31, 2017, we examined 82 women with clinically, histologically and mammographically confirmed breast cancer as well as 60 healthy women from the region of Varna, Bulgaria. The palmoscopic examination of these palmar traits was accomplished by the basic method of Cummins and Midlo. There were statistically significant differences in terms of the frequencies of the arches and loops in hypothenar as well as concerning the sum frequencies of the arches, loops, whorls and image traces in right-hand hypothenar between breast cancer patients and healthy females. The number and relative share of palmar traits in II-IV interdigital fields in left- and right hand hypothenar differed statistically reliably between both groups. These palmar dermatoglyphic traits could be used within a diagnostic algorithm for breast cancer screening among genetically predisposed population.

Key words: dermatoglyphics, breast cancer, hypothenar, thenar, region of Varna

Introduction

Dermatoglyphic investigations of some palmar traits such as hypothenar and thenar are relatively less popular than those of digital traits. However, they represent an essential component in the diagnostic and prognostic armamentarium of disease-oriented dermatoglyphics, too.

The true hypothenar patterns as a component of dermatoglyphic traits are analyzed in 386 individuals, 182 males and 204 females aged between 10 and 18 years from the central Rhodopes in South Bulgaria [10]. There is a hypothenar radial arch in 2,07% of the males and 2,82% of females in a sample of 2130 Bulgarians [9]. A well-expressed tendency of the hypothenar radial arch towards symmetrical occurrence is disclosed through the ratio between the actual and expected frequency of its bilateral occurrence.

There are several papers dealing with analyses of a palmar dermatoglyphics in children with acute lymphoblastic leukemia (acute lymphoblastic leukemia [3], larynx cancer [12], gastric cancer [18], ovarian cancer [4], uterine cervix and endometrial cancers [1] and other neoplasms.

The environmental and hereditary influence on tumour development using digito-palmar dermatoglyphic traits is assessed in 126 patients of both genders with pituitary tumors (60 non-functional and 66 functional pituitary tumour patients) in comparison to a control group of 400 phenotypically healthy individuals [8]. The use of these traits as screening markers of predisposition to pituitary tumour development facilitates the earlier detection of patients in addition to standard methods, possibly earlier treatment and higher survival rate.

Some papers are devoted to the peculiarities of digital [2, 7] and palmar dermatoglyphics [6, 13, 14] in breast cancer patients, too.

The purpose of this study was to comparatively analyze some peculiarities of hypothenar and thenar traits in female breast cancer patients and healthy women with a view of their possible diagnostic significance.

Material and Methods

The present investigation was performed during the period from January 1, 2014 till December 31, 2017. It covered 82 women with clinically, histologically and mammographically confirmed breast cancer as well as 60 healthy women from the region of Varna, Bulgaria. Breast cancer patients were aged between 36 and 80 years while healthy females were aged between 31 and 79 years. All of them were of Bulgarian ethnical origin.

The palmoscopic examination of palmar traits on hypothenar and thenar was accomplished by the basic method of Cummins and Midlo [5] as already described by us elsewhere [16]. Variation analysis and χ^2 test were applied. Statistical data processing was done by means of SPSS software package, version 19.

Results

Our results were presented on one table and four figures.

The number and relative share of palmar traits on hypothenar and thenar between breast cancer patients and healthy females were compared on **Table 1**.

Table 1. Number and relative share of palmar traits on hypothenar and thenar in breast cancer patients and healthy females

Palmar traits	Breast cancer patients (n=82)		Healthy females (n=60)		χ^2	p
	n	%	n	%		
Left hand						
hypothenar	31	37,8	13	21,7	4,220	**0,040**
thenar	6	7,3	3	5,0	0,366	0,545
Right hand						
hypothenar	38	46,3	16	26,7	5,691	**0,017**
thenar	5	6,1	3	5,0	0,230	0,632

The sum frequency of the palmar patterns including arches, loops, whorls and image traces on left- and right hand hypothenar was illustrated on **Fig.1** and **Fig. 2**.

The sum frequency of the palmar patterns including arches, loops, whorls and image traces on left- and right hand thenar was illustrated on **Fig. 3** and **Fig. 4**.

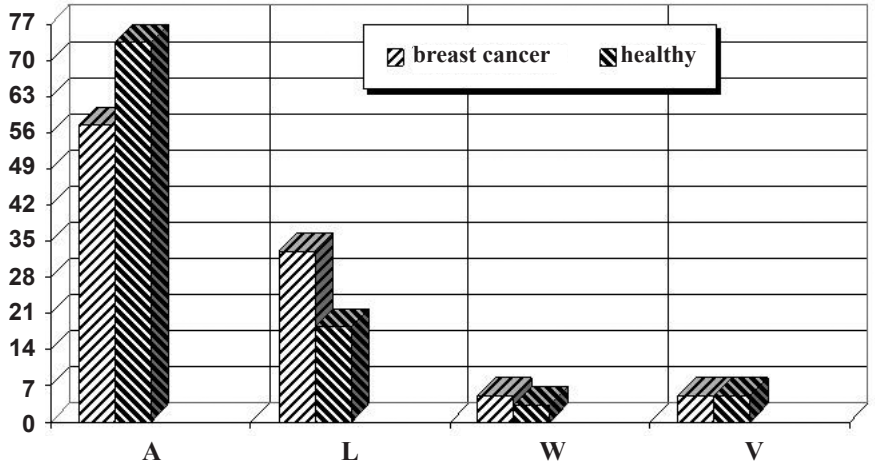

Fig. 1. Relative share of left hand palmar traits on hypothenar in breast cancer patients and healthy females

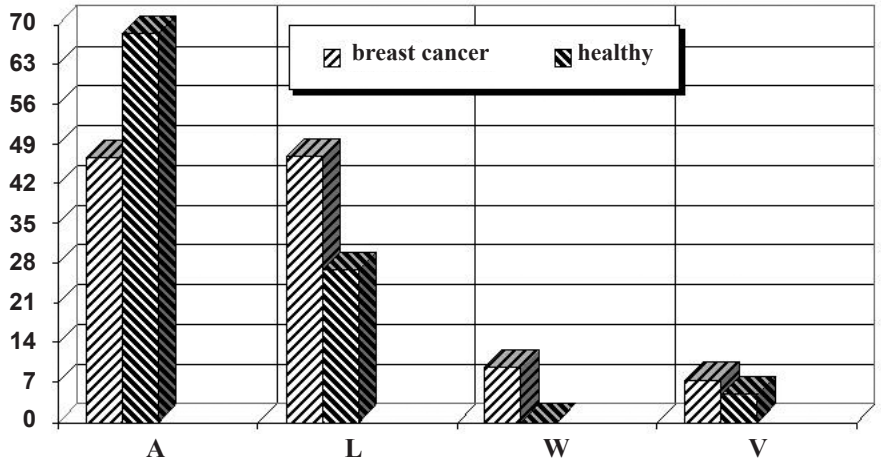

Fig. 2. Relative share of right hand palmar traits on hypothenar in breast cancer patients and healthy females

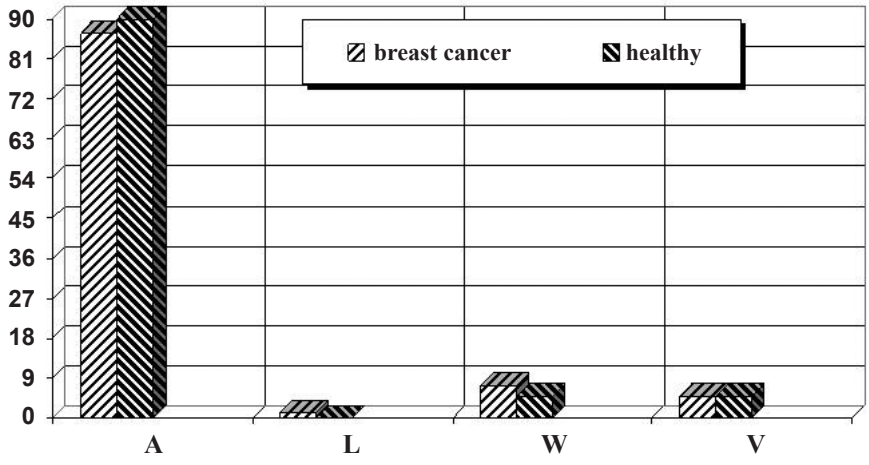

Fig. 3. Relative share of left hand palmar traits on thenar in breast cancer patients and healthy females

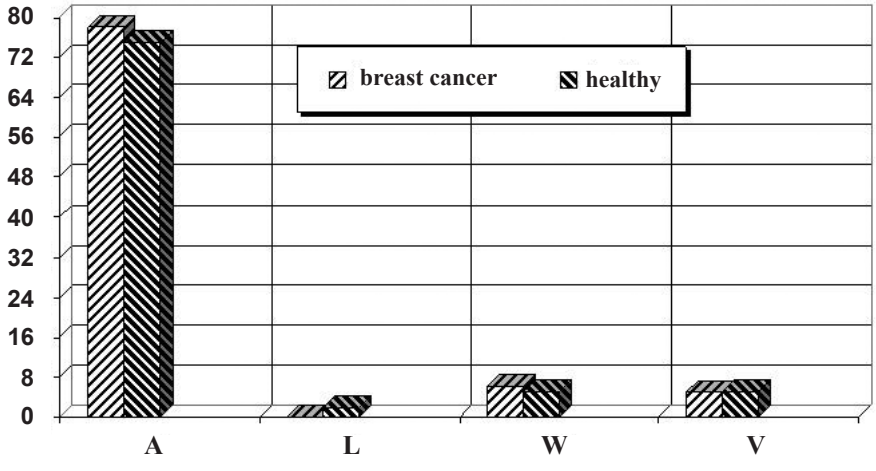

Fig. 4. Relative share of right hand palmar traits on thenar in breast cancer patients and healthy females

There was a statistically significant difference between breast cancer patients and healthy females in terms of the mean value of palmar thenar fields only (p=0,006).

There was a statistically significant difference in favour of breast cancer patients against healthy females in terms of the number and frequency of the palmar patterns in the interdigital fields of the hypothenar of the left hand (χ^2=4,220; p=0,040) and right hand (χ^2=5,691; p=0,017) only.

The frequencies of the arches in left hand (t=2,025; p<0,05) and in right-hand hypothenar (t=2,700; p<0,01) were statistically significantly less in breast cancer patients than in healthy females. The frequency of the loops in left hand hypothenar

(t=2,028; p<0,05) was statistically significantly higher in breast cancer patients than in healthy females.

The sum frequencies of the palmar patterns including arches, loops, whorls and image traces in right hand hypothenar differed statistically significantly between breast cancer patients and healthy females (χ^2=3,228; p=0,006) while that in left-hand hypothenar did not at all (χ^2=3,328; p=0,072). The corresponding frequencies in both right- and left hand thenar did not differ statistically significantly between breast cancer patients and healthy females (χ^2=0,172; p=0,678 and χ^2=0,327; p=0,568, respectively).

There was a statistically reliable difference concerning the number and relative share of palmar traits in II-IV interdigital fields in left- (χ^2=4,220; p=0,040) and right hand (χ^2=5,691; p=0,017) hypothenar between breast cancer patients and healthy females only. The corresponding difference in the thenar was, however, statistically insignificant (χ^2=0,366; p=0,545).

Discussion

Our results clearly indicate some statistically significant differences concerning certain hypothenar traits between the breast cancer patients and healthy females. Obviously, further research of larger samples is needed to warrant the suggested diagnostic potential of this parameter for breast cancer risk assessment as an additional screening marker.

The hypothenar patterns do not demonstrate any significant differences between breast cancer patients and healthy controls [17].

As a functional plug-in of the dermatoglyphic analysis and detection system, the template-based image preprocessing including histogram redistribution, ridge orientation, and skeletonization is effectively used for the automatic identification of palmar traits [11]. The method is feasible and can be applied as an auxiliary diagnostic tool for breast cancer and other diseases.

Palmar dermatoglyphics is simple, inexpensive, anatomical and non-invasive method [15, 16]. It may be used as a reliable indicator for screening of high-risk population in terms of breast cancer.

Conclusion

We establish statistically significant differences concerning the frequencies of the arches and loops in hypothenar as well as concerning the sum frequencies of the palmar patterns including arches, loops, whorls and image traces in right hand hypothenar between breast cancer patients and healthy females. The number and relative share of palmar traits in II-IV interdigital fields in left- and right hand hypothenar differ statistically reliably between breast cancer patients and healthy females only.

These palmar dermatoglyphic traits could be included in a diagnostic algorithm for breast cancer screening among genetically predisposed population, too.

References

1. **Bejerano, M., K. Yakovenko, M. B. Katznelson, E. Kobyliansky**. Relationship between genetic anomalies of different levels and deviations in dermatoglyphic traits. Part 7: Dermatoglyphic peculiarities of females with cervical and endometrial carcinoma. – *Z. Morphol. Anthropol*., **83** (1), 2001, 75-108.

2. **Bierman, H. R., M. R. Faith, M. E. Stewart**. Digital dermatoglyphics in mammary cancer. – *Cancer Invest*., **6** (1), 1988, 15-27.
3. **Bukelo, M. J., T. Kanchan, A. T. Rau, B. Unnikrishnan, M. F. Bukelo, V. N**. **Krishna.** Palmar dermatoglyphics in children with acute lymphoblastic leukemia - a preliminary investigation. – *J. Forensic Leg. Med*., **18** (3), 2011, 115-118.
4. **Buković, D., Z. Persec, N. Buković, P. Martinac**. Qualitative dermatoglyphic traits in ovarian cancer patients: a case-control study. – *Coll. Antropol*., **23** (2), 1999, 641-644.
5. **Cummins, H., C. Midlo**. *Finger prints palms and soles. An introduction in dermatoglyphics.* Blakinston, Philadelphia, New York, Reprinted Dower, 1961. 319 p.
6. **de Andrés Basauri, L., L. Barneo, J. Carulla**. Genetic factors in breast cancer. Identification of a high risk group by means of dermatoglyphic investigation. – *Oncology*, **32** (1), 1975, 27-33.
7. **Gamel, J. W**. Digital dermatoglyphics in mammary cancer. – *Cancer Invest*., **7** (3), 1989, 301-302.
8. **Gradiser, M., M. Matovinovic Osvatic, D. Dilber, I. Bilic-Curcic**. Assessment of environmental and hereditary influence on development of pituitary tumors using dermatoglyphic traits and their potential as screening markers. – *Int. J. Environ. Res. Public Health*, **13** (3), 2016.
9. **Karev, G. B.** Hypothenar radial arch in man: observations on its distribution, morphology, symmetry, and inheritance. – *Am. J. Phys. Anthropol*., **84** (4), 1991, 479-487.
10. **Kavgazova, L., R. Stoev, Z. Mitova**. Dermatoglyphic characteristics of a population from the central Rhodopes (South Bulgaria). – *Anthropol. Anz*., **57**(4), 1999, 349-360.
11. **Qiao, Y., Z. Li, Q. Wang, Y. Zeng, K. Liang**. Identification of palm print using dermatoglyphics analysis and detection system. – *Med. Eng. Phys*., **27** (3), 2005, 229-235.
12. **Rudić, M., J. Milicić, D. Letinić**. Dermatoglyphs and larynx cancer. – *Coll. Antropol*., **29** (1), 2005, 179-183.
13. **Sariri, E., M. Kashanian, M. Vahdat, S. Yari**. Comparison of the dermatoglyphic characteristics of women with and without breast cancer. – *Eur. J. Obstet. Gynecol. Reprod. Biol*., **160** (2), 2012, 201-204.
14. **Singh, D., B. R. Prabhakar, S. S. Bhalla**. Dermatoglyphic study in breast carcinoma. – *Indian J. Pathol. Microbiol*., **22** (1), 1979, 27-32.
15. **Sridevi, N. S., C. R. Delphine Silvia, R. Kulkarni, C. Seshagiri.** Palmar dermatoglyphics in carcinoma breast of Indian women. – *Rom. J. Morphol. Embryol*., **51** (3), 2010, 547-550.
16. **Yaneva, G., Ts. Dimitrova, Dj. Cherneva, N. Ivanova, I. Maslarski, S. Sivkov, D. Ivanov**. Comparative dermatoglyphic study of the palmar ridge count in breast carcinoma patients from Northeast Bulgaria. – *Acta morphol. anthropol*., **25**(1-2), 2018, 86-92.
17. **Zhou, Y., Y. Zeng, Lizhen, W. Hu**. Application and development of palm print research. – *Technol. Health Care*, **10** (5), 2002, 383-390.
18. **Zivanović-Posilović, G., J. Milicić, D. Bozicević**. Dermatoglyphs and gastric cancer. – *Coll. Antropol*., **27** (1) 2003, 213-219.

Institute of Experimental Morphology, Pathology and Anthropology with Museum
Bulgarian Anatomical Society

Acta morphologica et anthropologica, 25 (3-4)
Sofia ● 2018

Sperm Mitochondrial Biology During Spermatogenesis and Fertilization (Review)

E. Zvetkova[2], I. Ilieva[1], I. Sainova[1], B. Nikolov[1]*

[1] Dept. Experimental Morphology, Institute of Experimental Morphology, Pathology and Anthropology with Museum, Bulgarian Academy of Sciences, Sofia, Bulgaria
[2] Bulgarian Society of Biorheology, Institute of Mechanics, Bulgarian Academy of Sciences, Bulgaria

* Corresponding author e-mail: iilieva@abv.bg

The aim of our review article is related to the sperm mitochondrial biology during living cycle – spermatogenesis, when the sperm mitochondria are independent biomarkers of male germ cell differentiation, sperm capacitation and motility, as well as of spermatozoa health and fertility. An increased understanding of sperm mitochondrial structure, functions, bioenergetics, remodeling/plasticity and especially studies of the own mitochondrial genome (mtDNA), may be useful in the routine andrological clinical practice and assisted reproduction.

Key words: remodeling/plasticity, sperm mitochondrial genome, proteomics, fertilization, male pronucleus

Introduction

The mitochondrial morphology, functions, biodynamics, remodeling and plasticity have been elucidated on cellular, biochemical and molecular levels in plants, animals and humans, and could be characterized as species-specific features [4, 6, 18, 39, 40, 43, 57, 72]. During the mitotic- and meiotic cell divisions, as well as in the process of fertilization, the mitochondria form complexes with other cellular organelles (cytoskeleton, endoplasmic reticulum, ribosomal components, etc.) [5, 41, 43, 56, 59, 74, 81].

The mitochondria contain their own genome with a modified genetic code [74]. The human mitochondrial DNA/mtDNA (double-stranded circular molecule in the mitochondrial matrix) encodes two rRNAs, 22 tRNAs and many specific polypeptides [4, 74], related with normal cell development. In the last decades, new modern technologies give possibilities to be examined and evaluated the influence of mtDNA-mutations/ polymorphism on human diseases (genetic cases of "mitochondrial diseases") [16, 79], as well as with ageing [19].

Mitochondrial structure, functions and plasticity are closely related to the cellular oxidative metabolism and bio-energy production [46], but organelles also participate in the processes of apoptosis, reactive oxygen species ROS-generation, Ca^{2+} (calcium-)

homeostasis [2, 3, 21, 39, 40, 68, 72]. Having in view this specific mitochondrial functions the authors pointed out the significance of organelles as independent biomarkers of different health disorders ("mitochondrial diseases" including) [6, 18, 26, 46, 47, 50, 59, 60, 73, 78].

Sperm mitochondria differ from the same organelles of somatic cells participating in important spermatozoon functions, such as sperm viability, motility, activation, acrosomal reaction and fertilization. Further studies could be performed to determine the role of mitochondrial functions in male fertility/infertility. Recent data [45] supported idea that mitochondria during spermatogenesis affect sperm survival and preservation for the purposes of assisted reproduction. The question arises whether or not there are implications of spermatozoa damage due to the increasing ROS - simultaneously with high mitochondrial activity [12, 17, 45, 77]. As additional criteria for stratification of human sperm quality and fertility were proposed mitochondrial DNA amplification, but also further studies are necessary to understand mtDNA- (mitochondrial genome-) potential as a new independent biomarker for sperm health [2, 33, 39, 49]. The biological reactions occurring inside mitochondria as changes in their proteome, metabolome, respiratory functions, redox signaling and bioenergetics metabolism, cover their principal role as biomarkers – in health and diseases [4, 5, 12, 41, 45, 52, 53, 74].

The aim of this review article is to present and compare data from various studies focusing on mitochondria as special sperm organelles and independent biomarkers of male germ sells/spermatozoa health during spermatogenesis and fertilization, as well as to be used as new diagnostic tools of male fertility/infertility in clinical andrology.

Male germ cells mitochondrial morphology, functions, biodynamic and plasticity during spermatogenesis

During spermatogenesis, the mitochondrial plasticity/dynamics is related to organelle capability to change size, shape and number [58, 73]. Three different morphological types of mitochondria have been described during spermatogenesis – "orthodox", "condensed" and "intermediate", according to the states of expansion and/or contraction of the mitochondrial matrix (according to earlier data of Hackenbrock, 1968) [22, 43].

The mitochondria of "orthodox" type (characterized with a few cristae, contracted and dispersed in electron-translucent matrix) have been found in the various types of spermatogonia, in preleptotene and leptotene spermatocytes, as well as in the Sertoli cells [74]. In this male germ cells the number of mitochondria is small, the organelles are dispersed in the cytoplasm, and their shape is most often oval [13, 43, 53, 74].

In the early stages of meiosis – zygotene and early pachytene, the mitochondria with "intermediate" configuration prevail in the spermatocytes [43, 53, 55].

The "condensed" mitochondrial configuration could serve as biomarker of organelles in active functional state. The round-shaped "condensed" mitochondria – with small size, compressed matrix and dilated christae [43, 53, 55, 74], are localized in the male germ cells (including middle- and late pachytene spermatocytes) during meiotic cell division, as well as in the secondary spermatocytes and the early round spermatids [13, 43, 74].

The biological characteristics of mitochondria in male germ cells in the early prophase-I of meiosis (increased number, round/elongated shape, aggregation of mitochondria in clusters, located near to the nuclear membrane) [13, 43, 74], support the idea for active participation of the organelles in the early spermatogenesis.

In male germ cells (zygotene and pachytene spermatocytes) mitochondria form clusters and are associated with an amorphous electron-dense structure in the cytoplasm – without limiting membrane, termed "nuage" or germinal granules [9, 16, 58, 79]. Germinal granules are aggregates characterized as ribinucleoproteins (RNPs) – associated with RNA- and

protein metabolism, and interplaying with mitochondria. Some germ cell-specific proteins, including GASZ-, PIWI-, MIWI-families are associated with "nuage" [8, 9, 16, 19, 39, 58, 79]. Loss of function of these proteins usually leads to disrupted formation of "nuage", defective piRNA biosynthesis and male infertility [8, 9, 16, 19]. The role of "nuage" (first described ultrastructurally by Eddy et al. [16] and called also inter-mitochondrial cement – IMC or pi-body) in the small RNAs (sRNAs) biosynthesis and in the maintenance of genome integrity, was largely examined during male germ cell differentiation [16, 58, 79]. IMC was found in the embryonic gonocytes, in the post-natal spermatogonia and in spermatocytes with clustered mitochondria [79].

In the secondary spermatocytes, no mitochondrial clusters have been established near the cell nucleus, and the translocation of the organelles to the plasma membrane has been observed [74]. During spermatids' maturation (elongated spermatids) and their moving to the lumens of the seminiferous tubules of testes, the appearance of "intermediate" forms of mitochondria could be assessed [43, 74]. Some of the organelles are localized in the developing sperm flagellum, whereas others form the "residual bodies", subsequently phagocyted by Sertoli cells [14, 23, 43].

At the end of spermiogenesis, the sperm mitochondrial are again transformed into "orthodox" type, as well as could be "elongating" or "fusing" into larger organelles. They are grouped and helically arranged in the region of the sperm neck, as well as "enveloped" into the mitochondrial sheath, localized around the outer dense fibers (ODFs) and axoneme in the middle-piece (mid-piece) of flagellum (sperm tail) (Fig.1) [24, 26, 45, 53]. In the mitochondrial sheath the organelles are surrounded by specific selenoproteins and attached to the fibrose sheath. Additionally, the mitochondrial sheath provides structural support to the flagellum [53]. In the scientific literature a discussion existed if the sperm mid-piece tail is discarded outside the ovum in fertilization or the paternal mitochondria are degraded inside the zygote, following male gamete penetration [53]. The examination of this phenomenon needs of future investigations. (**Fig. 1**)

The male germ cells' survival in the testis depends also of the carbohydrate metabolism – anaerobic (glycolysis) and aerobic (OXPHOS) pathways [53]. In the inner mito-

Fig. 1. Electron image showing the immature human spermatozoa with mitochondrial sheath in mid-piece of the sperm tail: longitudinal section. TEM, × 20000 [24].

chondrial membrane (IMM) are arranged the respiratory enzyme complexes including NADH-dehydrogenase, succinate dehydrogenase, cytochrome oxidase, cytochrome C, etc. [45]. One of the respiratory complexes is responsible for ATP synthesis. The IMM and christae enclose a dense protein-rich mitochondrial matrix. Lactate dehydrogenase (LDH) activity within the mitochondrial matrix is unique to sperm cells and is related to the mitochondrial energy production too [70]. For energy production sperm mitochondrial matrix needs lactate/pyruvate, aspartate/malate and glycerol-3 phosphate: addition of lactate and pyruvate to the sperm media increases mitochondrial functions [12].

Dynamics and variations in mitochondrial morphology during spermatogenesis could be influenced by OXPHOS and respiration mitochondrial activity: in conditions of active respiration and functionality, most of the mitochondria rest in "condensed" state [41]. The changes in the mitochondrial dynamics are closely dependent to the metabolic and energetic status of cells and have shown a transition from slow to intensive male gamete metabolism [21, 43, 49]. The morphological mitochondrial transformations (orthodox configuration) in both spermatogonia and spermatocytes' in prophase stages (preleptotene, leptotene) include predominantly the glycolysis as a main source of ATP [21, 43, 49]. Condensed and intermediate mitochondria in the male germ cells during spermatogenesis are preliminary involved in the production of ATP by OXPHOS mechanism [7, 44, 47, 54]. Enhanced OXPHOS leads also to increased number and size (hypertrophy) of organelles [1, 5, 13].

A hypothesis about changes in the mitochondria architecture as a result of osmotic changes in the local cell tissue environment, has been also proposed [40]. The localization of many mitochondria in the mid-piece of the flagellum at the end of spermiogenesis is related to diffusion of more oxygen and mitochondrial energy (ATP) to the flagellum - of importance for spermatozoa motility [23, 27, 74].

Additionally to energy production, the mitochondria are also engaged in the processes of calcium homeostasis and apoptosis or "apoptotic-like" events in male germ cells during spermatogenesis [45]. All biological reactions occurring inside mitochondria lead to changes in their proteome-, metabolome-redox signaling, respiratory functions and bioenergetics [5, 40, 74].

Mitochondrial genome (mtDNA, RNAs and proteins) during spermatogenesis and fertilization

In the scientific literature was indicated the significance of mitochondrial DNA (mtDNA) as a non-invasive biomarker of sperm quality and fertility, but it is not clear whether mtDNA has a functional role in sperm when in cases of completed spermatogenesis [42, 64, 67].

Mitochondrial DNA copy number of sperm has been examined in human and mammalian and data demonstrated an increase in mtDNA copy number simultaneously with reduced sperm motility and quality [42, 64, 68]. Fragmented sperm genomes were also described within mitochondria [1]. The cellular and molecular mechanisms of epiphenomenon has not been elucidated but authors hypothesized that the mitochondrial transcription factor A (TFAM) is a key regulator of the mtDNA copy number in mammalian and human: the down-regulation of TFAM correlated to the lower mtDNA copy number – examined at the level of the round and elongated spermatides during spermatogenesis [2, 33, 34, 54]. Recently, as additional criteria for sperm quality were proposed mtDNA amplification and mtDNA/beta-globin ratio, which could be biomarkers for male infertility [41, 47].

Some types of mtDNA damages as specific point mutations and deletions in the mitochondrial genome (containing in mammalian 37 genes, which encode 13 peptides,

22 tRNAs and 2 rRNAs [50]) could affect synthesis of RNAs, proteins and respiratory enzymes also participating in the regulation of spermatogenesis in mammalians and humans [11, 20, 44, 46, 48]. Microarray analysis suggested that sperm from asthenozoospermic patients has altered levels of specific mtRNAs, as well as of nuclear transcripts, encoding several sperm mitochondrial proteins [28, 62, 80].

Nakada et al. [48] evaluated induction of mitochondrial dysfunction in the human spermatogenic cells due to accumulation of the pathogenic mutant DNAs in the testes – leading to the "meiotic arrest" in male germ cells during spermatogenesis. Accumulated mtDNA mutations in the spermatocytes and early spermatids during spermatogenesis in mammalians and humans suppress the respiratory functions of the sperm mitochondria, increase the number of apoptotic spermatogenic cells, induce respiration deficiency and spermatocyte degeneration and thus, male infertility [26, 46, 48, 55, 58, 78]. The presence of mutant mtDNA has been also evaluated in animal models [15, 46]. During spermatogenesis the mutant mtDNA accumulate preliminary in the early spermatids with induced mitochondrial dysfunction [26, 46, 48]. Deletions and other types of mutations in the mtDNA occur at a frequency of less than 1% in men and increase with aging [44]. However, few studies on the special role of mtDNA mutations/polymorphism in male fertility/infertility (disorders as oligozoospermia and asthenozoospermia) have been performed [31, 42, 48, 73, 78]. mtDNA-amplification was proposed as an additional criterion for human sperm quality and male fertility by WHO (1999) [42, 48].

Recent studies [1, 29, 46, 49, 50, 64, 66, 69] showed that pathological changes in the mtDNA during spermatogenesis affect male spermatogenic cell homeostasis and induce their degeneration and apoptosis. Degeneration of germ cells affects the quantitative and qualitative aspects of spermatogenesis [29, 30]. A significant male germ cells loss (36–45%) by degeneration occurs during the meiotic cell division [30]. The mitochondria thereby assuring that good quality meiotic products enter the process of spermatogenesis to yield good quality mature sperm [52]. MtDNA mutations in the etiopathogenesis of male infertility have been recently reviewed [1, 41, 59, 62, 73]. Data existed that remained in the egg cytoplasm paternal mitochondria after fertilization are eliminated, for example by ubiquitinization [68, 71].

The morphological and functional development of male germ cells is a reflection of the changes in the testicular microenvironment during spermatogenesis when expression of specific mitochondrial marker proteins was evaluated: with attention to hsp60, hsp70, protamin-1, Lon-protease, sulfhydryl-oxidase, cytochrome C, cytochrome Ct, endopeptidases, chaperonin 60, transition proteins 1, 2, etc. [32, 43]. The expression of several sperm mitochondrial proteins may be altered in asthenozoospermic patients [62]. The synthesis of the sperm mitochondrial fusion and fission factors – mitofusins 1, 2 (Mfn1 and Mfn2) and dynamin-related protein 1 (Drp1) was examined at the levels of the round and elongated spermatids (steps 8 - 12) of spermatogenesis [24].

Mitochondrial functions are preliminary related to the oxidative metabolism of cells and free oxidative radicals (ROS-) generation. To meet their energy demands, sperm utilize both pathways – oxidative and/or glycolytic energy metabolism. For example, bull sperm utilizes both OXPHOS and glycolysis with high efficiency [38]. The question arises if the stimulated and increased sperm mitochondrial function prior to sperm use in assisted reproduction may improve male fertility [12]. In this sense, mild oxidative stress (produced by ROS) is considered necessary for some sperm functions as motility, acrosome reaction and fertility [1]. On the other hand, high ROS activity/ oxidative stress are related to the respiration defects in mitochondria – including to the mitochondrial genome (mtDNA-) mutations and low male fertility: ROS production is necessary for normal sperm function [45], but in excess it could damage spermatozoa – with negative influence on fertility.

Evidence that human sperm mitochondria have the potential to generate ROS was obtained using a peroxide-based hemiluminescent system to detect the release of H_2O_2 into the extracellular space. Fluorescent probes (flow-cytometry) and ApoAllert mitochondrial membrane sensor kits – JC-1, TMRM and Mito Tracker Green (MT-G), were employed to assess mitochondrial membrane potential [12, 25, 45, 65]. The authors showed that MT-G-positive sperm has better fertilization potential: green-stained mid-pieces of spermatozoa could be biomarkers for the presence of high functional mitochondria, successfully participating in the processes of fertilization and early embryonic development. By this way MT-G test gives new possibilities to determine whether sperm would constitute a better - (MT-G-positive-) functional sperm subpopulation, or MT-G-negative non-functional male gametes - with low quality/ fertility parameters.

According to many studies, the changes in the mitochondrial morphology are dependent on the protein synthesis in the Sertoli cells (actively synthesizing paracrine mitochondrial maturation factors/PMMFs) [14, 43, 60]. These data have pointed out the protein activin A as a major paracrine modulator in the early male spermatogenesis. In addition, the Sertoli cells are the main lactate/pyruvate source required for OXPHOS and ATP-synthesis of mitochondria during meiosis and post-meiosis phases of spermatogenesis [13, 21, 43].

Sperm mitochondria during fertilization (male pronucleus development)

In this review we try to summarize insufficient literature data on the role of sperm mitochondria in the biology of fertilization [37]. Having in view our own *in vitro* studies in this field, we pointed out especially on data for sperm mitochondria participation in the development of the male pronucleus (breakdown of the sperm nuclear envelope; dispersion of the condensed sperm nuclear chromatin preliminary at the perinuclear regions; development of the male pronuclear envelope (**Fig. 2**).

Following fusion of male and female gametes and subsequent breakdown of the sperm nuclear envelope, the male nuclear chromatin is associated directly – without membranous boundary, with components of the egg cytoplasm. The conical sperm nucleus changes into spherical MP with decondensed (dispersed) nuclear chromatin. In the literature exists a hypothesis [37] related to the probable "agents" responsible for sperm nuclear chromatin dispersion – a process starting at the periphery of the nucleus (**Fig. 2D**). The authors concluded that events related to the MP formation are similar to those occurring in prophase and telophase of mitotically-active cells. There are lack of accurate data on the fate of incorporated sperm mitochondria, flagellum and perinuclear structures – well visualized on **Fig. 2**. For example data existed that after sperm incorporation in the egg the mitochondria are displaced from the sperm mid-piece and destruction of mitochondrial sheath occurs [71]. An aggregate of clustered unstained sperm mitochondria (as mitochondrial "crown") could be visualized around the sperm nucleus in the early stages of sperm penetration (**Fig. 2B**). These mitochondria are of very small size – probably result of fission [24]. Organelles are probably in active functional state – fusing in the MP and thus, participating in the chromatin activation/decondensation. Similar results were obtained in highly proliferated somatic cells [82, 84]. According to data of other authors about the fate of organelles - the mitochondrial clusters of this type remain in the vicinity of the MP and can later be seen at one of the poles of the metaphase spindle, as well as in one blastomer of the four-cell embryo, and are no longer detected in early embryogenesis [37]. Finally, a zygote nucleus formation is a result of fusion of the outer and inner membranes of the two pronuclear (MP-, FP-) envelopes.

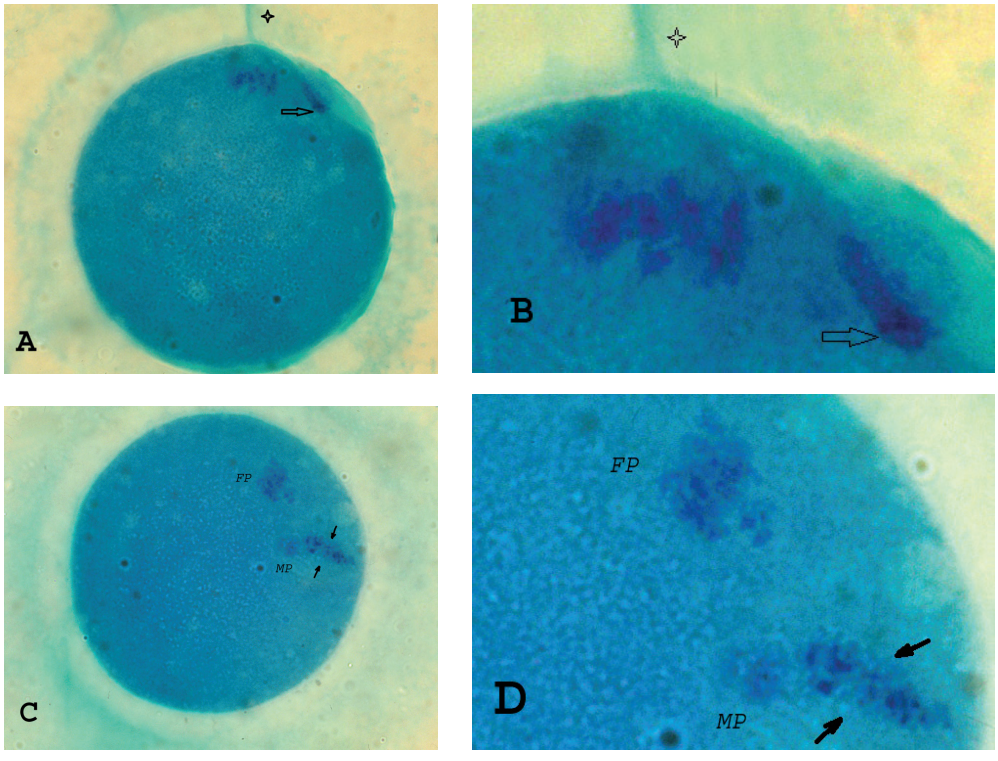

Fig 2. *In vitro* fertilization in mice. Remodeling of sperm nucleus into a male pronucleus during fertilization. A, B – The spermatozoon enters the cytoplasm of oocyte through the cone of fertilization (B – empty arrow). Desoxyribonucleoproteins (DNP) are blue-violet stained (with methylene blue) in both pronuclei (female – FP and male – MP). Decondenzation of the sperm nuclear chromatin could be visualized. Basic proteins in sperm head, neck and tail (asterisks) are green-stained (with fast green). C, D – DNP in the FP, MP and mitochondrial genome (mitochondria localized in the mid-piece of sperm tail – arrows), are blue-violet stained and one could see condensed chromosomal chromatin in FP and perinuclear chromatin decondensation in MP. Staining with methylene blue – fast green, after cold acid hydrolysis with 5N HCL for RNP-extraction (Zvetkova and Zvetkov [83]); × 200, 450.
Images have been originally made by assoc. prof. Elissaveta Zvetkova and prof. Pascale Debay – Institut de Biologie Physico-Chimique – INSERM, Paris – France, 1991.

One question remains - related to confusions still persisting in the literature: evaluation that the paternal sperm-born mitochondria of most mammalian species are targeted for lysosomal degradation by ubiquitin system (ubiquitination) during fertilization. Other authors supported the thesis that such widely disputed evidence warrants further investigations. The problem is also related to the major paradox in the developmental biology - for maternal inheritance of mtDNA and subsequent paternal genome elimination in the zygote, by unknown degradation mechanisms [71]. New methods for cytological/cytochemical *in situ* studies on sperm mitochondria could be recommended for better understanding of the sperm mitochondrial biology - in health and diseases.

Conclusion

Nowadays it is possible to evaluate sperm mitochondrial biology (structure, functions, biochemistry, biodynamics, remodeling, plasticity, etc.) during spermatogenesis/spermiogenesis. Biological characteristics of sperm mitochondria could serve as biomarkers and diagnostic tools for spermatozoa health and fertility in the clinical practice.

In conclusion, we could point out that morphological, biochemical, physiological and bioenergy parameters of sperm mitochondria correlate with sperm quality, health, functionality and fertilization properties. From epigenetic's point of view, it is important that a cross-talk between mitochondrial metabolism, functionality and genome activities could also exist.

References

1. **Amaral, A., B. Lourenço, M. Marques, J. Ramalho-Santos**. Mitochondria functionality and sperm quality. – *Reproduction*, **146**, 2013, 163-174.
2. **Amaral, A., J. Ramalho-Santos, J. C. St John**. The expression of polymerase gamma and mitochondrial transcription factor A and the regulation of mitochondrial DNA content in mature human sperm. – *Human Reprod.*, **22**, 2007, 1585-1596.
3. **Anderson, S., A. T. Bankier, B. G. Barrell, M. H. De Bruijn, A. R. Coulson, J. Drouin, I. C. Eperon, D. P. Nierlich, B. A. Roe, F. Sanger, P. H. Schreier, A. J. Smith, R. Staden, I. G. Young**. Sequence and organization of the human mitochondrial genome. – *Nature*, **290**, 1981, 457-465.
4. **Arismendi-Morillo, G**. Electron microscopy morphology of the mitochondrial network in human cancer. – *Int. J. Biochem. Cell Biol.*, **41**, 2009, 2062-2068.
5. **Bereiter-Hahn, J., M. Vöth**. Dynamics of mitochondria in living cells: shape changes, dislocations, fusion, and fission of mitochondria. – *Microsc. Res. Tech*., **27**, 1994, 198-219.
6. **Boussouar, F., M. Benahmed**. Lactate and energy metabolism in male germ cells. – *Trends Endocrinol. Metab*., **15**, 2004, 345-350.
7. **Campello, S., L. Scorrano**. Mitochondrial shape changes: orchestrating cell pathophysiology. – *EMBO Reports*, **11**, 2010, 678-684
8. **Carmell, M. A., A. Girard, H. J. van de Kant, D. Bourc'his, T. H. Bestor, D. G. de Rooij, G. J. Hannon**. MIWI2 is essential for spermatogenesis and repression of transposons in the mouse male germline. – *Dev. Cell*, **12**, 2007, 503-514.
9. **Chuma, S., M. Hosokawa, T. Tanaka, N. Nakatsuji**. Ultrastructural characterization of spermatogenesis and its evolutionary conservation in the germline: Germinal granules in mammals. – *Mol. Cell. Endocrinol*., **306**, 2009, 17-23.
10. **Clayton, D. A**. Transcription and replication of mitochondrial DNA. – *Hum. Reprod*., **2**, 2000, 11-17.
11. **Creasy, D., A. Bube, E. de Rijk, H. Kandori, M. Kuwahara, R. Masson, T. Nolte, R. Reams, K. Regan, S. Rehm, P. Rogerson, K. Whitney**. Proliferative and nonproliferative lesions of the rat and mouse male reproductive system. – *Toxicol. Pathol*., **40**, 2012, 40S-121S.
12. **Darr, C. R., G. A. Cotopassi, S. Datta, D. Varner, S. A. Meyers**. Mitochondrial oxygen consumption is a unique indicator of stallion sperm spermatozoal health and varies with cryopreservation media. – *Theriogenology*, **86**, 2016, 1382-1392.
13. **De Martino, C., A. Floridi, M. L. Marcante, W. Malorni, P. Scorza Barcellona, M. Bellocci, B. Silvestrini**. Morphological, histochemical and biochemical studies on germ cell mitochondria of normal rats. – *Cell Tissue Res*., **196**, 1979, 1-22.
14. **de Winter, J. P., H. M. J. Vanderstichele, M. A. Timmerman**. Activin is produced by rat Sertoli cells *in vitro* and can act as an autocrine regulator of Sertoli cell function. – *Endocrinology*, **123**, 1993, 975-982.
15. **Dunn, D. A., M. V. Cannon, M. H. Irwin, C. A. Pinkert**. Animal models of human mitochondrial DNA mutations. – *Biochim. Biophys. Acta*, **1820**, 2012, 601–607.
16. **Eddy, E. M**. Fine structural observations on the form and distribution of nuage in germ cells of the rat. – *Anat. Rec*., **178**, 1974, 731–197757.
17. **Gibb, Z., S. R. Lombourne, R. G. Aitken**. The paradoxal relationship between stallion fertility and oxidative stress. – *Biol. Reprod*., **91**, 2014, 77.

18. **Greaves, L. C., A. K. Reeve, R. W. Taylor, D. M. Turnbull**. Mitochondrial DNA and disease. – *J. Pathol.*, **226**, 2012, 274-286.
19. **Grivna, S. T., B. Pyhtila, H. Lin**. MIWI associates with translational machinery and PIWI-interacting RNAs (piRNAs) in regulating spermatogenesis. – *Proc. Natl. Acad. Sci. U.S.A.*, **103**, 2006, 13415-13420.
20. **Grivna, S. T., E. Beyret, Z. Wang, H. Lin**. A novel class of small RNAs in mouse spermatogenic cells. – *Genes Dev.*, **20**, 2006, 1709-1714.
21. **Grootegoed, J. A., R. Jansen, H. J. van der Molen**. Spermatogenic cells in the germinal epithelium utilize alpha-ketoisocaproate and lactate, produced by Sertoli cells from leucine and glucose. – *Ann. N. Y. Acad. Sci.*, **438**, 1984, 557-560.
22. **Hackenbrock, C. R**. Ultrastructural bases for metabolically linked mechanical activity in mitochondria. II. Electron transport-linked ultrastructural transformations in mitochondria. – *J. Cell Biol.*, **37,** 1968, 345-369.
23. **Ho, H. C., S. Wey.** Three dimensional rendering of the mitochondrial sheath morphogenesis during mouse spermiogenesis. – *Microsc. Res. Tech.*, **70**, 2007, 719-723.
24. **Honda, S., S. Hirose**. Stage-specific enhanced expression of mitochondrial fusion and fission factors during spermatogenesis in rat testis. – *Biochem. Biophys. Res. Commun.*, **311(2)**, 2003, 424-432.
25. **Hu, C. H., X. J. Zhuang, Y. M. Wei, M. Zhang, S. S. Lu, Y. Q. Lu, X. G. Yang, K. H. Lu**. Comparison of mitochondrial function in boar and bull spermatozoa throughout cryopreservation based on JC-1 staining. – *Cryo. Lett.*, **38**, 2017, 75-79.
26. **Ilieva, I**. Morphological changes in the structure of sperm in male infertility. – PhD Thesis, Bulgarian Academy of Sciences, Sofa, 2012, 215.
27. **Ilieva, I., I. Sainova, E. Zvetkova**. Sperm mitochondria-associated male infertility: sperm quality defects and mitochondria (mtDNA) anomalies. – *Acta morphol. anthropol.*, **24**, 2017, 114-122.
28. **Jodar, M., S. Kalko, J. Castillo, J. L. Ballesca, R. Oliva**. Differential RNAs in the sperm cells of asthenozoospermic patients. – *Hum. Reprod.*, **27**, 2012, 1431-1438.
29. **Johnson, L**. Increased daily sperm production in the breeding season of stallions is explained by an elevated population of spermatogonia. – *Biol. Reprod.*, **32**, 1985, 1181-1190.
30. **Johnson, L., C. S. Petty, W. B. Neaves**. Further quantification of human spermatogenesis: germ cell loss during postprophase of meiosis and its relationship to daily sperm production. – *Biol. Reprod.*, **1**, 1983, 207-215.
31. **Kao, S. H., H. T. Chao, Y. H. Wei**. Multiple deletions of mitochondrial DNA are associated with the decline of motility and fertility of human spermatozoa. – *Mol. Human Reprod.*, **4**, 1998, 657-666.
32. **Kleene, K. C., R. J. Distel, N. B. Hecht**. Translational regulation and deadenylation of a protamine mRNA during spermiogenesis in the mouse. – *Dev. Biol.*, **105**, 1984, 71-79.
33. **Kolmer, M., M. Pelto-Huikko, M. Parvinen, C. Höög, H. Alho**. The transcriptional and translational control of diazepam binding inhibitor expression in rat male germ-line cells. – *DNA Cell Biol.*, **16**, 1997, 59-72.
34. **Larsson, N. G., A. Oldfors, J. D. Garman, G. S. Barsh, D. A. Clayton**. Down-regulation of mitochondrial transcription factor A during spermatogenesis in humans. – *Human Molec. Genet.*, **6**, 1997, 185-191.
35. **Larsson, N. G., J.D. Garman, A. Oldorfs, G.S. Barsh, D.A. Clayton.** A single mouse gene encodes the mitochondrial transcription factor A and a testisspecific nuclear HMG box protein. – *Nat. Genet.*, **13**, 1996, 296-302.
36. **Lindemann, C. B., K. A. Lesich**. Functional anatomy of the mammalian sperm flagellum. – *Cytoskeleton*, **73,** 2016, 652-669.
37. **Longo, F. J., E. Anderson**. The fine structure of pronuclear development and fusion in the sea urchin, *Arbacia punctulata*. – *J. Cell Biol.*, **39**(2), 1968, 339-368.
38. **Losano, J. D. A., J. F. Padin, I. Mendez-Lopez, D. S. R. Angrimani, A. G. Garcia, V. H. Barnabe, M. Nichi**. The stimulated glycolytic pathway is able to maintain ATP levels and kinetic patterns of bovine epididymal sperm subjected to mitochondrial uncoupling. – *Oxid. Med. Cell. Longev*. **ID 1682393**, 2017, 1-8.
39. **Ma, L., G. M. Buchold, M. P. Greenbaum, A. Roy, K. H. Burns, H. Zhu, D. Y. Han, R. A. Harris, C. Coarfa, P. H. Gunaratne, W. Yan, M. M. Matzuk**. GASZ is essential for male meiosis and suppression of retrotransposon expression in the male germline. – *PLoS Genet.*, **5**, 2009, e1000635.

40. **Mannella, C. A**. Structural diversity of mitochondria, functional implications. – *Ann. N.Y. Acad. Sci*., **1147**, 2008, 171-179.
41. **Mannella, C. A**. Structure and dynamics of the mitochondrial inner membrane cristae. – *Biochim. Biophys. Acta – Molecular Cell Research*, **1763**, 2006, 542-548.
42. **May-Panloup**, **P., M. F. Chretien, F. Savagner, C. Vasseur, M. Jean, Y. Malthiery, P. Reynier**. Increased sperm mitochondrial DNA content in male infertility. – *Hum. Reprod*., **18**, 2003, 550-556.
43. **Meinhardt, A., B. Wilhelm, J. Seitz**. Expression of mitochondrial marker proteins during spermatogenesis. – *Human Reprod. Upd*., **5**, 1999, 108-119.
44. **Michikawa, Y., F. Mazzucchelli, N. Bresolin, G. Scarlato, G. Attardi**. Aging dependent large accumulation of point mutations in the human mtDNA control region for replication. – *Science*, **286**, 1999, 774-779.
45. **Moraes, C. R., S. Meyers**. The sperm mitochondrion: Organelle of many functions. – Animal Reprod. Sci., 2018, https://doi.org/10.1016/j.anireprosci.2018.03.0242018.
46. **Mota, P. C., S. Amaral, L. Martins, M. L. Pereira, P. J. Oliveira, J. Ramalho-Santos**. Mitochondrial bioenergetics of testicular cells from the domestic cat (felis catus) – a model for endangered species. – *Reprod. Toxicol*., **11**, 2009, 111-116.
47. **Moussa, F., R. Oko, L. Hermo**. The immunolocalization of small nuclear ribonucleoprotein particles in testicular cells during the cycle of the seminiferous epithelium of the adult rat. – *Cell Tissue Res*., **278**, 1994, 363-378.
48. **Nakada, K., A. Sato, K. Yoshida, T. Morita, H. Tanaka, S. Inoue, H. Yonekawa, J. Hayashi**. Mitochondria - related male infertility. – *Proc. Natl. Acad. Sci. U.S.A.*, **103**, 2006, 15148-15153.
49. **Nakamura, M., S. Okinaga, K. Arai**. Metabolism of pachytene primary spermatocytes from rat testes: pyruvate maintenance of adenosine triphosphate level. – *Biol. Reprod*., **30**, 1984, 1187-1197.
50. **Park, C. B., N.-G. Larsson**. Mitochondrial DNA mutations in disease and aging. – *J. Cell Biol*., **193**, 2011, 809-818.
51. **Pelliccione, F., A. Micillo, G. Cordeschi, A. D'Angeli, S. Necozione, L. Gandini, A. Lenzi, F. Francavilla S. Francavilla**. Altered ultrastructure of mitochondrial membranes is strongly associated with unexplained asthenozoospermia. – *Fertil. Steril.*, **95**, 2011, 641-646.
52. **Rajender, S., P. Rahul, A. A. Mahdi**. Mitochondria, spermatogenesis and male infertility. – *Mitochondrion*, **10**, 2010, 419-428
53. **Ramalho-Santos, J., S. Varum, S. Amaral, P. C. Mota, A. P. Sousa, A. Amaral**. Mitochondrial functionality in reproduction: from gonads and gametes to embryos and embryonic stem cells. – *Human Reprod. Upd*., **15**, 2009, 553-572.
54. **Rantanen, A., N. G. Larsson**. Regulation of mitochondrial DNA copy number during spermatogenesis. – *Hum. Reprod*., **15** (2), 2000, 86-91.
55. **Rato, L., M. G. Alves, S. Socorro, A. I. Duarte, J. E. Cavaco, P. F. Oliveira**. Metabolic regulation is important for spermatogenesis. – *Nat. Rev. Urol*., **9**, 2012, 330-338.
56. **Rube, D.A., A. M. van der Bliek**. Mitochondrial morphology is dynamic and varied. – *Mol Cell. Biochem*., **256/257**, 2004, 331-339.
57. **Ruiz-Pesini, E., C. Diez, A. Lapena, A. Perez-Martos, J. Montoya, E. Alvarez, J. Arenas**, **M. Lopez-Perez**. Correlation of sperm motility with mitochondrial enzymatic activities. – *Clin. Chem.*, **44**, 1998, 1616-1620.
58. **Russell, L., B. Frank**. Ultrastructural characterization of nuage in spermatocytes of the rat testis. – *Anat. Rec.*, **190**(1), 1978, 79-97.
59. **Scott, I., D. C. Logan**. Mitochondrial dynamics: the control of mitochondrial shape, size, number, motility, and cellular inheritance. – In: Plant Mitochondria, (Ed. David C Logan). – *Blackwell Publishing Ltd*., Oxford, UK, 2007, 1-35.
60. **Seitz, J., J. Möbius, M. Bergmann, A**. **Meinhardt**. Mitochondrial differentiation during meiosis of male germ cells. – *Int. J. Androl*., **2**, 1995, 7-11.
61. **Shamsi, M. B., R. Kumar, A. Bhatt, R. Bamezai, R. Kumar, N. Gupta, T. Das, R. Dada**. Mitochondrial DNA mutations in etiopathogenesis of male infertility. – *Ind. J. Urol.*, **24** (2), 2008, 150-154.
62. **Siva, A. B., D. B. Kameshwari, V. Singh, K. Pavani, C. S. Sundaram, N. Rangaraj, M. Deenadayal, S. Shivaji**. Proteomics-based study on asthenozoospermia: differential expression of proteasome alpha complex. – *Mol. Human Reprod.*, **16**, 2010, 452-462.
63. **Söderstrom**, **K. O., Parvinen, M**. Incorporation of (^{3}H) uridine by the chromatoid body during rat spermatogenesis. – *J. Cell Biol*., **70**, 1976, 239-246.

64. **Song, G. J., V. Lewis.** Mitochondrial DNA integrity and copy number in sperm from infertile men. – *Fert. Steril*., **90**, 2008, 2238-2244.
65. Sousa, A. P., A. Amaral, M. Baptista, R. Tavares, P. C. Campo, P. C. Peregrín, A. Freitas, A. Paiva, T. Almeida-Santos, J. Ramalho-Santos. Not all sperm are equal: functional mitochondria characterize a subpopulation of human sperm with better fertilization potential. – *PloS ONE*, 6(3), 2011, e18112.
66. **Srivastava, N., P. Megha**. Mitochondrion: Features, functions and comparative analysis of specific probes in detecting sperm cell damages. – *Asian Pacif. J. Reprod*., **5**(6), 2016, 445-452.
67. **St John, J. C., E. Bowles, A. Amaral**. Sperm mitochondria and fertilisation. – *Soc. Reprod. Fertil. Suppl*., **65**, 2007, 399-416.
68. **St John, J. C., R. P. Jokhi, C. L. Barratt.** The impact of mitochondrial genetics on male infertility. – *Int. J. Androl.*, **28**, 2005, 65-73.
69. **St John, J. C., J. Facucho-Oliveira, Y. Jiang, R. Kelly, R. Salah**. Mitochondrial DNA transmission, replication and inheritance: a journey from the gamete through the embryo and into offspring and embryonic stem cells. – *Human Reproduction Update*, **16**, 2010, 488-509.
70. **Storey, B. T.** Mammalian sperm metabolism: oxygen and sugar, friend and foe. – *Int. J. Dev. Biol*., **52**, 2008, 427-437.
71. **Sutovsky, P., R. D. Moreno, J. Ramalho-Santos, T. Dominko, C. Simerly, G. Schatten**. Ubiquitin tag for sperm mitochondria. – *Nature*, **402**, 1999, 371-372.
72. **Taanman, J. W**. The mitochondrial genome: structure, transcription, translation and replication. – *Biochim. Biophys. Acta,* **1410**(2), 1999, 103-123.
73. **Thangaraj, K., M. B. Joshi, A. G. Reddy, A. A. Rasalkar, L. Singh**. Sperm mitochondrial mutations as a cause of low sperm motility. – *J. Androl*., **24**, 2003, 388-392.
74. **Tzagoloff, A**. Mitochondria. Cellular organelles. (Ed. Philip Siekevitz), Plenum Press, New York and London, 1982, 15-23.
75. **Venkatesh, S., M. Deecaraman, R. Kumar, M. B. Shamsi, R. Dada**. Role of reactive oxygen species in the pathogenesis of mitochondrial DNA (mtDNA) mutations in male infertility. – *Indian J. Med. Res.,* **129**, 2009, 127-137.
76. **Wai, T., A. Ao, X. Zhang, D. Cyr, D. Dufort, E. A. Shoubridge**. The role of mitochondrial DNA copy number in mammalian fertility. – *Biology of Reproduction*, **83**(1), 2010, 52-62.
77. **Yeste, M., E. Estrada, L. G. Rocha, H. Marin, J. E. Rodriguez-Gil, J. Miro**. Cryotolerance of stallion spermatozoa is related to ROS production and mitochondrial membrane potential rather than to the integrity of sperm nucleus. – *Andrology*, **3**, 2015, 395-407.
78. **Zeviani, M., C. Antozzi**. Mitochondrial disorders. – Mol. Human Reprod. **3**, 1997, 133-148.
79. **Zhang, J., Q. Wang, M. Wang, M. Jiang, Y. Wang, Y. Sun, J. Wang, T. Xie, C. Tang, N. Tang, H. Song, D. Cui, R. Chao, S. Ding, B. Ni, X. Chen, Y. Wang**. GASZ and mitofusin-mediated mitochondrial functions are crucial for spermatogenesis. – *EMBO Reports*, **17**(2), 2016, 220-234.
80. **Zhao, C., R. Huo, F. Q. Wang, M. Lin, Z. M. Zhou, J. H. Sha**. Identification of several proteins involved in the regulation of sperm motility by proteomic analysis. – *Fertil. Steril.*, **87**, 2007, 436-438.
81. **Zvetkova, E.** Cytochemical detection and distribution of ribonucleoprotein complexes (rnpcs) during mitosis. – *Genetics and breeding*, **25**(3), 1992, 282-287.
82. **Zvetkova E**. Unstained mitochondria in nuclei of myeloblast-patients with CML; Unstained mitochondria in granulocytes' nuclei of cancer patients. – In: Thein S. L. (Ed.), BloodMed, www.bloodmed.com-SlideAtlas, 2006, Blackwell Publishing, Oxford, UK.
83. **Zvetkova, E., I. Zvetkov**. A cytological method for the simultaneous staining of nucleoproteins and some cationic proteins. – *Acta Histochem*., **57**, 1976, 1-13.
84. **Zvetkova E., R. Toshkova**. Unstained mitochondria in the cytoplasm and nucleus of atypical myeloid cell – *Graffi* myeloid tumor, induced in hamster. – In: Thein S. L. (Ed.), BloodMed, www.bloodmed.com-SlideAtlas, 2006, Blackwell Publishing, Oxford, UK.

Guidelines for Authors

Acta morphologica et anthropologica is an open access peer review journal and publishes original articles, short communications, reviews, letters to the Editors. The aim of the journal is to provide a forum for cytological, histological, anatomical and anthropological research community in life sciences, including cell biology, immunobiology, pathology, neurobiology, environmental and toxicological research, reproductive biology, pharmacology, physical development and medical anthropology, paleoanthropology, anatomy, paleoanatomy, etc.

Contact details and submission

Manuscripts should be in English with total length not exceeding 10 standard pages, line-spacing 1.5, justified with 2.5 cm margins. The authors are advised to use Times New Roman, 12 pt throughout the text. Pages should be numbered at the bottom right corner of the page. Manuscript submission is electronic only. The manuscripts should be sent to**: iempam@bas.bg and ygluhcheva@hotmail.com**

All correspondence, including notification for Editor's decision, requests for revision, is sent by e-mail. After acceptance of the manuscript a hard copy should be sent to Editorial Office address:

Institute of Experimental Morphology, Pathology and Anthropology with Museum
Bulgarian Academy of Sciences
Editorial Office of Acta morphologica et anthropologica
Acad. Georgi Bonchev Str., Bl. 25
1113 Sofia, Bulgaria

Article structure

The article should be arranged under the following headings: Introduction, Material and Methods, Results, Discussion, Conclusion, Acknowledgements and References.
Title page – includes:

- **Title** - concise and informative;
- **Author(s)' names and affiliations** – indicate the given name(s) and family name(s) of all authors. Present the authors' affiliation addresses below the names. Indicate all affiliations with a lower-case superscript after the author's name and in front of the appropriate address. Provide the full postal address information for each affiliation, including the country name.
- **Corresponding author** – clearly indicate who will handle the correspondence for refereeing, publication and post-publication. An e-mail should be provided.
- **Abstract** – state briefly the aim of the work, the principal results and major conclusions and should not exceed 150 words. References and uncommon, or non-standard abbreviations should be avoided.
- **Key words** – provide up to 5 key words. Avoid general, plural and multiple concepts. The key words will be used for indexing purposes.

Introduction – state the objectives of the work and provide an adequate background, avoiding a detailed literature survey or summary of the results.

Material and Methods – provide sufficient detail to allow the work to be reproduced. Methods already published should be indicated as a reference: only relevant modifications should be described.

Results – results should be clear and concise.

Discussion – should explore the significance of the results in the work, not repeat them. A combined *Results and Discussion* section is often appropriate. Avoid extensive citation and discussion of published literature.

Conclusions – the main conclusions of the study should be presented in a short section.

Acknowledgements – list here those individuals who provided help during the research and the funding sources.

Units – please use the International System of Units (SI).

Math formulae – please submit math equations as editable text, not as images.

Electronic artwork – number the tables and illustrations according to their sequence in the text. Provide captions for them on a separate page at the end of the manuscript. The proper place of each figure in the text should be indicated in the left margin of the corresponding page. **All illustrations (photos, graphs and diagrams)** should be referred to as "figures" and given in abbreviation "Fig.", and numbered in Arabic numerals in order of its mentioning in the manuscript. They should be provided in grayscale as JPEG or TIFF format, minimum 300 dpi. The illustrations should be submitted as separate files.

References – they should be listed in alphabetical order, indicated in the text by giving the corresponding numbers in parentheses. The "References" should be typed on a separate sheet. The names of authors should be arranged alphabetically according to family names. In the reference list titles of works, published in languages with non-Latin alphabet, should be translated, original language must be indicated at the end of reference (e.g., [in Bulgarian,]). Articles should include the name(s) of author(s), followed by the full title of the article or book cited, the standard abbreviation of the journal (according to British Union Catalogue), the volume number, the year of publication and the pages cited, for books - the city of publication and publisher. In case of more than one author, the initials of the second, third, etc. authors precede their family names.

For articles: Davidoff, M. S., R. Middendorff, G. Enikolopov, D. Riethmacher, A. F. Holstein, D. Muller. Progenitor cells of the testosterone-producing Leydig cells revealed. – *J. Cell Biol.,* **167**, 2004, 935-944.

Book article or chapter: Rodriguez, C. M., J. L. Kirby, B. T. Hinton. The development of the epididymis. – In: *The Epididymis - from molecules to clinical practice* (Eds. B. Robaire, B. T. Hinton), New York, Kluwer Academic Plenum Publisher, 2002, 251-269.

Electronic books: **Gray, H.** *Anatomy of the human body* (Ed. W.H.Lewis), 20th edition, NY, 2000. Available at http://www.Bartleby.com.

PhD thesis: **Padberg, G**. Facioscapulohumeral diseases. *PhD thesis*, Leiden University, 1982, 130 p.

Website: National survey schoolchildren report. National Centre of Public Health and Analyses, 2014. Available at http://ncphp.government.bg/files

Page charges

Manuscript publication is free of charges.

Ethics in publishing

Before sending the manuscript the authors must make sure that it meets the Ethical guidelines for journal publication of Acta morphologica et anthropologica.

Human and animal rights

If the work involves the use of human subjects, the authors should ensure that work has been carried out in accordance with *The Code of Ethics of the World Medical Association* (Declaration of Helsinski). The authors should include a statement in the manuscript that informed consent was obtained for experimentation with human subjects. The privacy rights of human subjects must always be observed.
All animal experiments should comply with the *ARRIVE guidelines* and should be carried out in accordance with the U.K. Animals (Scientific procedures) Act, 1986 and the associated guidelines *EU Directive 2010/63/EU* for animal experiments, or the National Institutes of Health guide for the care and use of Laboratory animals (NIH Publications No. 8023, revised 1978) and the authors should clearly indicate in the manuscript that such guidelines have been followed.

Submission declaration

Submission of the manuscript implies that the work described has not been published previously, is not considered under publication elsewhere, that its publication is approved by all authors, and that if accepted, it will not be published elsewhere in the same form, in English or in any other language, including electronically, without the informed consent of the copyright-holder.

Contributors

The statement that all authors approve the final article should be included in the disclosure.

Copyright

Upon acceptance of an article, the authors will be asked to complete a "Journal Publishing Agreement". An e-mail will be sent to the corresponding author with the Journal Publishing Agreement Form or a link to the online version of this agreement.

Peer review

This journal operates a single blind review process. All contributions will be initially assessed by the Editor for suitability for the journal. All suitable papers are then sent to two independent expert reviewers to assess the scientific quality of the paper. The Editor is responsible for the final decision regarding acceptance or rejection of articles.

After acceptance

Proof correction

The corresponding author will receive proofs by e-mail in PDF format and will be requested to return it with any corrections within a week.

Offprints

The journal provides free access to all papers in each volume that can be downloaded from the following website: http://www.iempam.bas.bg/journals/acta.html